

MIT/WHOI 2002-05

**Massachusetts Institute of Technology
Woods Hole Oceanographic Institution**



**Joint Program
in Oceanography/
Applied Ocean
Science
and Engineering**



DOCTORAL DISSERTATION

*Direct and Indirect Photoreactions of
Chromophoric Dissolved Organic Matter:
Roles of Reactive Oxygen Species and Iron*

by

Jared Verrill Goldstone

February 2002

DISTRIBUTION STATEMENT A

Approved for Public Release
Distribution Unlimited

20020924 017

MIT/WHOI

2002-05

**Direct and Indirect Photoreactions of
Chromophoric Dissolved Organic Matter:
Roles of Reactive Oxygen Species and Iron**

by

Jared Verrill Goldstone

Massachusetts Institute of Technology
Cambridge, Massachusetts 02139

and

Woods Hole Oceanographic Institution
Woods Hole, Massachusetts 02543

February 2002

DOCTORAL DISSERTATION

Funding was provided by the National Science Foundation under grants OCE-9529448, OCE-9521628, OCE-9811208, and OCE-9819089 and the Ralph M. Parsons Foundations.

Reproduction in whole or in part is permitted for any purpose of the United States Government.
This thesis should be cited as: Jared Verrill Goldstone, 2002. Direct and Indirect Photoreactions of Chromophoric Dissolved Organic Matter: Roles of Reactive Oxygen Species and Iron. Ph.D. Thesis. MIT/WHOI, 2002-05.

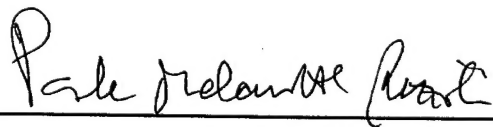
Approved for publication; distribution unlimited.

Approved for Distribution:



Mark D. Kurz, Chair

Department of Marine Chemistry and Geochemistry



Paola Malanotte-Rizzoli

Paola Malanotte-Rizzoli
MIT Director of Joint Program



John W. Farrington

John W. Farrington
WHOI Dean of Graduate
Studies

**DIRECT AND INDIRECT PHOTOREACTIONS OF CHROMOPHORIC
DISSOLVED ORGANIC MATTER: ROLES OF REACTIVE OXYGEN SPECIES
AND IRON**

by

JARED VERRILL GOLDSTONE

S.M., Massachusetts Institute of Technology (1996)
B.S., Yale University (1993)

submitted in partial fulfillment of the requirements for the degree of

Doctor of Philosophy

at the

MASSACHUSETTS INSTITUTE OF TECHNOLOGY

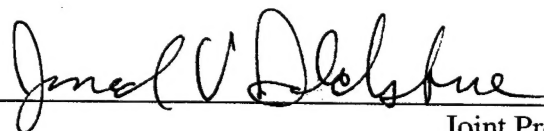
and the

WOODS HOLE OCEANOGRAPHIC INSTITUTION

February 2002

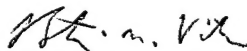
©Massachusetts Institute of Technology, 2002
All rights reserved

Signature of Author



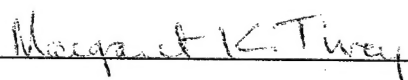
Joint Program in Oceanography
Massachusetts Institute of Technology
Woods Hole Oceanographic Institution

Certified by



Professor Bettina M. Voelker
Thesis Supervisor

Accepted by



Dr. Margaret Tivey, chair
Joint Committee for Chemical Oceanography
Woods Hole Oceanographic Institution

DIRECT AND INDIRECT PHOTOREACTIONS OF CHROMOPHORIC DISSOLVED ORGANIC MATTER: ROLES OF REACTIVE OXYGEN SPECIES AND IRON

by Jared Verrill Goldstone

Submitted to the Joint Committee on Chemical Oceanography, Massachusetts Institute of Technology and Woods Hole Oceanographic Institution on January 18, 2002, in partial fulfillment of the requirements for the degree of Doctor of Philosophy in Oceanography

ABSTRACT

Photochemical transformations of chromophoric dissolved organic matter (CDOM) are one of the principal processes controlling its fate in coastal waters. The photochemical decomposition of CDOM leads to the formation of a variety of biologically available carbon substrates. Photomineralization of CDOM to dissolved inorganic carbon may constitute a significant flux in the global carbon cycle.

Photoreactions ultimately lead to the destruction of the chromophores and hence to the loss of absorption and fluorescence (bleaching), thus acting as a sink for CDOM.

Photodecomposition may proceed both via direct photochemical reactions, following absorption of photons by CDOM, or via indirect processes, involving DOM reactions with photochemically generated intermediates such as reactive oxygen species (ROS).

The reactions of CDOM with two important ROS, superoxide (O_2^-) and hydroxyl radical ($OH\cdot$), have different consequences. Superoxide reactions with CDOM did not appear to degrade the CDOM. Instead, CDOM catalysed the dismutation of O_2^- to O_2 and HOOH. This reactivity has the effect of limiting the steady-state concentration of O_2^- in most coastal waters. In contrast, reactions of CDOM with radiolytically produced $OH\cdot$ formed CO_2 and several low molecular weight carboxylic acids, as well as bleached both the absorption and fluorescence at slow rates. These reactions did not increase the bioavailability of this material to a microbial consortium.

Both direct and indirect photochemical processes are expected to be accelerated by the presence of iron. However, addition of iron to several coastal seawater samples neither increased the rate of photobleaching nor the apparent quantum yield (AQY) of CO. Similarly, the addition of the siderophore desferrioxamine B did not change the photobleaching rates or the CO AQYs. The addition of 2 μM Fe to solutions of Suwannee River Fulvic Acid did not increase the photobleaching rates. In combination with prior results, these findings suggest that indirect photoreactions do not increase the photobleaching rates of CDOM in coastal systems.

A model of CDOM photobleaching based on the assumption of negligible indirect photobleaching processes and multiple non-interacting chromophores was created utilizing photobleaching data produced with monochromatic light to calculate the spectra and exponential decay rates of independent components. These components were then used to calculate bleaching spectra for broadband light and compared with actual bleaching spectra.

Thesis supervisor:

Bettina M. Voelker, Assistant Professor of Civil and Environmental Engineering, MIT

Sea-Fever

I must go down to the seas again, to the lonely sea and the sky,
And all I ask is a tall ship and a star to steer her by,
And the wheel's kick and the wind's song and the white sail's shaking,
And a gray mist on the sea's face and a gray dawn breaking.

I must go down to the seas again, for the call of the running tide
Is a wild call and a clear call that may not be denied;
And all I ask is a windy day with the white clouds flying,
And the flung spray and the blown spume, and the seagulls crying.

I must go down to the seas again to the vagrant gypsy life,
To the gull's way and the whale's way where the wind's like a whetted knife;
And all I ask is a merry yarn from a laughing fellow-rover,
And quiet sleep and a sweet dream when the long trick's over.

-John Masefield (1878-1967)

Acknowledgements

First, and most importantly, I need to thank my advisor, Tina Voelker. Tina not only got me into the Joint Program on extremely short notice (2 weeks in August!), but gave me free rein to develop my own research interests. I am also glad to have the unique opportunity of being her first graduate student. All the members of my thesis committee, Ed Boyle, Neil Blough, Dan Repeta, and Ollie Zafiriou, have been extremely generous with their time and attention. Ollie has also been generous with lab space and cruise time, two very precious commodities. Rossana Del Vecchio and Neil Blough have been extremely unselfish with their data, and Rossana in particular has been patient with my desperate, last-minute emails asking for data.

A large cast of other people have been of invaluable help on the various research cruises that I have managed to scrounge: Greg and Linda Cutter, Craig Taylor, John Tolli, Lori Ziolkowski, Ray Najjar, Jen Werner, Bob Kieber, and Xie Hui, as well as the crews of the R/V Cape Hatteras, R/V Cape Henlopen, R/V Endeavor and the R/V Weatherbird II. Dave Glover, Urs von Gunten, and Michael Elovitz were of great help for different aspects of this thesis. In particular, Dave's help with Matlab has allowed me to develop a tolerance, at least, for matrix algebra. The members of the Voelker group, Barbara Southworth, Megan Kogut (thanks for the 'Dissertation Station!'), Wai Kwan, Mike Pullin, and Stefan Bertilsson have been tolerant labmates, appreciative audiences for practice talks, and good friends. I must also thank Frieda for making a number of meetings with Tina an excuse to play with an amazingly cute (but large!) puppy.

As a Joint Program student, I have been very fortunate to be able to interact with two amazing communities: Woods Hole and Parsons Lab. The denizens of Fye Lab, including Jim Moffett, Ed Sholkovitz, Tim Eglinton, Dan, Ollie, Chris Reddy, and many others, have always been cheeful and welcoming. Parsons Lab has been my home for these past five and half years, sometimes almost literally, although I've only slept over once. Parsons could not be a home without a mom, and Sheila Frankel has amply filled that role. She's even been generous enough to allow her husband Don to play ice hockey with us. Through the years I've also managed to play soccer with an amazingly diverse

array of Parsonites, and I've always enjoyed the games, even when we lost. (Go Hydros!) Many fellow students and postdocs in both Woods Hole and Parsons have been good friends, willing to engage in both intellectual conversation and completely unintellectual chat: Rebecca Thomas (and Muddy), Steve Fries (and Jasmine), Bridget Bergquist, Emily Slaby, Mak Saito, Anna Cruise, Holly Michael, Matt Sullivan, Ana Lima, Vanya Klepac, Sam Arey (thanks for the late night company at the computers), Andy Tolonen, Daniel Pedersen, Janelle Thompson, Greg Noonan, John Gambino, Dave Senn, Nicole Keon, Dan Brabander, Jim Gawel, Jenny Jay, Rachel Adams, Kirsten Findell, Dror Angel, Debbie Lindel, and everyone else in Parsons who has ever spent time in the lunchroom.

My years in Cambridge and Somerville and at MIT have brought me many close friends. Chris Morse in particular has been an amazing friend, and labmate, and housemate. I'd give him his own paragraph, but I'm running out of room. Chris Long has been another amazing friend, starting from our first meeting as randomly joined roommates in Tang 19D eight! years ago. And 2 Brastow Ave. was never the same once Carlos Navas left. Thank you for the sangria recipe. Ann and Ray, Deb and Brian, Catharine and Brant, Tivol, and Rose and Brian have all made life enjoyable over the years here, especially for many memorable birthday dinners.

Many family members, and my parents in particular, have been enthusiastic supporters during my graduate career. Dad, thank you for asking if I was writing yet (every week for the past three years). My grandfather, John H. Welsh, has been an inspiration, even more so once I learned that he had been on research cruises aboard the original R/V Atlantis in 1930 (the year WHOI was founded). Judy and Mark Handley have been supportive and helpful throughout my years in the Joint Program, and I have greatly enjoyed sailing with them. Finally, and most importantly, I need to thank Heather Handley. This thesis would not have happened without her editing and support.

Research funding was provided by the National Science Foundation and the Ralph M. Parsons Foundation. Different aspects of this work was supported by NSF grants OCE-9529448, OCE-9521628, OCE-9811208, and OCE-9819089, which are acknowledged at the end of each relevant chapter.

TABLE OF CONTENTS

ABSTRACT	3
ACKNOWLEDGEMENTS	5
TABLE OF CONTENTS.....	7
LIST OF FIGURES	10
LIST OF TABLES.....	13
CHAPTER 1. INTRODUCTION: PHOTOCHEMISTRY OF CHROMOPHORIC DISSOLVED ORGANIC MATTER	15
INTRODUCTION.....	16
AQUATIC DISSOLVED ORGANIC MATTER: COMPOSITION AND PROPERTIES	16
Autochthonous and allochthonous DOM.....	17
Humic and fulvic acids	17
Marine humic substances	19
Ultrafiltered dissolved organic matter	19
CHROMOPHORIC DISSOLVED ORGANIC MATTER (CDOM).....	20
CDOM Absorption	21
Fluorescent dissolved organic matter (FDOM).....	22
CDOM and FDOM in estuaries.....	23
CDOM PHOTOCHEMISTRY.....	23
Photochemistry as a sink of CDOM	24
Photochemical Mechanisms: Direct versus Indirect Photochemistry	24
MECHANISMS OF DIRECT CDOM PHOTOCHEMISTRY.....	26
MECHANISMS OF INDIRECT CDOM PHOTOCHEMISTRY	27
Reactive Oxygen Species.....	27
Fate of ROS: Reaction with DOM and metals	28
ROLES OF FE	29
MECHANISMS OF PHOTOBLEACHING	30
CONTRIBUTIONS OF THIS THESIS.....	31
REFERENCES	32
CHAPTER 2. CHEMISTRY OF SUPEROXIDE RADICAL (O_2^-) IN SEAWATER: CDOM ASSOCIATED SINK OF SUPEROXIDE IN COASTAL WATERS	57
ABSTRACT	58
INTRODUCTION.....	59
METHODS.....	60
Samples	60
Kinetics	61
RESULTS	63
DISCUSSION	65

Redox activity.....	65
Steady state O ₂ ⁻ concentrations	67
ACKNOWLEDGMENTS	68
REFERENCES	70
CHAPTER 3. REACTIONS OF HYDROXYL RADICAL WITH HUMIC SUBSTANCES: BLEACHING, MINERALIZATION, AND PRODUCTION OF BIOAVAILABLE CARBON SUBSTRATES.....	91
ABSTRACT	92
INTRODUCTION.....	93
METHODS.....	96
Materials.....	96
Radiolysis.....	97
Analytical Techniques	98
Determination of low-molecular weight carboxylic acids.....	99
Bioassays.....	100
RESULTS	102
DISCUSSION	106
LMW acid production.....	106
Production of bioavailable carbon substrates.....	107
DIC production.....	108
Bleaching.....	109
OH [•] as a mechanism of DOM photoproduct formation	109
ACKNOWLEDGEMENTS	111
REFERENCES	112
SRHA.....	116
SRFA	116
CHAPTER 4: A MULTICOMPONENT MODEL OF CDOM PHOTOBLEACHING.....	131
ABSTRACT	132
INTRODUCTION.....	133
Theory	136
METHODS.....	140
Data/Bleaching Samples	140
Modeling	141
Broadband reconstruction	144
RESULTS	145
Broadband reconstruction	147
DISCUSSION	148
ACKNOWLEDGEMENTS	150
REFERENCES	151
APPENDIX	176

CHAPTER 5. IRON EFFECTS ON THE PHOTOBLEACHING OF CDOM AND THE PHOTOPRODUCTION OF CO.....	187
ABSTRACT	188
INTRODUCTION.....	189
Photobleaching	190
Estuarine processes	193
METHODS.....	195
Samples	195
Photobleaching	196
Gamma Radiolysis.....	197
Analyses	198
Carbon Monoxide Apparent Quantum Yields.....	199
Carbon Monoxide Optical Buoy Incubations.....	200
RESULTS	201
Photobleaching of fluorescence.....	202
Effect of Fe on photobleaching	202
Excitation-emission spectroscopy	202
CO photoproduction	203
Fe effects on CO photoproduction.....	204
DISCUSSION	205
Photobleaching of Absorption.....	205
Photobleaching of Fluorescence.....	207
Excitation-Emission Spectra	207
Fe effects on photobleaching.....	209
Fe effects on CO photoproduction in estuarine waters.....	210
Conclusions	211
ACKNOWLEDGEMENTS	211
REFERENCES	213
CHAPTER 6. THESIS DISTILLATION AND FUTURE WORK.....	249
GEOCHEMICAL SIGNIFICANCE.....	250
FUTURE WORK.....	252
REFERENCES	254
AUTHOR'S BIOGRAPHY.....	255

LIST OF FIGURES

Figure 1.1 UV-visible absorption spectrum of three different CDOM samples.....	38
Figure 1.2 Primarily photochemical reactions of CDOM.....	40
Figure 1.3 Photogeneration of reactive oxygen species via secondary CDOM reactions	42
Figure 1.4 Mechanism of photodecarboxylation	44
Figure 1.5 Potential mechanism of photodecarbonylation	46
Figure 1.6 Interconversion between the various oxidation states of oxygen.....	48
Figure 1.7 The most important mechanisms of OH• reactions with lignin models	50
Figure 1.8 Redox cycling of dissolved and particulate Fe	52
Figure 1.9 Two mechanisms of the role of Fe in CDOM photochemistry.....	54
Figure 2.1 An example of a plot of k_{pseudo} versus percent-sample-added.....	72
Figure 2.2 The correlation between the observed k_{pseudo} and the absorbance of the water samples.....	74
Figure 2.3 The relationship between the observed k_{pseudo} values and chlorophyll a (A), nitrate (B), phosphate (C), and silicate (D) concentrations.....	76
Figure 2.4 The effects of several different sample treatments on k_{pseudo}	78
Figure 2.5 Hydrogen peroxide produced during either the self-dismutation or the DOM catalyzed dismutation of superoxide.....	80
Figure 2.6 The variation of observed k_{pseudo} with initial superoxide concentration.....	82
Figure 2.7 Suggested redox cycle between quinone, semiquinone radical, and hydroquinone.....	84
Figure 2.8 The observed k_{pseudo} versus the optical absorption at 300 nm for several 10 mg/L humic and fulvic acid solutions.....	86
Figure 2.9 Correlation between the observed k_{pseudo} and (A) the organic radical content and (B) the percent aromaticity	88

Figure 3.1 Mineralization of ^{14}C -formate in 5 mg l ⁻¹ SRFA and SRHA solutions	118
Figure 3.2 Measured formation of formic, acetic, malonic, and oxalic acids from the reaction of OH• with SRFA (A) and SRHA (B).	120
Figure 3.3 Average bacterial abundance in incubated cultures of GF/F filtered seawater amended 25% (v/v) with Suwannee River Fulvic Acid, SRFA, (A) or Suwannee River Humic Acid, SRHA (B) with or without γ -radiolysis treatment	122
Figure 3.4 DIC production from irradiated SRFA without and with 0.3 M <i>tert</i> -butanol as a radical scavenger.....	124
Figure 3.5 DIC production divided by OH• generated ($\mu\text{M}/\mu\text{M}$) for various treatments of SRFA and SRHA solutions	126
Figure 3.6 Bleaching of SRFA at 300 nm with and without oxygen, SRHA solutions with and without oxygen, DOC-free seawater amended with SRFA prior to irradiation , and a coastal seawater sample	128
Figure 4.1 Fit components to monochromatic bleaching of 10mg l ⁻¹ SRFA at different wavelengths.	156
Figure 4.2 Decrease in the reduced χ^2 for the residual values of the model fit to the data	158
Figure 4.3 Absorbance values of the four (top) and six (bottom) component fit to the monochromatic bleaching data of SRFA.	160
Figure 4.4 Four component fit to monochromatic bleaching data of 10mg l ⁻¹ SRFA at different wavelengths.....	162
Figure 4.5 Six component fit to monochromatic bleaching data of 10mg l ⁻¹ SRFA at different wavelengths.	164
Figure 4.6 Graphical analysis for the determination of constant quantum yield for the four component fit.	166
Figure 4.7 Graphical analysis for the determination of constant quantum yield for the six component fit.....	168

Figure 4.8 Comparison of reconstructed spectra calculated with different numbers of components with observed absorption values for broadband ($\lambda_j > 320$ nm) irradiation of SRFA.	170
Figure 4.9 Expanded view of the early timepoints for the comparison of the reconstructed spectra	172
Figure 4.10 Percent residual ((data-fit)/data) x 100% for the calculation of broadband bleaching spectra of SRFA.	174
Figure 5.1 Schematic diagram of the photobleaching apparatus	224
Figure 5.2 Irradiance spectrum of the solar simulator and a solar spectrum.....	226
Figure 5.3 Normalized photobleaching curves of CDOM absorption in three unaltered seawater samples from the Delaware Bay	228
Figure 5.4 Normalized photobleaching curves of CDOM fluorescence F/R values for three unaltered seawater samples from the Delaware Bay and SRFA	230
Figure 5.5 Normalized bleaching curves of CDOM absorption and fluorescence F/R values for three treatments of two different seawater samples Fe, DFOM, and unamended	232
Figure 5.6 Normalized bleaching curves of CDOM absorption and fluorescence F/R values for additions of Fe to SRFA solutions	234
Figure 5.7 Excitation-emission matrix spectra (EEMs) for 4 different water samples...	236
Figure 5.8 EEMs difference spectra showing the bleaching of the two peaks, A and H	238
Figure 5.9 EEMS difference spectra showing the bleaching of fluorescence by radiolytically-produced OH•	240
Figure 5.10 Apparent quantum yields (AQY) of CO photoproduction from estuarine seawater for different treatments: Fe added, DFOM added, and unaltered	242
Figure 5.11 CO photoproduction from Sargasso Sea water during one daylight period as determined using an optical buoy.....	244
Figure 5.12 Bleaching of fluorescence versus bleaching of absorption for 4 different samples: SRFA S4, S20FeB, and S29	246

LIST OF TABLES

Table 2.1 Calculated O ₂ ⁻ steady state concentrations in coastal waters	69
Table 3.1 OH• reaction rate constants with SRFA and SRHA as a function of cumulative OH• exposure	115
Table 3.2 Ratio of mol carboxylic acid produced per mol OH• for SRFA and SRHA...	115
Table 3.3 Initial DOC measured in dilution culture bioassays and bacterial abundance, cellular carbon content and total bacterial carbon at day 6.....	116
Table 4.1 ANOVA results testing goodness-of-fit for multicomponent fits to monochromatic irradiation data sets.....	153
Table 4.2 ANOVA tests of the significance of adding a component to multicomponent fits of monochromatic irradiations of SRFA.....	153
Table 4.3 The relative bleaching decay constants (in units of hr ⁻¹ (mol photons m ⁻²) ⁻¹) for the best fits to the monochromatic data sets.....	154
Table 4.4 Sum of squared residuals for the comparison of calculated broadband bleaching spectra with observed spectra	154
Table 5.1 Characteristics of water samples used in photobleaching experiments	217
Table 5.2 Measured Fe concentrations in irradiation samples.....	217
Table 5.3 Spectral slopes (S) of absorption curves determined from least-squares regression of log-linearized absorption values.....	218
Table 5.4 Fitting constants for bi-exponential fits of absorption photobleaching	219
Table 5.5 Fitting constants for bi-exponential fits of photobleaching of fluorescence...	220
Table 5.6 Excitation and emission peak wavelengths determined from EEMS	221
Table 5.7 Apparent quantum yields of CO from seawater samples in mole per photon absorbed at 3 different wavelengths	222

CHAPTER 1.

INTRODUCTION: PHOTOCHEMISTRY OF CHROMOPHORIC DISSOLVED ORGANIC MATTER

Introduction

The fate of dissolved organic carbon (DOC) is an important part of the global carbon cycle (1). Approximately 0.25×10^{15} g (0.25 Pg) of terrestrially-derived DOC is discharged annually via rivers into estuaries and the coastal ocean. This represents about 60% of the annual total delivery of terrestrial organic carbon to the world's oceans (2,3). This rate of discharge of terrestrial DOC is sufficient to replace the entire oceanic DOC inventory every 3000 years, yet there is no evidence that this material accumulates in marine systems (1,4-7). Well characterized removal processes, such as net heterotrophy (8,9) and burial in coastal sediments (10), account for only 50% of the total input. Photochemical reactions, such as DOC photomineralization to dissolved inorganic carbon (DIC) and increases in DOC bioavailability, may represent a significant portion of the remaining missing sink (11). This thesis is part of an investigation into the mechanisms involved in photochemical processes affecting DOC in marine systems.

Aquatic dissolved organic matter: Composition and Properties

In order to determine the processes governing the cycling of DOM in natural systems, the composition and properties of this complex material must be understood. A significant confounding issue in aquatic chemistry is the use by different research communities of a range of terminology and definitions, both operative and conceptual, for components of the material that makes up dissolved organic carbon. Defining the nature and components of aquatic DOC is an extremely complex problem that has not been fully solved. An immediate distinction must be made between dissolved organic carbon (DOC), which is actually the measured or calculated carbon content, and dissolved organic matter (DOM), which is a more inclusive term that addresses the extreme heterogeneity of this material. DOM contains large amounts of organic carbon, but also can contain other associated elements such as nitrogen, phosphorus, and sulfur bound in organic molecules. I will refer to DOM rather than DOC throughout this thesis to distinguish between measured (or calculated) carbon and the general definition

presented here. Broadly, natural DOM is material derived from organic (biological in origin) sources that passes through a 0.2 µm filter (or, less commonly, a 0.45 µm or GF/F filter, depending on the study). DOM contains almost every type of biomolecule, including carbohydrates (polysaccharides), cellulose, lignins, proteins, tannins, cutins, amino acids, and sugars, as well as abiotically modified and condensed products (1,12-20).

Autochthonous and allochthonous DOM

Freshwater aquatic chemists have traditionally divided DOM into two classes: allochthonous (produced *ex situ*, or outside the aquatic system in question) and autochthonous (produced *in situ*). These terms imply a further division between algal and microbial DOM and terrestrial material, usually derived from decaying plant matter and containing large concentrations of biomolecules that are highly specific to terrestrial sources, such as lignins, cellulose, cutins, and tannins. Terrestrial sources of aquatic DOM include organic carbon leached from decaying trees, leaves, grasses, and other terrestrial plants into the soil, where it may be substantially altered by various microbial and fungal decay mechanisms. This material may be immediately leached into surface or groundwater or may persist in the soil for long periods of time, eventually reaching ponds, lakes, and rivers with significant surface residence times (19,21).

The terms ‘autochthonous’ and ‘allochthonous’ have generally not been applied in estuarine and coastal marine systems. However, these terms can provide useful distinctions between DOM carried in by freshwater inflows and that created within the marine ecosystem. A portion of both humic and fulvic acids in estuaries under this definition will be allochthonous. The fraction of DOM that is formed within the estuary is then ‘autochthonous.’

Humic and fulvic acids

A portion of the total aquatic DOM pool can be separated and concentrated by manipulating the pH and extracting the organic material from the water samples using an organic resin. The sample to be fractionated is acidified with HCl to pH 2 and passed through a hydrophobic resin column, such as XAD-8. The material that sorbs to the

column and can be eluted with 0.1 M sodium hydroxide contains a mixture of humic and fulvic acids. The fraction that precipitates in acid solution is known as humic acid, while the supernatant contains the fulvic acid (22,23). Hydrophilic molecules such as simple sugars and amino acids are not readily sorbed to the XAD-8 column, and thus are not separated using this method. The terms ‘humic acid’ and ‘fulvic acid’ are operational definitions based on the chemical behavior of the DOM fractions, and care must be used when applying these terms. In this thesis, they are applied only to specifically defined materials extracted using the published procedures (24).

The assignment of any fraction of DOM to a certain source based on these operational definitions is necessarily extremely inexact, yet some useful generalities have been drawn. Humic acids are generally both more aromatic and more chromophoric (colored) per unit carbon than fulvic acids (15,25-29). The greater aromaticity in the humic fraction of terrestrially-derived DOM relative to both fulvic acids and marine humic acids is often ascribed to a larger lignin- and tannin-derived fraction. As these products are solely derived from vascular plants, they have been used as biomarkers to trace the persistence of terrestrial DOM in marine systems (1,5,13,14).

In addition to being more aromatic, humic acids are generally more hydrophobic than fulvic acids, a property that has been exploited in their isolation. The portion of DOM that is isolated by sorption onto hydrophobic columns such as XAD resins is generally referred to as ‘humic substances,’ as a large portion of such material behaves in a manner similar to the classically defined humic acids (30). Often this material is subdivided into humic acid and fulvic acids based on the precipitation steps outlined above. This hydrophobic extraction avoids the extremely alkaline conditions that may cause structural changes in the traditional method of humic and fulvic acid extraction (22).

Humic acids in general appear to be a more biologically recalcitrant fraction of DOM than fulvic acids (31). Studies of the microbial utilization of DOM have indicated that biological availability of terrestrial DOM to microbial assemblages appears to be

positively correlated with aliphatic (saturated) carbon content and negatively correlated with aromatic carbon content and color (32-34).

Marine humic substances

Humic substances isolated from marine sources can be fractionated into humic and fulvic acids using the same procedures applied to freshwater DOM. Similarly to freshwater humic substances, marine humic acids (MHA) display a greater aromatic content, increased hydrophobicity, and larger optical absorption per unit carbon than marine fulvic acids (MFA) (1,20,29,35). However, it has been observed that MHA and MFA share far more characteristics than the corresponding freshwater isolates, leading to the hypothesis that MFA and MHA are part of a continuum of marine DOM that share a common source material and mechanism of formation (20).

Humic substances isolated from the open ocean have been found to be primarily non-terrestrial in origin (1). Thus, while the largest proportion of humic substances in coastal regions is terrestrial in origin, marine humic substances become relatively more important farther from the riverine sources. Studies utilizing both ultrafiltration to isolate the larger molecular weight fraction of DOM and XAD extraction to isolate hydrophobic portions have found very small concentrations of lignin phenols in remote marine systems, indicating that there is indeed a small quantity of terrestrial DOM (estimated to be 2-10% of the total DOM) in remote marine systems (1,5,7). The extremely small amount of terrestrial DOM raises a question regarding the fate of the terrestrially-derived organic matter in the ocean. Only 50% of the terrestrial DOM can be well accounted for by known processes, leaving a large flux of organic carbon to an unknown set of sinks.

Ultrafiltered dissolved organic matter

DOM can also be divided into high molecular weight fractions (HMW, >1 kDa) and low molecular weight fractions (LMW, <1kDa) by ultrafiltration (36,37). This size fractionation provides both a gentler method of separation of DOM from dissolved inorganic material and a more complete picture of the different hydrophilic fractions of DOM than acidification and XAD resin extraction. Ultrafiltration can also provide information about the different size pools of DOM. For example, most of the color of

swamp and river water samples is contained in the HMW fraction (>1 kDa) of the DOM isolates (38). In contrast, more of the color of marine samples is contained in the lower molecular weight fraction (37).

Certain processes can alter the size distribution of DOM in different ways. Increasing ionic strength, e.g. by mixing riverine water with seawater in an estuary, can cause flocculation of a portion of the DOM (39-42). Photochemical reactions are generally thought to increase the percentage of DOM in the smallest size class (43), although ‘photo-coagulation’ of DOM has been observed in an iron-rich river (44).

Chromophoric Dissolved Organic Matter (CDOM)

A portion of the DOM in all aquatic systems is highly colored. This material is known as chromophoric (or colored) dissolved organic matter (CDOM), or ‘gilvin’ or ‘gelbstoff’ due to the yellow color (45,46). CDOM is mostly composed of both freshwater and marine humic and fulvic acids, and is both autochthonous and allochthonous in origin, and constitutes a varying portion of the total DOM pool. The percentage of DOM constituted by CDOM is unknown because the extinction coefficients, ϵ , and concentrations, c , of specific chromophores are unknown. In freshwater systems the ratio of absorbance per mol carbon can be very large, as in the case of humic bogs and blackwater rivers (46). Terrestrial DOM contains a higher concentration of more intensely absorbing chromophores per unit carbon than aquatic autochthonous DOM (46,47). In contrast, many oceanic systems have mostly non-colored DOM (48). CDOM formation and dynamics in remote marine systems has been thoroughly investigated only recently, but seems to follow similar source (condensed biomolecules) and sink (photochemical) processes as in freshwater systems (48).

Coastal and estuarine systems generally fall between the two extremes. The relationship between color and measured DOC concentration in coastal waters has been explored a number of times (49-53). These studies have confirmed the presence of uncolored DOM and in some cases attempted to calculate the conversion (presumably via both photochemical and biological mechanisms) of CDOM to uncolored DOM (49).

CDOM Absorption

The UV-visible absorption spectrum of CDOM is generally featureless, increasing in a log-linear fashion with decreasing wavelength ((46); **Figure 1.1**). Different water samples may have slightly different curves, but surprisingly, almost every CDOM sample studied has exhibited the same type of smooth exponential absorption (46). The principal transitions in organic compounds that produce absorption bands in the ultraviolet and visible wavelengths are $n-\pi^*$, and $\pi -\pi^*$, typically observed in C=C, C=O, and aromatic groups (54). These moieties exist in significant concentrations in the highly colored portions of DOM, and are present at lesser concentrations in uncolored DOM. The extended conjugation of these electronic systems in highly colored CDOM samples is at least as important as the concentrations of these moieties for the absorption of UVB, UVA, and visible radiation, although almost all organic compounds will absorb far UV (UVC and below) radiation.

There are several possible explanations for the broad, featureless absorption behavior of CDOM, none of which has been successfully tested. CDOM may consist of a set of independent chromophores with overlapping absorption spectra, or it may be instead a smaller set of extensively coupled chromophores. The superposition of a number of vibrationally broadened electronic absorption bands in a molecule or molecules with solvent broadening would produce spectra with the observed featureless CDOM spectra (54).

CDOM in natural waters is the dominant absorber of light in the near UV region, and often in the visible region as well (46). Thus, CDOM controls the penetration depth of biologically harmful UV-B radiation and can contribute substantially to attenuation with depth of photosynthetically active radiation (PAR) (46,55-57). Furthermore, CDOM absorption of solar radiation can significantly influence the thermal structure of the water column (46,58).

CDOM absorption significantly complicates the application of remote sensing to the determination of chlorophyll in coastal waters (46,59), and renders remote sensing all but useless without extensive *in situ* validation in inland waters (60). Substantial effort has been aimed at determining the contributions of CDOM to remote measurements of

color (47,49,55,61-63). It has been argued that CDOM in coastal environments contributes far more color to remote observations than has been previously accounted for, thus biasing the interpretation of remote sensing data (49,55,62,64).

Fluorescent dissolved organic matter (FDOM)

CDOM also exhibits significant fluorescence, a property that has been utilized to examine the cycling of organic matter in a number of systems (49,65-69). CDOM fluorescence must occur *after* absorption of light, indicating that fluorescence properties are intimately tied to absorption properties and that fluorescence can act as a sensitive probe into the photophysical and photochemical properties of CDOM (70,71). Thus, fluorescent DOM (FDOM) is a subset of CDOM, although it is not currently possible to determine what percentage of CDOM (or bulk DOM) is fluorescent. Reemission of absorbed light as fluorescence also can have an impact on remote sensing in coastal waters. CDOM fluorescence has a broad maximum in the 400-550 nm range, potentially impacting the remote detection of chlorophyll absorption (62,72).

Progress in our understanding of the fluorescence properties of DOM has been made recently using excitation-emission matrix (EEM) fluorescence spectroscopy (68,73-76). Scanning the fluorescence emission of CDOM at many excitation wavelengths has allowed investigators to begin characterizing the fluorescence behavior of this material, and to differentiate between CDOM sources based on EEMS fluorescence patterns. These studies have focused on characterization of the fluorescent properties of various DOM samples and the alterations that may take place during mixing, rather than on investigations into photochemical alterations to DOM fluorescence. EEM spectroscopy is a useful tool for probing photochemical bleaching processes because EEM spectra can provide information about fluorophores that are not as easily visualized with conventional fluorescence spectroscopy. For example, the use of EEMS allows simultaneous observation of the bleaching of fluorophores that are excited at light wavelengths below those used in irradiations relative to fluorophores excited by longer wavelengths.

CDOM and FDOM in estuaries

CDOM and FDOM are involved in the many processes affecting organic matter in estuaries. These include chemicophysical processes - coagulation, flocculation, and sedimentation; biological modification and production; and photochemical alteration (77,78). The transport of terrestrial DOM from some rivers through estuaries to the coastal ocean has been observed to be relatively conservative (14,79,80), although the loss of some fraction (an estimated 20%) has been observed in a number of other cases (1,39,42,81). Humic acids may compose the largest fraction of DOM removed by estuarine flocculation.

Thus it is surprising that despite the attention paid to DOM transportation in estuaries, very few studies have focused on CDOM. A recent study found 21% of the CDOM in the Tyne estuary was removed by adsorption onto suspended sediments (82). However, this study is in contrast to other investigations that have found CDOM to be relatively conservative in several systems (63,68,83). In fact, one of these studies also observed an apparent strong, possibly seasonal source of CDOM to the Orinoco Estuary (63).

A linear relationship between DOM absorption and fluorescence has been observed in a variety of different systems (47,49-51,53,61,65). Fluorescent DOM (FDOM) exhibits relatively conservative behavior in many estuaries (73,84), although there is some evidence of slight FDOM production in some estuaries (66,67,69). Estuarine optical properties (both absorption and fluorescence) have not been studied in enough detail to determine if these are representative observations.

CDOM photochemistry

The photochemical decomposition of CDOM leads to a variety of organic products including low molecular weight carbonyl compounds, dissolved inorganic carbon (DIC), and carbon monoxide (11,85-91). Photochemical alterations of CDOM can also lead to increased microbial availability of what would otherwise be recalcitrant organic matter, thus ultimately allowing recycling of organic carbon to DIC as a crucial part of the carbon cycle (11,92-96). Interestingly, photochemical alterations of *algal*

DOM actually reduced its bioavailability, presumably through the photopolymerization of biomolecules to recalcitrant products (97-99). This finding lends support to the practice of distinguishing allochthonous terrestrial DOM and autochthonous aquatic DOM.

Photochemistry as a sink of CDOM

Absorption of light by CDOM leads both to the production of various photointermediates and products and to the eventual loss of CDOM absorption ('bleaching' or 'fading'). Thus photobleaching reactions act as a sink for CDOM (49,100). Previous studies of CDOM photobleaching have demonstrated that this sink is significant compared to the mixing residence time of CDOM in both coastal and freshwaters. Bleaching half-lives on the order of days have been found in bottle experiments in sunlight or simulated sunlight (11,100-102). Field studies of photobleaching have found significant decreases in CDOM absorption in both stratified ocean water and in lakes during the summer (49,103). Under certain conditions, the seasonal stratification of the water column in marine systems causes CDOM photobleaching to significantly increase the optical transparency of surface seawaters (48,49,103).

CDOM light absorption drives all subsequent CDOM photochemistry. Hence an understanding of the bleaching properties of CDOM is necessary for a thorough understanding of the ultimate significance of CDOM photochemistry to the global carbon cycle. In addition, because of the profound impact of CDOM light absorption on the underwater light field (reduction of UVB, attenuation of PAR, effects on remote sensing), understanding the mechanisms of CDOM photobleaching is also essential for understanding other biogeochemical systems.

Photochemical Mechanisms: Direct versus Indirect Photochemistry

The investigation of photochemical mechanisms involved in the photobleaching and photooxidation of DOM is complicated by the heterogeneity of the material and the multiple reactions occurring in both the DOM matrix and the aqueous solvent. Conceptually, CDOM photochemistry can be divided into two mechanistic pathways:

direct and indirect. Direct photochemistry involves processes such as photofragmentation or photoionization after absorption of photons by CDOM (**Figure 1.2**; (104-107)).

Indirect photochemistry involves the production of reactive intermediates arising from primary photochemistry that react with CDOM to produce a chemical change.

Photointermediates include reactive oxygen species (ROS) such as superoxide, hydroxyl radical, singlet oxygen, hydrogen peroxide, and peroxy radicals (**Figure 1.3**). Other radical photointermediates include the carbonate radical and the dibromide ion. A final important class of photointermediates is composed of reduced metals such as Fe(II), Cu(I), and Mn(II). Since these metals are potentially important in both primary and secondary photoprocesses, investigations into their redox reactions as well as their direct photochemistry have provided some insight into the relative contribution of direct and indirect photoprocesses in the generation of various photoproducts (44,108,109).

The relative importance of direct versus indirect photochemical pathways must be understood in order to be able to utilize laboratory studies of DOM photodecomposition and product formation rates to estimate the rates of these processes in the environment. If direct photochemical processes dominate, only the chromophoric portion of the DOM will be broken down, and the rates of photodecomposition and product formation will be proportional to the amount of light absorbed by CDOM. If indirect processes are important, decomposition of non-chromophoric material is also possible, and the rate of light absorption by CDOM will only control the rates of CDOM photo-oxidation and photobleaching if CDOM photoreactions are the main source of the intermediates involved.

There is no reason to assume *a priori* that the same general mechanism is responsible for different processes of interest. For instance, photobleaching could proceed mostly via direct mechanisms while photomineralization and photoproduction of low molecular weight (LMW) organic compounds could proceed mostly via indirect mechanisms.

Mechanisms of direct CDOM photochemistry

Direct photochemistry of CDOM is difficult to investigate mechanistically due to the heterogeneous nature of natural systems. Thus, many photochemical studies have not attempted to separate the effects of direct versus indirect photoprocesses. One common method of reducing the importance of indirect photochemical effects is to exclude dioxygen (O_2) from the system being studied, reducing the formation of ROS (43,44,110,111). For example, Gao and Zepp noted that the photoproduction rates of both CO_2 and CO decreased during irradiation under an N_2 atmosphere (44). It is often difficult to completely exclude O_2 from these systems, so if small concentrations of ROS are important to the process of interest then the contribution of direct photoprocesses may be overstated. The relative contribution of the two general pathways, direct and indirect, may be assessed by explicitly examining the role of ROS or other reactive photointermediates generated using non-photochemical methods or by using radical scavengers.

Direct photochemical reactions often lead to the production of radical species within the CDOM. These reactions lead to various fragmentation reactions, including the photomineralization of DOM to both CO_2 and to carbon monoxide, CO (112). These reactions are known as (photo)decarboxylation and (photo)decarbonylation, and most have been proposed to proceed via radical intermediates (Figures 1.4 and 1.5). One of the postulated mechanisms of CO generation has been suggested to involve the acyl radical as an intermediate (113).

The photoproduction of CO_2 (DIC) is at least one order of magnitude more efficient than the photoproduction of CO, at least in river water (11,44). CO photoproduction in the world's oceans has been calculated at 15 - 1400 Tg yr^{-1} , indicating the potential size of DIC photoproduction (130-12 000 Tg yr^{-1}). However, CO is potentially an important tracer of photochemical mechanisms, especially in seawater or other high-carbonate waters in which measurement of DIC photoproduction is extremely difficult.

Mechanisms of indirect CDOM photochemistry

The photochemical production of reactive oxygen species (ROS) via secondary reactions between initial organic intermediates and dissolved oxygen (*vide infra*) can affect metal redox speciation and influence the cycling of carbon, oxygen, and sulfur in both marine and freshwater systems (106,109,114). Indirect CDOM photochemistry is the reaction of intermediates formed during photolysis of CDOM with other solutes or with CDOM. These reactions can have the same ultimate consequences that direct processes do, but the mechanisms are very different since they involve reactive intermediates that are distinct from CDOM and can thus also react with many other constituents of the photolyzed system.

Reactive Oxygen Species

The processes and rates leading to the production of various reactive oxygen species (ROS) have been thoroughly reviewed (106). Because of the relative reactivity and high concentration (~250 μM) of O_2 in surface waters, it dominates the secondary photochemical reactions involving CDOM. This reactivity has given rise to what Zafiriou *et al.* term ‘the oxygen wall,’ a kinetic barrier set up by oxygen reactions that separates the primary photochemical processes from the secondary processes (115). The oxygen wall causes the time scale of primary radical interaction with the medium (water, O_2 , and Br^-) to be ~1 μs . A variety of mechanisms transfer electrons from primary photoproducts to O_2 to produce secondary photoproducts (see **Figure 1.3**). Because of the unpaired electron (triplet) ground state configuration of O_2 , a number of different states are readily accessible (see **Figure 1.6**). Singlet oxygen ($^1\text{O}_2$) can be generated from singlet-triplet intersystem crossing, and superoxide (O_2^\bullet , O-O bond order of 1.5) from single electron transfer. Hydrogen peroxide (HOOH , O-O bond order of 1) results from either two electron transfer (most likely consecutive, rather than concerted) or from superoxide dismutation. Finally, hydroxyl radical (OH^\bullet) is produced by reduction of HOOH , from hydrogen atom (H^\bullet) abstraction from water by excited states of CDOM, or from photolysis of nitrate and nitrite (non-CDOM-dependent).

The rates of photoproduction of all of the ROS (except nitrate/nitrite produced OH[•]) are dependent on the amount and composition of available sunlight and CDOM. Like other photochemical processes, ROS photoproduction increases with wavelength from the visible into the ultraviolet. Midday formation rates range from 10^{-12} (OH[•]) to 10^{-8} (O₂[•]) M⁻¹ s⁻¹ (106). In all coastal seawater samples examined, O₂[•] seems to be the major radical photoproduct, composing at least one-third of the total radical flux (116,117). As HOOH is produced from both the catalyzed and uncatalyzed dismutation of superoxide, and possibly from other photochemical reactions as well, it may be nearly as important a photoproduct as O₂[•] (106,118). More importantly, the slower reaction kinetics of HOOH relative to other photointermediates allows HOOH to persist and build up concentrations of 10^{-7} M or greater in some systems (106). High concentrations of HOOH can have a variety of biogeochemical consequences, possibly including direct effects on phytoplankton ecology (119).

Fate of ROS: Reaction with DOM and metals

Some of the specific rates and mechanisms of ROS reactions with their ultimate sinks are well known (106). These sinks include H₂O, DOM, Br⁻, CO₃²⁻, and dissolved and particulate metals. The dominant loss pathway of ¹O₂ is rapid solvent relaxation, as there are few ¹O₂-reactive constituents under most circumstances (106). The primary decay pathway for HOOH is particle associated, usually assumed to be reaction with the biologically produced enzymes catalase and peroxidase (106,120). The steady-state concentrations of HOOH in sunlit surface waters can be substantial enough to be significant sources of OH[•] via Fenton-like reactions with reduced metals such as Fe(II) and Cu(I)) (106,118,121). In aqueous systems, DOM is the principal sink of OH[•], an important sink of O₂[•], and a possible sink of peroxy radicals. Neither the rates nor the ultimate consequences of many of the reactions of ROS with DOM are well known.

Superoxide reacts rapidly with reduced or oxidized metals to produce HOOH and oxidized metals or O₂ and reduced metals, respectively. Reduced metals, such as Fe(II), may participate in the production of OH[•] via Fenton reactions with HOOH (108,109,122,123). However, O₂[•] also reacts with DOM, producing HOOH in a fashion

similar to its redox reactions with metals. Chapter 2 is an examination of this mechanism and its consequences for sunlit surface waters.

DOM is most likely the ultimate sink for the radical products of OH[•] reactions with Br⁻ and CO₃²⁻ as well as for OH[•] itself (124-127). Reactions of OH[•] with model lignin phenols suggest a number of different reaction mechanisms are possible with some of the components of fulvic and humic acids (128-130). Some reaction pathways are shown in **Figure 1.7**. Although many of these pathways do not lead directly to the production of CO₂, continued reaction of OH[•] and O₂/O₂⁻ with the intermediate carbon radicals formed by hydrogen atom extraction and aromatic ring hydroxylation will eventually mineralize DOM. Furthermore, intermediate oxidation of acid residues can lead to decarboxylation and formation of both R[•] and CO₂. Mineralization of photoproduced intermediate low molecular weight carboxylic acids can also add to DIC production, and hence the net photomineralization of DOM. The consequences of these reactions are the subject of Chapter 3.

Roles of Fe

CDOM photochemistry may be important in the geochemical cycling of Fe in aquatic systems (108,109,131-142). **Figure 1.8** presents some of the possible light- and ROS- driven reactions of both dissolved and particulate Fe. However, the converse importance of Fe photochemistry to CDOM cycling has not received much attention (44,85,108,143). A few investigators have noted the apparent catalytic effect of Fe in the photochemical production of both DIC and CO in freshwater samples (44,85,144). No studies have been performed in marine systems.

Despite the extreme insolubility of Fe in most natural waters, its abundance and reactivity may make Fe photoreactions very important in DOM and ROS photochemistry. Direct photochemical transformations of CDOM may be accelerated by Fe-induced ligand to metal charge transfer (LMCT) reactions (**Figure 1.9**). Fenton chemistry, the reaction of Fe(II) with HOOH to produce OH[•], may also accelerate the mineralization of DOM (121). The work presented in Chapter 5 is an examination of the role of Fe in the photobleaching and photomineralization reactions of CDOM, primarily in a set of

estuarine samples, but also in an extracted fulvic acid (Suwannee River Fulvic Acid, SRFA).

Mechanisms of Photobleaching

The principal theories regarding the origin of CDOM absorption suggest distinct chemical and photochemical behaviors that may be amenable to experimental testing. CDOM may be a large set of independent chromophores with overlapping absorption spectra, or it may be instead a small set of extensively coupled chromophores. Because the absorption spectra of independent chromophores would be expected to be extensively broadened by thermal (vibrational) effects, it might be possible to describe the absorption spectra and photochemical behavior with a relatively small number of distinct chromophore classes.(145,146). If, in contrast, CDOM were to contain chromophores that are extensively electronically coupled, even a very large number of independent chromophores might not be sufficient to describe the photobleaching behavior. A model developed in Chapter 4 is an initial attempt at addressing this question.

A complicating issue is that CDOM may in fact exhibit mixed behavior: a few independent chromophores with extensive photophysical and photochemical coupling. A fourth possibility is that indirect photochemistry may play a significant role in the overall photochemical behavior of CDOM. Secondary photoproducts, most notably reactive oxygen species, may have a significant effect on CDOM photobleaching. The relative contribution of several of these intermediates to photobleaching processes remains to be completely determined.

The two different models of CDOM photoabsorption lead to different photobleaching behaviors. A superposition of multiple independent chromophores leads to the possibility of bleaching a ‘hole’ in the CDOM spectrum by using monochromatic light to ‘burn out’ the chromophores absorbing at the irradiation wavelength. If instead CDOM consists of molecules that absorb at many different wavelengths simultaneously or otherwise electronically coupled chromophores, then irradiation at one wavelength would cause the loss of absorption at distant wavelengths. As mentioned above, indirect photobleaching processes could be a significant complicating factor in testing these

theories. CDOM bleaching by ROS or by other photointermediates should be independent of observation wavelength. The wavelength dependence of the bleaching behavior of one ROS, OH[•], is examined in Chapter 5.

Contributions of this thesis

The mechanisms of DOM photobleaching and photooxidation, particularly the relative contributions of direct and indirect processes, are still poorly understood. Chapters 2 and 3 represent attempts to improve our understanding of the reactions of two different indirect photoproducts, O₂⁻ and OH[•], with DOM. The apparent catalytic dismutation of superoxide by CDOM is described in Chapter 2, and steady state concentrations of O₂⁻ are calculated for a variety of surface waters. This chapter was previously published as a paper co-authored with Bettina Voelker (147).

Chapter 3 examines the reaction of OH[•] with two extracted humic substances, Suwannee River Fulvic Acid and Suwannee River Humic Acid, as well as some bleaching reactions of OH[•] with a coastal seawater sample. The OH[•]-driven production of low molecular weight carboxylic acids and alteration to the bioavailability of the extracted humic and fulvic acids by reaction with OH[•] was also probed. That chapter has been accepted for publication, and was co-authored with two postdoctoral fellows in addition to Bettina Voelker (148). Dr. Michael Pullin performed the carboxylic acid analyses, and Dr. Stefan Bertilsson performed the analyses of the biological assays.

Chapter 4 details the development of a model for CDOM photobleaching that begins to addresses the issues surrounding the different hypotheses regarding the chromophoric properties of CDOM (*vide supra*). This model was developed using monochromatic and polychromatic photobleaching data provided by Rossana Del Vecchio and Neil Blough of the University of Maryland at College Park.

Chapter 5 addresses the both the role of Fe in CDOM photobleaching and CO photoproduction and the relative contributions of the direct and indirect mechanisms to the photobleaching of CDOM. Taken together, this thesis examines the mechanisms of CDOM photobleaching and photomineralization, with emphasis on ROS-mediated processes.

References

1. Hedges, J. I.; Keil, R. G.; Benner, R. *Org. Geochem.* **1997**, 27, 195-212.
2. Spitz, A.; Ittekkot, V. *Ocean Margins Processes in Global Change*; Mantoura, R. F. C., Martin, J. M. and Wollast, R., Ed.; John Wiley and Sons Ltd.: New York, 1991, pp 5-17.
3. Meybeck, M. *Am. J. Sci.* **1982**, 282, 401-450.
4. Williams, P. M.; Druffel, E. R. M. *Nature* **1987**, 330, 246-248.
5. Meyers-Schulte, K.; Hedges, J. I. *Nature* **1986**, 321, 61-63.
6. Druffel, E. R. M.; Williams, P. M.; Bauer, J. E.; Ertel, J. R. *J. Geophys. Res.* **1992**, 97, 15639-15659.
7. Opshal, S.; Benner, R. *Nature* **1997**, 386.
8. Smith, S.; Hollibaugh, J. *Rev. Geophys.* **1993**, 31, 75-89.
9. Raymond, P. A.; Bauer, J. E.; Cole, J. J. *Limnol. Oceanogr.* **2000**, 45, 1707-1717.
10. Berner, R. A. *Am. J. Sci.* **1982**, 282, 451-473.
11. Miller, W. L.; Zepp, R. G. *J. Geophys. Res.* **1995**, 22, 417-420.
12. Aluwihare, L. I.; Repeta, D. J.; Chen, R. F. *Nature* **1997**, 387, 166-169.
13. Benner, R.; Pakulski, J. D.; McCarthy, M.; Hedges, J. I.; Hatcher, P. G. *Science* **1992**, 255, 1561-1564.
14. Benner, R.; Opsahl, S. *Organic Geochemistry* **2001**, 32, 597-611.
15. Choudhry, G. G. *Humic Substances*; Gordon and Breach Science Publishers: New York, 1984; Vol. 7.
16. Hedges, J. I.; Hatcher, P. G.; Ertel, J. R.; Meyers-Schulte, K. *J. Geochim. Cosmochim. Acta* **1992**, 56, 1753-1757.
17. Hope, D.; Billett, M. F.; Cresser, M. S. *Environmental Pollution* **1994**, 84, 301-324.
18. Opshal, S.; Benner, R. *Limnol. Oceanogr.* **1998**, 1297-1304.
19. Raymond, P. A.; Bauer, J. E. *Org. Geochem.* **2001**, 32, 469-485.
20. Harvey, G. R.; Boran, D. A.; Chesal, L. A.; Tokar, J. M. *Mar. Chem.* **1983**, 12, 119-132.
21. Hedges, J. I.; Ertel, J. R.; Quay, P. D.; Grootes, P. M.; Richery, J. E.; Devol, A. H.; Farwell, G. W.; Schmidt, F. W.; Salati, E. *Science* **1986**, 231, 1129-1131.
22. Gaffney, J. S.; Marley, N. A.; Clark, S. B. *Humic and Fulvic Acids: Isolation, Structure, and Environmental Role*; Gaffney, J. S., Marley, N. A. and Clark, S. B., Ed.; American Chemical Society: Washington, DC, 1996; Vol. ACS Symposium Series 651.
23. Schnitzer, M.; Kahn, S. U. *Humic Substances in the Environment*; Marcel Dekker: New York, 1972.
24. "I.H.S.S. Standard and Reference Collection," Internation Humic Substances Society, 2001.
25. McKnight, D. M.; Andrews, E. D.; Spaulding, S. A.; Aiken, G. R. *Limnol. Oceanogr.* **1994**, 39, 1972-1979.
26. Aiken, G. R.; McKnight, D. M.; Wershaw, R. L.; MacCarthy, P. *Humic Substances in Soil, Sediment, and Water: Geochemistry, Isolation, and*

- Characterization*; Aiken, G. R.; McKnight, D. M.; Wershaw, R. L.; MacCarthy, P., Ed.; Wiley-Interscience: New York, 1985, pp 691.
27. Scott, D. T.; McKnight, D. M.; Blunt-Harris, E. L.; Kolesar, S. E.; Lovley, D. R. *Environ. Sci. Technol.* **1998**, *32*, 2984-2989.
28. Westerhoff, P.; Aiken, G.; Amy, G.; Debroux, J. *Wat. Res.* **1999**, *33*, 2265-2276.
29. Carder, K. L.; Steward, R. G.; Harvey, G. R.; Ortner, P. B. *Limnol. Oceanogr.* **1989**, *34*, 68-81.
30. Amador, J. A.; Milne, P. J.; Moore, C. A.; Zika, R. G. *Mar. Chem.* **1990**, *29*, 1-17.
31. Moran, M. A.; Hodson, R. E. *Limnol. Oceanogr.* **1990**, *35*, 1744-1756.
32. Leff, L. G.; Meyer, J. L. *Limnol. Oceanogr.* **1991**, *36*, 315-323.
33. Sun, L.; Perdue, E. M.; Meyer, J. L.; Weis, J. *Limnol. Oceanogr.* **1997**, *42*, 714-721.
34. Hopkinson, C. S.; Buffam, I.; Hobbie, J.; Vallino, J.; Perdue, M.; Eversmeyer, B.; Prahl, F.; Covert, J.; Hodson, R.; Moran, M. A.; Smith, E.; Baross, J.; Crumb, B.; Findlay, S.; Foreman, K. *Biogeochem.* **1998**, *43*, 211-234.
35. Stuermer, D. H.; Payne, J. R. *Geochim. Cosmochim. Acta* **1976**, *40*, 1109-1114.
36. Buessler, K. O.; Bauer, J. E.; Chen, R. F.; Eglington, T. I.; Gustafsson, O.; Landing, W.; Mopper, K.; Moran, S. B.; Santschi, P. H.; Wells, M. L. *Mar. Chem.* **1996**, *55*, 1-31.
37. Mopper, K.; Feng, Z.; Bentjen, S. B.; Chen, R. F. *Mar. Chem.* **1996**, *55*, 53-74.
38. Everett, C. R.; Chin, Y.-P.; Aiken, G. R. *Limnol. Oceanogr.* **1999**, *44*, 1316-1322.
39. Sholkovitz, E. R. *Geochim. Cosmochim. Acta* **1976**, *40*, 831-845.
40. Eisma, D. *Netherlands Journal of Sea Research* **1986**, *20*, 183-199.
41. Forsgren, G.; Jansson, M.; Nilsson, P. *Estuarine Coastal and Shelf Science* **1996**, *43*, 259-268.
42. Fox, L. E. *Geochim. Cosmochim. Acta* **1984**, *48*, 879-884.
43. Schmitt-Kopplin, P.; Hertkorn, N.; Schulten, H.-R.; Kettrup, A. **1998**.
44. Gao, H. Z.; Zepp, R. G. *Environmental Science & Technology* **1998**, *32*, 2940-2946.
45. Kirk, J. T. O. *Aust. J. Mar. Freshwater Res.* **1976**, *27*, 61-71.
46. Kirk, J. T. O. *Light and Photosynthesis in Aquatic Ecosystems*; 2 ed.; Cambridge University Press: Cambridge, 1994.
47. Vodacek, A.; Hoge, F. E.; Swift, R. N.; Yungel, J. K.; Peltzer, E. T.; Blough, N. V. *Limnol. Oceanogr.* **1995**, *40*, 411-415.
48. Nelson, N. B.; Siegel, D. A.; Michaels, A. F. *Deep-Sea Research Part I-Oceanographic Research Papers* **1998**, *45*, 931-957.
49. Vodacek, A.; Blough, N. V.; DeGrandpre, M. D.; Peltzer, E. T.; Nelson, R. K. *Limnol. Oceanogr.* **1997**, *42*, 674-686.
50. Ferrari, G. M.; Dowell, M. D. *Estuarine Coastal and Shelf Science* **1998**, *47*, 91-105.
51. Ferrari, G. M. *Marine Chemistry* **2000**, *70*, 339-357.

52. Stedmon, C. A.; Markager, S.; Kaas, H. *Estuarine Coastal and Shelf Science* **2000**, *51*, 267-278.
53. Ferrari, G. M.; Dowell, M. D.; Grossi, S.; Targa, C. *Mar. Chem.* **1996**, *55*, 299-316.
54. Turro, N. J. *Modern Molecular Photochemistry*; University Science Books: Sausalito, CA, 1991.
55. DeGrandpre, M. D.; Vodacek, A.; Nelson, R. K.; Bruce, E. J.; Blough, N. V. *J. Geophys. Res.* **1996**, *101*, 22727-22736.
56. Schindler, D. W.; Curtis, P. J. *Biogeochem.* **1997**, *36*, 1-8.
57. Williamson, C. E.; Stemberger, R. S.; Morris, D. P.; Frost, T. M.; Paulsen, S. G. *Limnol. Oceanogr.* **1996**, *41*, 1024-1034.
58. Kirk, J. T. O. *J. Geophys. Res.* **1988**, *93*, 10897-10908.
59. Kirk, J. T. O. *Arch. Hydrobiol. Bieh. Ergebn. Limnol.* **1994**, *43*, 1-16.
60. Bukata, R. P.; Jerome, J. H.; Kondratyev, K. Y.; Pozdnyakov, D. V.; Kotykhov, A. A. *J. Great Lakes Res.* **1997**, *23*, 254-269.
61. Hoge, F. E.; Vodacek, A.; Blough, N. V. *Limnol. Oceanogr.* **1993**, *38*, 1394-1402.
62. Vodacek, A.; Green, S.; Blough, N. V. *Limnol. Oceanogr.* **1994**, *39*, 1-11.
63. Blough, N. V.; Zafiriou, O. C.; Bonilla, J. *J. Geophys. Res.* **1993**, *98*, 2271-2278.
64. Muller-Karger, F. E.; McClain, C. R.; Fisher, T. R.; Esaias, W. E.; Varela, R. *Prog. Oceanogr.* **1989**, *23*, 23-64.
65. Green, S. A.; Blough, N. V. *Limnol. Oceanogr.* **1994**, *39*, 1903-1916.
66. Chen, R. F.; Bada, J. L. *Mar. Chem.* **1992**, *37*, 191-221.
67. Chen, R. F. *Organic Geochemistry* **1999**, *30*, 397-409.
68. Del Castillo, C. E.; Gilbes, F.; Coble, P. G.; Muller-Karger, F. E. *Limnology and Oceanography* **2000**, *45*, 1425-1432.
69. Klinkhammer, G. P.; McManus, J.; Colbert, D.; Rudnick, M. D. *Geochim. Cosmochim. Acta* **2000**, *64*, 2765-2774.
70. Power, J. F.; Sharma, D. K.; Langford, C. H.; Bonneau, R.; Joussot-Dubien, J. *Photochemistry of Environmental Aquatic Systems*; Zika, R. G. and Cooper, W. J., Ed.; American Chemical Society: Washington, DC, 1987; Vol. ACS Symposium Series 327.
71. Milne, P. J.; Odum, D. S.; Zika, R. G. *Photochemistry of Environmental Aquatic Systems*; Zika, R. G. and Cooper, W. J., Ed.; American Chemical Society: Washington, DC, 1987; Vol. ACS Symposium Series 327.
72. Spitzer, D.; Dirks, R. W. *J. Appl. Opt.* **1985**, *24*, 444-445.
73. Coble, P. G. *Mar. Chem.* **1996**, *51*, 325-346.
74. Coble, P. G.; Schultz, C. A.; Mopper, K. *Mar. Chem.* **1993**, *41*, 173-178.
75. Baker, A. *Environ. Sci. Technol.* **2001**, *35*, 948-953.
76. Mobed, J. J.; Hemmingsen, S. L.; Autry, J. L.; McGown, L. B. *Environ. Sci. Technol.* **1996**, *30*, 3061-3065.
77. Mitra, S.; Bianchi, T. S.; Guo, L.; Santschi, P. H. *Geochim. Cosmochim. Acta* **2000**, *64*, 3547-3557.
78. Raymond, P. A.; Bauer, J. E. *Limnology and Oceanography* **2001**, *46*, 655-667.

79. Mantoura, R. F. C.; Woodward, E. M. S. *Geochim. Cosmochim. Acta* **1983**, *47*, 1293-1309.
80. Miller, A. E. J. *Estuarine Coastal and Shelf Science* **1999**, *49*, 891-908.
81. Sholkovitz, E.; Boyle, E. A.; Price, N. B. *Earth Planet. Sci. Lett.* **1978**, *40*, 130-136.
82. Uher, G.; Hughes, C.; Henry, G.; Upstill-Goddard, R. C. *Geochem. Res. Lett.* **2001**, *28*, 3309-3312.
83. Bowers, D. G.; Harker, G. E. L.; Smith, P. S. D.; Tett, P. *Estuarine, Coastal, Shelf Sci.* **2000**, *50*, 717-726.
84. De Souza Sierra, M. M.; Donard, O. F. X.; Lamotte, M.; Ewald, M. *Mar. Chem.* **1994**, *47*, 124-144.
85. Miles, C. J.; Brezonik, P. L. *Environ. Sci. Technol.* **1981**, *15*, 1089-1095.
86. Bertilsson, S.; Tranvik, L. *Limnol. Oceanogr.* **1998**, *43*, 885-895.
87. Granéli, W.; Lindell, M.; Tranvik, L. *Limnol. Oceanogr.* **1996**, *41*, 698-706.
88. Zuo, Y.; Jones, R. D. *Naturwissenschaften* **1995**, *82*, 472-474.
89. Zhou, X.; Mopper, K. *Mar. Chem.* **1997**, *56*, 201-213.
90. Mopper, K.; Stahovec, W. L. *Mar. Chem.* **1986**, *19*, 305-321.
91. Kieber, R. J.; Zhou, X.; Mopper, K. *Limnol. Oceanogr.* **1990**, *35*, 1503-1515.
92. Amon, R. M.; Benner, R. *Geochim. Cosmochim. Acta* **1996**, *60*, 1783-1792.
93. Amon, R. M. W.; Benner, R. *Limnol. Oceanogr.* **1996**, *41*, 41-51.
94. Bertilsson, S.; Tranvik, L. *Limnol. Oceanogr.* **2000**, *45*, 753-762.
95. Bertilsson, S.; Allard, B. *Arch. Hydrobiol./Advanc. Limnol.* **1996**, *48*, 133-141.
96. Lindell, M. J.; Granelli, W.; Tranvik, L. J. *Limnol. Oceanogr.* **1995**, *40*, 195-199.
97. Anesio, A.; Denward, C. M. T.; Tranvik, L. J.; Granéli, W. *Aquat. Microb. Ecol.* **1999**, *17*, 159-165.
98. Anesio, A.; Theil-Nielsen, J.; Granéli, W. *Microbial Ecol.* **2000**, *40*, 200-208.
99. Tranvik, L.; Kokalj, S. *Aq. Microb. Ecol.* **1998**, *14*, 301-307.
100. Kouassi, A. M.; Zika, R. G. *Toxicol. Env. Chem.* **1992**, *35*, 195-211.
101. Grzybowski, W. *Chemosphere* **2000**, *40*, 1313-1318.
102. Reche, I.; Pace, M. L.; Cole, J. J. *Biogeochemistry* **1999**, *44*, 259-280.
103. Morris, D. P.; Hargreaves, B. R. *Limnol. Oceanogr.* **1997**, *42*, 239-249.
104. Zafiriou, O. C. *Chemical Oceanography*; Academic Press: London, 1983; Vol. 8.
105. Zafiriou, O. C.; Joussot-Dubien, J.; Zepp, R. G.; Zika, R. *Environ. Sci. Technol.* **1984**, *18*, 358A-371A.
106. Blough, N. V.; Zepp, R. G. *Active Oxygen in Chemistry*; Foote, C. S. and Valentine, J. S., Ed.; Chapman and Hall: New York, 1995, pp 280-333.
107. Cooper, W. J.; Zika, R. G.; Petasne, R. G.; Fischer, A. M. *Aquatic Humic Substances: Influence on Fate and Treatment of Pollutants*; Suffet, I. H. and MacCarthy, P., Ed.; American Chemical Society: Washington, DC, 1989; Vol. Advances in Chemistry Series No. 219.
108. Voelker, B. M.; Sedlak, D. L. *Mar. Chem.* **1995**, *50*, 93-102.
109. Voelker, B. M.; Morel, F. M. M.; Sulzberger, B. *Environ. Sci. Technol.* **1997**, *31*, 1004-1011.

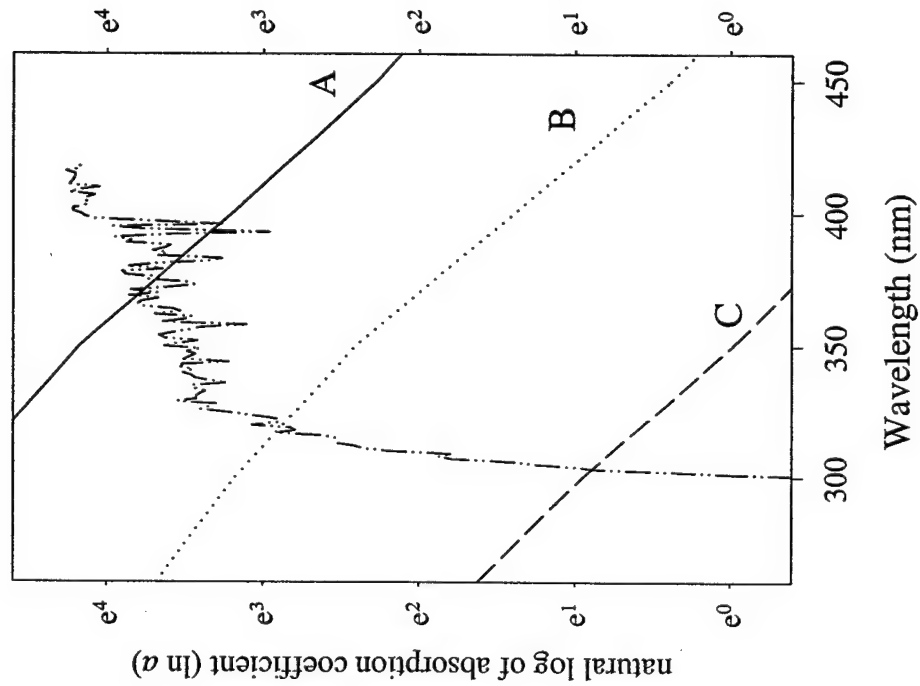
110. Vaughn, P. P.; Blough, N. V. *Environ. Sci. Technol.* **1998**, *32*, 2947-2953.
111. Andrews, S. S.; Caron, S.; Zafiriou, O. C. *Limnol. Oceanogr.* **2000**, *45*, 267-277.
112. Budac, D.; Wan, P. J. *Photochem. Photobiol. A: Chem.* **1992**, *67*, 135-166.
113. Pos, W. H.; Riemer, D. D.; Zika, R. G. *Mar. Chem.* **1998**, *62*, 89-101.
114. Zepp, R. G.; Callaghan, T. V.; Erickson, D. J. *J. Photochem. Photobiol. B: Biology* **1998**, *46*, 69-82.
115. Zafiriou, O. C.; Blough, N. V.; Micinski, E.; Dister, B.; Kieber, D.; Moffett, J. *Marine Chemistry* **1990**, *30*, 45-70.
116. Zafiriou, O. C.; Dister, B. *J. Geophys. Res.* **1991**, *69*, 99-4945.
117. Dister, B.; Zafiriou, O. C. *J. Geophys. Res.* **1993**, *98*, 2341-2352.
118. Cooper, W. J.; Shao, C. W.; Lean, D. R. S.; Gordon, A. S.; Scully, F. E. *Environmental Chemistry of Lakes and Reservoirs*, 1994; Vol. 237, pp 391-422.
119. Willey, J. D.; Paerl, H. W.; Go, M. *Marine Ecology-Progress Series* **1999**, *178*, 145-150.
120. Moffett, J. W.; Zafiriou, O. C. *Limnol. Oceanogr.* **1990**, *35*, 1221-1229.
121. Zepp, R. G.; Faust, B. C.; Hoigne, J. *Environ. Sci. Technol.* **1992**, *26*.
122. Voelker, B. M.; Sedlak, D. L.; Zafiriou, O. C. *Environ. Sci. Technol.* **2000**, *34*, 1038-1042.
123. Zafiriou, O. C.; Voelker, B. M.; Sedlak, D. L. *J. Phys. Chem. A* **1998**, *102*, 5693-5700.
124. Huang, J.; Mabury, S. A. *Environ. Toxicol. Chem.* **2000**, *19*, 2181-2188.
125. Zafiriou, O. C.; True, M. B.; Hayon, E. *Photochemistry of Environmental Aquatic Systems*; Zika, R. G. and Cooper, W. J., Ed.; American Chemical Society: Washington, DC, 1987.
126. Zafiriou, O. C., Personal communication.
127. Umschlag, T.; Herrmann, H. *Acta Hydrochim. Hydrobiol.* **1999**, *27*, 214-222.
128. Gierer, J. *Holzforschung* **1997**, *51*, 34-46.
129. Machado, A. E. H.; Furuyama, A. M.; Falone, S. Z.; Ruggiero, R.; da Silva Perez, D.; Castellan, A. *Chemosphere* **2000**, *40*, 115-124.
130. Hobbs, G. C.; Abbot, J. J. *Wood Chem. Tech.* **1994**, *14*, 195-225.
131. Johnson, K. S.; Coale, K. H.; A., E. V.; Tindale, N. W. *Mar. Chem.* **1994**, *46*, 319-334.
132. Miller, W. L.; King, D. W.; Lin, J.; Kester, D. R. *Mar. Chem.* **1995**, *50*, 63-77.
133. Sulzberger, B.; Laubscher, H. *Mar. Chem.* **1995**, *50*, 103-115.
134. Wells, M. L.; Price, N. M.; Bruland, K. W. *Marine Chemistry* **1995**, *48*, 157-182.
135. O'Sullivan, D. W.; Hanson Jr., A. K.; Kester, D. R. *Mar. Chem.* **1995**, *49*, 65-77.
136. Wells, M. L.; Mayer, L. M. *Deep-Sea Res.* **1991**, *38*, 1379-1395.
137. Fukushima, M.; Tatsumi, K. *Colloids and Surfaces a-Physicochemical and Engineering Aspects* **1999**, *155*, 249-258.
138. Faust, B. C. *Aquatic and Surface Photochemistry*; Helz, G. R., Zepp, R. G. and Crosby, D. G., Ed.; Lewis Publishers: Boca Raton, FL, 1994, pp 3-38.

139. Waite, T. D.; Szymczak, R. *Aquatic and Surface Photochemistry*; Helz, G. R., Zepp, R. G. and Crosby, D. G., Ed.; Lewis Publishers: Boca Raton, FL, 1994, pp 39-52.
140. Colliene, R. H. *Limnol. Oceanogr.* **1983**, *28*, 83-100.
141. McKnight, D. M.; Kimball, B. A.; Bencala, K. E. *Science* **1988**, *240*, 637-640.
142. Stumm, W.; Sulzberger, B. *Geochim. Cosmochim. Acta* **1992**, *56*, 3233-3257.
143. Faust, B. C.; Zepp, R. G. *Environmental Science & Technology* **1993**, *27*, 2517-2522.
144. Zuo, Y.; Jones, R. D. *Water. Res.* **1997**, *31*, 850-858.
145. Lawrence, J. *Wat. Res.* **1980**, *14*, 373-377.
146. Korshin, G. V.; Li, C. W.; Benjamin, M. M. *Water Research* **1997**, *31*, 1787-1795.
147. Goldstone, J. V.; Voelker, B. M. *Environ. Sci. Technol.* **2000**, *34*, 1043-1048.
148. Goldstone, J. V.; Pullin, M. J.; Bertilsson, S.; Voelker, B. M. *Environ. Sci. Technol.* **in press**.

Figure 1. 1

UV-visible absorption spectrum of three different CDOM samples: A: a humic bog water B: an extracted fulvic acid (5mg/l SRFA) C: coastal seawater (Delaware Bay S29). Also shown is the solar irradiance at the earth's surface in $\text{W m}^{-2} \text{ nm}^{-1}$ (x 50) (right axis, dotted line).

natural log of solar irradiance $\times 50$



Solar irradiance ($\text{W m}^{-2} \text{ nm}^{-1}$) $\times 50$

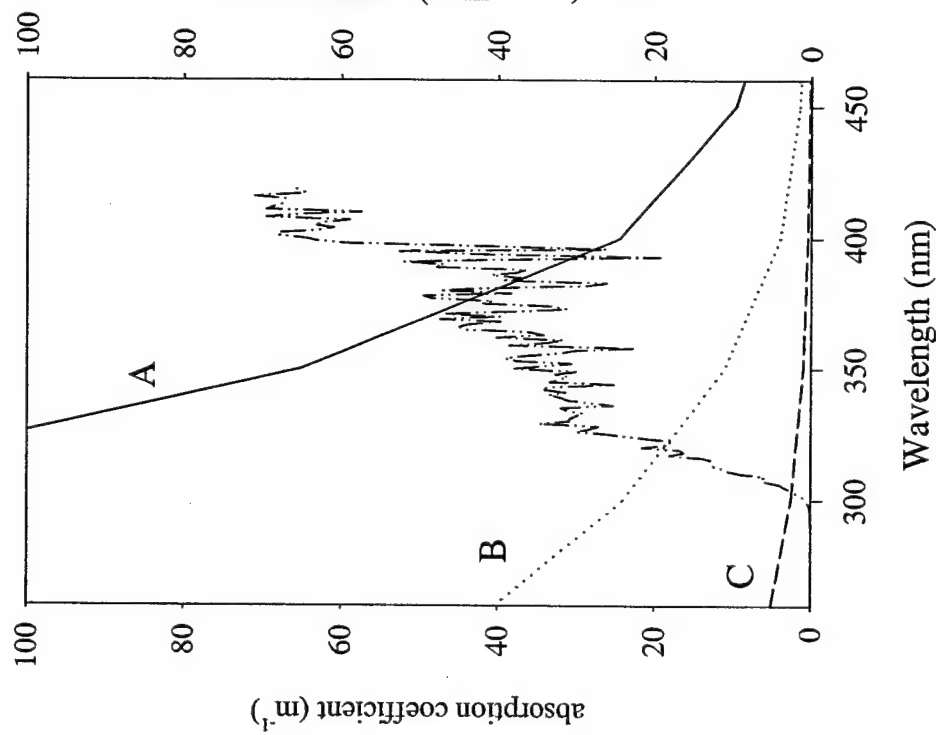


Figure 1. 2

Primary photochemical and photophysical processes of CDOM. CDOM* represents the excited state (usually S_1) formed after photon absorption by the singlet ground state ($^1\text{CDOM}$, S_0). Radiative (fluorescence) and non-radiative relaxation return the excited state CDOM chromophore to the ground state. This excited state can go on to form more stable species, such as excited triplet states ($^3\text{CDOM}$, T_1), internally charge separated radicals ($\text{CDOM}^{\pm\cdot}$), and radical products ($R\cdot$). Radical pairs produced from the singlet state are likely to recombine, relaxing to the ground state with excess heat. Radicals produced from triplet states are more likely to escape from the solvent cage and to take part in further chemistry.

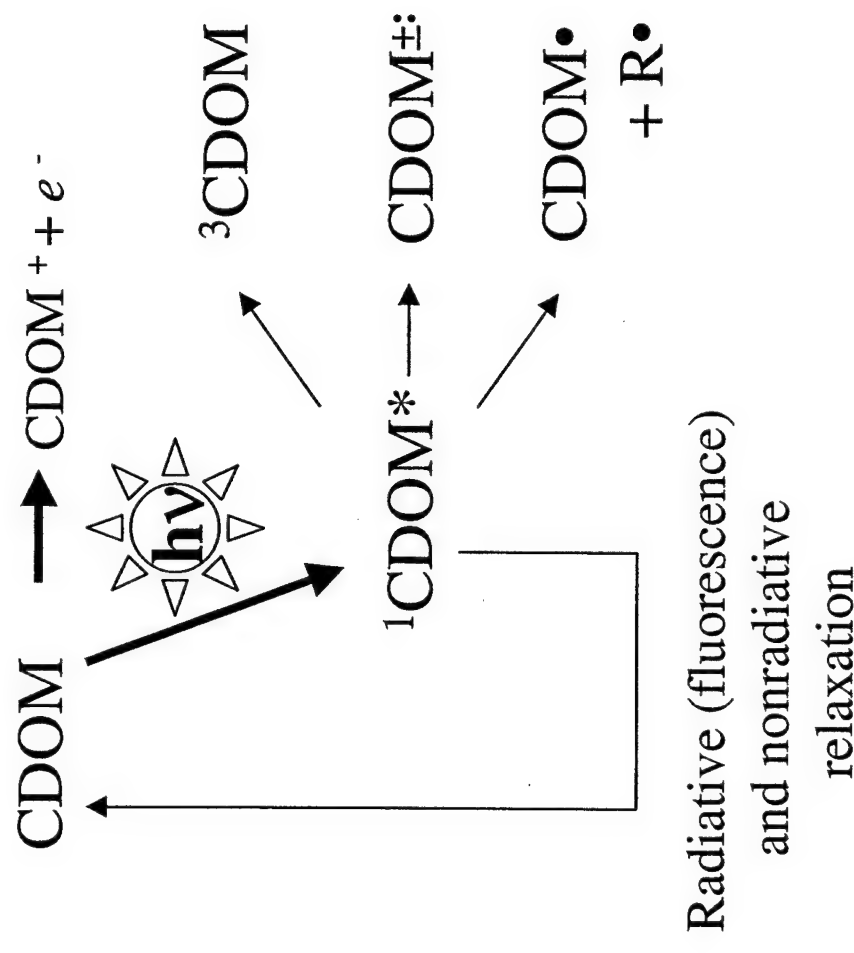


Figure 1. 3

Photogeneration of reactive oxygen species via secondary reactions of CDOM photointermediates with O₂ and H₂O. Adapted from Blough and Zepp (1995).

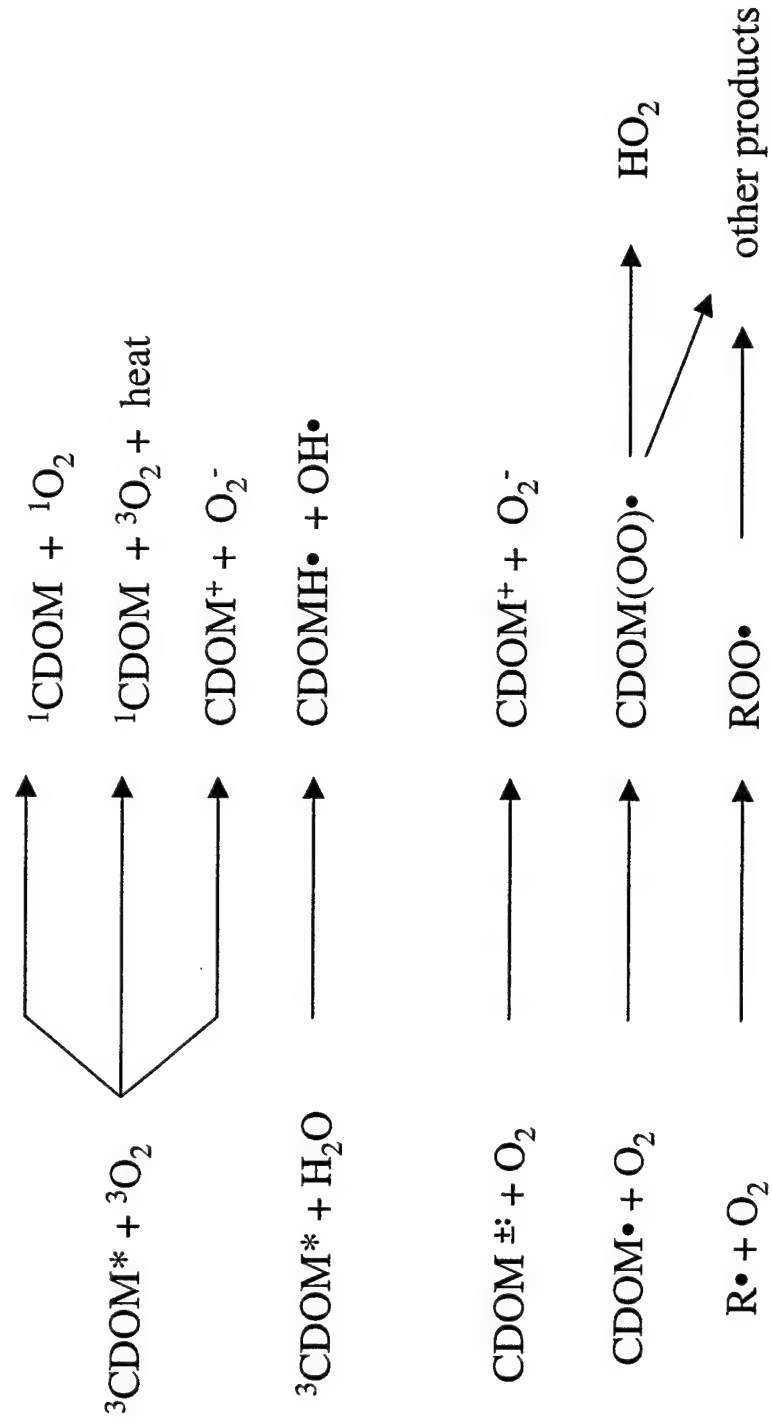


Figure 1. 4

Mechanism of photodecarboxylation, including mesolytic (bond cleavage of a photoionized product), homolytic (equal electron partitioning) , and heterolytic (unequal electron partitioning) cleavage mechanisms. Also shown is photodecarboxylation initiated by indirect oxidation of an aromatic ring. Adapted from (112).



mesolytic

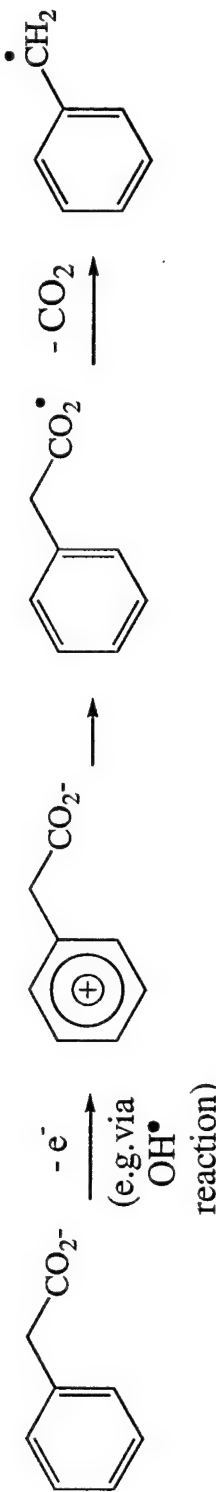


Figure 1. 5

Potential mechanism of photodecarbonylation from CDOM involving the formation of an acyl radical (a) within a solvent cage, followed by a variety of reactions including recombination, decarbonylation, intramolecular recombination with another portion of the CDOM molecule, intermolecular reaction with oxygen to form peroxy radicals, and hydrogen abstraction with different intermolecular reactants ($R'H$).

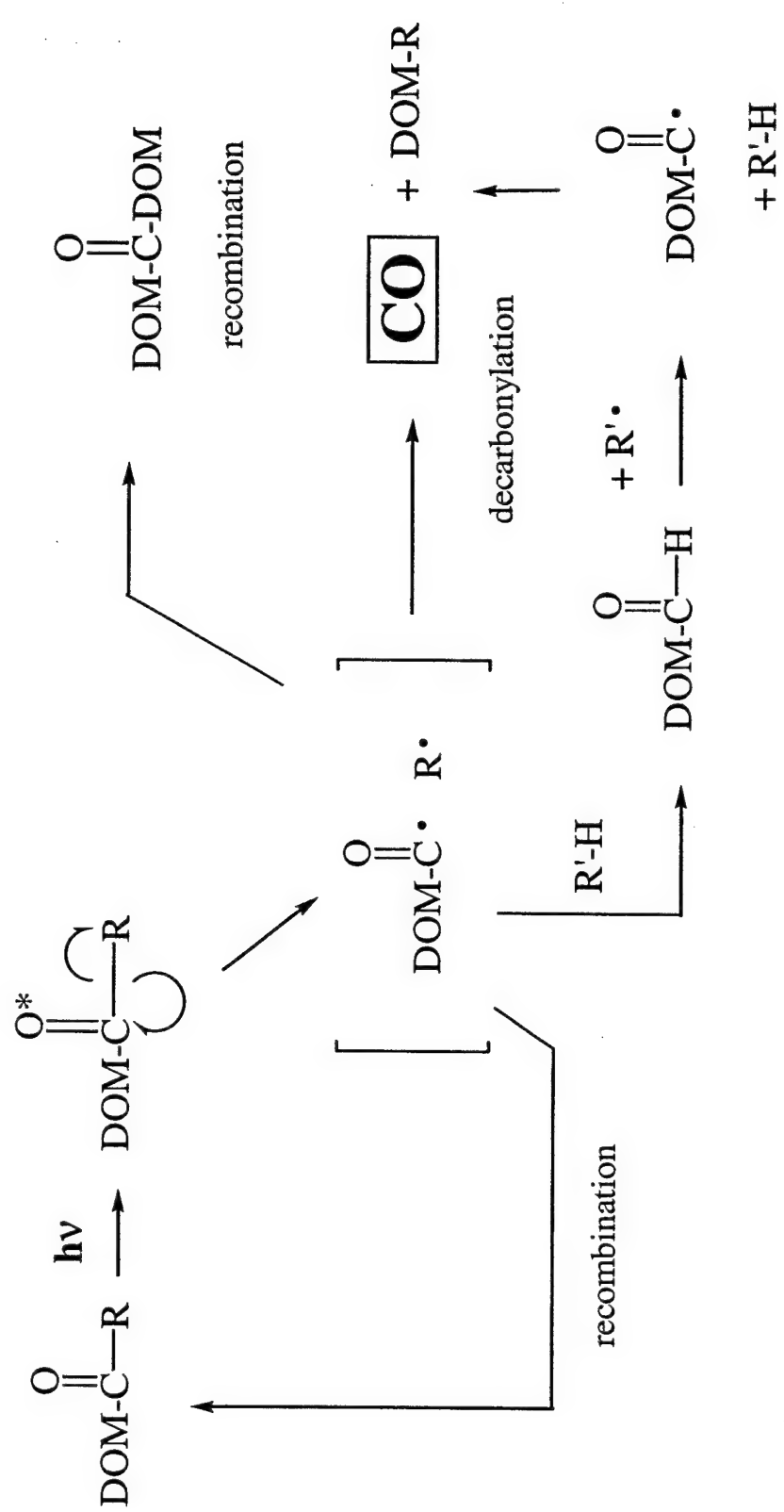


Figure 1. 6

Interconversion between the various oxidation states of oxygen, centering on the ground state triplet oxygen (${}^3\text{O}_2$). Sequential one electron processes produce most of the different ROS. Intersystem crossing (ISC) between the triple ground state and the excited singlet state results in singlet oxygen.

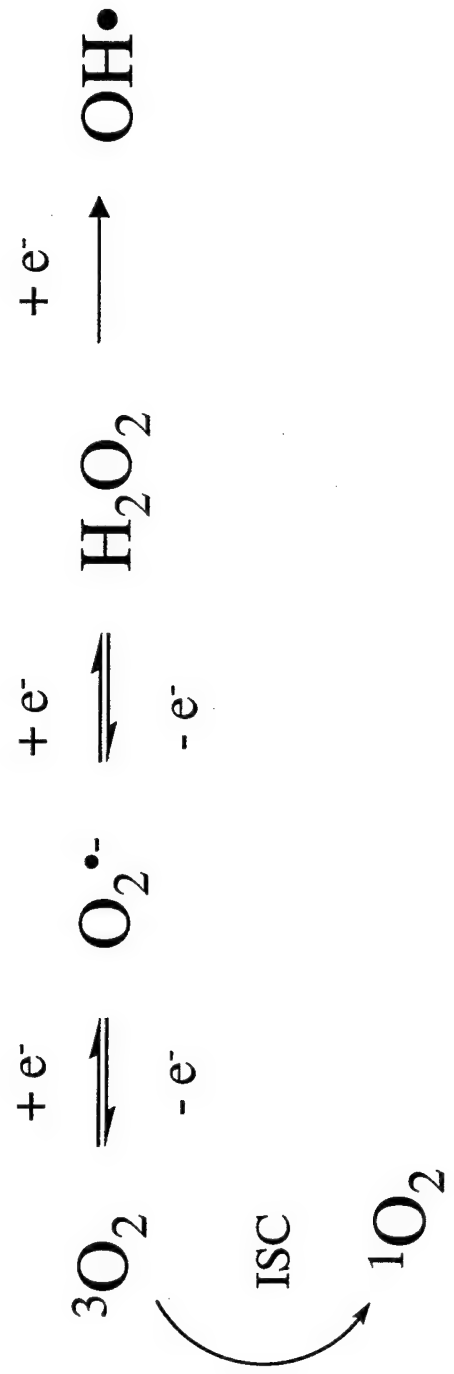


Figure 1. 7

The most important mechanisms of OH[•] reactions with lignin models, including ring opening, demethoxylation, and C_α-C_β bond scission. Adapted from Gierer (1998).

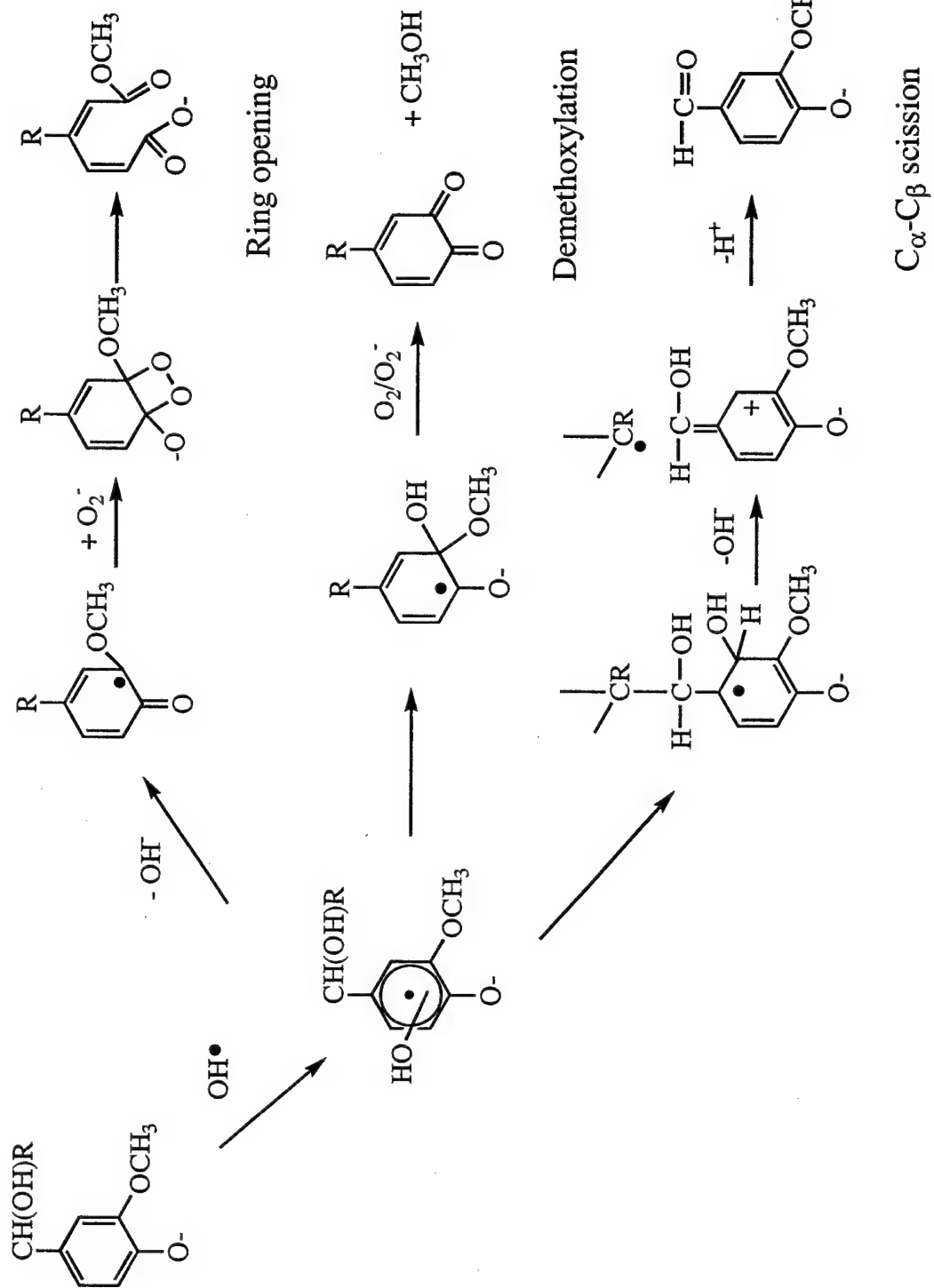


Figure 1.8

Redox cycling of dissolved (right hand side) and particulate Fe (left hand side) with reactive oxygen species and light. Adapted from B. Voelker (1996).

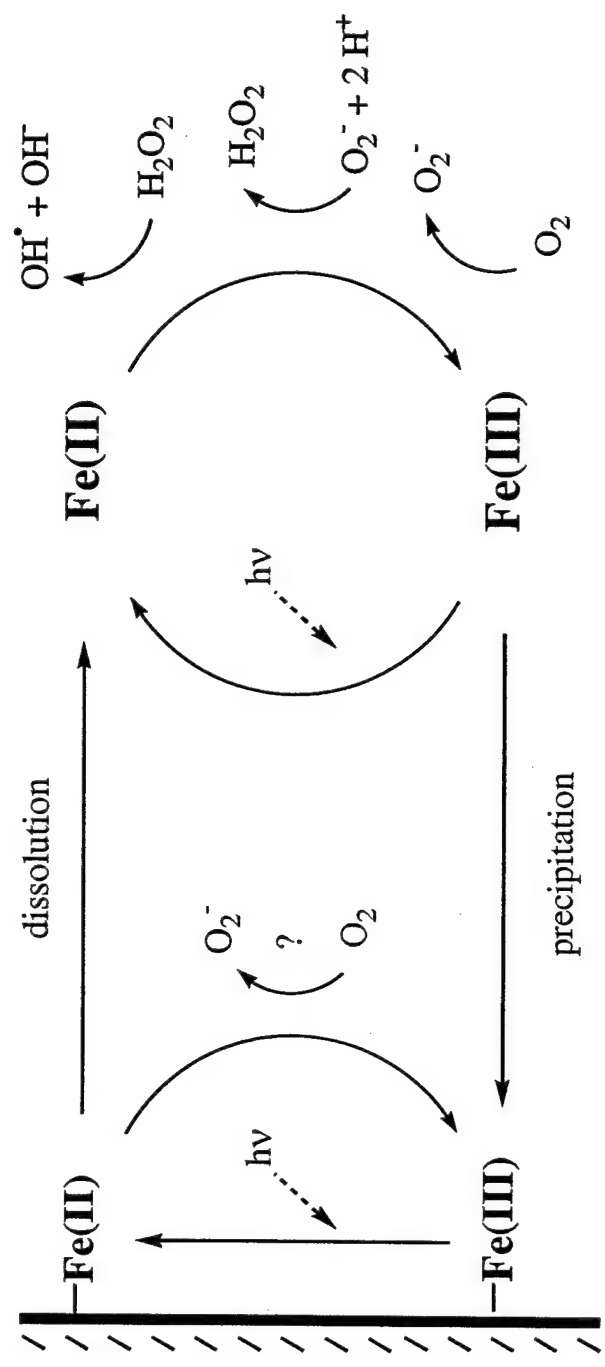
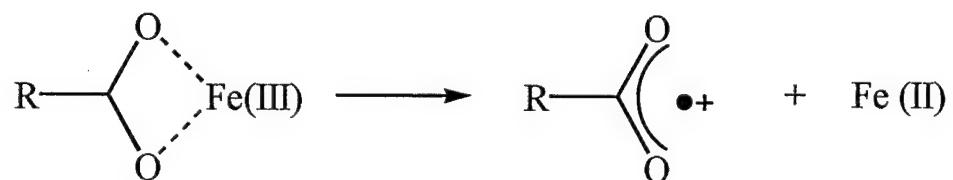


Figure 1.9

Two mechanisms of the role of Fe in CDOM photochemistry. Top: Direct ligand to metal charge transfer (LMCT) reaction. Bottom: Indirect Fenton chemistry of photoproduced Fe(II) (formed via LMCT or reaction of Fe(III) with O_2^-) with photoproduced HOOH to form the indirect oxidant $OH\cdot$.



CHAPTER 2.

CHEMISTRY OF SUPEROXIDE RADICAL (O_2^-) IN SEAWATER: CDOM ASSOCIATED SINK OF SUPEROXIDE IN COASTAL WATERS

Reproduced with permission from

Jared V. Goldstone and Bettina M. Voelker, The chemistry of superoxide in seawater:
CDOM associated sink of superoxide in coastal waters. *Environmental Science and
Technology*, 34 (6), 1043-1048 (2000).

© 2000 American Chemical Society.

Abstract

Colored dissolved organic matter (CDOM) and humic substances contain a non-metallic redox-cycling component capable of catalyzing superoxide (O_2^-) dismutation. First-order rate coefficients (k_{pseudo}) measured for this O_2^- sink in a number of coastal and Chesapeake Bay water samples range up to 1.4 s^{-1} , comparable in magnitude to catalyzed dismutation by Cu species. A significant ($r^2=0.73$) correlation is observed between k_{pseudo} and the optical absorption and salinity of individual coastal water samples, suggesting an association with non-marine-derived CDOM. The activity of this sink is not changed by acidification or boiling of samples, but is removed by photooxidation, indicating that it is an organic compound, but that it is neither enzymatic nor likely to consist of tightly bound metals. The stoichiometry of hydrogen peroxide formation from O_2^- decay indicates that this sink is capable of a redox cycle catalyzing the dismutation of O_2^- . This CDOM sink combined with the organic copper sink previously described will produce a steady-state superoxide concentration in coastal waters that is 100- to 1000-fold lower than predicted from bimolecular dismutation alone. Catalyzed O_2^- decay was also observed in a variety of humic and fulvic acid samples, possibly occurring through quinone functionalities. Although the presence of quinone moieties in humic and fulvic acids has been demonstrated, there do not appear to be good correlations between several measures of quinone content and the O_2^- dismutation rates of these samples.

Introduction

Superoxide radical (O_2^-) is the principal redox intermediate formed in sunlit natural waters through the reduction of oxygen by photochemically excited colored dissolved organic matter (CDOM). Superoxide plays a significant role in the redox cycling of dissolved trace metal species in natural waters (1-5), may play a role in redox transformations of aquatic pollutants (6), and is the key intermediate in the formation of photochemically generated hydrogen peroxide (7-9). An understanding of the reactions controlling the steady-state concentration of O_2^- is necessary to elucidate its role in photochemical redox processes.

The steady-state concentration of superoxide ($[O_2^-]_{ss}$) is given by the balance of its rates of production and destruction:

$$\begin{aligned} [O_2^-]_{ss} &= \text{Production} \\ &2k_D [O_2^-]_{ss} + \sum k_M [M]_x + k_{\text{pseudo}} \end{aligned} \quad (1)$$

where k_D is the pH dependent effective bimolecular dismutation rate constant for O_2^- ($k_D = 5 \pm 1 \times 10^{12} [H^+] M^{-2}s^{-1}$ in seawater (10)), k_M is the second-order rate constant of reaction of O_2^- with metal species M_x (1, 2), and k_{pseudo} is the sum of pseudo-first-order rate constants of O_2^- with additional sinks. O_2^- production rates in several Caribbean waters have been determined to be $10^{-11} - 10^{-10} Ms^{-1}$, at least one-third of the total radical flux in seawater (11). The role of Cu in controlling the steady-state concentration of superoxide ($[O_2^-]_{ss}$) in coastal waters is discussed in the preceding paper in this issue (1).

The contribution of non-metallic sinks has not previously been examined in detail. Unknown sinks of O_2^- in coastal and riverine waters were observed in earlier work (9, 10). Zafiriou (1990) determined the rate of an unknown pseudo-first-order decay sink in water from the Orinoco River and the Gulf of Paria to be $1-5 s^{-1}$ by utilizing diethylenetriaminepentaacetic acid (DTPA) to remove the effects of kinetically labile metals on O_2^- decay. Zafiriou calculated that this unknown riverine sink would

outcompete bimolecular dismutation as the dominant sink of O_2^- in coastal waters even if extremely diluted.

Our purpose in this work was to examine the rates of non-metal catalyzed O_2^- decay (k_{pseudo}) in a number of coastal waters and to identify the unknown sink or sinks if possible. The use of high concentrations of O_2^- and natural pH values in the previous work by Zafiriou (1990) prevented the differentiation of slower first-order decay processes in the presence of second-order bimolecular dismutation (k_D in Equation 1). The detection limit for k_{pseudo} imposed by second-order decay under the conditions used was $>1.5\text{ s}^{-1}$, thus giving rise to the large uncertainties in his calculated sink rates. By photochemically generating lower concentrations of O_2^- at higher pH values we have avoided competition from second-order decay. This method allows us to detect any sinks that are at least as important as organically complexed Cu ($k_{pseudo} > 0.1\text{ s}^{-1}$) (1). Furthermore, we have investigated the apparent catalytic activity of this sink by examining both the kinetics of O_2^- decay and the production of hydrogen peroxide. Treatment of samples to eliminate the influence of potential sinks has allowed us to narrow the identity of the sink, as has a field study in the Chesapeake Bay. In addition, we have investigated the catalytic activity of a number of standard humic and fulvic substances, including both allochthonous and autochthonous fulvic acids.

Methods

Samples

Surface seawater samples from the Chesapeake Bay were collected using Go-Flo bottles in late July 1997 during a cruise of the R/V Cape Hatteras. Supporting chlorophyll and nutrient data were obtained from Greg Cutter (Old Dominion University). Other samples were collected using stainless steel or plastic buckets or acid washed PTFE containers from several sites near Cape Cod, Massachusetts, including Woods Hole Harbor, Vineyard Sound, Stellwagen Bank, and Waquoit Bay. Seawater samples were 0.2 μM filter sterilized and refrigerated or frozen in acid-washed PTFE bottles until analysis. Absorbance measurements were made in 5-cm quartz cuvettes using either a Hewlett Packard 8452A or 8453 diode array spectrophotometer and referenced to Nanopure

water. Acid-treated samples were acidified to pH 2 with HCl and returned to pH 8 with NaHCO₃. Boiled samples were boiled for 10 minutes in acid-washed Pyrex flasks. Photo-oxidation of seawater samples was performed using a medium pressure Hg lamp. Humic and fulvic acid samples were obtained from the International Humic Substance Society (IHSS) or from Durelle Scott and Diane McKnight (Institute of Arctic and Alpine Research, University of Colorado). IHSS terrestrial humic substances used were: soil humic acid (S-HA), Leonardite humic acid (L-HA), peat humic acid (P-HA), Summit Hill humic acid (SH-HA), Suwannee River fulvic acid (SRFA) and Suwannee River humic acid (SRHA). Other humic substances used were: Lake Fryxell fulvic acid (LF-FA) and Nymph Lake sediment fulvic acid (NL-FA) (12). Humic and fulvic acid solutions (10 mg/L in 1 mM NaHCO₃) were created by dissolving the samples in 0.2 M NaOH and adjusting the pH to ca. 8.3 with HCl and NaHCO₃. All chemicals were used as received from Aldrich Chemical Company.

Kinetics

Superoxide was photochemically generated in 0.5 M NaCl solutions containing isopropanol and benzophenone buffered with sodium borate (13). Volume percentages of sample were added to O₂⁻ solutions and the resulting first-order decay curves were fit using non-linear least squares regression (Figure 1 inset). Decay kinetics were observed directly at 240 nm in 5-cm quartz cuvettes using the diode array spectrophotometer. This method was chosen over traditional methods of superoxide detection, as indirect methods such as ferricytochrome c reduction may be subject to interferences arising from alternative reductants or oxidants present in natural waters (14).

The experimental design allowed us to eliminate the first two terms of the O₂⁻ decay equation:

$$-\frac{d[O_2^-]}{dt} = 2k_D[O_2^-]^2 + \Sigma k_M[M]_x[O_2^-] + k_{pseudo}[O_2^-] \quad (2)$$

To avoid competition from metal-catalyzed dismutation, 15 μM diethylenetriaminepentaacetic acid (DTPA) was added to all solutions, and allowed to equilibrate overnight. MINEQL+ speciation calculations show that this concentration of DTPA is sufficient to chelate >99.9% of trace Fe and Cu even in the presence of strong ligands ("L₁") known to complex Fe and Cu in seawater ($\beta_{\text{Fe}}=10^{18}$, $[\text{L}_{\text{Fe}}]=10^{-8} \text{ M}$, $\beta_{\text{Cu}}=10^{15}$, $[\text{L}_{\text{Cu}}]=10^{-8} \text{ M}$). (15, 16). DTPA complexation constants were taken from the National Institute of Standards and Technology Critical Stability Constants for Metal Complexes Database (NIST Standard Reference Database 46, 1993). To avoid competition from second-order bimolecular dismutation, solutions were buffered at pH 9.5 ($k_D = 1600 \text{ M}^{-1}\text{s}^{-1}$) and initial O₂⁻ concentrations were below 10 μM . At seawater pH (8.3), k_D is 25 000 $\text{M}^{-1}\text{s}^{-1}$, precluding differentiation between first and second-order decay rates (10). Data was plotted as sample percentage of total solution volume versus calculated first-order fits to Equation 2 (Figure 1). By extrapolating to 100% sample, the unknown pseudo-first-order rate constant k_{pseudo} was obtained.

A significant aspect of the aqueous chemistry of O₂⁻ is the ability of O₂⁻ to act as both a one-electron oxidant and reductant:



Pseudo-first-order decay of [O₂⁻] will be observed if the concentration of X_{red} or Y_{ox} is much greater than [O₂⁻]. For simplicity, we assume a single significant X_{red} or Y_{ox} species; the arguments are easily extended to include the sum of the effects of a number of different species. If a sink reaction is irreversible, the ratio of H₂O₂ generated per O₂⁻ should be 1 (sink is a reductant, X_{red} in Equation 3) or 0 (sink is an oxidant, Y_{ox} in Equation 4). This behavior also implies that the k_{pseudo} is equal to some decay constant k_{red} multiplied by the concentration of the sink, [X_{red}], or similarly, some k_{ox} multiplied

by some sink concentration, $[Y_{ox}]$. If both X_{red} and Y_{ox} are present these reactions occur simultaneously, and Equation 5 describes k_{pseudo} :

$$k_{pseudo} = k_{red}[X_{red}] + k_{ox}[Y_{ox}] \quad (5)$$

If a species is capable of functioning as both X and Y, that is, $X_{red} = Y_{red}$ and $X_{ox} = Y_{ox}$, (e.g. Cu(I) and Cu(II) (1, 4)) then a redox cycle may be established that catalyzes the dismutation of O_2^- . A catalytic redox cycle would produce a stoichiometry of 0.5 H_2O_2 per O_2^- , and k_{pseudo} would be described by a catalytic rate constant with $[cat] = [X_{red}] + [Y_{ox}]$:

$$k_{pseudo} = k_{cat}[cat] \quad (6)$$

In addition, while k_{pseudo} will be indifferent to increases in initial superoxide concentrations ($[O_2^-]_0$) if the sink is catalytic, pseudo-first-order decay will no longer be observed in the non-catalytic case when $[O_2^-]_0$ approaches initial concentrations of X_{red} or Y_{ox} . By examining both the stoichiometry of H_2O_2 generation and the dependence of k_{pseudo} on $[O_2^-]_0$ we can distinguish between these two models. $[H_2O_2]$ was determined using the diethyl *p*-phenylene diamine (DPD) peroxidase method (17). Large but consistent blanks derived from the isopropanol and benzophenone in the O_2^- solution were observed using this method, decreasing its precision.

Results

The values of k_{pseudo} measured in a number of local coastal waters and the Chesapeake Bay range between 0.1 s^{-1} and 1.4 s^{-1} . A significant ($r^2=0.73$, $P<0.001$) correlation is observed between the first-order O_2^- decay fits (k_{pseudo}) and the optical absorption of the individual water samples (Figure 2). The data point shown with an absorption at 300nm of 2.5 m^{-1} was not included in the fit, as later measurements of the same sample did not reproduce these results. The poor reproducibility of this one measurement may be due to contamination of the sample with particulate material during

filtration. k_{pseudo} did not correlate well with chlorophyll *a* ($r^2 = 0.46$), phosphate ($r^2 = 0.07$), nitrate ($r^2 = 0.37$), or silicate ($r^2 = 0.45$) concentrations in a transect of the Chesapeake Bay (Figure 3).

To examine the identity of the unknown sink, we applied a number of treatments to the seawater samples (Figure 4). Overnight equilibration of seawater samples with DTPA is expected to eliminate the O_2^- dismutation effects of most metal species, and a control experiment in which 100nM Cu as copper sulfate was added to a UV photo-oxidized sample containing 15 μ M DTPA confirmed this expectation ($k_{pseudo} \leq 0.02 s^{-1}$). However, kinetically inert metal species (e.g. those chelated by phytochelatins, porphyrins, or siderophores) might not be chelated by DTPA on this time scale. To release tightly bound metals from such complexes, we acidified the samples to pH 2 in the presence of DTPA prior to measuring k_{pseudo} at pH 9.5. A second treatment involved boiling the seawater samples for several minutes. Boiling has been shown to remove most of the activity of mammalian and bacterial superoxide dismutases (18), presumably by denaturing the enzymes and releasing the metals that compose the active sites. Neither boiling nor acidification removed the superoxide dismutation activity. The only treatment that eliminated the observed k_{pseudo} was UV-photooxidation, which also eliminated any spectrophotometrically observable light absorption due to CDOM. Treatment of other samples with the same or a similar UV-photooxidation apparatus has been shown to remove all DOC. Control experiments in which UV-photooxidized samples were acidified or boiled showed no first-order superoxide dismutation ($k_{pseudo} \leq 0.02 s^{-1}$).

The observed stoichiometry of O_2^- decay in the seawater is approximately the same as for bimolecular dismutation - that is, 0.5 H_2O_2 produced per O_2^- input into the system (Figure 5). In addition, k_{pseudo} does not change if the initial concentration of O_2^- in the system is increased, as shown in Figure 6.

Freshwater fulvic and humic substances are also capable of catalytically decomposing O_2^- . The $[O_2^-]_0$ -independent catalytic behavior of k_{pseudo} and the stoichiometry of hydrogen peroxide formation in the fulvic and humic acid solutions is similar to that of the seawater samples.

Discussion

The data presented above show that a non-metallic component of DOM is a ubiquitous and significant sink of O_2^- in coastal waters. This sink does not seem to be a biological product of marine organisms, such as superoxide dismutase (SOD) or a marine-derived porphyrin, as suggested by the boiling and acidification experiments (Figure 4), as well as the lack of correlation between sink activity and marine chlorophyll *a* concentrations. Furthermore, UV-photooxidation destroys the activity of this sink. Photooxidation would not remove dissolved metal oxyanions such as molybdate and vanadate that are present in significant concentrations in seawater, thus demonstrating that this sink is a part of the DOM rather than an inorganic constituent of seawater.

Both the k_{pseudo} and the optical absorption of samples from the Chesapeake Bay decrease with distance from land and are similarly correlated to salinity, suggesting that CDOM and the associated O_2^- sink are dominated by terrestrial sources in this system. Samples taken from the vicinity of Cape Cod (open symbols in Figure 2) and data from the Orinoco River and the Gulf of Paria ((10), inset, Figure 2) also fit the correlation derived from the samples taken from the Chesapeake Bay, indicating that there may be a general similarity in the behavior of CDOM taken from different locations.

Redox activity

Redox cycling of portions of the CDOM may be responsible for the correlation between k_{pseudo} and CDOM color. This idea of a catalytic organic redox cycle is supported by both the measurements of the stoichiometry of hydrogen peroxide generation from O_2^- decay and the unchanging relationship between the initial O_2^- concentration and the observed k_{pseudo} . The measurements of hydrogen peroxide stoichiometry suggest that either this sink is catalytic, as in Equation 6, or the unlikely situation that $k_{red}[X_{red}]$ is equal to $k_{ox}[Y_{ox}]$, producing reduced and oxidized O_2^- (H_2O_2 and O_2) in equal proportions (see Equation 5). For non-catalytic sinks to produce pseudo-first-order behavior with $[O_2^-]_0$ as large as 24 μM (Figure 6), they would have to be present in excess concentrations, which is unlikely given that concentrations of DOC in coastal marine systems are generally less than 300 μM (19). Furthermore, this material

has been previously exposed to sunlight, and thus to O_2^- , suggesting that the redox active portions of DOM are resistant to alterations in redox activity over intermediate time scales.

These redox-active structures might be quinone-hydroquinone functionalities (Figure 7) which are considered to be ubiquitous components of terrestrial humic materials (20). Zafiriou (1990) speculated that purely organic molecules such as quinone-semiquinone or semiquinone-hydroquinone couples are plausible natural catalysts due to their favorable redox potentials and demonstrated presence in natural organic matter (10, 12, 20-22). Various quinones, semiquinones, and hydroquinones have been shown to react with O_2^- (23, 24), and we have observed that 1,10-anthraquinone-2,6-disulphonate (AQDS) displays O_2^- dismutation activity similar to that of the CDOM (e.g. pseudo-first-order decay of 0.04 s^{-1} observed with $1\text{ }\mu\text{M}$ AQDS and $10\text{ }\mu\text{M}$ O_2^- at pH 9.5). However, it is not clear that this AQDS dismutation activity is equivalent to the k_{cat} mentioned above as decay rates comparable to those observed for CDOM would require AQDS concentrations large enough to invalidate the pseudo-first-order assumption.

The hypothesis that the O_2^- dismutase activity in CDOM is due only to a quinonoid component of humic substances may be overly simplistic, however. Although solutions of several humic and fulvic acids display similar O_2^- dismutase activity (Figure 8), these solutions display much lower k_{pseudo} values per absorbance unit than coastal CDOM samples. Furthermore, there is no clear correlation between the observed k_{pseudo} and the organic free radical content of these humic and fulvic acids determined by electron spin resonance (ESR) spectroscopy ($r^2=0.46$) as taken from Scott *et al.* (1998), although there are slightly better correlations between k_{pseudo} and the ^{13}C NMR-derived concentration of aromatic functionalities ($r^2=0.56$) (Figure 9). Both of these measurements have been taken to represent in some way the quinone content of non-marine derived humic and fulvic acids (12).

The observed differences between isolated humic substances and the coastal samples may indicate that quinones are not the only redox-cycling moieties in CDOM. These differences might also be due to alterations in the properties of these humic

substances during extraction, or to inefficient extraction of the unknown sinks by the standard humic isolation procedures. Alternatively, it may indicate that these standard humic substances are not well representative of the material found in the coastal systems that we examined.

Despite the differences between the humic and CDOM samples, broad similarities remain. There exists an intriguing possibility that the redox cycling portion of CDOM could transfer electrons from O_2^- to other substances. Humic materials have been demonstrated to act as electron shuttles in other contexts. Bacterial reduction of humic material by *Geobacter metallireducens* has been observed, followed by reduction of iron oxides by the reduced humic materials (12, 25). Reduced humic materials produced by chemical reactions with a bulk reductant such as sulfide have also been shown to reduce aquatic pollutants such as nitroaromatic compounds (26). Superoxide creates reduced humic materials during catalytic dismutation, and therefore electron transfer to other substances such as iron oxides or aquatic pollutants might occur at significant rates if the steady-state concentration of reduced humic materials is high enough. This process might be important in the photoreductive dissolution of iron oxides and in the photoreduction of aquatic pollutants associated with DOM.

Steady state O_2^- concentrations

The results presented here indicate that $[O_2^-]_{ss}$ in marine waters is at the lower end of previously calculated ranges, that is, at most $10^{-11} - 10^{-10}$ M in near surface waters. In coastal waters where CDOM is dominated by terrestrial sources, both the O_2^- production rate (11) and the sink examined here are well correlated to the sample absorption (a_{300}). This implies that whenever the CDOM-correlated sink is the principal O_2^- sink, increasing CDOM concentration will not increase $[O_2^-]_{ss}$. We can thus estimate a general upper limit of 8×10^{-11} M for $[O_2^-]_{ss}$, using an absorption-normalized O_2^- production rate for near surface solar noon (as approximately one-third of the total photoproduced radical flux) of $\sim 2 \times 10^{-11}$ $M s^{-1} m$ based on the findings of Micinski *et al.* (1993) and Dister and Zafiriou (1993) (11, 27), and the absorption-normalized O_2^- sink measured in this study ($k_{pseudo}/a_{300} = 0.27 s^{-1} m$). Calculations of $[O_2^-]_{ss}$ including the reactions with Cu discussed

in the companion paper (1), suggest that Cu can substantially lower $[O_2]_{ss}$ from this upper limit, either when CDOM is fairly dilute or when waters are contaminated with Cu (see Table 1). Due to the fact that most of the superoxide decay kinetics were observed at pH 9.5 (*vide supra*), these results may not precisely represent the behavior of these sinks at natural pH values (8.1-8.3 for seawater). However, no differences in k_{pseudo} were observed over the pH range 9.4 to 11, suggesting that any pH effect is small. This analysis also assumes that other redox reactions do not become important at low natural levels of O_2^- .

Inclusion of the O_2^- production rates with estimates of the known O_2^- destruction rates leads to the conclusion that the non-metallic sink represents a dominant sink for O_2^- in coastal waters, and thus may represent a significant intermediate in DOM photochemistry. If this is indeed the case, then the indirect photoredox cycling of humic substances by superoxide in aquatic environments warrants further study.

Acknowledgments

We would like to thank Katharyn Jeffries for help in the lab, Durelle Scott and Diane McKnight for humic acid samples, Oliver Zafiriou for many helpful discussions, and Greg and Linda Cutter and the captains and crews of the R/V Cape Hatteras and the SSV Corwith Cramer for assistance with sampling. This work was supported by NSF Grants OCE-9529448 and OCE-9521628 and the Ralph M. Parsons Foundation. This is WHOI Contribution No. 10081.

Table 2. 1

Calculated O_2^- steady state concentrations in coastal waters. These calculations assume a O_2^- photoproduction rate of 10^{-10} Ms^{-1} for the high CDOM cases and 10^{-11} Ms^{-1} for the low CDOM case (11). Values for Cu sinks are taken from Table 4 in Reference 1. Case 1 represents a relatively pristine estuarine environment, with low natural levels of Cu and a high optical density. Case 2 represents a similar estuarine environment with significant Cu contamination, while Case 3 represents a low DOM, low Cu environment.

	CDOM sink (k_{pseudo})	Cu sinks ($\Sigma k_M [M]_x$)	$[O_2^-]_{ss}$ (calculated)
Case 1: "High CDOM" "Low Cu"	1.4 s^{-1}	$0.2-0.5 \text{ s}^{-1}$	$5 - 7 \times 10^{-11} \text{ M}$
Case 2: "High CDOM" "High Cu"	1.4 s^{-1}	7 s^{-1}	$1 \times 10^{-11} \text{ M}$
Case 3: "Low CDOM" "Low Cu"	0.1 s^{-1}	$0.2-0.5 \text{ s}^{-1}$	$2 - 3 \times 10^{-11} \text{ M}$

References

- (1) Voelker, B. M.; Sedlak, D. L.; Zafiriou, O. C. *Environ. Sci. Technol.* **1999**, this issue.
- (2) Voelker, B. M.; Sedlak, D. L. *Mar. Chem.* **1995**, *50*, 93-102.
- (3) Voelker, B. M.; Morel, F. M. M.; Sulzberger, B. *Environ. Sci. Technol.* **1997**, *31*, 1004-1011.
- (4) Zafiriou, O. C.; Voelker, B. M.; Sedlak, D. L. *J. Phys. Chem. A* **1998**, *102*, 5693-5700.
- (5) Sunda, W. G.; Huntsman, S. A. *Mar. Chem.* **1994**, *46*, 133-152.
- (6) Schwarzenbach, R. P.; Angst, W.; Hollinger, C.; Hug, S. J.; Klausen, J. *Chimia* **1997**, *51*, 908-914.
- (7) Moffett, J. W.; Zafiriou, O. C. *Limnol. Oceanogr.* **1990**, *35*, 1221-1229.
- (8) Zika, R. G. In *Marine Organic Chemistry*; Duursma, E., Dawson, R., Eds.; Elsevier: Amsterdam, 1981, pp 299-338.
- (9) Petasne, R. G.; Zika, R. G. *Nature* **1987**, *325*, 516-518.
- (10) Zafiriou, O. C. *Mar. Chem.* **1990**, *30*, 31-43.
- (11) Micinski, E.; Ball, L. A.; Zafiriou, O. C. *J. Geophys. Res.* **1993**, *98*, 2299-2306.
- (12) Scott, D. T.; McKnight, D. M.; Blunt-Harris, E. L.; Kolesar, S. E.; Lovley, D. R. *Environ. Sci. Technol.* **1998**, *32*, 2984-2989.
- (13) McDowell, M. S.; Bakac, A.; Espenson, J. H. *Inorg. Chem.* **1982**, *22*, 847-848.
- (14) Kownatzki, E.; Uhrich, S.; Bethke, P. *Agents and Actions* **1991**, *34*, 393-396.
- (15) Moffett, J. W.; Brand, L. E.; Croot, P. L.; Barbeau, K. A. *Limnol. Oceanogr.* **1997**, *42*, 789-799.
- (16) Rue, E. L.; Bruland, K. W. *Mar. Chem.* **1995**, *50*, 117-138.
- (17) Bader, H.; Sturzenegger, V.; Hoigne, J. *Wat. Res.* **1988**, *22*, 1109-1115.
- (18) McCord, J. M.; Fridovich, I. *J. Biol. Chem.* **1969**, *244*, 6049-6055.
- (19) Mantoura, R. F. C.; Woodward, E. M. S. *Geochim. Cosmochim. Acta* **1983**, *47*, 1293-1309.
- (20) Choudhry, G. G. *Humic Substances*; Gordon and Breach Science Publishers: New York, 1984.
- (21) Thorn, K.; Arterburn, J.; Mikita, M. *Environ. Sci. Technol.* **1992**, *26*, 107.
- (22) Senesi, N.; Steelink, C. In *Humic Substances II: In Search of Structure*; Hayes, M., MacCarthy, P., Malcolm, R., Swift, R., Eds.; John Wiley and Sons: New York, 1989, pp 373-408.
- (23) Bielski, B. H. J.; Cabelli, D. E.; Arudi, R. L.; Ross, A. B. *J. Phys. Chem. Ref. Data* **1985**, *14*, 1041-1100.
- (24) Ilan, Y. A.; Czapski, G.; Meisel, D. *Biochim. Biophys. Acta* **1976**, *430*, 209-224.
- (25) Lovley, D. R.; Coates, J. D.; Blunt-Harris, E. L.; Phillips, E. J. P.; Woodward, J. C. *Nature* **1996**, *382*, 445-448.
- (26) Dunnivant, F. M.; Schwarzenbach, R. P.; Macalady, D. L. *Environ. Sci. Technol.* **1992**, *26*, 2133-2141.
- (27) Dister, B.; Zafiriou, O. C. *J. Geophys. Res.* **1993**, *98*, 2341-2352.

Figure 2. 1

An example of a plot of k_{pseudo} versus percent-sample-added. The linear fit is extrapolated to 100% sample in order to obtain the k_{pseudo} for the sample. This sample is surface water from Station 11 ($S = 26.2 \text{ ‰}$) in the Chesapeake Bay, collected on 31 July 1997 during a cruise of the R/V Cape Hatteras. The extrapolated fit is $0.38 \pm 0.1 \text{ s}^{-1}$, $r^2 = 0.87$. Inset is an example of a kinetic decay experiment showing data and non-linear regression fit with seawater sample added to make up 20% of the total solution.

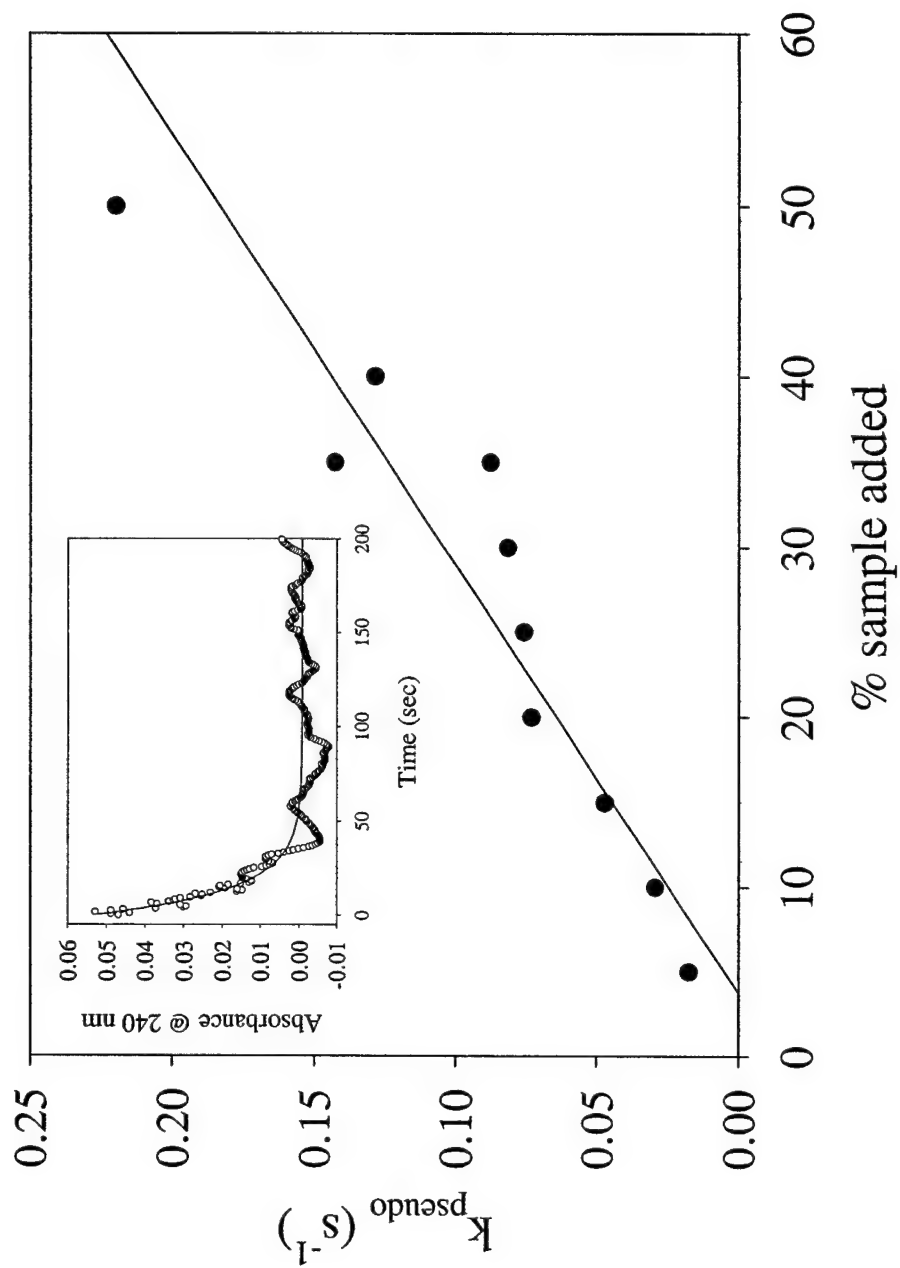


Figure 2. 2

The correlation between the observed k_{pseudo} and the absorbance of the water samples at 300 nm (in m^{-1}), taken as a measure of CDOM in coastal waters. The solid circles are samples from the Chesapeake Bay and the open circles are samples from the vicinity of Woods Hole and Cape Cod Bay. The fit produces an r^2 of 0.75 excluding the point at 2.5 m^{-1} (see text). The vertical error bars represent one standard deviation in the extrapolation of the kinetics data as in Figure 1. The inset shows the same fit and data, with the axes expanded to include data taken from Zafiriou (1990) and Micinski *et al.* (1993) for samples from the Orinoco River and the Gulf of Paria (diamonds).

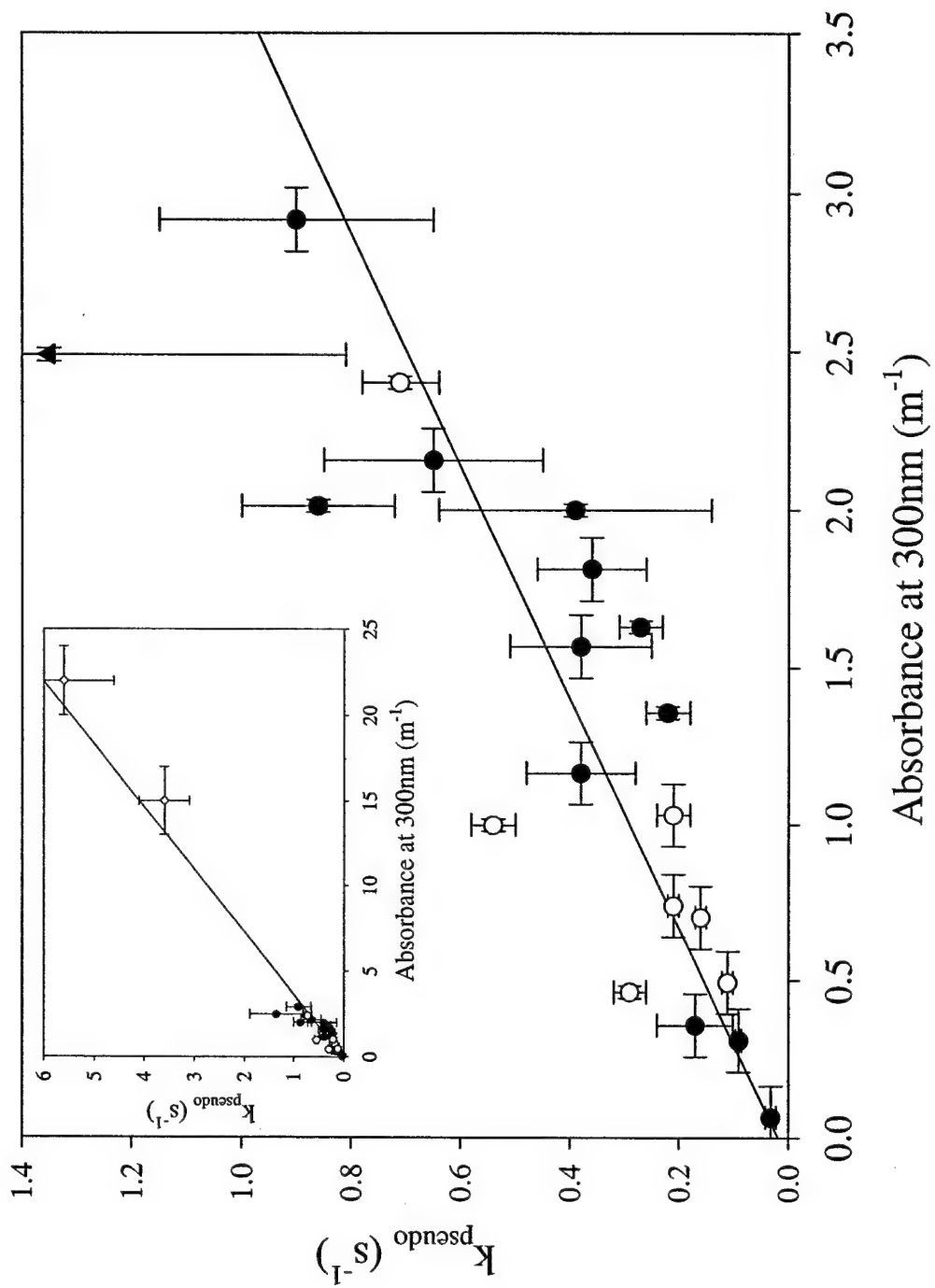


Figure 2. 3

The relationship between the observed k_{pseudo} values obtained in the Chesapeake Bay and chlorophyll α (A), nitrate (B), phosphate (C), and silicate (D) concentrations.

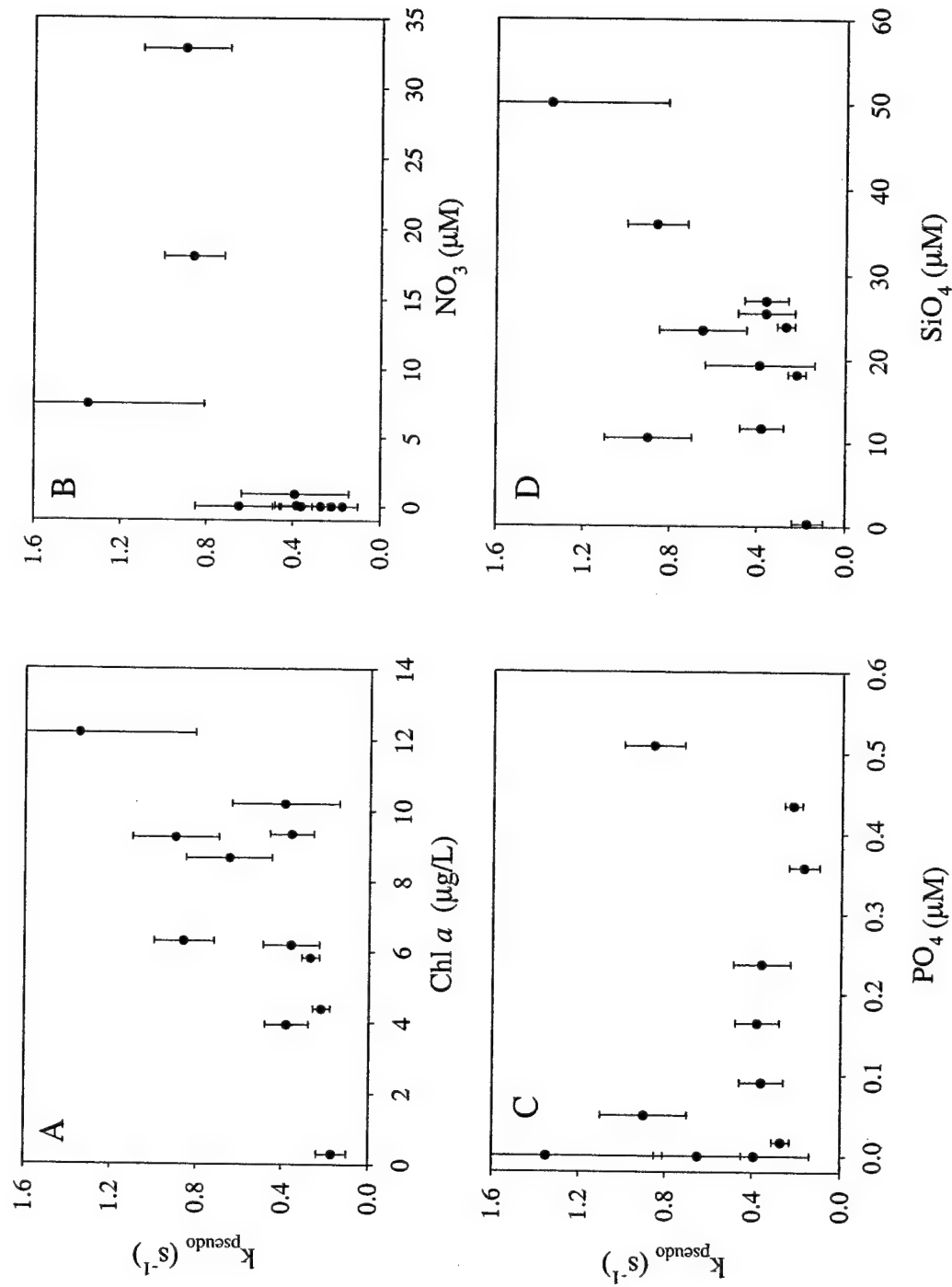


Figure 2. 4

The effects of several different sample treatments on k_{pseudo} . Samples were boiled for 5 minutes to remove enzyme activity, stored at pH 2 overnight in the presence of DTPA to remove metals from any inert complexes, or photo-oxidized to destroy CDOM. Only photo-oxidation removed the activity of the superoxide sink.

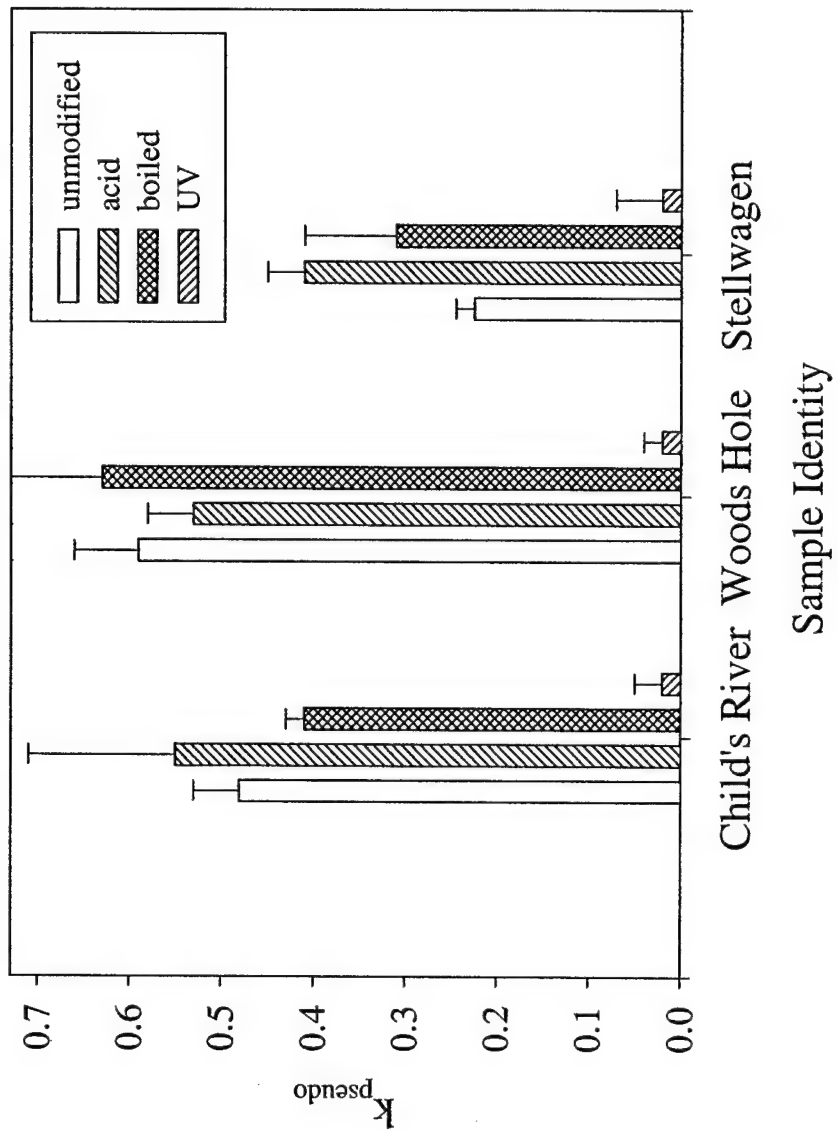


Figure 2. 5

Hydrogen peroxide produced during either the self-dismutation or the DOM catalyzed dismutation of superoxide measured using the diethyl *p*-phenylene diamine (DPD) peroxidase method.

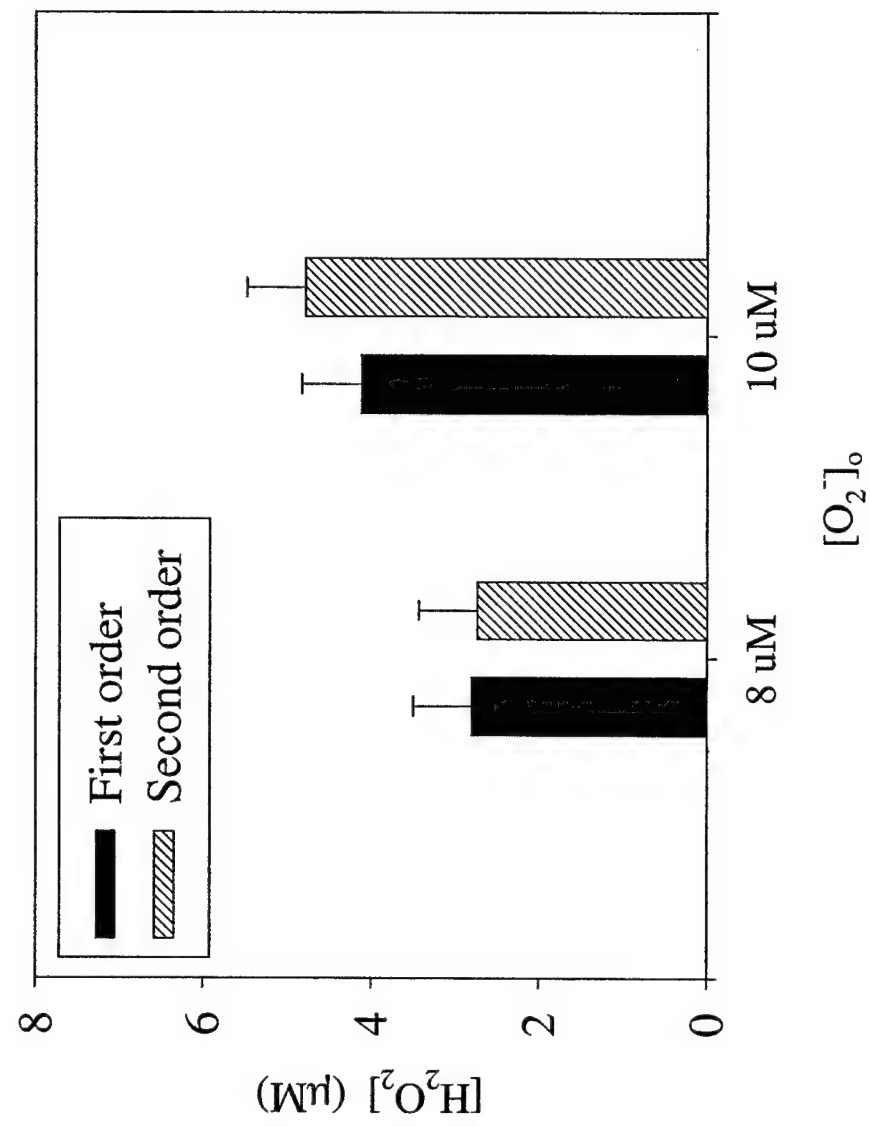


Figure 2. 6

The variation of observed k_{pseudo} with initial superoxide concentration. Different concentrations of superoxide were generated and the same seawater sample was used throughout the experiment.

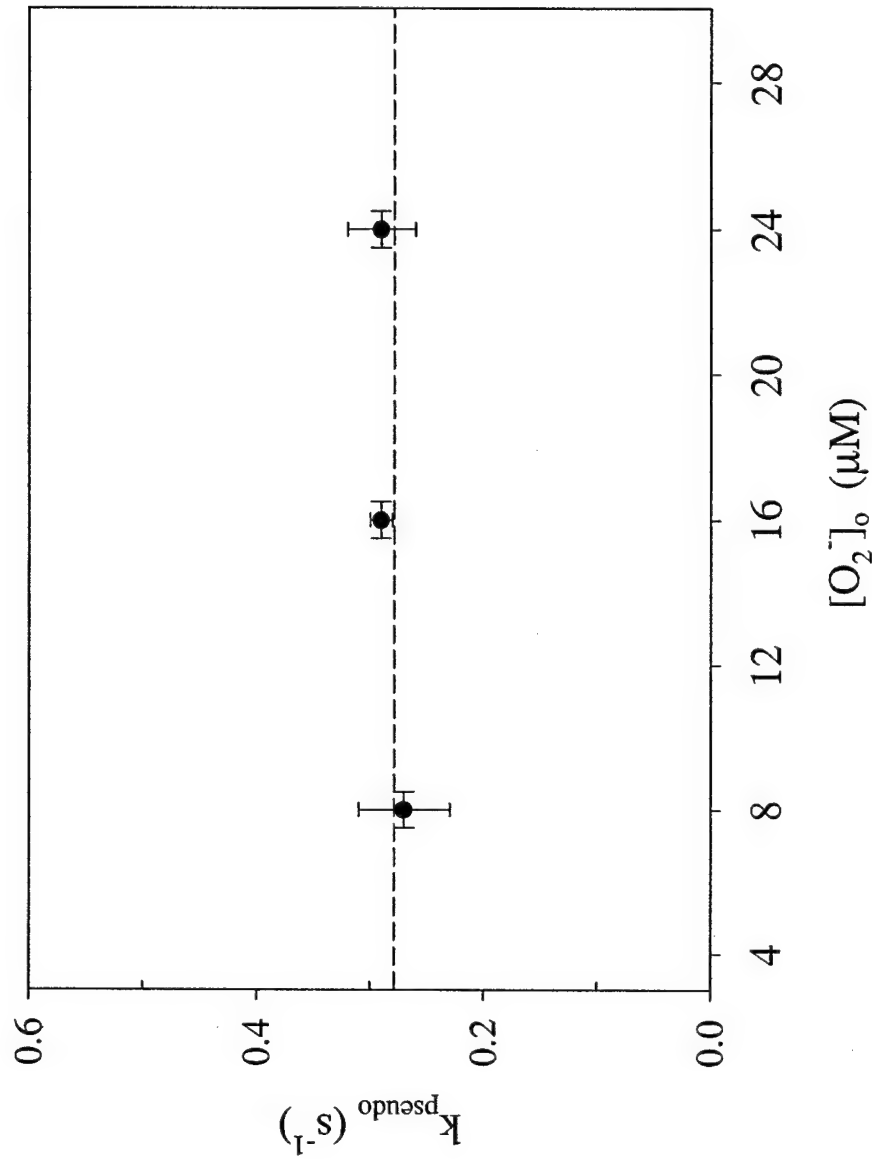


Figure 2. 7

Suggested redox cycle between quinone, semiquinone radical, and hydroquinone that could catalyze the dismutation of superoxide into hydrogen peroxide and dioxygen.

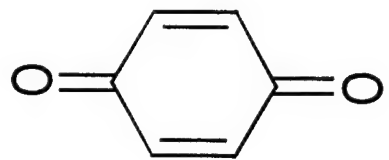
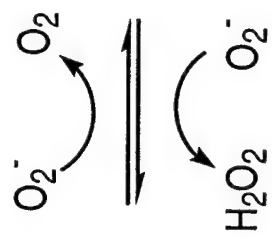
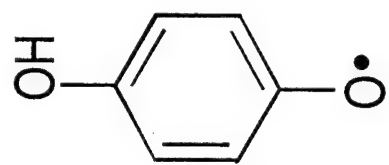
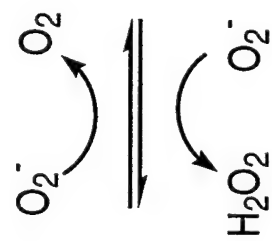
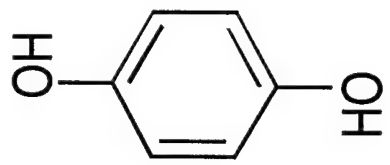


Figure 2. 8

The observed k_{pseudo} versus the optical absorption at 300 nm for several 10 mg/L humic and fulvic acid solutions. There does not appear to be as significant a linear correlation as observed for coastal seawater samples ($r^2=0.65$).

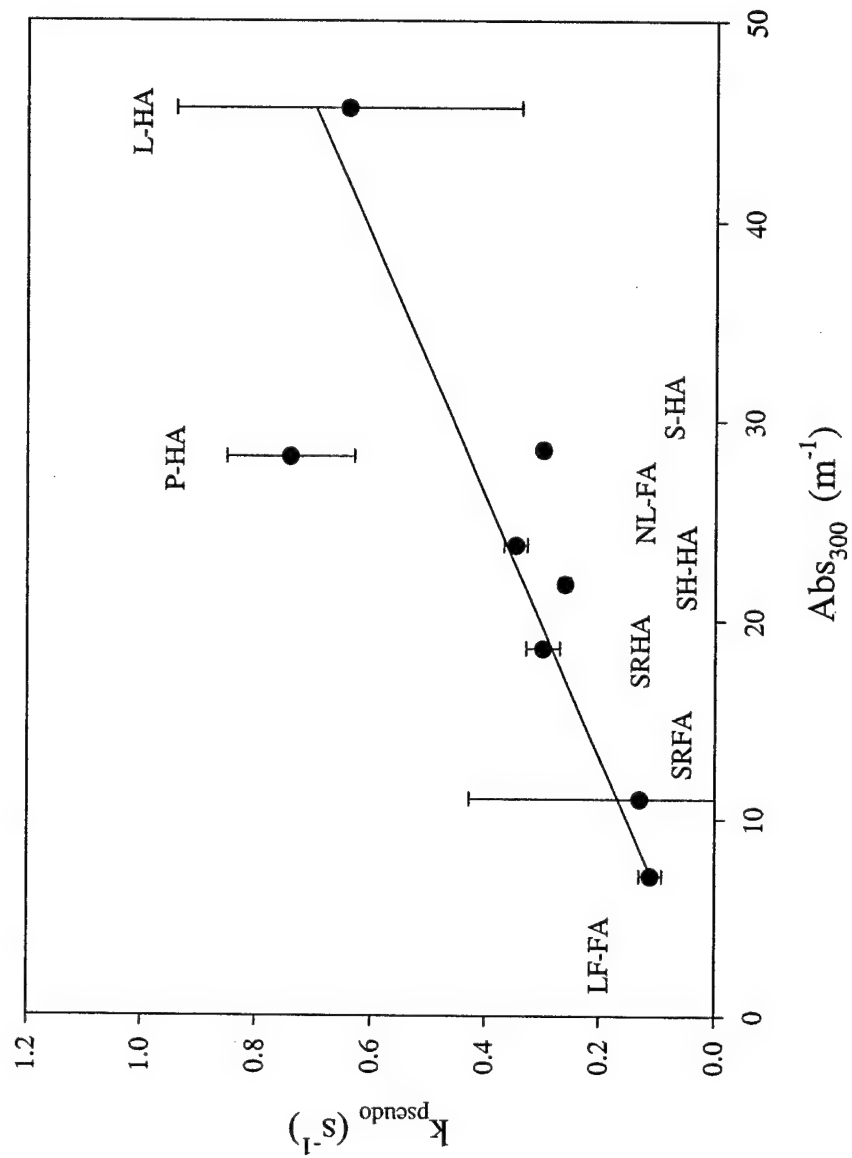
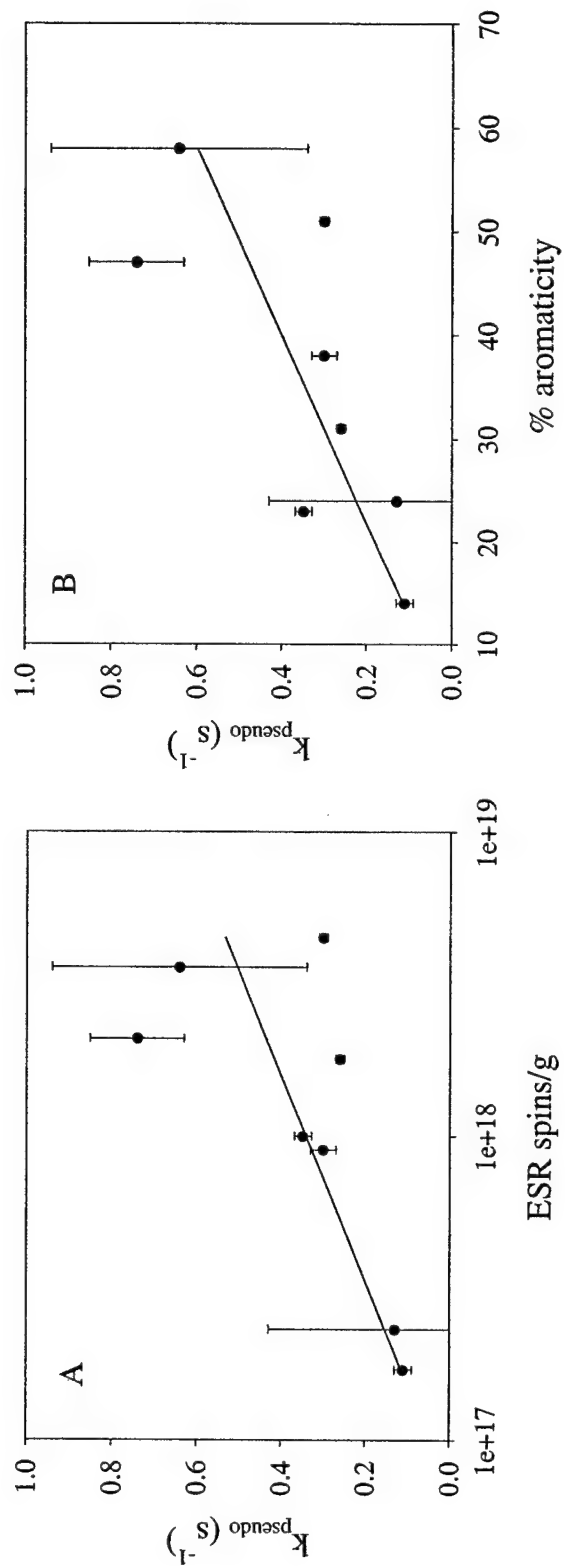


Figure 2. 9

Correlation between the observed k_{pseudo} and (A) the organic radical content (spins/g) determined by ESR ($r^2=0.46$) and (B) the percent aromaticity determined by ^{13}C NMR ($r^2=0.56$). Data from Scott *et al.* (1998).



CHAPTER 3.

REACTIONS OF HYDROXYL RADICAL WITH HUMIC SUBSTANCES: BLEACHING, MINERALIZATION, AND PRODUCTION OF BIOAVAILABLE CARBON SUBSTRATES

Environmental Science and Technology

Submitted May 7 , 2001

Revised October 6, 2001

Accepted October 16, 2001

Reproduced with permission from *Environmental Science and Technology* in press as
Goldstone, J. V.; Pullin, M. J.; Bertilsson, S. ; and Voelker, B. M. Reactions of hydroxyl
radical with humic substances: Bleaching, mineralization, and production of bioavailable
carbon substrates.

Unpublished work ©2002 American Chemical Society.

Abstract

In this study, we examine the role of hydroxyl ($\text{OH}\cdot$) radical as a mechanism for the photodecomposition of chromophoric dissolved organic matter (CDOM) in sunlit surface waters. Using gamma-radiolysis of water, $\text{OH}\cdot$ was generated in solutions of standard humic substances in quantities comparable to those produced on time scales of days in sunlit surface waters. The second-order rate coefficients of $\text{OH}\cdot$ reaction with Suwannee River Fulvic ($2.7 \times 10^4 \text{ s}^{-1} (\text{mg C/l})^{-1}$) and Humic Acids ($1.9 \times 10^4 \text{ s}^{-1} (\text{mg C/l})^{-1}$) are comparable to those observed for DOM in natural water samples and DOM isolates from other sources, but decrease slightly with increasing $\text{OH}\cdot$ doses. $\text{OH}\cdot$ reactions with humic substances produced dissolved inorganic carbon (DIC) with a high efficiency of $\sim 0.3 \text{ mol CO}_2$ per mol $\text{OH}\cdot$. This efficiency stayed approximately constant from early phases of oxidation until complete mineralization of the DOM. Production rates of low molecular weight (LMW) acids including acetic, formic, malonic, and oxalic acids by reaction of SRFA and SRHA with $\text{OH}\cdot$ were measured using HPLC. Ratios of production rates of these acids to rates of DIC production for SRHA and for SRFA were similar to those observed upon photolysis of natural water samples. Bioassays indicated that $\text{OH}\cdot$ reactions with humic substances do not result in measurable formation of bioavailable carbon substrates other than the LMW acids. Bleaching of humic chromophores by $\text{OH}\cdot$ was relatively slow. Our results indicate that $\text{OH}\cdot$ reactions with humic substances are not likely to contribute significantly to observed rates of DOM photomineralization and LMW acid production in sunlit waters. They are also not likely to be a significant mechanism of photobleaching except in waters with very high $\text{OH}\cdot$ photoformation rates.

Introduction

Aquatic dissolved organic matter (DOM) is in part composed of light-absorbing polymers that are resistant to microbial assimilation and breakdown. The photodecomposition of this chromophoric DOM (CDOM) in natural waters is of interest for a number of reasons. First, CDOM photolysis could represent an important source of nutrients and carbon substrates to microorganisms. Biologically available photoproducts that have been identified include CO (1), low molecular weight (LMW) organic compounds, including carboxylic acids and carbonyl compounds (2-7), and ammonia (8). Second, CDOM has further ecological significance as the main absorber of UV-A and UV-B radiation in natural waters, shielding aquatic organisms from sunlight's harmful effects (9). Photodecomposition of this material results in the destruction of its light-absorbing properties (photobleaching). Finally, photomineralization of CDOM to dissolved inorganic carbon (DIC) may constitute a significant flux in the global carbon cycle (10). In some cases, utilization of photoproduced carbon substrates by bacteria seems to be the more significant pathway to mineralization (11-13), while in other systems abiotic photomineralization of DOM is more significant (10,14,15).

Photodecomposition may proceed both via direct photochemical reactions, involving energy and electron transfer after absorption of photons by CDOM, (16-19), or via indirect (sensitized) processes, involving DOM reactions with photochemically generated intermediates such as reactive oxygen species (ROS). The relative importance of these two general classes of mechanisms must be understood in order to be able to utilize laboratory studies of DOM photodecomposition and product formation rates to estimate the rates of these processes in the environment. If direct photochemical processes dominate, only the chromophoric portion of the DOM will be broken down by this mechanism, and the rates of photodecomposition and product formation will be proportional to the amount of light absorbed by the CDOM. If indirect photochemical processes are important, photodecomposition of non-chromophoric material is also possible, and the rate of light absorption by CDOM will only control the rates if CDOM photoreactions are the main source of the intermediates involved. There is no reason to

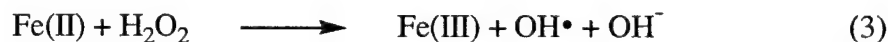
assume that the same general mechanism is responsible for different processes of interest; for instance, photobleaching could proceed mostly via direct mechanisms while photomineralization and photoproduction of LMW organic compounds could proceed mostly via indirect mechanisms.

Of the various reactive intermediates produced in sunlit natural waters, hydroxyl radical (OH^\bullet) is the likeliest candidate for having significant effects on DOM decomposition. OH^\bullet is a powerful oxidant known to react with many organic compounds at nearly diffusion-limited rates. Reaction rate constants of OH^\bullet with DOM measured in a number of natural water samples and isolates, typically $1\text{-}7 \times 10^4 \text{ s}^{-1} (\text{mg-C/l})^{-1}$ (20-24), imply that DOM is the primary sink of OH^\bullet in most freshwaters. The rate of DOM oxidation by OH^\bullet must then be approximately equal to the photoproduction rate of OH^\bullet . Sources of OH^\bullet in sunlit waters include nitrate photolysis (22,25) and DOM photolysis (26) (Equations 1-2).



OH^\bullet production rates are dependent on the concentrations of these sources as well as on the available sunlight. Mid-day near-surface production rates range from $10^{-13} \text{ M s}^{-1}$ to $10^{-10} \text{ M s}^{-1}$ in most natural waters, although production rates as high as 10^{-9} M s^{-1} have been observed in samples from the Florida Everglades (27). Steep attenuation of OH^\bullet production rates with water depth are expected, as UV irradiation is needed to produce OH^\bullet .

Photo-Fenton reactions, the oxidation of photoproduced Fe(II) by photoproduced HOOH, have also been suggested as a significant source of OH^\bullet in sunlit natural waters (28,29) (Equation 3).



Ongoing studies in our own laboratory suggest that Fenton's reaction could potentially result in OH• photo-production rates as high as 10^9 M s^{-1} in sunlit, organic-rich, iron-rich, mildly acidic waters (30). Increases in OH• production rates due to Fenton chemistry may explain observed increases in the rate of photoproduction of DIC and other DOM photoproducts in the presence of Fe (14,31), as well as positive correlations of photoproduction rates of DIC with Fe content in a number of Swedish lake water samples (12). Alternatively, the Fe effect may be attributable to a direct photochemical process, ligand to metal charge transfer (LMCT) reactions, that entail the oxidation of CDOM with the concurrent reduction of Fe(III) to Fe(II) (29,31,32). While Fe effects on LMW acid production were not observed in the Swedish lake study, Mopper and Zhou (1990) suggest OH• involvement in the photoproduction of LMW carboxyl compounds in seawater (27).

Although the effects of OH• on the decomposition of DOM have not been extensively investigated in natural waters, these reactions have been studied in engineered systems. Both the pulp and paper and the drinking water treatment industries have been interested in the oxidative reactions of OH• with organic matter. Hydrogen peroxide (HOOH) has been used as a bleaching reagent in the pulp and paper industry for more than 50 years (33). Until recently, the perhydroxyl radical anion, HO₂⁻, was believed to be the active species present during alkaline bleaching processes (33,34). However, a number of studies have shown that OH• is an integral part of the bleaching process (34-38).

The production of OH• is also thought to be one of the important processes occurring during Advanced Oxidation Process (AOP) treatments of paper pulp, wastewater, and drinking water, which replace chlorine-based oxidants with use of ozone, ozone-hydrogen peroxide, UV-ozone, UV-hydrogen, or photo-Fenton chemistries (39-41). Rapid bleaching and mineralization, as well as production of LMW mono- and diacids, are observed during ozonation and other AOP and total-chlorine-free (TCF) bleaching treatments (35,42-44). The specific contributions of OH• reactions to the

observed rates of product formation from DOM decomposition processes has generally not been assessed.

The purpose of this study is to determine whether reactions of DOM with OH• play a role in the photomineralization and photobleaching of DOM and the photoproduction of biologically available carbon sources in natural waters. Gamma radiolysis of water was used to produce OH• non-photolytically, avoiding the complicating effects of multiple reactions occurring in the DOM matrix and the aqueous solvent during irradiation with light. Rates of bleaching and mineralization of extracted fulvic and humic acids standards (Suwannee River humic and fulvic acids) by OH• were examined under a range of conditions representative of natural waters. In addition, we have examined the role of OH• in the production of LMW organic acids which are important products of DOM photolysis. Because the production of LMW carboxylic acids is not the only potential effect of OH on DOM bioavailability, we also used dilution cultures with bacterial growth potential as an indirect measure of the impact of hydroxyl radical on DOM substrate quality and bioavailability (45).

Methods

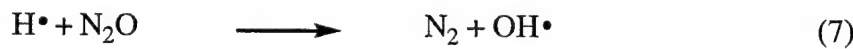
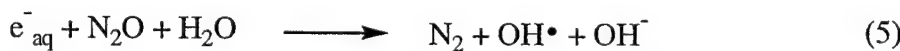
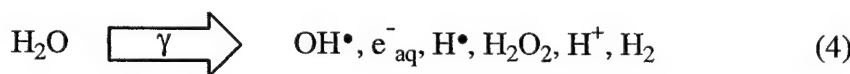
Materials

Suwannee River Humic and Fulvic Acid reference materials (SRHA 1R103H and SRFA 1R101F) were obtained from the International Humic Substances Society. Seawater samples were collected from Delaware Bay using the Teflon flow system of the R/V Cape Henlopen. Samples were 0.45µm and 0.2µm filtered through acid-washed and extensively pre-rinsed cartridge filters and stored in the dark at 4°C in fluorinated HDPE carboys. DOC-free seawater was produced by UV irradiating 0.2µm filtered Sargasso Sea using an air-cooled medium pressure Hg lamp. Massachusetts Bay water for bacterial growth experiments was sampled at Revere State Beach using an acid-washed Teflon bottle and filtered through precombusted Whatman GF/F filters (3 hours at 450 °C, nominal pore-size 0.7 µm). Argon (Grade 4.8), oxygen (Grade 4.4), CO₂-free air (TOC

grade), and N₂O (Grade 2) were obtained from BOC Gases. All reagents were purchased from Sigma-Aldrich and used as received unless otherwise specified.

Radiolysis

By gamma radiolysis of N₂O-saturated aqueous solutions, the radiolytic decomposition of water can be exploited to produce a stable, steady flux of OH• via the reactions of hydrated electrons (e⁻_(aq)) and hydrogen atoms (H•) with N₂O (Equations 4-8;(46)). In the presence of O₂, the reducing radical H• is instead converted into HO₂ (Eq 8) (>93 % and >98% with 4:1 N₂O/air and N₂O/oxygen mixtures) while the reaction of O₂ with e⁻_(aq) is less significant, so that e⁻_(aq) is still converted (>99 and >98 %,



respectively) into OH•. Gamma radiolysis was performed using a ⁶⁰Co source (GammaCell-220) emitting 0.13 kGy/hr of gamma radiation (1.2 MeV). Dosimetry was performed using the standard Fricke dosimeter (47), and also by measuring hydrogen peroxide production rates using acridinium ester chemiluminescence (48) or the N,N'-diethyl-p-phenylenediamine - peroxidase method (49). Samples were saturated with N₂O or with a 4:1 mixture of N₂O and either CO₂-free air or O₂, transferred under constant gas purge to pre-combusted amber glass vials with Teflon®-lined silicone septa, and irradiated in the GammaCell. The net radiation-chemical yield (G-value) for OH• in the absence of O₂ is 5.9 molecules/100 eV, while in the presence of O₂ it drops to 5.3 molecules/100 eV (46). These values correspond to OH• production rates of 1.9 x 10⁻⁸

and $1.7 \times 10^{-8} \text{ M s}^{-1}$ in N_2O and $\text{N}_2\text{O}/\text{air}$ or oxygen-saturated solutions respectively.

Analyses were performed immediately after irradiation.

Phosphate buffers were used to control the pH of the solutions where indicated. Because the reaction rate constants of phosphate species with $\text{OH}\cdot$ are all $< 3 \times 10^6 \text{ M}^{-1}\text{s}^{-1}$ (46), keeping the buffer concentrations low ($\leq 2\text{mM}$) assured that phosphate reactions with $\text{OH}\cdot$ would be negligible.

Analytical Techniques

Measurements of $[\text{OH}\cdot]_{ss}$ were accomplished using ^{14}C -labeled formate as an $\text{OH}\cdot$ probe. In the presence of O_2 , formate anion reacts with $\text{OH}\cdot$ to produce CO_2 with a rate constant of $3.2 \times 10^9 \text{ M}^{-1}\text{s}^{-1}$ (46). Formate does not react with O_2^- , the only other radical present in significant steady-state concentrations during these radiolysis experiments ($k < 0.01 \text{ M}^{-1}\text{s}^{-1}$) (50). Irradiations were performed in glass scintillation vials with foil-lined caps. To measure ^{14}C -formate remaining in solution, $^{14}\text{CO}_2$ was purged from the pH 6-buffered sample with argon prior to the addition of scintillation fluid in a 6:1 ratio of ScintiSafe Econo1 (Fisher Scientific) to sample. Scintillation counting was performed using a Beckman Model 6500 Scintillation Counter.

Measurements of DIC were performed using a TOC-5000 (Shimadzu Corp.) in IC mode. In order to eliminate the interference of N_2O during the near-infrared (NDIR) detection of CO_2 , all samples were purged with argon following the addition of CO_2 -free NaOH to prevent the loss of the CO_2 . Measurements of DOC were performed using a TOC-5000 (Shimadzu Corp.) on samples acidified with concentrated HCl to pH ≤ 1 . Samples to be analyzed were purged for 4 minutes using CO_2 -free air (TOC grade) to remove DIC prior to injection. Optical spectra were obtained on a HP8453 diode-array spectrophotometer (Agilent Technology) using 10cm quartz cuvettes and referenced to Milli-Q water. Hydrogen peroxide was analyzed using the chemiluminescent acridinium ester method (48).

Determination of low-molecular weight carboxylic acids

Low-molecular weight (LMW) carboxylic acids were determined by HPLC of their 2-nitrophenylhydrazide derivatives (51-53). The HPLC separation was optimized to detect a set of carboxylic acids previously observed to be produced by the irradiation of natural waters or aqueous solutions of humic materials: formic, acetic, oxalic, malonic, and levulinic acids (3,12,54,55).

2-nitrophenylhydrazine (2-NPH) was purchased from Acros Organics and was recrystallized from hot water, removed from the supernatant by filtration, and stored as a wet paste at room temperature until use. 1-ethyl-3-(3-dimethylaminopropyl) carbodiimide hydrochloride (SigmaUltra grade) (EDC) was obtained from Sigma Chemical Company. Pyridine (99.9+%) and concentrated HCl (99.999%) were obtained from Aldrich Chemicals and used without further purification. Stock solution of the 2-NPH (0.050 M in 0.25 M HCl) and EDC (0.30 M) were made in advance and frozen in 5-10 ml aliquots, which were defrosted immediately prior to use. Concentrated HCl and pyridine were mixed in 1:1.25 volume ratio to make the derivatization reaction buffer. In our low alkalinity samples, this gave a reaction pH of 4.5 which is ideal for the derivatization reaction (52,56).

The derivatization reaction was carried out in acid washed (10% HNO₃ overnight), rinsed (UV treated 18 MΩ water), and combusted (450 °C for 12 hours) 8 ml glass vials with Teflon®-lined silicone septa closures (acid washed and rinsed). 0.1 ml buffer, 0.1 ml EDC stock, and 0.2 ml 2-NPH stock were added (in order) per 1 ml sample and allowed to stand in the dark at room temperature for 1.5 hours. 0.1 ml 40% w/w KOH (SigmaUltra) per 1 ml sample was then added and the vial was heated at 70 °C for 10 minutes in a water bath. The derivatized sample was either analyzed immediately or stored overnight at 4 °C.

The various acids derivatives were quantified using a Hewlett Packard 1150 HPLC system. The samples were preconcentrated on a polymeric reversed phase guard column (Dionex IonPac NG1 10 μm, 4 x 35 mm) used in place of the manual injector sample loop (52). 100 μl of sample were passed through the concentrator column,

followed by 1.0 ml water to expel the alkaline derivatization reaction medium and remove some interfering reaction byproducts.

Separation used an isocratic ion-pairing eluent with a reversed phase column and (Phenomenex Luna 5 μ m C18(2), 250 x 4.6 mm) and guard cartridge (Phenomenex Securityguard C18, 4 X 3.0 mm). The mobile phase consisted of 20% acetonitrile and 80% aqueous phase containing 7.5 mM tetrabutylammonium bromide and 3 mM phosphate at pH 7.0. This system gave baseline resolution of the five acids in 35 minutes.

The derivatives were detected by absorbance at 230 and 400 nm. Quantitation used external standardization with solutions containing known concentrations of the derivatives of the pure acids and SRFA or SRHA in the same concentration as in the related experiments. The system responded linearly up to 100 μ M, with a detection limit of approximately 100 nM. It should be noted that even the high concentration of humic substances used here do not interfere in the determination of the small organic acids using this method. It is not surprising that the presence of measurable concentrations of LMW acids in unirradiated SRFA and SRHA solutions has not been previously reported, as the concentration of acids observed in these solutions is less than 0.2% of the total organic carbon.

Bioassays

Dilution cultures were prepared from Massachusetts Bay water sampled at Revere State Beach filtered through precombusted Whatman GF/F filters (3 hours at 450 °C, nominal pore-size 0.7 μ m) to remove bacterivorous protists. This filtering also resulted in a reduction in bacterial abundance from 6×10^6 cells ml^{-1} to 6×10^5 cells ml^{-1} . The final concentration of DOC in the filtered sample was 3.6 mg C l^{-1} (300 μ M C). This coastal water was amended with filter-sterilized aqueous solutions of SRHA (36 mg C liter $^{-1}$, 3mM C) and SRFA (45 mg C liter $^{-1}$, 3.75 mM C) dissolved in Milli-Q water. Identical solutions of SRHA (36 mg C liter $^{-1}$) and SRFA (45 mg C liter $^{-1}$) that had been exposed to gamma radiolysis for 30 minutes (approximately 30 μ M OH•) as described above were also added to seawater (γ -SRHA, γ -SRFA). In each case, one part of humic or fulvic

solution was added to 3 parts of seawater (v/v) so that the final DOC concentrations in the incubated cultures were 11.7 mg C l⁻¹ (SRHA) and 14.1 mg C l⁻¹ (SRFA), of which 2.7 mg C l⁻¹ (225 µM C) were from the DOC originally present in the coastal seawater. Each culture was also amended with NaH₂PO₄ and NH₄Cl to final N and P concentrations of 100 µM to achieve carbon limited growth conditions. For each amendment, triplicate cultures were incubated in darkness at 23 °C in acid-washed glass bottles sealed with Teflon-lined screw caps. Samples for bacterial abundance were taken daily from the cultures during the 6 day incubation and were preserved by adding 0.2 µm-filtered sodium tetraborate buffered formaldehyde to 2 % final concentration. Samples were kept at 4 °C until analysis (within 2 weeks). As a result of the gamma radiolysis, initial hydrogen peroxide concentrations were 1.8 µM but declined to less than 500 nM by the fourth day of the incubation.

Bacterial abundance was analyzed using a FACScan flowcytometer (Becton Dickinson) (57). Samples containing formaldehyde-fixed bacterial cells were stained with the nucleic acid stain Syto 13® (50 µM final concentration, Molecular Probes). Counting was performed at low flow (12 µl minute⁻¹) with detector voltages set to 400 (side scatter) and 560 (green fluorescence). Fluorescent microspheres (Carboxy YG, 1.58 µm diameter, Polysciences) were added to all samples at a final concentration of 4.5 x 10⁶ beads ml⁻¹ for use as internal reference. Cells were separated from fluorescent beads in a log-log dot plot of side scatter and green fluorescence and bacterial cell abundance was determined using the fluorescent beads as an internal standard. Samples were run for 20 seconds or until a minimum of 2000 beads had been counted.

Epifluorescence microscopy and image analysis were used to estimate bacterial cell size and to assure that predatory flagellates were absent in the cultures at the end of the incubations. Formaldehyde-fixed bacterial samples were stained with 4'6-diamidino-2-phenylindole (DAPI) (58) and cells were visualized with an Axioskop 2 fluorescence microscope (Zeiss) equipped with an Atto-Arc variable light source. For each culture, duplicate images were acquired with a Magnafire cooled CCD camera (Optronics). Images were exported to the Scion Image 4.0.2 image analysis software and an edge

detection operator was used to define individual area, length, and width of >100 cells per individual culture. Cell volumes were then estimated by approximating the shape of bacterial cells as a cylindrical cell with hemispherical end caps. Volumes were converted to bacterial carbon biomass for individual cells using the volume to dry weight relationship previously reported by Loferer-Krößbacher et al. (1998) and assuming that carbon comprises 50 % of the bacterial dry weight (59). Total bacterial carbon was calculated using bacterial abundance and average carbon content per cell in individual cultures.

Results

We have determined the second-order reaction rate coefficients for OH[•] with 5mg/L (416 μM C) SRFA and SRHA using ¹⁴C-labeled formate as a probe for OH[•] in solutions of the acids saturated with a 4:1 N₂O/O₂ mixture and buffered at pH 6. By utilizing ¹⁴C-formate we can add very small probe concentrations (100 nM), and as DOM is the only significant sink of OH[•] in this system, we can assume that the OH[•] steady state concentration ([OH[•]]_{ss}) is determined by the scavenging rate of the DOM in the system. The concentration of formate anion after irradiation time t, [formate]_t, is described by the equation:

$$\ln [\text{formate}]_t / [\text{formate}]_0 = -k_{\text{formate}} [\text{OH}^{\bullet}]_{\text{ss}} t \quad (9)$$

where [formate]₀ is the initial formate concentration and k_{formate} is the second-order rate constant of reaction of OH[•] with formate (the reaction of OH[•] with formic acid is insignificant at this pH). If [OH[•]]_{ss} is constant, a plot of ln[formate]_t/[formate]₀ versus t should be linear, and [OH[•]]_{ss} can then be obtained from the slope. Since the OH[•] production rate P_{OH} in our radiolysis apparatus is known ($1.7 \times 10^{-8} \text{ Ms}^{-1}$ in the presence of O₂), [OH[•]]_{ss} can then be used to determine the sum of the rates of the reactions of OH[•] with its sinks, where each rate is given by the second-order rate constant of the reaction of OH[•] with sink *i*, k_{S,i}, multiplied by the concentration of the sink, [S]_i:

$$\Sigma k_{S,i} [S]_i = P_{OH}/[OH^{\bullet}]_{ss} \quad (10)$$

Plots of $\ln[\text{formate}]_t/[\text{formate}]_0$ versus irradiation time in fulvic and humic acid solutions exhibit a slope becoming steeper with increasing irradiation time, indicating that $[OH^{\bullet}]_{ss}$ is also increasing (Figure 1) and therefore that $\Sigma k_{S,i} [S]_i$ is decreasing. Values of $\Sigma k_{S,i} [S]_i$ calculated from the observed slopes all greatly exceeded the contributions of formate and phosphate species to the sum, showing that DOM is the only significant sink of OH^{\bullet} in this system, and that $\Sigma k_{S,i} [S]_i$ is therefore equal to $k_{DOM}[DOM]$. DIC measurements (see below) indicate that $[DOM]$ did not decrease significantly during the course of this experiment so that the observed decreases in $\Sigma k_{S,i} [S]_i$, with longer irradiation time must be due to decreases in k_{DOM} . Calculated k_{DOM} values for SRFA and SRHA in the early, middle, and later parts of the irradiations (normalized to carbon content) are shown in Table 1.

We have observed the production of LMW carbon acids during the reaction of OH^{\bullet} with SRFA and SRHA (Figure 2). Production rates of acetic, formic, malonic, and oxalic acids per mole of OH^{\bullet} were approximately constant in the SRFA and in the SRHA solutions (Figure 2). Production rates of these acids determined from least squares regression of the data are shown in Table 2. No production of levulinic acid was observed in our experiments. The large flux of OH^{\bullet} used in these experiments could also react with the acids, reducing their observed concentration and cause an underestimation of their production rates. However, maximum loss rates from reaction with OH^{\bullet} of oxalic and acetic acids were less than 4% of the net production rates shown in Table 2 ($[OH^{\bullet}]_{ss} = 4 - 6 \times 10^{-14} M$, rate constants of deprotonated acids with $OH^{\bullet} < 10^8 M^{-1} s^{-1}$ (50)). The loss rate of malonic acid is at most 17% of the production rate in the SRFA experiment and 18% in the SRHA experiment (rate constant of the malonate reaction with OH^{\bullet} is $3 \times 10^8 M^{-1}s^{-1}$). In the case of formic acid, the rate of reaction with OH^{\bullet} is much faster (rate constant of formate $3 \times 10^9 M^{-1}s^{-1}$; (46)). The observed net formate production rates of $3.2 \times 10^{-10} M s^{-1}$ (SRFA) and $7.3 \times 10^{-10} M s^{-1}$ (SRHA) can be corrected for the loss of formate by two independent methods. The half-life of loss due to reaction with OH^{\bullet} is 60

minutes (SRHA) or 90 minutes (SRFA), so that approach of a formate steady-state concentration might be expected in our 120 minute irradiation experiments. By assuming the maximum formate concentration represents a steady state concentration and using calculated $[\text{OH}^\bullet]_{\text{ss}}$ concentrations of 4×10^{-14} M (SRFA) and 6×10^{-14} M (SRHA), formate production rates of 4.9×10^{-10} M s⁻¹ (SRFA) and 9.9×10^{-10} M s⁻¹ (SRHA) can be calculated. Dividing these calculated formation rates by the OH[•] production rate of 1.6×10^{-8} M s⁻¹ leads to the calculated production ratio of 0.03 μM formic acid/ μM OH[•] for SRFA, and the corresponding SRHA value of 0.06 μM acid/ μM OH[•] (Table 2). The larger correction for the SRHA solutions is due to the lower reaction rate constant of OH[•] with SRHA and hence a larger calculated $[\text{OH}^\bullet]_{\text{ss}}$. These revised rates can be arrived at independently by calculating the formate loss rate at each time point and performing a linear regression of the resulting corrected data. The values arrived at by this method are within 2% of those derived from the steady-state calculation.

The microbial growth experiment provided a measure of the total change in bioavailable substrates by the OH[•]-driven alteration of SRFA and SRHA. Samples exposed to 30 μM OH[•], a dose equivalent to 15 days of near-surface solar irradiation assuming a relatively high OH[•] production rate of 10^{-10} M s⁻¹ for six hours per day (see Introduction), were inoculated with a natural consortium of coastal bacteria and incubated for six days. During the course of the six day incubation, bacterial abundance increased > 10-fold in all cultures. There were no visible protozoan contaminants in any of the cultures at the end of this period. Radiolysis treatment of SRHA and SRFA resulted in a slightly lower bacterial abundance throughout the incubation (Figure 3), but neither the cell abundances nor the carbon content per cell differed significantly between irradiated samples and controls at maximum cell concentration (Students-t, p> 0.1; Table 3).

Radiolysis of the SRFA and SRHA solutions produced significant concentrations of DIC, showing that OH[•] and/or O₂[−] reactions with DOM macromolecules are important in photomineralization processes. Since DIC production can be eliminated by the addition of *t*-butanol, which scavenges OH[•] but not O₂[−], OH[•] must be responsible for this mineralization (Figure 4). The rate of DIC production from a 0.5 mg C l⁻¹ (42 μM DOC)

solution of SRFA remains relatively constant until complete mineralization occurred (40 μM DIC produced, Inset Figure 4). A further indication that neither O_2^- nor O_2 is responsible for a significant portion of the DIC production comes from the fact that there is no significant decrease in the DIC production rate when O_2 is excluded from the radiolysis experiments, as shown in Figure 5. The molar ratio of DIC produced to OH^\bullet generated is approximately 0.3 both in the SRFA solutions and in the SRHA solutions. This ratio is not significantly altered within the range of pH values found in natural waters (pH 4- pH 10).

OH^\bullet radical reacts very rapidly with Br^- in seawater (60) and in other bromide-containing natural waters (61) to produce Br_2^- and BrO^\bullet , which may then react with CO_3^{2-} to produce CO_3^\bullet radical (60,62). Any of these intermediate radicals may react more selectively with DOM than OH^\bullet does. Large concentrations of added Br^- (up to 0.1M) do not affect the production of DIC (Figure 5), indicating that these intermediate radicals are as effective as OH^\bullet in mineralizing DOM. Bromine species (BrO^\bullet and BrOH) have been shown to be rapidly reduced by DOM at doses of 1.6 μM (mgC l^{-1})⁻¹ (63). Thus, although >97% of OH^\bullet in seawater reacts initially with Br^- (60), the final sink of these radicals is most likely DOM.

OH^\bullet was observed to be capable of bleaching SRFA and SRHA in the UV-B region of CDOM (300 nm) at a rate of approximately $2.1 (\pm 0.1) \times 10^4 \text{ m}^{-1}$ per molar OH^\bullet produced for SRFA and $4.3 (\pm 0.06) \times 10^4 \text{ m}^{-1}$ per molar OH^\bullet for SRHA (Figure 6). Both DOC-free seawater amended with SRFA and coastal seawater samples from Delaware Bay exhibited similar bleaching rates ($1.3 (\pm 0.2) \times 10^4 \text{ m}^{-1}$ per molar OH^\bullet). These rates were only slightly lower than the bleaching observed in N_2O -saturated, buffered Milli-Q solutions of SRFA (Figure 6), although there is significant scatter, possibly due to pH changes in these unbuffered solutions. The addition of O_2 to the radiolysis solutions increased the bleaching efficiency of OH^\bullet to $3.0 (\pm 0.1) \times 10^4 \text{ m}^{-1}$ per molar OH^\bullet for SRFA and $5.1 (\pm 0.1) \times 10^4 \text{ m}^{-1}$ per molar OH^\bullet for SRHA, possibly by increasing the efficiency of the OH^\bullet -mediated aromatic-ring opening reactions (see Discussion).

Discussion

The second order reaction rate coefficients of OH[•] with SRFA and SRHA (k_{DOM}) determined in this work (Table 1) fall within the range of values for aquatic DOM determined by previous investigators ($1.7 \times 10^4 \text{ s}^{-1}$) (20,21,64). Previous investigators have used similar techniques to determine the rate coefficients of the OH[•] reactions with SRFA and SRHA (23,24). The rate constants determined were 30-40% lower than those found in this work, but were determined at OH[•] doses that were 30% higher than used here. A decrease in the rate coefficients with increasing OH[•] dose, which cannot be accounted for by mineralization of the organic matter, has not been previously reported, although Peyton (1993) speculated that this result might occur (65). The decrease is not unexpected, since these rate coefficients are the averages of the reaction rate constants of OH[•] with the many different constituent parts of the fulvic and humic acids. As the more rapidly-reacting portions of the DOM are oxidized, the average rate coefficient decreases. The rate of DOM scavenging of OH[•] in natural waters, which often determines [OH[•]]_{ss}, should therefore be considered a function not only of the DOM concentration, but also of the extent of DOM oxidation, although the magnitude of the effect that we observed is small compared to the variability in reactivity of DOM from different sources observed by others (20,21,23,24,28).

LMW acid production

OH[•] reactions with organic compounds fall into two basic mechanisms: addition (hydroxylation), generally to an aromatic ring, or hydrogen atom (H[•]) abstraction, both of which may lead to formation of LMW acids. Hydroxylation of aromatic moieties of the precursor material followed by ring opening can produce both mono- and diacids (35,44,66). Both hydroxylation and H[•] abstraction from phenols can break the aromaticity of an aromatic ring, forming hydroxycyclohexadienyl radicals (35,44). Rearomatization is a significant driving force towards O₂/O₂⁻-driven scission of conjugated carbon-carbon bonds adjacent to the aromatic ring (C_α-C_β), leading to subsequent fragmentation and the formation of smaller oxidized products (see Figure 6 in (36)). Another possible mechanism is H[•] abstraction from an unsaturated carbon-carbon

bond to form a carbon-centered radical ($R\cdot$) followed by reaction with O_2 to form a peroxy radical and subsequent decomposition to a carboxylic acid (67,68).

We observed that the production of LMW acids from $OH\cdot$ reactions with SRFA was very similar to the rates observed in the SRHA solutions. In principle, SRFA represents a fraction of humic substances that contain more extensively substituted aromatic rings (69), which exhibit increased reactivity towards $OH\cdot$ (70), and are thus more easily broken down further by $OH\cdot$. However, we did not observe large differences between SRFA and SRHA in the overall LMW acid production. Both SRFA and SRHA contain significant concentrations of carboxylic acid (11.2 versus 7.85 mol kg⁻¹) and phenolic (2.89 versus 1.86 mol kg⁻¹) residues (69). Substituted phenolic residues in particular might contribute to the production of LMW acids (35,36).

Production of bioavailable carbon substrates

The exposure of SRFA and SRHA samples to an environmentally relevant dose of $OH\cdot$ (30 μM) did not have any measurable effect on bacterial growth potential (differences between irradiated and unirradiated incubations 1 (± 2) $\times 10^6$ cells ml⁻¹, 0.1 (± 0.4) mg C l⁻¹ for SRHA; 2 (± 2) $\times 10^6$ cells ml⁻¹, 0.1 (± 0.2) mg C l⁻¹ for SRFA; Figure 3; Table 3). There is an extensive literature supporting a photochemically driven increase in bioavailability of terrestrially derived DOM such as humic materials (reviewed by Moran and Zepp, 1997). Furthermore, $OH\cdot$ has been shown to selectively depolymerize cellulose in pulps (37) and has also been suggested to cleave cross-links in the rigid lignin matrix (34). Either of these mechanisms would serve to facilitate enzymatic degradation of high molecular weight DOM (e.g. humic and fulvic acids) into monomeric compounds that are available for bacterial utilization (45). In contrast, some recent studies have demonstrated that photochemical processes can have a negative impact on the ability of DOM to support bacterial growth (71-73), but these negative effects have generally been associated with the presence of more recent, algal-derived DOM and are therefore less likely to be significant in our experiment. While the simplest explanation of our result is that the reaction of DOM with $OH\cdot$ does not result in measurable formation

of bioavailable products, we cannot rule out the possibility of counteractive positive and negative effects on DOM bioavailability with a zero net result.

The low production rates of LMW carbon acids by OH• are consistent with the lack of effect of OH• on bacterial growth in the bioassay results. The 30 µM dose of OH• used for the bioassay experiments would have produced total LMW acid carbon concentrations of ~ 0.07 mg C l⁻¹ (5.5 µM C) in the solutions (Table 2). Conservatively assuming a 50 % growth efficiency and a carbon content of 106 fg C cell⁻¹ (Table 3), the carboxylic acid carbon produced in SRFA or in SRHA cultures could support the growth of 3.3 x 10⁵ cells. Although there is considerable uncertainty in the growth efficiency of microbial communities on carboxylic acids (range of 20-80%; (3)), the formation rates of the LMW acids we measured are clearly too low to be a significant source of bioavailable carbon in these experiments.

The bacterial growth in our dilution cultures suggests that a fraction of the added SRFA and SRHA was bioavailable; the yield of biomass we observed is consistent with what we would expect based on observations made on a variety of other humic materials (74,75). While the contribution of the 2.7 mg C l⁻¹ (300 µM C, 19-23% of total) DOC originally present from the Massachusetts Bay seawater is not clear, previous reports of “labile” fractions of natural aquatic DOM (19 ± 12% for marine DOM; (76)) and an expected growth yield of less than 50% suggest that the bacterial growth is not attributable solely to this material.

DIC production

Since the average oxidation state of carbon in SRFA and SRHA is approximately zero (69), an average DIC production rate of 0.25 mol DIC per mol OH• would be expected if OH• is the only oxidant participating in the mineralization reaction. Given the lack of effect of oxygen on the rate of mineralization, then, the observed production of ~0.3 mol DIC per mol OH• is consistent with our expectations. The same is true in the presence of Br⁻, as long as Br⁻ is ultimately regenerated so that the overall outcomes of the reaction are reduction of OH• to OH⁻ and oxidation of DOM to DIC. Our parallel measurements of LMW acid production during irradiation show that production of DIC

from OH[•] reaction with LMW acids is an insignificant fraction of the overall DIC formation rate, indicating that most of the mineralization of humic substances does not proceed via LMW acids as intermediates. The observation that the rate of DIC production remains relatively constant from the beginning of the experiment until complete mineralization of the DOM (Inset, Figure 4) suggests that breakdown of DOM into LMW molecules other than the LMW acids we measured is also not a necessary precursor for mineralization.

Bleaching

Bleaching (or ‘fading’) of CDOM is an important photoprocess that leads to increased light penetration into the water column and to decreased photochemical rates (since light must be absorbed in order to cause a photochemical reaction). The addition of O₂ to these solutions increases the bleaching rates of SRFA by 35% and SRHA by about 20% (Figure 6), possibly due to the formation of peroxy radicals followed by the decomposition of aromatic rings and conjugated double bonds. The presence of oxygen has been shown to increase the bleaching of paper pulps, most likely through a similar mechanism (35,36,38). Solutions of humic acids display increased bleaching relative to fulvic acid solutions (Figure 6). These differences may be due to the greater aromatic content of the humic reference material (77), which may be more readily bleached by OH[•] without being mineralized. Although the reactions of OH[•] with Br⁻ in seawater result in intermediates which we expected to react more selectively with chromophoric material, we did not observe an increase in the effectiveness of bleaching per OH[•] generated in seawater.

OH[•] as a mechanism of DOM photoproduct formation

Assuming that the product formation efficiencies (mol product per mol OH[•]) for the materials we examined are similar to those for DOM from other sources, we can assess whether OH[•] could be a significant mechanism for photoformation of these products observed in previous studies. For example, in sunlight irradiation of water from Lake Skarshultsjon, a humic-rich, iron-rich Swedish Lake (12.4 mg C l⁻¹ (1.03 mM C), ~300 µg Fe l⁻¹), a total LMW acid production rate of 1.6 µM C per hour was observed,

with formic acid being produced in greatest amount (3). In addition, photochemical irradiations of a series of lake waters showed that LMW acid carbon production was 20–30% of the concurrent DIC production (12). We observed formation of similar relative abundances of individual acids to each other and to DIC in both of these samples, including LMW acid carbon production rates of 30–40% of concurrent DIC production. Although it is difficult to generalize from SRFA and SRHA to other materials, if SRHA and Lake Skarshultsjon DOM behave similarly, a photoproduction rate of 8–9 $\mu\text{M OH}\cdot$ per hour ($\sim 2 \times 10^{-9} \text{ M s}^{-1}$) would be required to produce the quantities of LMW acids and DIC observed to be photoproduced in Lake Skarshultsjon. Similarly, to explain the difference in DIC photoproduction in Satilla River water with and without addition of a ligand to eliminate Fe photoreactions (14), a difference in $\text{OH}\cdot$ production rates of $\sim 16 \mu\text{M OH}\cdot$ per hour is required if indirect, $\text{OH}\cdot$ -mediated chemistry is solely responsible for the Fe-related DIC production. Based on these estimates, it seems unlikely that $\text{OH}\cdot$ is responsible for a large fraction of the photochemical production of DIC or LMW acids observed in these waters. In addition, exposure to $\text{OH}\cdot$ corresponding to an average solar exposure of 15 days (assuming $\text{OH}\cdot$ photoproduction rates of $10^{-10} \text{ M s}^{-1}$ for 6 hours per day) did not have any significant effect on bacterial growth potential (Figure 3; Table 3), in contrast to previous work that has shown enhanced bacterial growth potential after only 12 hours of simulated surface UV radiation (73). Finally, for an $\text{OH}\cdot$ production rate of $2 \mu\text{M d}^{-1}$ ($10^{-10} \text{ M s}^{-1}$ for six hours/day), the maximum bleaching rate of SRFA due to reactions with $\text{OH}\cdot$ was $6 \times 10^{-2} \text{ m}^{-1} \text{ d}^{-1}$, less than 20% of photobleaching rates of $\sim 0.33 \text{ m}^{-1} \text{ d}^{-1}$ observed in similar solutions irradiated by simulated sunlight (Chapter 5; (78)). Thus, indirect photobleaching of SRFA via the photointermediate $\text{OH}\cdot$ is only a candidate as a significant mechanism of total photobleaching in waters with very high $\text{OH}\cdot$ photoproduction rates, for example in iron-rich acidic systems where Fenton chemistry may be important. To the extent that SRFA and SRHA are representative of aquatic DOM, then, we can eliminate $\text{OH}\cdot$ reactions with humic substances as a significant mechanism for formation of DOM photoproducts.

Acknowledgements

We would like to thank Phil Gschwend for the loan of the HPLC, and Urs von Gunten and Michael Elovitz for helpful discussions. This work was funded by NSF-OCE 9819089. MJP was supported by a NSF Earth Sciences Postdoctoral Fellowship. SB was supported by a Wallenberg Postdoctoral Fellowship. This is WHOI publication number 10468.

References

1. Zuo, Y.; Jones, R. D. *Naturwissenschaften* **1995**, *82*, 472-474.
2. Zhou, X.; Mopper, K. *Mar. Chem.* **1997**, *56*, 201-213.
3. Bertilsson, S.; Tranvik, L. *Limnol. Oceanogr.* **1998**, *43*, 885-895.
4. Kieber, D. J.; Mopper, K. *Mar. Chem.* **1987**, *21*, 135-149.
5. Kieber, R. J.; Zhou, X.; Mopper, K. *Limnol. Oceanogr.* **1990**, *35*, 1503-1515.
6. Mopper, K.; Stahovec, W. L. *Mar. Chem.* **1986**, *19*, 305-321.
7. Kieber, D. J.; McDaniel, J.; Mopper, K. *Nature* **1989**, *341*, 637-639.
8. Bushaw, K. L.; Zepp, R. G.; Tarr, M. A.; Schulz-Janders, D.; Bourbonniere, R. A.; Hodson, R. E.; Miller, W. L.; Bronk, D. A.; Moran, M. A. *Nature* **1996**, *381*, 404-407.
9. Williamson, C. E. *Limnol. Oceanogr.* **1995**, *40*, 386-392.
10. Miller, W. L.; Zepp, R. G. *J. Geophys. Res.* **1995**, *22*, 417-420.
11. Bertilsson, S.; Allard, B. *Arch. Hydrobiol./Advanc. Limnol.* **1996**, *48*, 133-141.
12. Bertilsson, S.; Tranvik, L. *Limnol. Oceanogr.* **2000**, *45*, 753-762.
13. Bano, N.; Moran, M. A.; Hodson, R. E. *Aquat. Microb. Ecol.* **1998**, *16*, 95-102.
14. Gao, H.; Zepp, R. G. *Environ. Sci. Technol.* **1998**.
15. Granéli, W.; Lindell, M.; Tranvik, L. *Limnol. Oceanogr.* **1996**, *41*, 698-706.
16. Zafiriou, O. C. *Chemical Oceanography*; Academic Press: London, 1983; Vol. 8.
17. Zafiriou, O. C.; Joussot-Dubien, J.; Zepp, R. G.; Zika, R. *Environ. Sci. Technol.* **1984**, *18*, 358A-371A.
18. Blough, N. V.; Zepp, R. G. *Active Oxygen in Chemistry*; Foote, C. S. and Valentine, J. S., Ed.; Chapman and Hall: New York, 1995, pp 280-333.
19. Cooper, W. J.; Zika, R. G.; Petasne, R. G.; Fischer, A. M. *Aquatic Humic Substances: Influence on Fate and Treatment of Pollutants*; Suffet, I. H. and MacCarthy, P., Ed.; American Chemical Society: Washington, DC, 1989; Vol. Advances in Chemistry Series No. 219.
20. Brezonik, P. L.; Fulkerson-Brekken, J. *Environ. Sci. Technol.* **1998**, *32*, 3004-3010.
21. Westerhoff, P.; Aiken, G.; Amy, G.; Debroux, J. *Wat. Res.* **1999**, *33*, 2265-2276.
22. Zepp, R. G.; Hoigne, J.; Bader, H. *Environ. Sci. Technol.* **1987**, *21*, 443-450.
23. Elovitz, M. S., personal communication.
24. Elovitz, M. S.; von Gunten, U. *ACS Conference Proceedings - Division of Environmental Chemistry Preprints and Extended Abstracts* **1999**, *39*, 123, March.
25. Wagner, I.; Strehlow, H.; Busse, G. *Z. Phys. Chem. (Munich)* **1980**, *123*, 1-33.
26. Vaughn, P. P.; Blough, N. V. *Environ. Sci. Technol.* **1998**, *32*, 2947-2953.
27. Mopper, K.; Zhou, X. *Science* **1990**, *250*, 661-664.
28. Zepp, R. G.; Faust, B. C.; Hoigne, J. *Environ. Sci. Technol.* **1992**, *26*.
29. Voelker, B. M.; Morel, F. M. M.; Sulzberger, B. *Environ. Sci. Technol.* **1997**, *31*, 1004-1011.
30. Southworth, B.; Voelker, B. M. unpublished data.
31. Miles, C. J.; Brezonik, P. L. *Environ. Sci. Technol.* **1981**, *15*, 1089-1095.

32. Faust, B. C.; Hoigne, J. *Atmos. Environ.* **1990**, *24A*, 79-89.
33. Hobbs, G. C.; Abbot, J. J. *Wood Chem. Tech.* **1994**, *14*, 195-225.
34. Gierer, J.; Jansbo, K. *J. Wood Chem. Technol.* **1993**, *13*, 561-581.
35. Gierer, J. *Holzforschung* **1997**, *51*, 34-46.
36. Gierer, J. *Lignin: Historical, Biological, and Materials Perspectives*; Glasser, W. G., Northey, R. A. and Schultz, T. P., Ed.; ACS Symposium Series: Washington, DC, 2000; Vol. 742.
37. Chirat, C.; Lachemal, D. *Holzforschung* **1997**, *51*, 147-154.
38. Ragnar, M.; Eriksson, T.; Reitberger, T. *Holzforschung* **1999**, *53*, 292-298.
39. Staehelin, J.; Hoigne, J. *Environ. Sci. Technol.* **1985**, *19*, 1206-1213.
40. Hoigne, J.; Bader, H. *Water. Res.* **1976**, *10*, 337-386.
41. Hoigne, J. *The Handbook of Environmental Chemistry V5. Part C: Quality and Treatment of Drinking Water II*; Hrubec, J., Ed.; Springer-Verlag: Heidelberg, 1998.
42. Gagnon, G. A.; Booth, S. D. J.; Peldszus, S.; Mutti, D.; Smith, F.; Huck, P. M. *J. Am. Water Works Assoc.* **1997**, *89*, 88-97.
43. Kuo, C.-Y.; Wang, H.-C.; Krasner, S. W.; Davis, M. K. *Water Disinfection and Natural Organic Matter*; Minear, R. A. and Amy, G. L., Ed.; ACS Symposium Series: Washington, D.C., 1996; Vol. 649.
44. Lanzalunga, O.; Bietti, M. *Photochem. Photobio. B: Biology* **2000**, *56*, 85-108.
45. Tranvik, L. J. *Aquatic Humic Substances: Ecology and Biogeochemistry*; Hessen, D. O. a. T., L. J., Ed.; Springer Verlag: Berlin, 1998, pp 259-283.
46. Buxton, G. V.; Greenstock, C. L.; Helman, W. P.; Ross, A. B. *J. Phys. Chem. Ref. Data* **1988**, *17*, 513-889.
47. Spinks, J. W. T.; Woods, R. J. *An Introduction to Radiation Chemistry*; 3 ed.; John Wiley & Sons: New York, 1990.
48. Cooper, W. J.; Moegling, J. K.; Kieber, R. J.; Kiddle, J. J. *Mar. Chem.* **2000**, *70*, 191-200.
49. Bader, H.; Sturzenegger, V.; Hoigne, J. *Wat. Res.* **1988**, *22*, 1109-1115.
50. NDRL-RCDC *Notre Dame Radiation Laboratory Radiation Chemistry Data Center*; NDRL-RCDC, Ed.
51. Miwa, H.; Hiyama, C.; Yamamoto, M. *Journal of Chromatography* **1985**, *321*, 165-174.
52. Albert, D. B.; Martens, C. S. *Marine Chemistry* **1997**, *56*, 27-37.
53. Muellerharvey, I.; Parkes, R. J. *Estuarine Coastal and Shelf Science* **1987**, *25*, 567-579.
54. Wetzel, R. G.; Hatcher, P. G.; Bianchi, T. S. *Limnol. Oceanogr.* **1995**, *40*, 1369-1380.
55. Bertilsson, S.; Bergh, S. *Chemosphere* **1999**, *39*, 2289-2300.
56. Vairavamurthy, A.; Mopper, K. *Analytica Chimica Acta* **1990**, *237*, 215-221.
57. del Giorgio, P. A.; Bird, D. F.; Prairie, Y. T.; Planas, D. *Limnol. Oceanogr.* **1996**, *41*, 783-789.
58. Porter, K. G.; Feig, Y. S. *Limnol. Oceanogr.* **1980**, *25*, 943-948.

59. Loferer-Kröbbacher, M.; Klima, J.; Psenner, R. *Appl. Environ. Microbiol.* **1998**, 64.
60. Zafiriou, O. C.; True, M. B.; Hayon, E. *Photochemistry of Environmental Aquatic Systems*; Zika, R. G. and Cooper, W. J., Ed.; American Chemical Society: Washington, DC, 1987.
61. von Gunten, U.; Hoigne, J. *Environ. Sci. Technol.* **1994**, 28, 1234-1242.
62. True, M. B.; Zafiriou, O. C. *Photochemistry of Environmental Aquatic Systems*; Zika, R. G. and Cooper, W. J., Ed.; American Chemical Society: Washington, DC, 1987; Vol. ACS Symposium Series, pp 106-115.
63. Song, R. G.; Westerhoff, P.; Minear, R. A.; Amy, G. L. *Water Disinfection and Natural Organic Matter*; American Chemical Society: Washington DC, 1996; Vol. ACS Symposium Series 649, pp 298-321.
64. Hoigné, J.; Bader, H. *Ozone Sci. Eng.* **1979**, 1.
65. Peyton, G. R. *Mar. Chem.* **1993**, 41, 91-103.
66. Gopalan, S.; Savage, P. E. *Journal of Physical Chemistry* **1994**, 98, 12646-12652.
67. von Sonntag, C.; Schuchmann, H.-P. *Peroxyl Radicals*; Alfassi, Z. B., Ed.; John Wiley and Sons: New York, 1997.
68. Passi, S.; Picardo, M.; De Luca, C.; Nazzaro-Porro, M.; Rossi, L.; Rotilio, G. *Biochim. Biophys. Acta* **1993**, 1168, 190-198.
69. "I.H.S.S. Standard and Reference Collection," Internation Humic Substances Society, 2001.
70. Barnes, A. R.; Sugden, J. K. *Pharm. Acta Helv.* **1986**, 61, 218-227.
71. Benner, R.; Biddanda, B. *Limnol. Oceanogr.* **1998**, 43, 1373-1378.
72. Obernosterer, I.; Reiner, B.; Herndl, G. J. *Limnol. Oceanogr.* **1999**, 44, 1645-1654.
73. Tranvik, L. J.; Bertilsson, S. *Ecology Lett.* In press.
74. Moran, M. A.; Hodson, R. E. *Limnol. Oceanogr.* **1990**, 35, 1744-1756.
75. Sun, L.; Perdue, E. M.; Meyer, J. L.; Weis, J. *Limnol. Oceanogr.* **1997**, 42, 714-721.
76. Søndergaard, M.; Middelboe, M. *Mar. Ecol. Prog. Ser.* **1995**, 118, 283-294.
77. Ravichandran, M.; Aiken, G. R.; Reddy, M. M.; Ryan, J. N. *Environ. Sci. Technol.* **1998**, 32, 3305-3311.
78. Goldstone, J. V.; Voelker, B. M. unpublished data.

Table 3. 1

$\text{OH}\cdot$ reaction rate constants with SRFA and SRHA as a function of cumulative $\text{OH}\cdot$ exposure. Standard errors derived from the slopes of the lines in Figure 1 are in parentheses.

	$\text{OH}\cdot$ range	SRFA ($10^4 \text{ s}^{-1} (\text{mg C/l})^{-1}$)	SRHA ($10^4 \text{ s}^{-1} (\text{mg C/l})^{-1}$)
Early	(0-2 μM)	3.8 (0.6)	3.8 (1.8)
Middle	(5.2-10.3 μM)	2.5 (0.1)	2.4 (0.2)
Late	(15.5-30.9 μM)	2.7 (0.2)	1.6 (0.07)
All data		2.7 (0.05)	1.9 (0.05)

Table 3. 2

Ratio of mol carboxylic acid produced per mol $\text{OH}\cdot$ for SRFA (14.0 mgC l^{-1}) and SRHA (14.2 mgC l^{-1}). Ratios were calculated by linear regression of the individual experiments for which the average values are show in Figure 2. The numbers in brackets are the standard errors of the slopes calculated during the regression analysis. Corrected formic acid production ratios from SRFA and SRHA were calculated by assuming the maximum formate concentrations represent steady-state concentrations and using calculated $[\text{OH}\cdot]_{ss}$ to obtain formate production rates (see Results). Losses of other acids via reaction with $\text{OH}\cdot$ are less significant compared to formation rates and were neglected.

acid	Acid produced per $\text{OH}\cdot$	
	SRFA	SRHA
formic	0.020 (0.003)	0.045 (0.003)
formic (corrected)	0.031	0.061
acetic	0.013 (0.003)	0.008 (0.001)
malonic	0.017 (0.005)	0.028 (0.008)
oxalic	0.032 (0.005)	0.017 (0.004)
total C	0.17	0.19

Table 3. 3

Initial DOC measured in dilution culture bioassays and bacterial abundance, cellular carbon content and total bacterial carbon at day 6 (final day of the dilution culture bioassay). Mean values of triplicate incubations are given with standard deviations in parentheses.

Material	Treatment	Initial DOC	Bacterial biomass		
		(mg C l ⁻¹)	(cells ml ⁻¹)	(fg C cell ⁻¹)	(mg C l ⁻¹)
SRHA	Control	11.7	1.3x10 ⁷ (0.2x10 ⁷)	82 (34)	1.0 (0.4)
	γ	11.7	1.2x10 ⁷ (0.03x10 ⁷)	91 (8)	1.1 (0.1)
SRFA	Control	14.1	1.3x10 ⁷ (0.05x10 ⁷)	102 (16)	1.2 (0.2)
	γ	14.0	1.1x10 ⁷ (0.2x10 ⁷)	106 (24)	1.1 (0.2)

Figure 3. 1

Mineralization of ^{14}C -formate in 5 mg C l⁻¹SRFA (●) and SRHA (○) solutions saturated with N₂O and O₂ (4:1) and buffered to pH 6 with phosphate. Initial ^{14}C counts are 8000 and 7800 dpm for SRFA and SRHA respectively, approximately 42 nCi (100 nM formate). The error bars are derived from counting statistics.

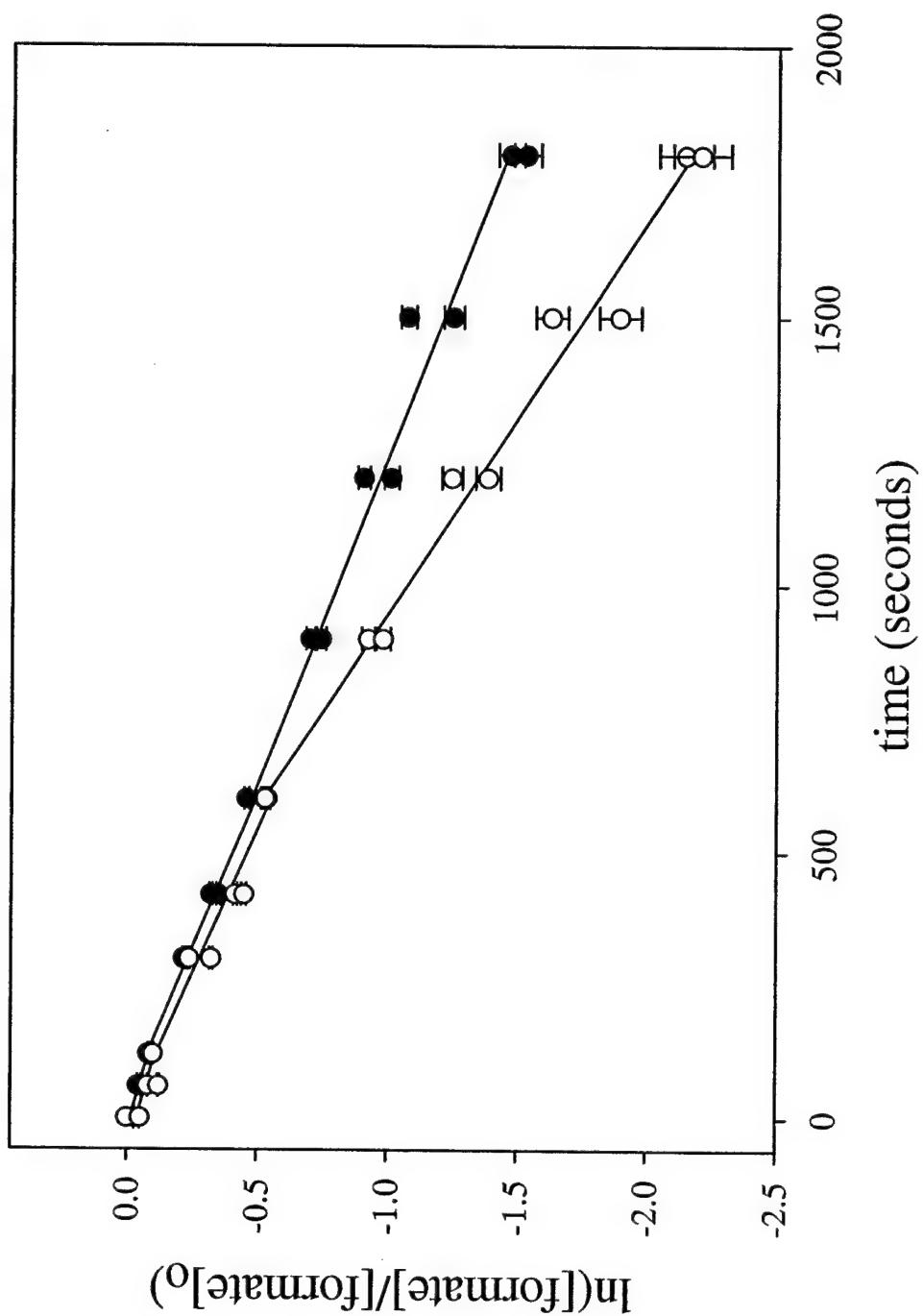


Figure 3.2

Measured formation of acetic (●), formic (▽), malonic (■), and oxalic (◊) acids from the reaction of OH[•] with SRFA (A) and SRHA (B). Error bars represent one standard deviation from the mean values of three separate irradiations. The analytical error for each determination would be smaller than the symbol.

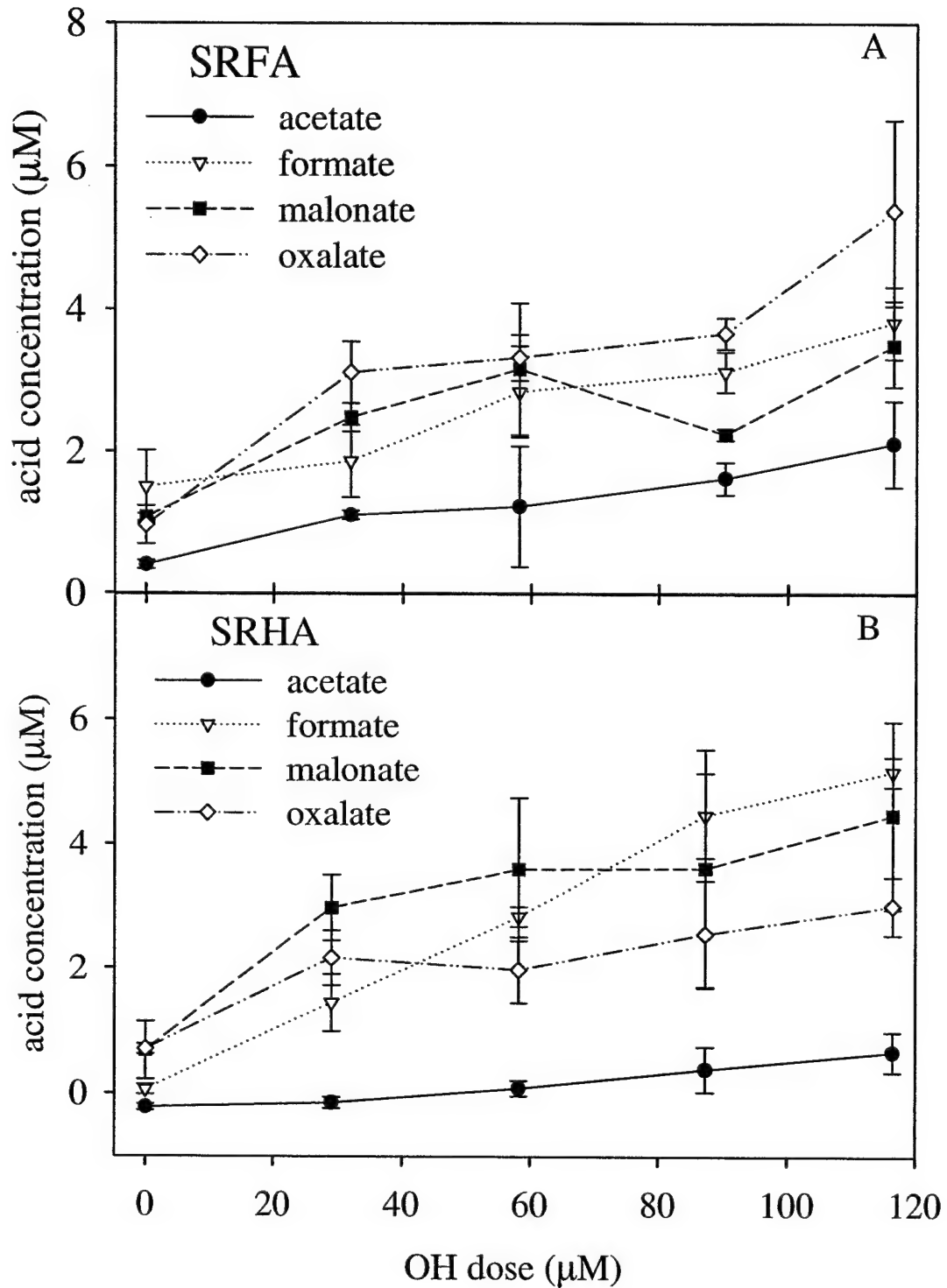


Figure 3. 3

Average bacterial abundance in incubated cultures of GF/F filtered seawater amended 25% (v/v) with Suwannee River Fulvic Acid, SRFA, (A) or Suwannee River Humic Acid, SRHA (B) with (○) or without (●) γ -radiolysis treatment. Initial DOC concentrations were 11.7 mgC l^{-1} for SRHA cultures and 14.1 mgC l^{-1} for SRFA cultures, of which 2.7 mgC l^{-1} was from the seawater inoculum and the rest from the humic substances. Error bars represent the standard deviation of triplicate incubations.

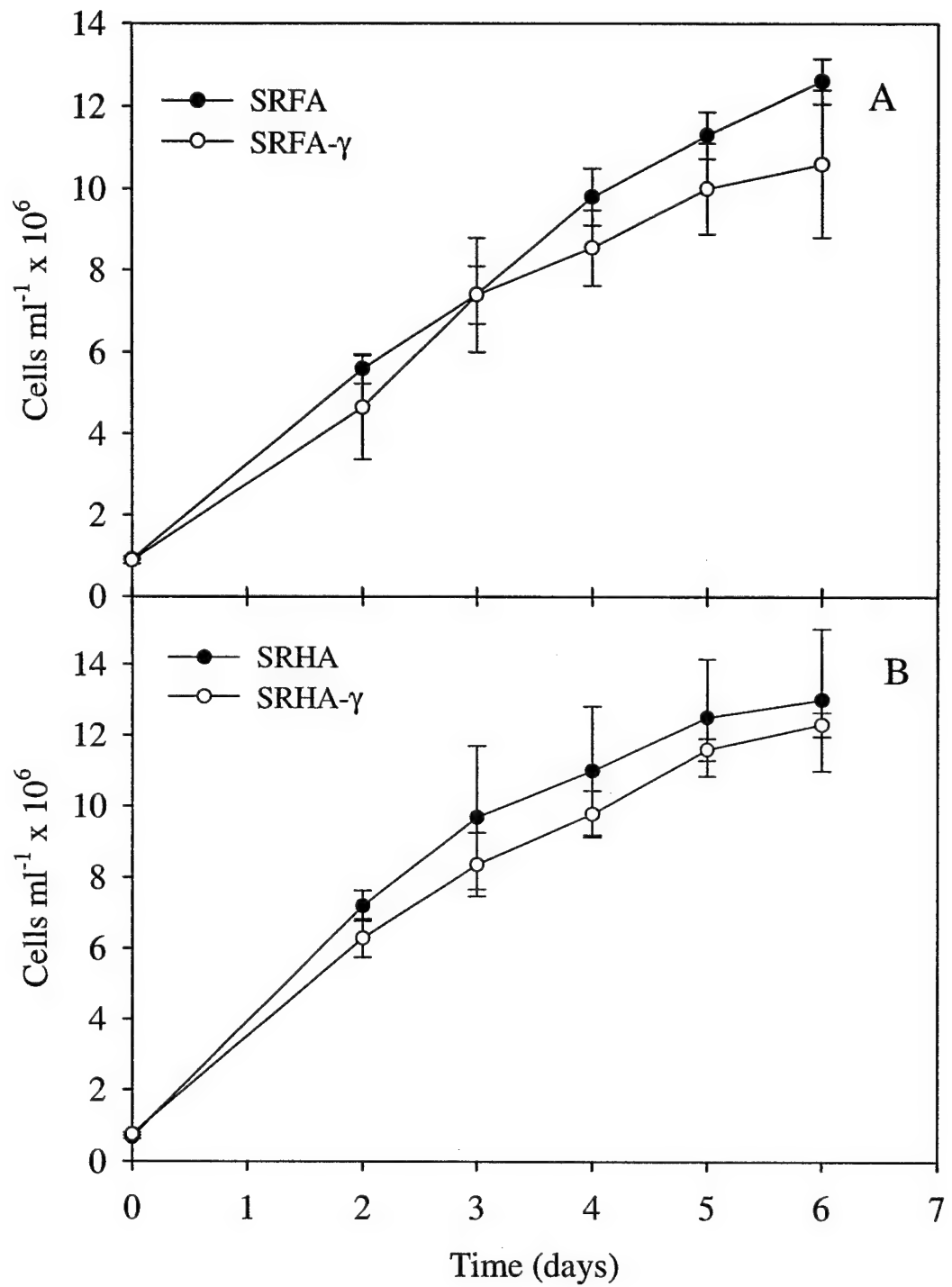


Figure 3. 4

DIC production from irradiated SRFA (5mg C l^{-1} ($430\text{ }\mu\text{M C}$), 2mM phosphate buffer at pH 6), without (\blacktriangledown) and with (\circ) 0.3 M *tert*-butanol as a radical scavenger. Also shown is the lack of production of DIC from 0.3 M *t*-butanol (\bullet). Solid lines are linear fits to all the data. DIC is produced at a similar rate from a lower concentration of SRFA (\square , 0.5 mg C l^{-1} ($43\text{ }\mu\text{M C}$)). The inset shows the complete mineralization of the $43\text{ }\mu\text{M C}$ SRFA solution at very high $\text{OH}\cdot$. The dashed lines represent a theoretical formation rate of 1 mol DIC per 4 mol $\text{OH}\cdot$ until complete mineralization of $43\text{ }\mu\text{M C}$.

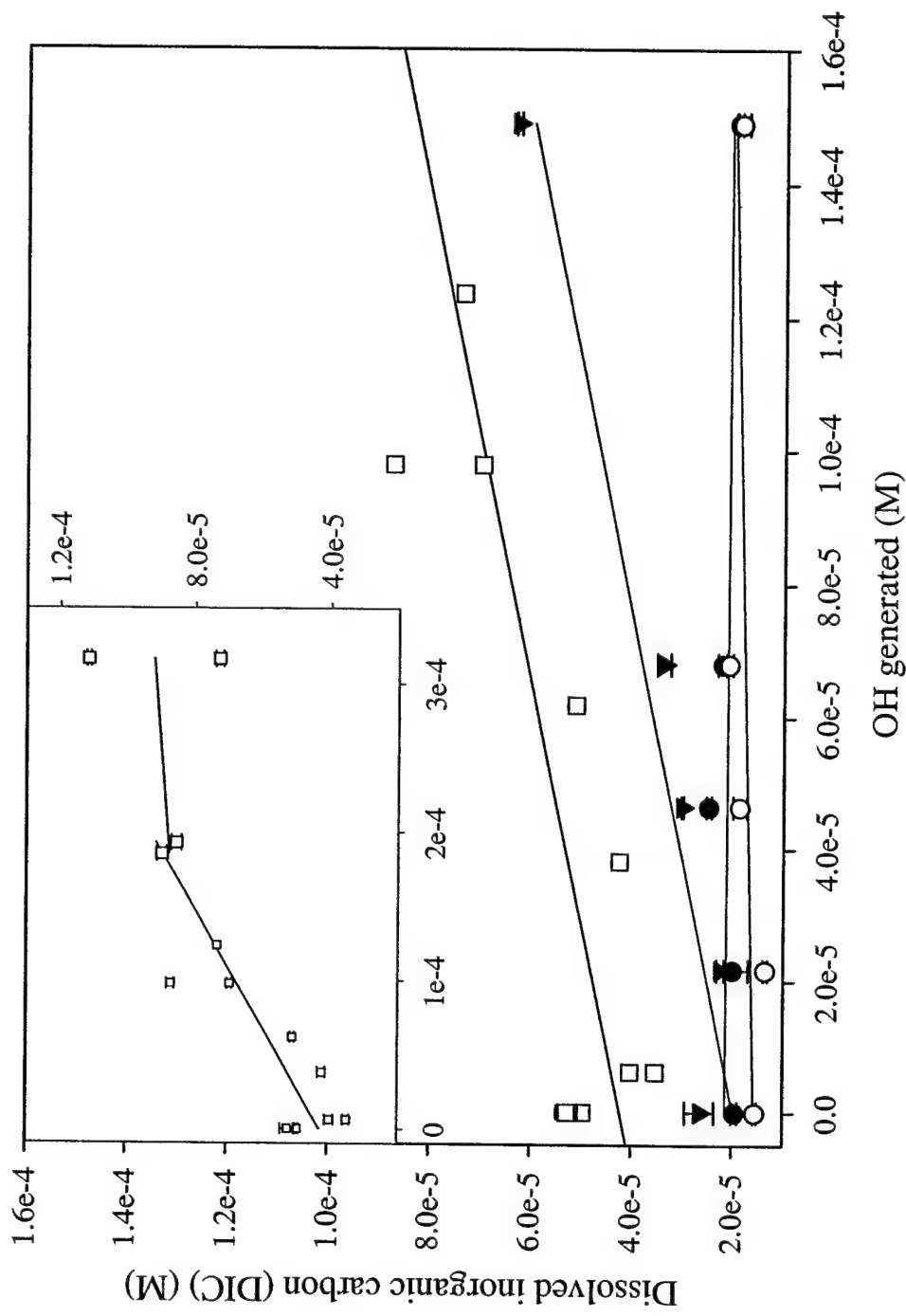


Figure 3. 5

DIC production divided by OH• generated ($\mu\text{M}/\mu\text{M}$) for various treatments of SRFA and SRHA solutions. Unless specified otherwise, all solutions are 5 mg C l^{-1} ($430 \mu\text{M C}$) SRFA, 2 mM pH 6 phosphate buffered, and saturated with both N_2O and O_2 . The first bar (FA avg) is the average of 3 different SRFA irradiations, with the error bar as the 95% confidence limit. Other error bars represent one standard deviation of the linear fits to the data.

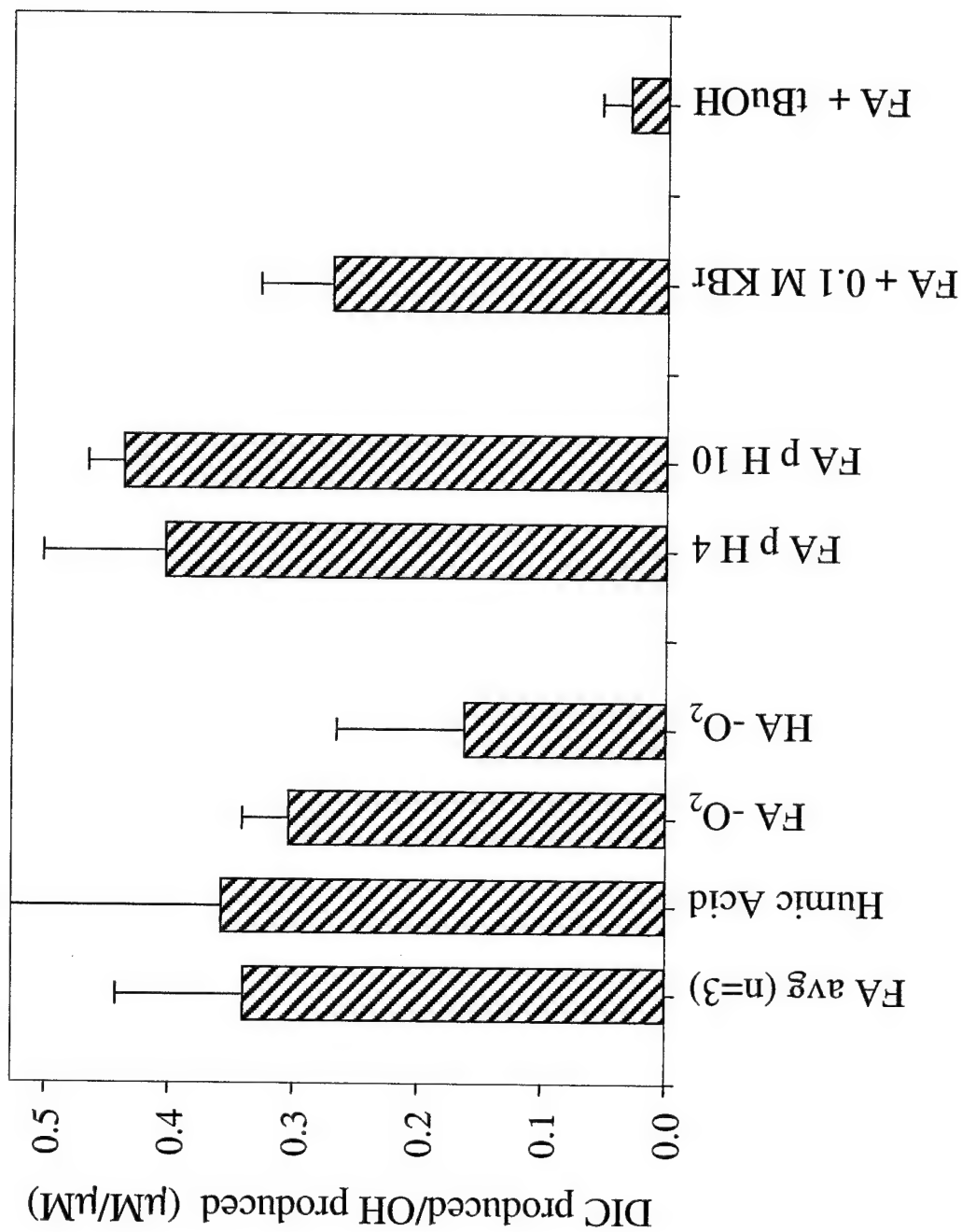
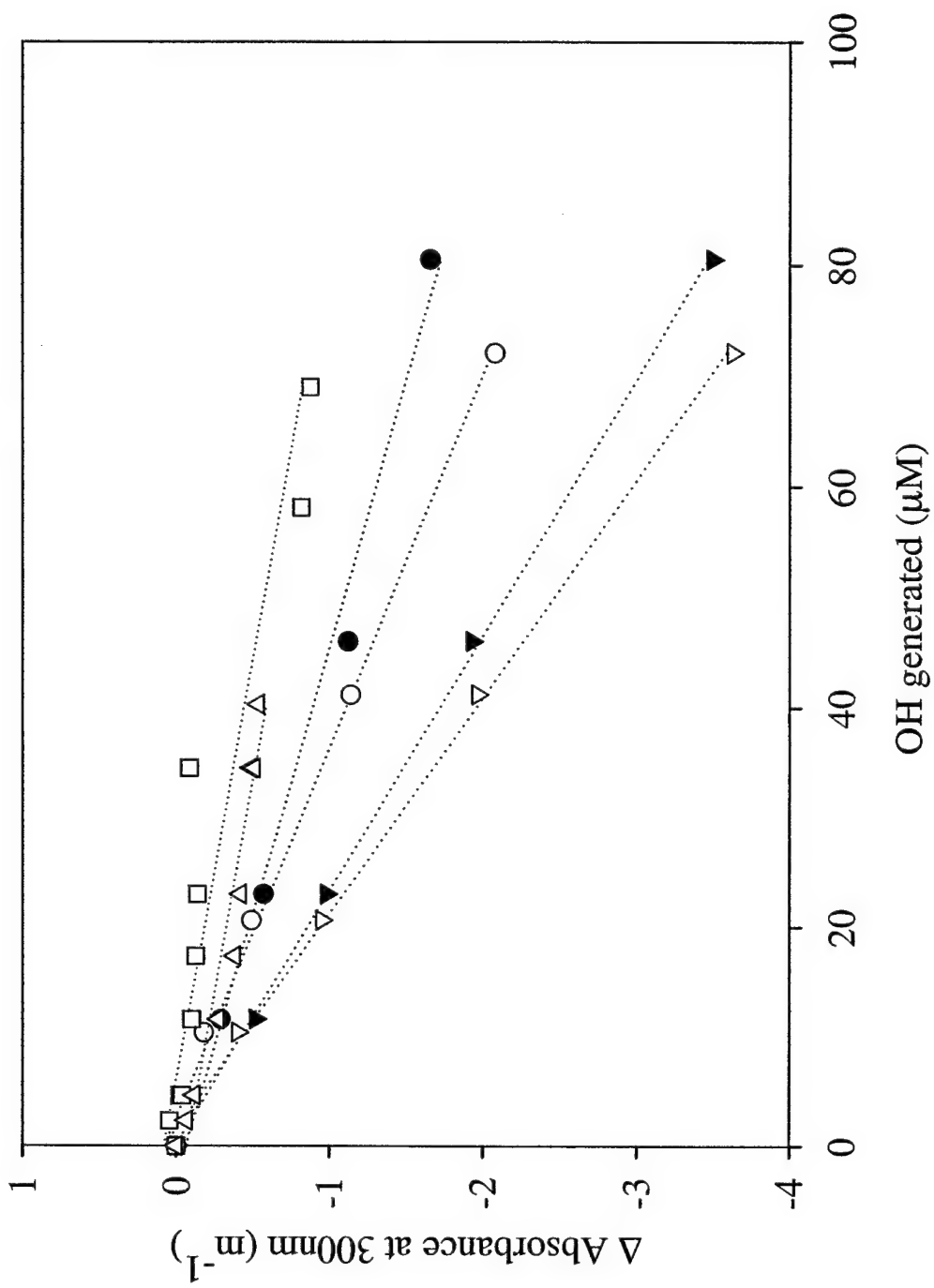


Figure 3. 6

Bleaching of SRFA at 300 nm with (○) and without (●) oxygen, SRHA solutions with (▽) and without (▼) oxygen, DOC-free seawater amended with 5 mg C l⁻¹ (430 μM C) SRFA prior to irradiation and saturated with N₂O/O₂ (□), and a coastal seawater sample from Delaware Bay saturated with N₂O/O₂ (Δ). All SRFA and SRHA solutions are 5 mg C l⁻¹ (430 μM C), 2 mM pH 6 phosphate buffer and saturated with N₂O or N₂O/O₂ as noted in the Methods. The dotted lines are linear fits (all r² >0.88).



CHAPTER 4:

A MULTICOMPONENT MODEL OF CDOM PHOTOBLEACHING

Abstract

Light absorption by the chromophore-containing constituents of dissolved organic matter (CDOM) plays a number of roles in aquatic systems, including both control of the underwater light field and the initiation of many photochemical reactions. We have developed a multicomponent model describing the effects of monochromatic UV and visible radiation on the optical absorption spectra of CDOM in a Suwannee River fulvic acid standard (SRFA). This model used a constrained minimization technique to fit exponentially bleaching independent spectral components to the observed bleaching behavior of SRFA under monochromatic irradiation. Bleaching spectra calculated from the components derived from these fits have been compared to the bleaching behavior of SRFA under polychromatic irradiation ($\lambda > 320\text{nm}$). The calculated spectra underpredict the bleaching at longer irradiation times, but reproduce the broadband photobleaching behavior very well at times < 48 hours.

Introduction

Light absorption by the chromophore-containing constituents of dissolved organic matter plays a number of roles in aquatic systems. Absorption of ultraviolet wavelengths has important ecological consequences (1,2), and the transformation of UV and visible wavelengths to heat can influence the thermal structure of aquatic systems (3). Another significant process is the formation of many primary and secondary photoproducts, such as dissolved inorganic carbon (4), carbon monoxide (5), low molecular weight carbonyl compounds (6), and various reactive oxygen species (7,8). Light absorption also leads to alterations in the bioavailability of CDOM (1,9-15).

The absorption and fluorescence spectra of CDOM in surface waters have a significant effect on the remote sensing of ocean color and therefore the remote determination of chlorophyll (3,16-20). The optical properties of ocean waters are typically divided into two principal domains: those in which phytoplankton absorption dominates the variable component (Case I) and those in which detritus particles and terrestrially derived CDOM play an important role (Case II; (21)). Case II waters incorporate the majority of coastal regions throughout the globe. Thus, the determination of the component of light absorption due to CDOM is essential to the remote determination of other optical properties, such as chlorophyll absorption.

The various photochemical reactions initiated by light absorption eventually lead to the destruction of the chromophores, and thus to the loss of CDOM light absorption (22-26). The CDOM ‘bleaching’ that ensues causes changes in the rates of photoprocesses such as reemission of light as fluorescence (27-29). In addition, the absorption of light is a necessary precursor to all CDOM-initiated photochemical processes.

Bleaching spectra of marine CDOM have been commonly described at various observation wavelengths, λ_{obs} , by a bi-exponential decay equation (24-26):

$$a_{\lambda_{\text{obs}}}/a_{0,\lambda_{\text{obs}}} = f_r e^{-k_r(\lambda_{\text{obs}}) t} + f_s e^{-k_s(\lambda_{\text{obs}}) t} \quad (1),$$

where $a_\lambda/a_{0,\lambda}$ is the normalized absorption at wavelength λ_{obs} , and f_r and f_s are amplitude factors corresponding to wavelength-specific exponential decay functions, $k_r(\lambda_{\text{obs}})$ and $k_s(\lambda_{\text{obs}})$, that describe the rapid (f_r, k_r) and slow (f_s, k_s) parts of the total decay at that wavelength. Attempts to replace bi-exponential bleaching functions with simple exponential terms tend to underpredict the early, fast bleaching phase, and overpredict the slower, longer-term bleaching phase. This empirical bi-exponential description is unsatisfactory for compressing the data into matrices suitable for predictive manipulations because of the non-linearity of these functions.

A larger problem is that in most of the exponential fits described above, each different observation wavelength must be described by a different set of exponential decay functions and amplitude factors. The two exponential amplitude factors cannot be thought of as two chromophores, as chromophore bleaching rate coefficients should be independent of the observation wavelengths. Furthermore, combining the modeling of photochemical O₂ uptake and associated CDOM photobleaching required at least three chromophore pools, suggesting that seawater CDOM photolysis cannot be thought of in terms of only two pools of photoreactive material (30). A possible solution to this problem is the description of CDOM absorption spectra as multiple chromophores with narrow absorption bands. A problem with this theoretical description of CDOM spectra is the bleaching of absorption at wavelengths far from the irradiation wavelengths ('off axis') observed during monochromatic photobleaching experiments (31).

A description of the 'off-axis' bleaching due to monochromatic irradiation requires the invocation of different mechanisms. Chromophores that have broad or multiple absorption bands, including the irradiation wavelength(s) of photobleaching, would be bleached at wavelengths other than the irradiation wavelengths. The rate of photobleaching of these chromophores at wavelengths away from the irradiation wavelength would be directly proportional to the rate of light absorption at the irradiation wavelength(s). Clearly, more than two such chromophores would be necessary in order to describe the observed photobleaching behavior. A second possible mechanism is indirect photobleaching of CDOM by photoproduced reactive intermediates such as OH•. This

process is expected to display little wavelength selectivity in bleaching reactions, although there is a wavelength dependence of OH[•] formation from CDOM (32).

A third mechanism that might account for the bleaching at wavelengths away from the irradiation wavelengths is electronic coupling of the absorbing chromophore with another portion of the CDOM (e.g. via energy or charge transfer). One method of describing this situation is to propose ‘inter-chromophore’ interactions (33). These interactions arise from electronic coupling, and are most likely to be large for species that are closely adjacent to each other, and should decrease rapidly with distance. A conformational change, e.g. induced by a pH change, or a chemical disruption that alters the orientation or distance between two interacting species will also alter the magnitude of this electronic coupling. pH-induced changes in absorption and fluorescence spectra of CDOM have been observed for a number of different CDOM sources, although it is not clear that these changes are due to this phenomenon (34,35).

One method of investigating the various possibilities for chromophore behavior is to model the bleaching behavior of CDOM under monochromatic irradiation. By limiting the irradiation wavelengths to a narrow band it is possible to examine the absorption loss at wavelengths that are not irradiated. The different hypotheses explaining off-axis photobleaching (bleaching at wavelengths other than irradiation wavelengths), namely, several independent chromophores; indirect, sensitized photobleaching; or coupled electronic states, might plausibly result in different kinetic behavior. Indirect bleaching caused by OH[•], as noted above and described in Chapters 3 and 5, does not contribute substantially to short-term photobleaching of CDOM. OH[•] may, however, have some effect on the long-term bleaching behavior of freshwater samples (see Chapter 5).

The simplest photochemical hypothesis of photobleaching consists of independent, non-interacting chromophores each bleaching with a constant quantum yield to transparent products (the ‘simple hypothesis’). If CDOM bleaching reactions arise from a *single* excited state (most likely the lowest excited singlet state, S₁), then the quantum yield of bleaching of each independent chromophore (ϕ_i) should be independent of the wavelength of light used to excite the chromophore (the irradiation wavelength,

λ_j). Many other more complicated photochemical reaction pathways are possible. For example, the population in the S_1 excited state might not react to produce a bleached product, but might instead undergo intersystem crossing (ISC) to form triplet states (T_1). It is also possible that charge transfer to solvent (CTTS) states are important parts of photochemical bleaching mechanisms. These mechanisms would not necessarily have the same hypothesized wavelength-independent quantum yields.

The successful application of the ‘simple hypothesis’ to the modeling of spectra of CDOM samples bleached with monochromatic light would argue that simple multicomponent chromophore behavior was the dominant mechanism of photobleaching. In this work, an initial model was developed by loosening the constraints of the ‘simple’ hypothesis. This ‘relaxation’ is performed by allowing the bleaching quantum yield (ϕ_{i,λ_j}) to vary as a function of irradiation wavelength, λ_j (the ‘relaxed model’). By relaxing these constraints, we can still attempt to fit photobleaching data and examine the simple hypothesis. If the simple hypothesis of wavelength-independent quantum yields is a reasonable approximation of chromophore behavior, it should produce a minimum in the solution space of the model fit. Thus the relaxed model should still allow us to investigate the validity of some of the assumptions of the simple hypothesis. We plan to address the simple hypothesis more directly in the future with a more constrained model.

Regardless of the ability of the relaxed model to address the simple hypothesis, the development of a fitting method based on monochromatic bleaching data sets that can be used to successfully reproduce broadband bleaching spectra would be of general utility in the modeling of photochemical phenomena.

Theory

An approach to modeling photo-bleaching rates is possible if CDOM behaves as a mixture of independent chromophores that bleach to uncolored products (i.e. minimal electronic coupling, no significant sensitization by other chromophores, and no intermediate chromophore formation). These are important, non-trivial assumptions. This model may hold true even if the different molecular components are chemically bonded to each other, as long as the chromophores are not electronically coupled and do not

sensitize chromophore destruction through the production of reactive intermediates. An important assumption is that these components bleach to uncolored products, that is, that there is not the production of intermediate products with different bleaching rates. This assumption cannot be readily tested with the model presented here, but it is an issue that should be addressed in future work.

The direct proportionality of bleaching rate with photon absorption rate is derived as follows. The rate of destruction of a chromophore i present at concentration c_i is described by:

$$\frac{dc_i}{dt} = \sum_j \frac{W_{i,\lambda_j} \phi_{i,\lambda_j}}{1000D} \quad (2)$$

where W_{i,λ_j} is the rate of photon absorption of chromophore i ($\text{E}/\text{m}^2\text{day}$), ϕ_{i,λ_j} is the quantum yield of i (moles of i bleached per E of photon absorbed) at wavelength λ_j , D is the depth of the water column, and the factor 1000 converts m^3 to 1. The sum over wavelengths λ_j is the sum over multiple irradiation wavelengths. The observed loss of absorption as a function of time for such a mixture of chromophores can then be derived from the treatments outlined in (36) and (37):

In the presence of a mixture of chromophores, the solution's total absorption a (in m^{-1}) at wavelength λ is given by:

$$a(\lambda) = \alpha_w(\lambda) + \sum \epsilon_i(\lambda) c_i \quad (3)$$

where $\alpha_w(\lambda)$ represents the absorption coefficient of the medium (water), and $\epsilon_i(\lambda)$ is the molar extinction coefficient (in $\text{M}^{-1}\text{m}^{-1}$) of chromophore i . $a(\lambda)$ is easily measured, but this measurement provides no information about the individual chromophores present. If light scattering is insignificant (i.e. under conditions of low turbidity) and if the light beam enters the solution perpendicular to the surface, the attenuation of light intensity with depth z is given by:

$$I_{z,\lambda} = I_{o,\lambda} (e^{-a(\lambda)z}) \quad (4)$$

where $I_{o,\lambda}$ ($\text{E/m}^2 \text{ day}$) is the intensity of light at wavelength λ entering the water and $I_{z,\lambda}$ is the intensity penetrating to depth z . By Beer's Law, for a pathlength dz short enough so that $I_{z+dz,\lambda} \approx I_{z,\lambda}$, the rate of light absorption by chromophore i at wavelength λ_j in this thin slice of solution is given by:

$$dW_{i,\lambda_j} = I_{z,\lambda} \epsilon_i(\lambda) c_i dz \quad (5)$$

The rate of absorption of light of wavelength λ_j by chromophore i , W_{i,λ_j} , for a water column of depth D is obtained by integration (Equation 7, below):

$$W_{i,\lambda_j} = \int_0^D I_{z,\lambda} \epsilon_i(\lambda) c_i dz = I_{o,\lambda} \epsilon_i(\lambda) c_i \int_0^D e^{-a(\lambda)z} dz = \frac{I_{o,\lambda} \epsilon_i(\lambda) c_i}{a(\lambda)} (1 - e^{-a(\lambda)D}) \quad (6)$$

For optically thin solutions ($a(\lambda)D \ll 1$) the above simplifies to

$$W_{i,\lambda_j} = I_{o,\lambda} \epsilon_i(\lambda) c_i D \quad (7)$$

A first-order decay of each chromophore will thus be observed:

$$\frac{dc_i}{dt} = -k'_i c_i \quad (8)$$

where, from Equations 2 and 7,

$$k'_i = \sum_j \frac{I_{o,\lambda_j} \epsilon_i(\lambda_j) \phi_{i,\lambda_j}}{1000} \quad (9)$$

Given an observation wavelength λ and n chromophores, the initial contribution of chromophore i to $a(\lambda)$ is defined as $b_i(\lambda)$ so that

$$b_i(\lambda) = \epsilon_i(\lambda)c_{i,0} \quad (10),$$

and from Equation 4, referenced to water to eliminate the $\alpha_w(\lambda)$ term,

$$a(t=0, \lambda) = \sum_{i=1 \text{ to } n} b_i(\lambda) \quad (11)$$

From Equation 8,

$$c_{i,t} = c_{i,0} e^{-k'_i t} \quad (12)$$

so that

$$a(t, \lambda) = \sum_{i=1 \text{ to } n} b_i(\lambda) e^{-k'_i t} \quad (13)$$

For monochromatic irradiations at wavelength λ_j , as are modeled here,

$$k'_{i,\lambda_j} = k_i I_{0,\lambda_j} \quad (14).$$

The bleaching rate coefficient of the i th component chromophore, k_{i,λ_j} , must be independent of observation wavelength for a given irradiation wavelength, since these photobleaching kinetic constants are directly proportional to the absorption of light at the irradiation wavelength, b_{i,λ_j} , the apparent quantum yield of photobleaching, ϕ_i , and the irradiance at wavelength λ_j , I_{0,λ_j} . For example, a single chromophore absorbing at multiple wavelengths would exhibit the same bleaching rates at different observation wavelengths under monochromatic irradiation.

The simplest hypothesis of photobleaching mechanisms leads to the quantum yield of photobleaching, ϕ_i , being independent of the irradiation wavelength:

$$k_i(\lambda_j) \propto b_{i,\lambda_j} \cdot \phi_i \cdot I_{0,\lambda_j} \quad (15).$$

In the model presented here (the ‘relaxed model’) this constraint is relaxed by allowing the quantum yield to be a function of the irradiation wavelength, such that

$$k_i(\lambda_j) \propto b_{i,\lambda_j} \cdot \phi_{i,\lambda_j} \cdot I_{0,\lambda_j} \quad (16).$$

Methods

Data/Bleaching Samples

Data for this modeling effort was provided by Rossana Del Vecchio and Neil Blough (31). Briefly, monochromatic bleaching spectra were obtained by irradiating several Suwannee River Fulvic Acid (SRFA) samples with monochromatic light. The samples were bleached using five wavelengths between 296 nm and 407 nm corresponding to the maximum emission lines of a high pressure mercury lamp. These wavelengths also span the range of energy considered most effective for photochemical and photobleaching reactions: UV B (280-315 nm) through blue-violet (400-430nm). A monochromator was used to isolate 10 nm band widths. Spectral absorption values are reported as absorption coefficients in units of m^{-1} .

Broadband irradiation experiments were also conducted on the same samples. High pressure xenon arc systems were used to simulate solar radiation, with cutoff filters used to exclude wavelengths below 320 nm and water filters used to exclude infrared radiation (heat) so as to avoid thermal effects.

Bleaching spectra were obtained using a Hewlett Packard HP8452A diode-array spectrophotometer or a Shimadzu 2401-PC spectrophotometer using quartz cuvettes and

referenced to Milli-Q water. Irradiation intensities were determined using both a IL 1700 radiometer and a Licor UW1800 spectroradiometer.

Modeling

All calculations were performed in MATLAB (Mathsoft Corp., Malden, MA.).

Absorption spectra were measured as a function of observation wavelength, irradiation time, and irradiation wavelength and arranged in a matrix **A**. Bleaching spectra as a function of time are arranged such that each column represents a spectrum. Each row is thus a set of absorption values at observation wavelength λ (280 nm – 410 nm in 10 nm intervals) as a function of time. This data set is composed of five different sets of bleaching spectra, with each set being an experiment in which the CDOM sample was bleached with monochromatic light at a different wavelength λ_j (296, 313, 334, 366, 407 nm). Because we are attempting to use the same set of chromophores to describe all the different data sets, we have concatenated the five different experiments. The first subscript on the t 's indicates the time point of the measurement, while the second subscript denotes the different irradiation wavelengths for each monochromatic bleaching experiment. The values after the commas are the observation wavelengths at which the absorption value is measured. Thus $a(t_0,296,280)$ is the initial absorption at time zero (t_0) of the bleaching experiment irradiated with light at 296 nm (λ_j) and observed at 280 nm (λ), and the array has the form:

A=

$a(t_0,296,280)\dots$	$a(t_f,296,280)$	$a(t_0,313,280)$	\dots	$a(t_0,407,280)\dots$	$a(t_f,407,280)$
$a(t_0,296,290)\dots$:	$a(t_0,313,290)$	\dots	$a(t_0,407,290)\dots$:
$a(t_0,296,300)\dots$:	:	\dots	$a(t_0,407,300)\dots$:
:	:	:	\dots	:	:
$a(t_0,296,410)\dots$	$a(t_f,296,410)$	$a(t_0,313,410)$	\dots	$a(t_0,407,410)\dots$	$a(t_f,407,410)$

Two matrices **B** and **P** need to be determined such that **B** times **P** (**B** x **P**) is a good fit to the data matrix, **A**. The matrix **B** contains the spectra of the n chromophores arranged in

columns such that each column is the spectrum of the i th chromophore b_i , where the numbers in parentheses are the observation wavelengths (λ):

B=

$$\begin{bmatrix} b_1(280) & b_2(280) & \dots & b_n(280) \\ b_1(290) & : & & : \\ : & : & & : \\ b_1(410) & b_2(410) & \dots & b_n(410) \end{bmatrix}$$

P is a ‘model’ of the behavior of the spectral components in **B**. We have assumed that each spectral component in **B** behaves independently, that is, that components do not become different absorbing species but instead bleach towards zero independently of each other. We have further approximated that these bleaching experiments were carried out under optically thin conditions. We can thus derive first order decay behavior for each component b_i (see Theory section) so that each b_i has been bleached by a factor of $\exp(-k_{i,\lambda_j} I_{0,\lambda_j} t)$ at time t . For example, the column of **A** corresponding to the spectrum of SRFA bleached with light of intensity I at wavelength 313 nm (I_{313}) at time x is:

$$A(t_{x,313}, \lambda) = b_1(\lambda) \exp(-k_{1,313} I_{313} t_{x,313}) + b_2(\lambda) \exp(-k_{2,313} I_{313} t_{x,313}) + \dots \dots + b_n(\lambda) \exp(-k_{n,313} I_{313} t_{x,313}) \quad (17)$$

Note that in this model, because the irradiance values, I_{λ_j} , are known, we explicitly include them in the exponential term (see Equation 14).

Our model matrix **P** is a description of the bleaching behavior of the chromophores in **B**, which each row representing a different component and each column a different time point of a monochromatic bleaching experiment:

P=

$$\begin{bmatrix} \exp(-k_{1,296}t_{0,296}I_{296}) & \exp(-k_{1,296}t_{f,296}I_{296}) & \exp(-k_{1,313}t_{0,313}I_{313}) & \exp(-k_{1,407}t_{f,407}I_{407}) \\ \exp(-k_{2,296}t_{0,296}I_{296}) & \exp(-k_{2,296}t_{f,296}I_{296}) & \dots & \exp(-k_{2,407}t_{f,407}I_{407}) \\ \exp(-k_{3,296}t_{0,296}I_{296}) & : & \dots & : \\ \vdots & \vdots & \dots & \vdots \\ \exp(-k_{n,296}t_{0,296}I_{296}) & \exp(-k_{n,296}t_{f,296}I_{296}) & \exp(-k_{n,313}t_{0,313}I_{313}) & \exp(-k_{n,407}t_{f,407}I_{407}) \end{bmatrix}$$

Because different experiments used different wavelengths of light to produce the bleaching, we have fit *different* rate constants k_{i,λ_j} (where k_i is the rate constant appropriate to chromophore i at bleaching wavelength λ_j , where λ_j is 296, 313, 334, 366, or 407 nm) for the *same* chromophore set bleached in each experiment. Therefore, our results are expressed in a $n \times 5$ matrix of k_{i,λ_j} 's, representing the 5 different wavelengths of light used in bleaching and the n different chromophores:

$k =$

$$\begin{bmatrix} k_{1,296} & k_{1,313} & \dots & k_{1,407} \\ k_{2,296} & : & & k_{2,407} \\ k_{n,296} & \dots & & k_{n,407} \end{bmatrix}$$

In order to determine these rate constants and the spectra of the independent chromophores, we have set up an algorithm to find the **B** and **P** that gives us the best fit to **A**:

$$\mathbf{A} = \mathbf{B}^* \mathbf{P} \quad (18)$$

- (1) Initial guess at k_{i,λ_j} gives an initial guess at **P**
- (2) Initial guess at **B**
- (3) Calculation of the sum of squared residuals of $\mathbf{A} - \mathbf{B}\mathbf{P}$ as the cost function.
- (4) Iteration to determine a better set of k_{i,λ_j} and **B** using a geometric search algorithm in Matlab (boundary constrained search routine utilizing sequential quadratic programming, fmincon). The search routine was constrained to find only positive values of k_{i,λ_j} and **B**.

An additional constraint held the sum of $b_{i,\lambda}$ less than or equal to the initial $a_{0,\lambda}$. For any irradiation experiment, then, A can be calculated if the spectral characteristics of the light source, I_{0,λ_j} , the irradiation-wavelength dependent bleaching characteristics (product of $\epsilon_{i,\lambda_j} \phi_{i,\lambda_j}$ in Equation 16, that is, k_{i,λ_j}), and the spectrum (**B** matrix) of each chromophore are known. This algorithm does not provide protection against finding local minima (see below).

Broadband reconstruction

The determination of the spectral components and decay rates from the monochromatically bleached SRFA spectra is an exercise in model fitting. That is, model parameters were adjusted according to criteria (defined above) to produce a good match between the model and the observed data. Reconstruction of the broadband bleaching spectra is not a fitting exercise, but instead a calculation produced by applying the experimental parameters of the polychromatic irradiation experiments (time and irradiance) to the model obtained during the monochromatic fitting exercise.

Reconstruction of broadband bleaching spectra was performed by binning the polychromatic irradiance in 10nm wide bins around the monochromatic bleaching wavelength bands, λ_j . The decay rate constant k_{i,λ_j} determined for each component b_i at monochromatic irradiation wavelength λ_j from the monochromatic bleaching experiments was multiplied by the appropriate irradiance value, producing the exponential rate coefficients k_i' from Equation 15. The decay rate coefficients for each component b_i are thus the sum over i of the irradiation-specific rate constants multiplied by the irradiance at each irradiation wavelength λ_j : $\sum_i k_{i,\lambda_j} I_{\lambda_j}$. The spectra were reconstructed by assuming single exponential decay of each independent component i using this decay constant and the times, t_{bb} , from the broadband photobleaching experiment and summing the resulting contributions of each component. Thus, each component i contributes $b_i \exp(-[\sum_i k_{i,\lambda_j} I_{\lambda_j}] t_{bb})$ total absorption at time t_{bb} . These calculated broadband predictions were then compared with the actual broadband bleaching spectra obtained using a 320 nm cutoff filter.

Results

Utilizing the 'relaxed model' of independently varying component spectra, b_i , and irradiation-wavelength-dependent decay constants, k_{i,λ_j} , we have been able to determine the spectra of independent components and the associated decay constants for a series of monochromatic bleaching data sets using the minimization technique described above and included in the Appendix. To examine the possibility of returning local minima as solutions, the algorithm was initiated with different initial values, including minimum (zero) and maximum (maximum absorption at observation wavelength) values of the components and rates. Iteration of the minimization algorithm using previous solutions was also performed. Identical solutions were returned with up to four components. The use of more than four components (5-9), in some cases returned very slightly different solutions for the same number of components.

The component spectra for the monochromatic bleaching of a SRFA solution are shown in **Figure 4.1**. Obviously, different numbers of distinct components can be used to describe all the monochromatic bleaching series. By employing statistical methods we can begin to deal with the empirical questions of how many components are necessary to arrive at a good description of the data and whether or not adding a component improves the fit.

One method of deciding the significant number of spectral components involves the use of a generalized analysis of variance (ANOVA) test of goodness-of-fit. This test is based on the assumption that the population of the dependent variables (the data) is normally distributed around the regression lines. A series of F-tests may be performed after separating the total variation into variation due to the fit and variation due to the deviation from the fit (38). The F-test for significance of fit is a ratio of the mean sum of squares of the model fit to the mean sum of squares of the residual value. It is a test of the null hypothesis that there is not a significant regression. If the computed value of F exceeds the critical value of the F distribution, then the null hypothesis is rejected with a given probability level. In a similar manner, an F-test for the significance of added terms can also be performed, in which the contribution of additional components to the fit can be assessed. Again, the null hypothesis that the added component does not increase the

goodness of fit significantly is rejected if the computed value of F exceeds the critical value of the F-value at a given probability level. The F values for the significance of fit and for the significance of added terms are given in **Tables 4.1** and **4.2**, respectively.

Another measure of the goodness-of-fit, the reduced chi-squared value of the residual, χ_r^2 , is plotted as a function of number of distinct components in **Figure 4.2**. The χ_r^2 is also based on the assumption that the residuals (data-fit) are normally distributed. This measure includes an estimate of analytical uncertainty, in this case approximated as both an absolute uncertainty of $\pm 0.04 \text{ m}^{-1}$ and a relative uncertainty of $\pm 0.4\%$, based both on our experience with this instrumentation and on an estimation of the error in the monochromatic bleaching data. As the χ_r^2 is the root mean squared deviation normalized to the measurement error, if the model is an accurate description of the data, the χ_r^2 will tend towards one. **Figure 4.2** shows that after four components the χ_r^2 does not continue to decrease rapidly, although the minimum value for χ_r^2 is found with six components. As the χ_r^2 appears to approach seven, rather than one, it is likely that our estimation of the analytical uncertainty has been overly optimistic.

The ANOVA tests show that six components supplies the largest F value for goodness of fit, and that adding a seventh component does not significantly increase the fit quality for the SRFA monochromatic bleaching data set. In fact, the fit quality declines very slightly upon addition of an eighth and ninth component. There is no guarantee that, although these are significant fits, these computed components represent the *best* fits (the global minima). The four component fit is also a reasonable choice for a good fit, based on a large F-value for the goodness of fit from **Table 4.1**, and a large reduction in the significance of adding another component from **Table 4.2** (although it is still above the $p < 0.01$ value of significance to add another component). Both the four component fit and the six component fit are show in an expanded view in **Figure 4.3**. The values of the bleaching rate constants for these two different fits are shown in **Table 4.3**.

The multicomponent fits to the monochromatic data share some general characteristics. Each fit contains a single component contributing a large portion of the absorption that has a shape similar to the original SRFA spectrum. This component is

slow bleaching (see b_3 and b_5 in **Table 4.3** for the four and six component fits, respectively). Both the four and the six component models produce excellent fits at all wavelengths in the time courses of absorption loss in each individual monochromatic bleaching experiment (**Figures 4.4 and 4.5**).

The four and six component fit values of rate constants for the monochromatic bleaching experiments are shown in **Table 4.3**. Note again that the quantum yield, ϕ_{i,λ_j} , has not been constrained to be wavelength-independent here. However, by plotting the rate constants, k_{i,λ_j} versus the absorption values of the spectral components at the irradiation wavelengths, the relationship between the rate constants and the absorption values of the spectral components can be investigated. If there is a direct proportionality (a straight line with an intercept of zero) between the rate constants and the calculated component absorption, then the quantum yield is independent of irradiation wavelength. If this analysis is performed (see **Figure 4.6** and **Figure 4.7**), only a subset of the components in each fit appear to have a constant quantum yield. These are b_2 for the four component fit and b_3 and b_6 for the six component fit. Interestingly, component b_2 in the four component fit and b_6 in the six component fit have approximately the same shape and amplitude. The largest component in each set (b_4 and b_5 , respectively, for the four and six component fits) displays a smoothly curving relationship between the absorbance value of the component and the rate.

Broadband reconstruction

The calculation of the monochromatic fits is valuable as a probe of chromophore behavior, as noted above, but is also valuable as a possible applied model of broadband bleaching. Broadband bleaching spectra calculated from the components and rate constants determined from the monochromatic bleaching experiments were used to reconstruct the spectra of a CDOM sample bleached with broadband light ($\lambda_{bb} > 320$ nm). The computed absorption bleaching curves (lines) are shown in **Figures 4.8 and 4.9**, and compared to actual broadband bleaching spectra obtained on the same water samples (circles). The percent residual values ((data-predicted)/data) at each wavelength for increasing numbers of components used to model the broadband bleaching data are

presented in **Figure 4.10**. The summed squared residual values are presented in **Table 4.4**. These residual values suggest that six components provides a good reconstruction of the broadband data. However other numbers of components also provide reasonable reconstructions of the data. This result can be observed in **Figure 4.10** as well: there are few obvious differences in the percent residual values after three components. In fact, one component provides a reasonably good reconstruction of the broadband bleaching data! However, as can be noted by the disagreement between the computed broadband spectra (lines) and observed absorption values (circles) in **Figure 4.8**, and more obviously in **Figure 4.10**, the computed broadband spectra slightly underestimate the bleaching of all wavelengths at long time periods.

Discussion

The utilization of a constrained minimization technique has allowed us to determine multiple sets of spectral components and associated decay rate constants that successfully model the photochemical bleaching behavior of SRFA under monochromatic irradiation. As discussed above, this model includes decay rates that were allowed to vary with irradiation wavelength (k_{i,λ_j}).

Iteration of the model with different initialization points produced slightly different results for both b_i and k_{i,λ_j} . A comparison between the different results indicated that these differences were very slight (a shift of < 10nm in the peak locations of similar components), suggesting that the calculated ‘best-fit’ solutions are reasonably robust. However, it is not currently possible to definitively state that these solutions represent global minima.

The broadband bleaching spectra calculated by the insertion of broadband irradiance values into this multicomponent model match the observed bleaching spectra quite well. The development of a fitting method based on monochromatic bleaching data sets that can be used to successfully reproduce broadband bleaching spectra may be of general utility in the modeling of photochemical phenomena. Although the reconstructed spectra are in excellent agreement with the observed bleaching behavior at short times (< 30 hours), they do not reproduce the observed bleaching behavior at long time periods.

More specifically, the reconstructed spectra bleach more slowly than the observed behavior of the SRFA. Because this model *underestimates* the bleaching due to broadband irradiations, while assuming negligible electronic interactions and sensitized (ROS-mediated) photoreactions, this result suggests that a portion of the photobleaching occurring at longer time scales could be due to these two mechanisms or to another mechanism that performs similarly.

Despite these shortcomings, this multicomponent model does appear to create a reasonable approximation of the time evolution of CDOM photochemical bleaching. A prior model of the photochemical bleaching spectra based on a mono-exponential decay function underestimated the bleaching at all wavelengths and all times (31). The approximation developed here may be useful in the modeling of the alterations to the underwater light field caused by CDOM photobleaching, the development of which is necessary for the accurate assessment of the production of important photochemical products such as carbon monoxide and carbon dioxide.

We can begin to examine the validity of the simple hypothesis by investigating the relationship between the calculated decay constants, k_{λ_j} , and the spectral components, b_i . As discussed above, only a subset of the components in the different calculated fits appear to have a direct proportionality between their decay rate constants and their absorption values. Assuming that these calculated solutions represent true solution minima, this result argues that the simple hypothesis is not the correct description of photobleaching. An interesting result that arises from this analysis, however, is that there may be a (few) components that do behave as ‘simple’ chromophores (i.e. have a wavelength-independent quantum yield and bleach to transparent products), an idea that deserves further investigation.

This model only represents an initial investigation of the photobleaching behavior of CDOM. The ‘relaxed’ constraints included in this model do not constitute a direct test of the ‘simple hypothesis’ of photobleaching. It is also unclear that the solutions determined here represent global minima, and hence the results of graphical analysis of the decay constant-component absorption relationship presented above should be taken

cautiously. In order to fully examine this hypothesis, the full constraints of this conception of photobleaching must be incorporated into a version of this model.

Acknowledgements

Rossana Del Vecchio and Neil Blough provided both the bleaching data and much helpful discussion. David Glover helped greatly with the statistical analysis.

References

1. Zepp, R. G.; Callaghan, T. V.; Erickson, D. J. *J. Photochem. Photobiol. B: Biology* **1998**, *46*, 69-82.
2. Williamson, C. E. *Limnol. Oceanogr.* **1995**, *40*, 386-392.
3. Kirk, J. T. O. *Light and Photosynthesis in Aquatic Ecosystems*; 2 ed.; Cambridge University Press: Cambridge, 1994.
4. Miller, W. L.; Zepp, R. G. *J. Geophys. Res.* **1995**, *22*, 417-420.
5. Zuo, Y.; Jones, R. D. *Naturwissenschaften* **1995**, *82*, 472-474.
6. Mopper, K.; Stahovec, W. L. *Mar. Chem.* **1986**, *19*, 305-321.
7. Cooper, W. J.; Shao, C. W.; Lean, D. R. S.; Gordon, A. S.; Scully, F. E. *Environmental Chemistry of Lakes and Reservoirs*, 1994; Vol. 237, pp 391-422.
8. Blough, N. V.; Zepp, R. G. *Active Oxygen in Chemistry*; Foote, C. S. and Valentine, J. S., Ed.; Chapman and Hall: New York, 1995, pp 280-333.
9. Bertilsson, S.; Allard, B. *Arch. Hydrobiol./Advanc. Limnol.* **1996**, *48*, 133-141.
10. Bertilsson, S.; Tranvik, L. *Limnol. Oceanogr.* **1998**, *43*, 885-895.
11. Anesio, A.; Denward, C. M. T.; Tranvik, L. J.; Granéli, W. *Aquat. Microb. Ecol.* **1999**, *17*, 159-165.
12. Anesio, A.; Theil-Nielsen, J.; Granéli, W. *Microbial Ecol.* **2000**, *40*, 200-208.
13. Tranvik, L.; Kokalj, S. *Aq. Microb. Ecol.* **1998**, *14*, 301-307.
14. Moran, M. A.; Sheldon, W. M.; Zepp, R. G. *Limnology and Oceanography* **2000**, *45*, 1254-1264.
15. Moran, M. A.; Zepp, R. G. *Limnol. Oceanogr.* **1997**, *42*, 1307-1316.
16. Carder, K. L.; Steward, R. G.; Harvey, G. R.; Ortner, P. B. *Limnol. Oceanogr.* **1989**, *34*, 68-81.
17. Twardowski, M. S.; Donaghay, P. L. *Journal of Geophysical Research-Oceans* **2001**, *106*, 2545-2560.
18. Hoge, F. E.; Vodacek, A.; Blough, N. V. *Limnol. Oceanogr.* **1993**, *38*, 1394-1402.
19. Hoge, F. E.; Lyon, P. E. *Applied Optics* **1999**, *38*, 1657-1662.
20. Hoge, F. E.; Wright, C. W.; Lyon, P. E.; Swift, R. N.; Yungel, J. K. *Applied Optics* **1999**, *38*, 7431-7441.
21. Morel, A.; Prieur, L. *Limnol. Oceanogr.* **1977**, *22*, 709-722.
22. Reche, I.; Pace, M. L.; Cole, J. J. *Ecosystems* **2000**, *3*, 419-432.
23. Reche, I.; Pace, M. L.; Cole, J. J. *Biogeochemistry* **1999**, *44*, 259-280.
24. Kouassi, A. M.; Zika, R. G. *Toxicol. Env. Chem.* **1992**, *35*, 195-211.
25. Grzybowski, W. *Chemosphere* **2000**, *40*, 1313-1318.
26. Vodacek, A.; Blough, N. V.; DeGrandpre, M. D.; Peltzer, E. T.; Nelson, R. K. *Limnol. Oceanogr.* **1997**, *42*, 674-686.
27. Kouassi, A. M.; Zika, R. G.; Plane, J. M. C. *Netherl. J. Sea Res.* **1990**, *27*, 33-41.
28. Kramer, C. J. M. *Netherlands J. Sea Res.* **1979**, *13*, 325-329.
29. Hayasi, K.; Tsubota, H.; Sunada, I.; Goda, S.; Yamazaki, H. *Mar. Chem.* **1988**, *25*, 373-381.
30. Andrews, S. S.; Caron, S.; Zafiriou, O. C. *Limnol. Oceanogr.* **2000**, *45*, 267-277.

31. Del Vecchio, R.; Blough, N. V. *Mar. Chem.* submitted.
32. Vaughn, P. P.; Blough, N. V. *Environ. Sci. Technol.* **1998**, *32*, 2947-2953.
33. Korshin, G.; Benjamin, M. M.; Li, C.-W. *Wat. Sci. Tech.* **1999**, *40*, 9-16.
34. Pullin, M. J.; Cabaniss, S. E. *Limnology and Oceanography* **1997**, *42*, 1766-1773.
35. Gennings, C.; Molot, L. A.; Dillon, P. J. *Biogeochemistry* **2001**, *52*, 339-354.
36. Leifer, A. *The kinetics of environmental aquatic photochemistry: theory and practice*; American Chemical Society: Washington, DC, 1988.
37. Schwarzenbach, R. P.; Gschwend, P. M.; Imboden, D. M. *Environmental Organic Chemistry*; Wiley: New York, 1993.
38. Davis, J. C. *Statistics and Data Analysis in Geology*; 2nd ed.; John Wiley & Sons: New York, 1986.

Table 4. 1

ANOVA results testing goodness-of-fit for multicomponent fits of monochromatic irradiations of SRFA. The F-test value is a ratio of the variance due to regression and the variance due to deviation. This ratio is taken as a measure of 'goodness-of-fit' and used to determine whether the fit is a significant description of the variation in the data. These values are all significant ($p < 0.01$).

Number of Components	F-test value for goodness of fit SRFA
1	15561
2	15874
3	24235
4	35165
5	30917
6	37732
7	28997
8	29135
9	24817

Table 4. 2

ANOVA tests of the significance of adding a component to multicomponent fits of monochromatic irradiations of SRFA. All of the significant values ($p < 0.01$) are indicated by a star. The negative F-test values are due to a decrease in the fit quality.

Number of Components	F-test value for increasing the number of components SRFA
1	246.5*
2	163.0*
3	217.5*
4	45.0*
5	76.8*
6	14.0
7	-5.7
8	-5.7
9	

Table 4. 3

The relative bleaching decay constants (in units of hr^{-1} ($\text{mol photons m}^{-2} \text{s}^{-1}$) $^{-1}$) for the best fit to the monochromatic data sets. Also shown are the irradiance values for the SRFA monochromatic bleaching experiments (in $\text{mol photons m}^{-2} \text{s}^{-1} \times 10^{-5}$).

Sample identity	Component number	Bleaching decay constants at monochromatic wavelengths				
		k^{296}	k^{313}	k^{336}	k^{366}	k^{407}
SRFA	b_1	332	1313	1294	751	0
4 components	b_2	16868	7747	26	0	1970
	b_3	106	81	84	975	1671
	b_4	237	87	39	12	0
SRFA	b_1	213	112	98	643	3202
6 components	b_2	681	297	253	513	0
	b_3	0	3795	6709	13160	48
	b_4	0	8420	13780	7	3158
	b_5	174	72	27	5	4
	b_6	7710	3871	54	0	0
Irradiance		2.72	6.60	2.57	7.25	3.68

Table 4. 4

Sum of squared residuals ($\Sigma(\text{data}-\text{model})^2$) for the comparison of calculated broadband bleaching spectra with observed spectra obtained under polychromatic irradiation (>320 nm).

Number of Components	Sum of squared residuals SRFA
1	253
2	263
3	326
4	191
5	176
6	125
7	134
8	220
9	128

Figure 4. 1

Fit components to monochromatic bleaching of 10mg l^{-1} SRFA at different wavelengths.

These components are calculated using a constrained minimization technique.

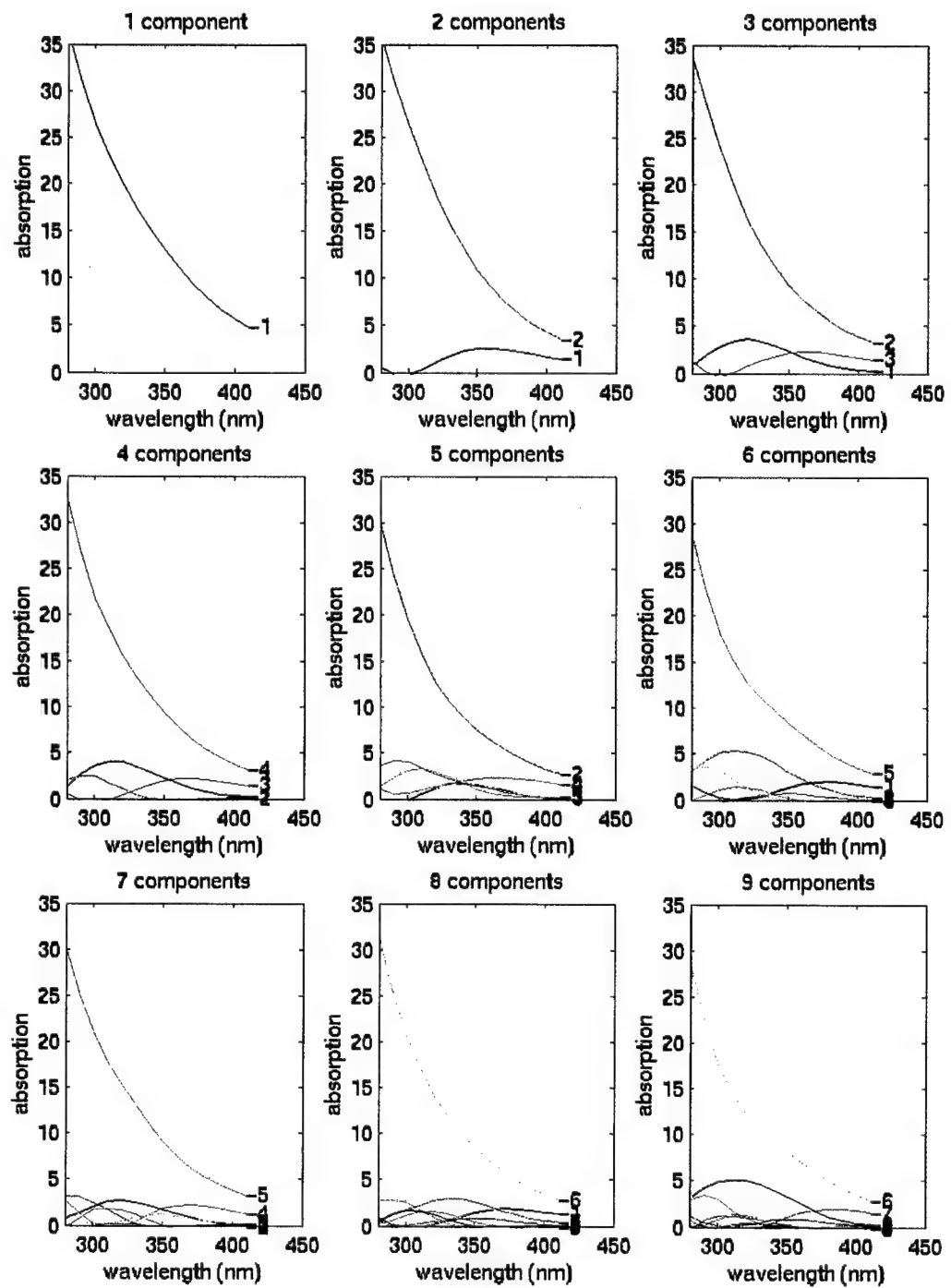


Figure 4. 2

Decrease in the reduced χ^2 for the residual values of the model fit to the data, $\Sigma(A - B^*P)^2/(v_D * \sigma^2)$, where v_D is the degrees of freedom and σ is an estimate of the error in each measurement. This error is approximated as both an absolute uncertainty of ± 0.04 m^{-1} and a relative uncertainty of $\pm 0.4\%$.

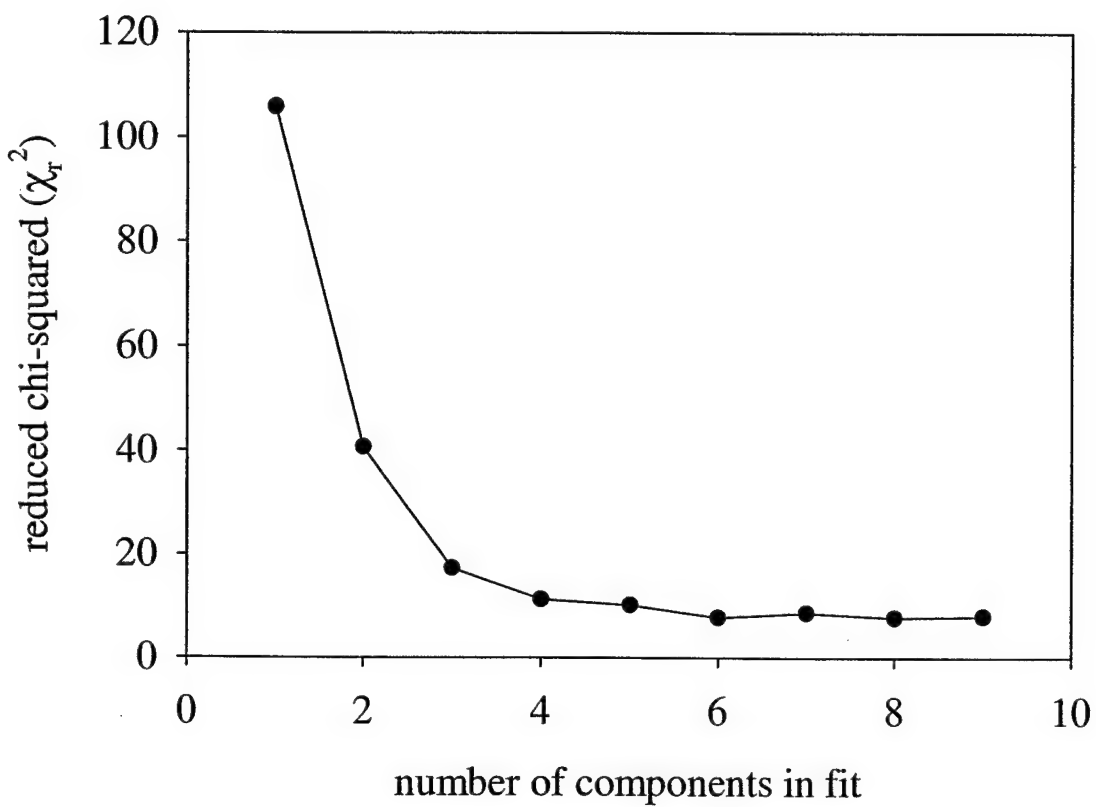


Figure 4.3

Absorbance values of the four (top) and six (bottom) component fit to the monochromatic bleaching data of SRFA. This figure is an expanded view of the four and six component fits from **Figure 4.1**. The rate constants presented in the top part of **Table 4.3** correspond to the four component fit, while those in the bottom half are for the six component fit.

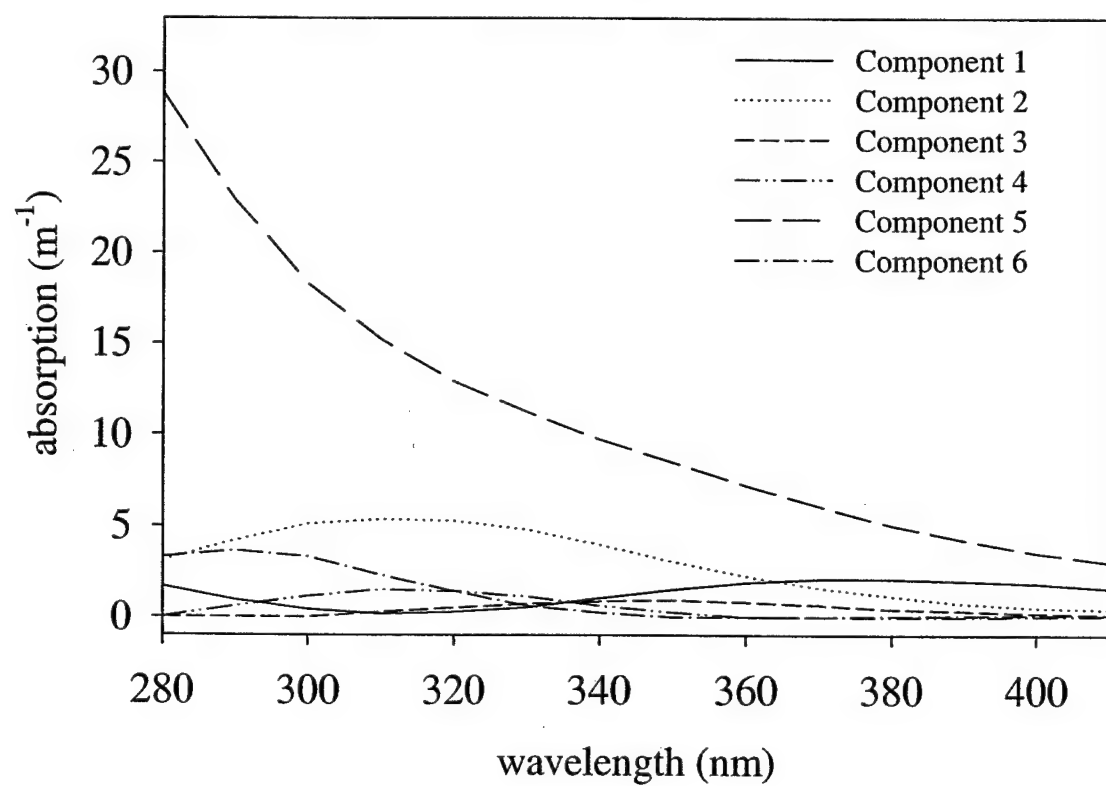
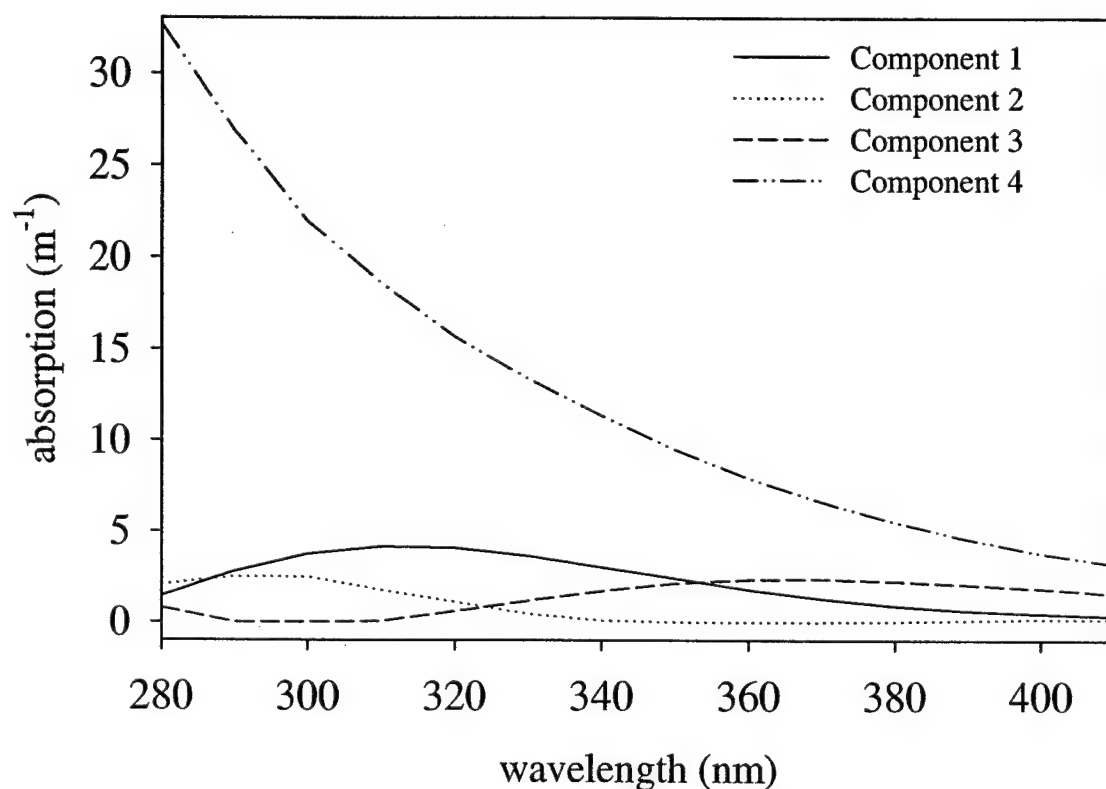


Figure 4. 4

Four component fit to monochromatic bleaching data of 10mg l^{-1} SRFA at different wavelengths. The model results are lines, while the data is shown as points. Only selected wavelengths are shown, with colors corresponding to 300 nm (blue), 320 nm (green), 340 nm (red), 360 nm (cyan), 380 nm (magenta), and 400 nm (yellow). The legends indicate the irradiation wavelengths: A. 296 nm B. 313 nm C. 336 nm D. 366 nm E. 407 nm. Composite residuals (the difference between the model and the data) are provided for all observation and irradiation wavelengths to show that the residuals are all less than 3%.

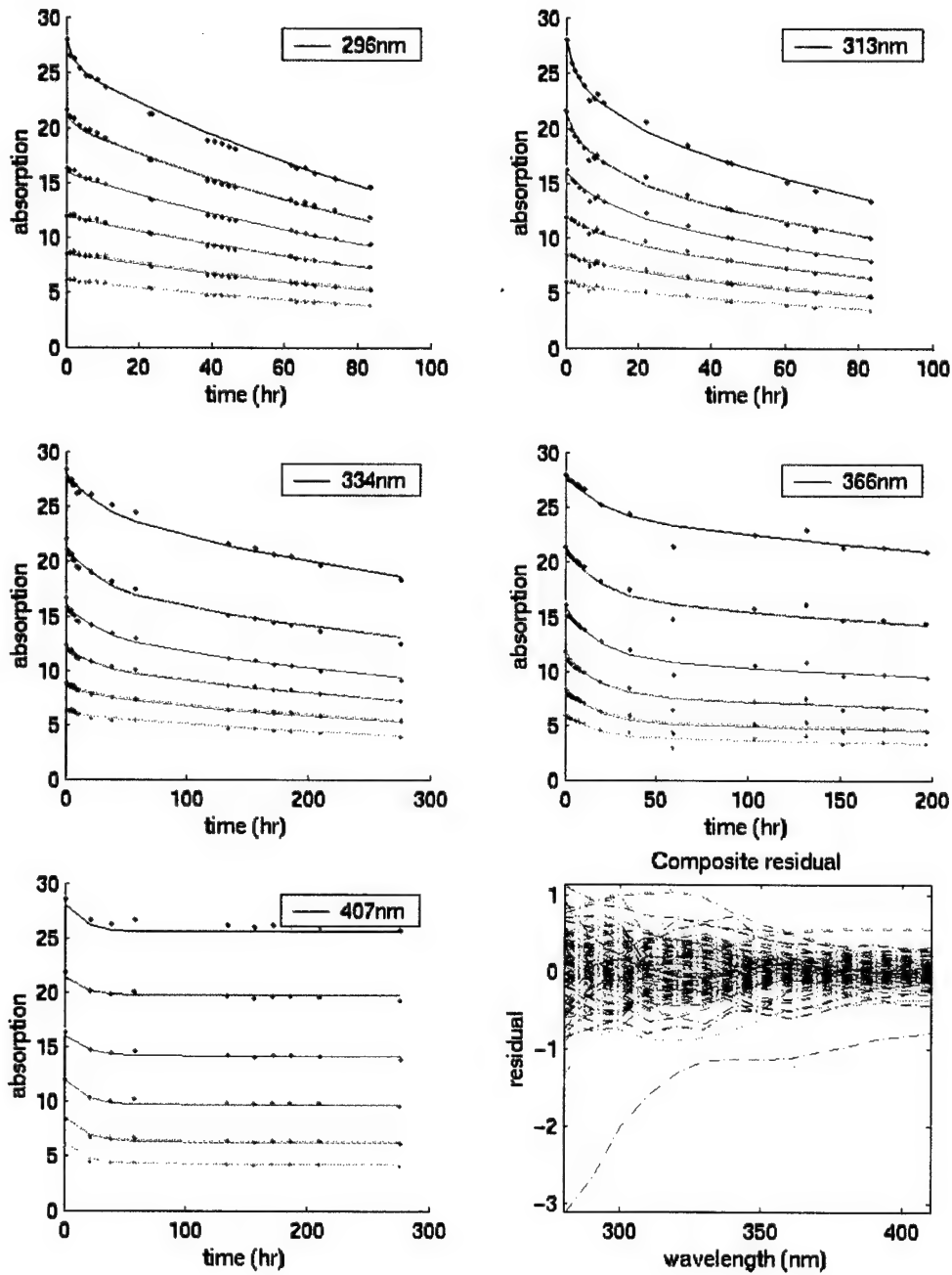


Figure 4.5

Six component fit to monochromatic bleaching data of 10mg l^{-1} SRFA at different wavelengths. The model results are lines, while the data is shown as points. Only selected wavelengths are shown, with colors corresponding to 300 nm (blue), 320 nm (green), 340 nm (red), 360 nm (cyan), 380 nm (magenta), and 400 nm (yellow). The legends indicate the irradiation wavelengths: A. 296 nm B. 313 nm C. 336 nm D. 366 nm E. 407 nm. Composite residuals (the difference between the model and the data) are provided for all observation and irradiation wavelengths to show that the residuals are all less than %.

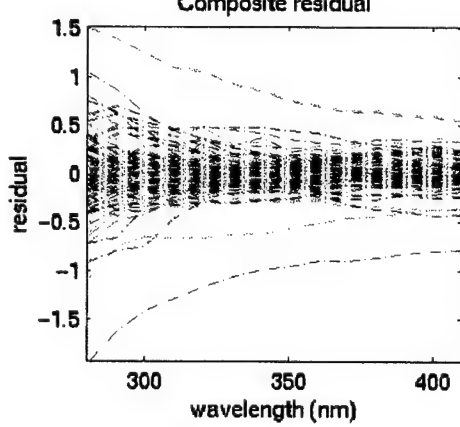
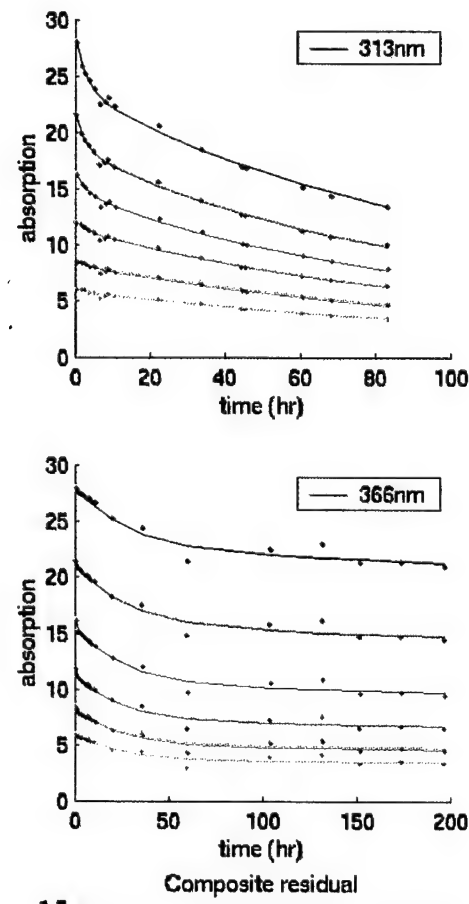
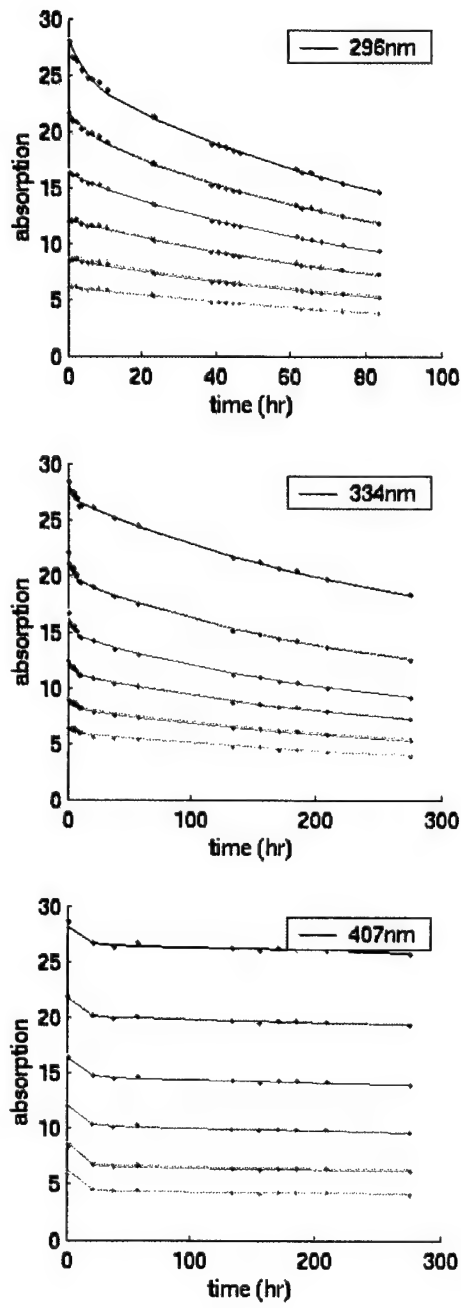


Figure 4. 6

Graphical analysis for the determination of constant quantum yield for the four component fit. The absorbance of each component, b_i , at the irradiation wavelengths is plotted against the wavelength-dependent kinetic rate constants determined by the model, $k_{\lambda j}$. A straight line with intercept near zero would be produced if there is a direct proportionality between the two variables. As can be observed, only one of the components exhibits this behavior (b_2), indicating that this model does not fulfil the requirement of a wavelength-independent quantum yield for each modeled component. The inset shows the zero intercepts. Component b_4 has a significantly non-zero intercept.

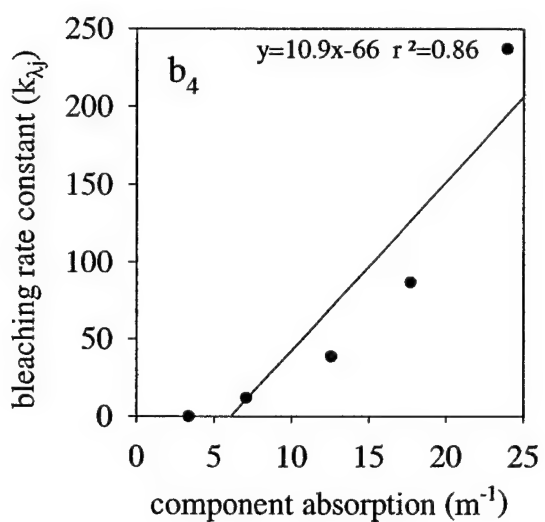
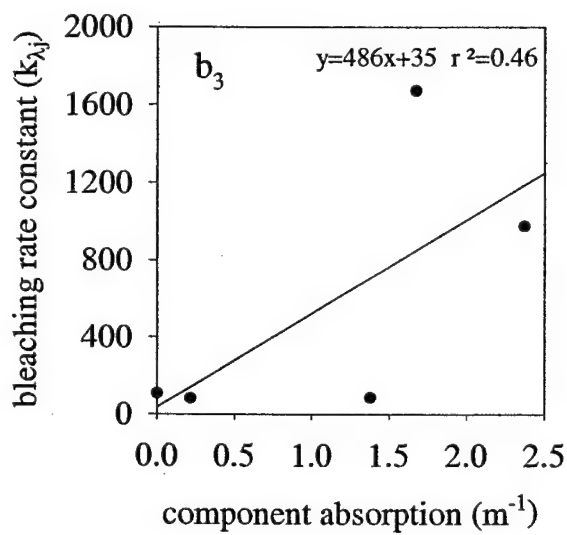
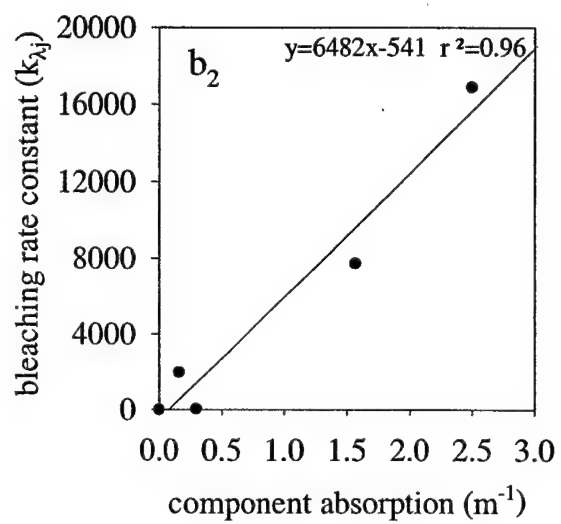
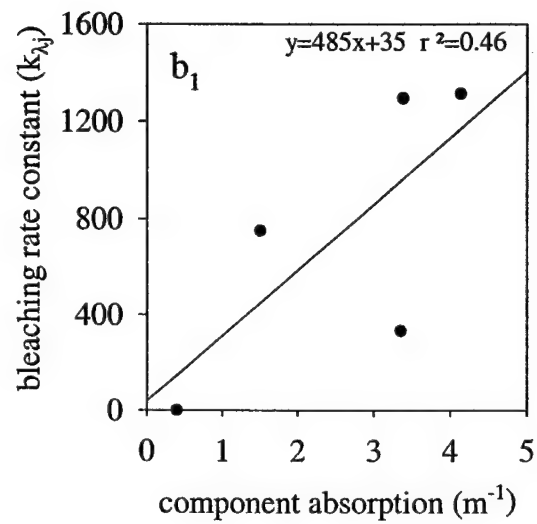


Figure 4. 7

Graphical analysis for the determination of constant quantum yield for the six component fit. The absorbance of each component, b_i , at the irradiation wavelengths is plotted against the wavelength-dependent kinetic rate constants determined by the model, $k_{\lambda j}$. A straight line with intercept near zero would be produced if there is a direct proportionality between the two variables. As can be observed, only two of the components exhibit this behavior (b_3 and b_6), indicating that this model does not fulfil the requirement of a wavelength-independent quantum yield for each modeled component. The inset shows the zero intercepts. Component b_5 has a significantly non-zero intercept.

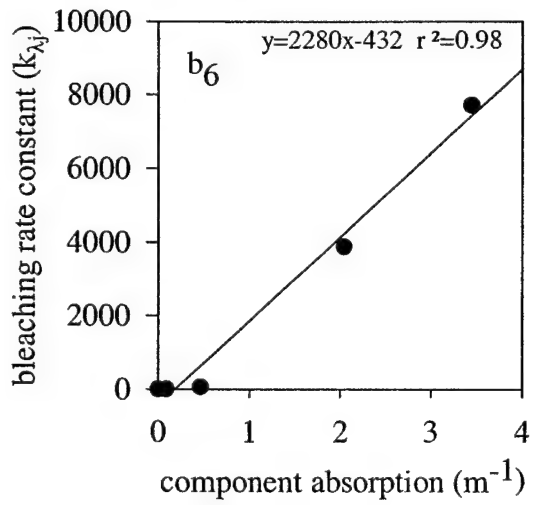
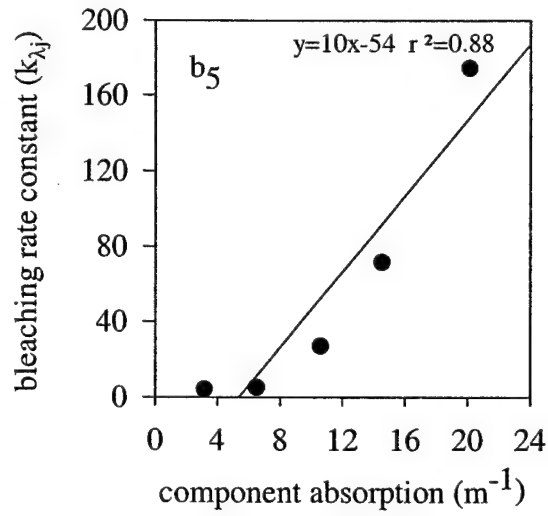
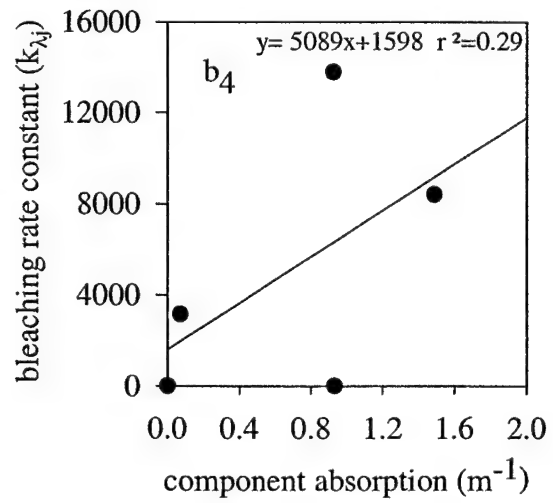
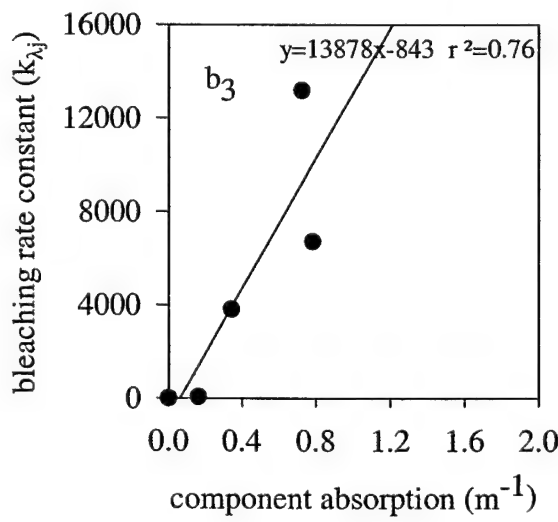
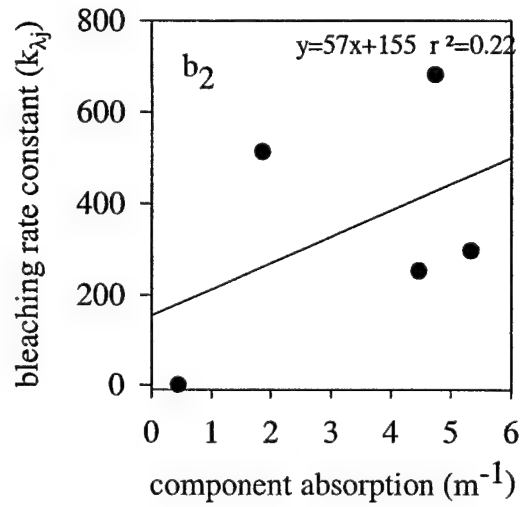
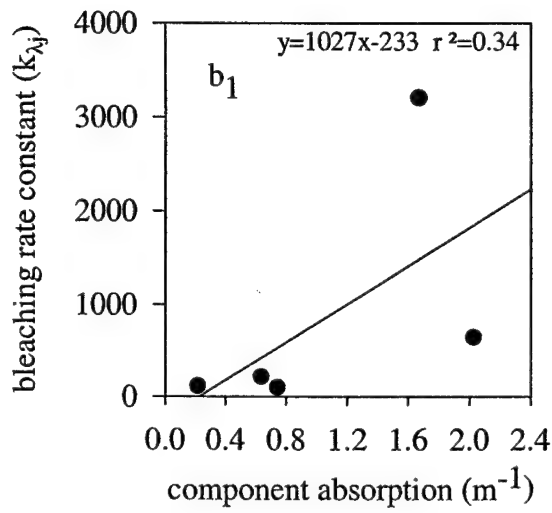


Figure 4.8

Comparison of reconstructed spectra calculated with different numbers of components with observed absorption values for broadband ($\lambda_j > 320$ nm) irradiation of SRFA. The six component fit is the best fit to the monochromatic data, and also provides the best fit to the broadband data. Only selected observation wavelengths are shown, with colors corresponding to 300 nm (blue), 320 nm (green), 340 nm (red), 360 nm (cyan), 380 nm (magenta), and 400 nm (yellow).

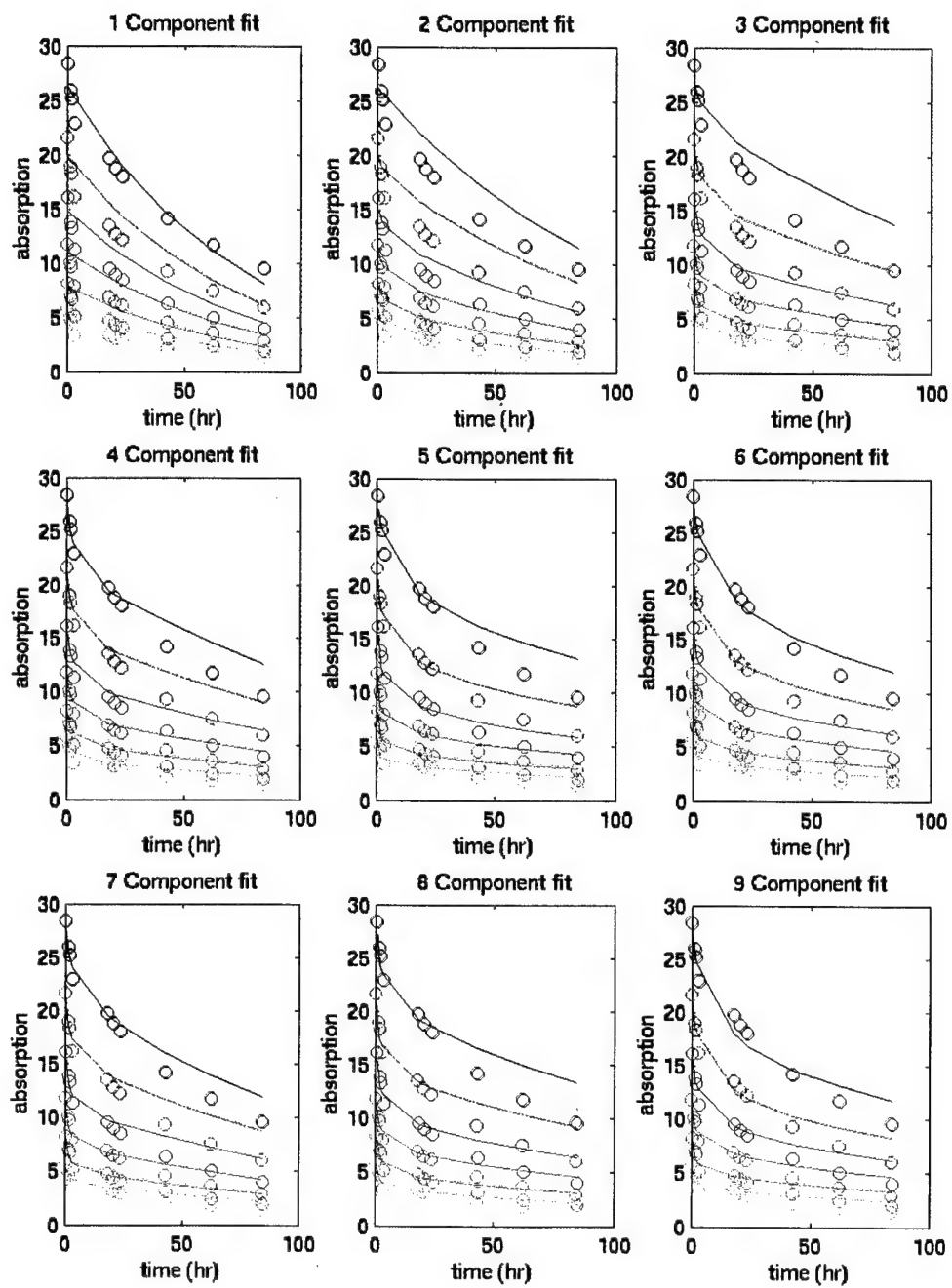


Figure 4.9

Expanded view of the early timepoints for the comparison of the reconstructed spectra calculated with different numbers of components with observed absorption values for broadband ($\lambda_j > 320$ nm) irradiation of SRFA. Only selected observation wavelengths are shown, with colors corresponding to 300 nm (blue), 320 nm (green), 340 nm (red), 360 nm (cyan), 380 nm (magenta), and 400 nm (yellow).

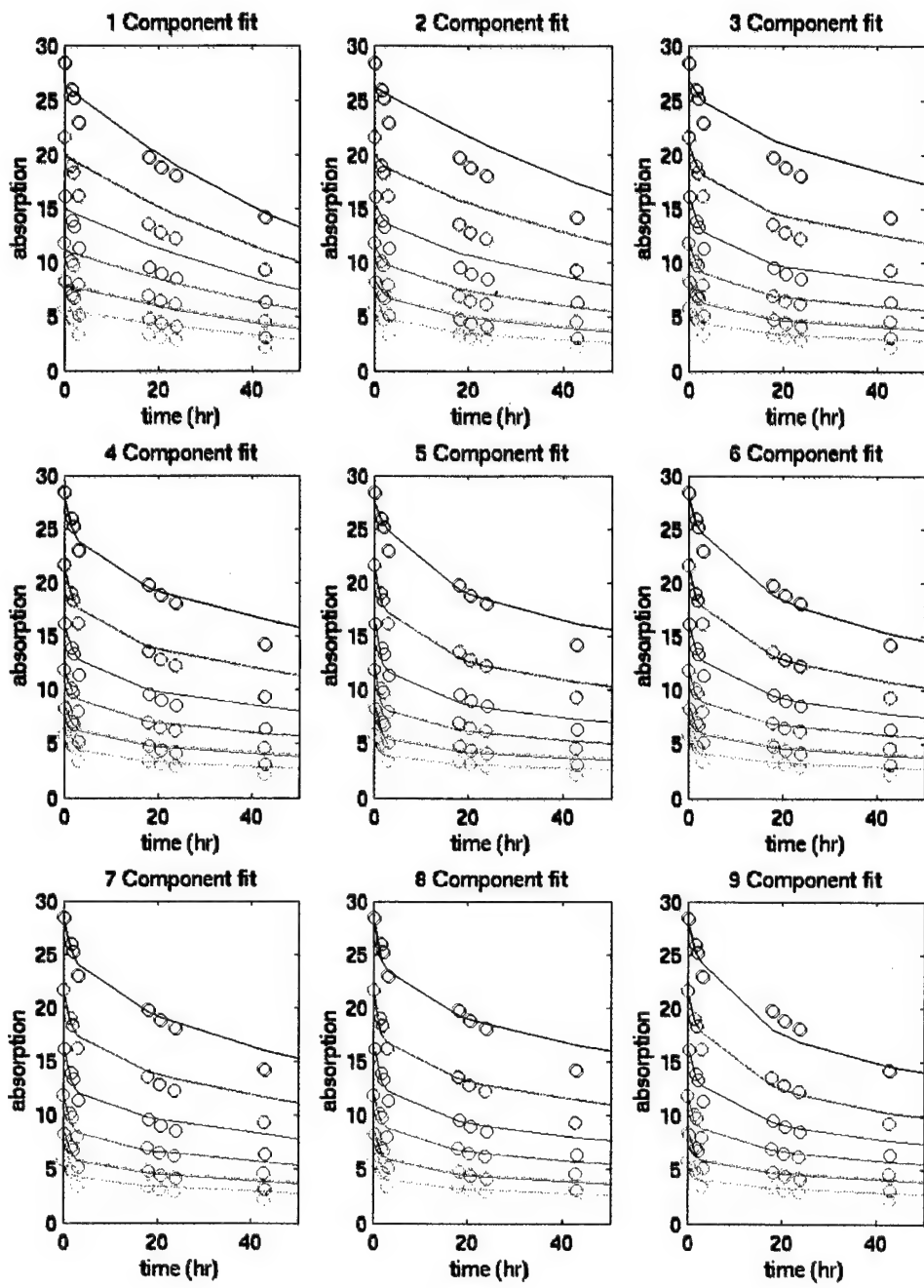
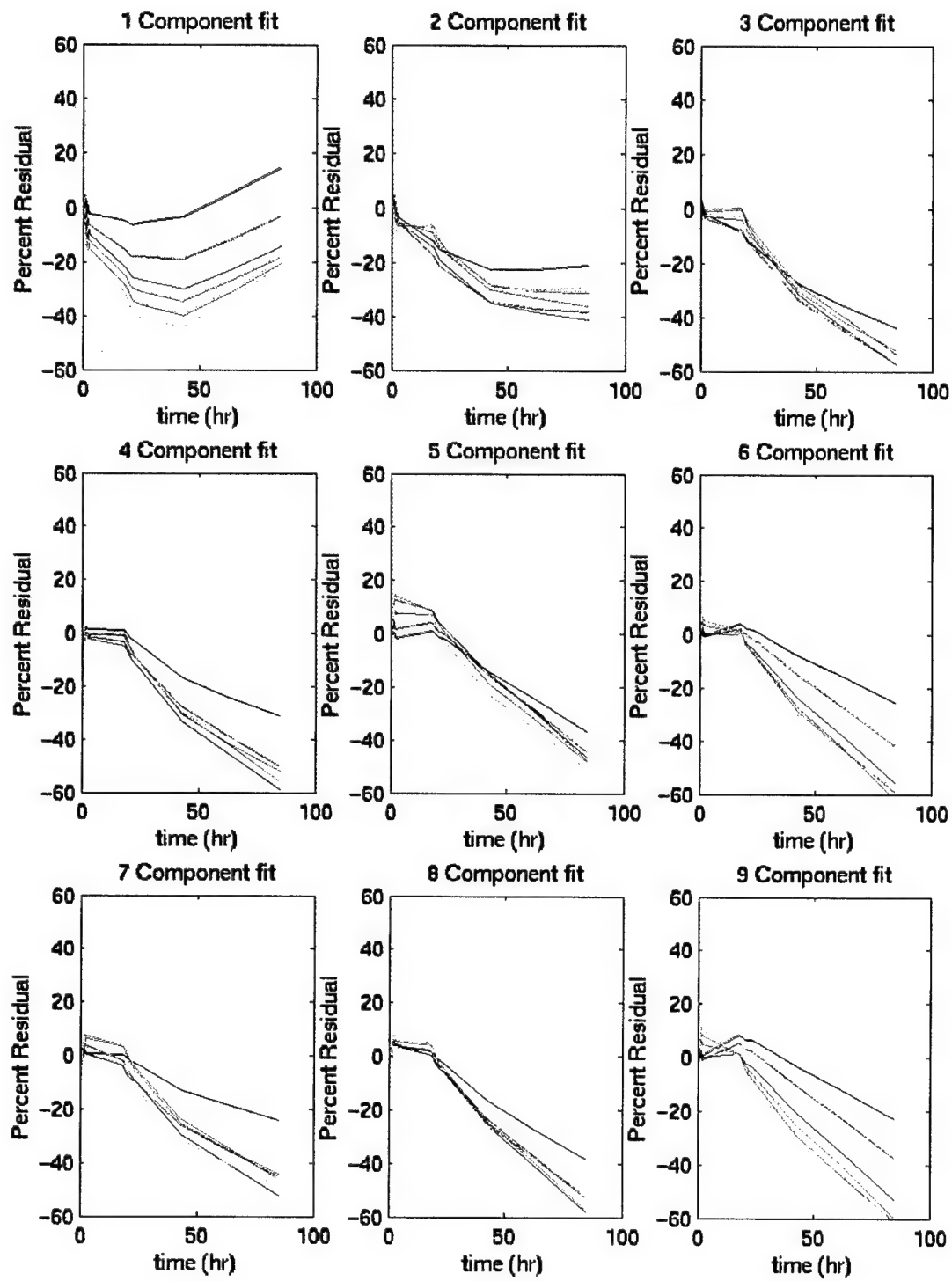


Figure 4. 10

Percent residual ((data-fit)/data) x 100% for the calculation of broadband bleaching spectra of SRFA. Only selected observation wavelengths are shown, with colors corresponding to 300 nm (blue), 320 nm (green), 340 nm (red), 360 nm (cyan), 380 nm (magenta), and 400 nm (yellow). The bleaching spectrum at time ~3.5 hours appears to have a significant analytical error, and hence that time point is not included in these residual plots.



Appendix

This appendix consists of the Matlab m-files (program) for the minimization and plotting routines. The percent sign is used in Matlab to indicate comments, and is reproduced here as well. The three routines presented here are mrunmodel3.m, the initial data management and iteration program, model3fun.m, the minimization function, and statistics.m, the function created to compare modeled broadband spectra with the actual data and to perform the statistical analysis of goodness-of-fit for all the components of the models.

```
% This program is a revised attempt to fit multiple
% chromophores to bleaching spectra.
% Rather than fitting a set of decay constants, k, and
% pseudoinverting an exponential decay term P to
% calculate the components, B, this model
% fits both B and k simultaneously using fmincon
% Requires model function model2fun.m and
% data to be in the form [ 0 T
%                         x A ]
%
% Created 1/7/02

R=input('File name to load:\n','s')      %loading data
files

eval(sprintf('load %s.txt',R));
eval(sprintf('data=%s',R));
tic
[y,z]=size(data);
x=data(2:y,1);                      %first column minus first row
T=data(1,2:z);                      %first row minus first colum
A=data(2:y,2:z);                    %rest of data.txt

q= input('Select maximum number of factors to use: ');
iternum= input('Select number of iterations: ');

Rcomp='srfa2'; % srfa2 is slightly cut (at 407 esp) raw
data
if strcmpi(R,Rcomp)==1
    t1=T(1:21);                  %298nm irr
```

```

t2=T(22:37); %313nm irr
t3=T(38:54); %334nm irrs
t4=T(55:71); %365nm irrs
t5=T(72:81); %407nm irrs
id=4;
end

Rcomp='delaware10';
if strcmpi(R,Rcomp)==1
    t1=T(1:20); %298nm irr
    t2=T(21:38); %313nm irr
    t3=T(39:54); %334nm irrs
    t4=T(55:69); %365nm irrs
    t5=T(70:91); %407nm irrs
    id=2.2;
    factor=[11.5188 9.67588 8.13954 6.84869 5.77028
4.85115 4.06296 3.3965 2.83441 2.36735 1.99281
1.68691];
A=factor*ones(1,z-1).*A;
end

Bff=[];
rchi2ff=[];
koutff=[];
reconall=[];
runt=[];
for n=1:q

t1m=ones(n,1)*t1; t2m=ones(n,1)*t2; t3m=ones(n,1)*t3;
t4m=ones(n,1)*t4;
t5m=ones(n,1)*t5;
m1=length(t1);
m2=length(t2); m3=length(t3); m4=length(t4); m5=length(t5);

irrwav=[298 313 334 366 407]; %irradiation wavelengths

I = 1e-6*ones(n,1)*[27.2 66.0 25.7 72.5 36.8]; %in E m-2 s-
1 (mol photons)

options=optimset('DiffMaxChange',0.0005,'LargeScale','off',
'MaxFunEvals', 2e6, 'MaxIter',5e4,'TolFun',1e-
8,'TolCon',1e-7,'TolX', 1e-7);%, 'Display','iter');

```

```

%upper and lower bounds for k

lb=zeros(y+4,n);
ub=[max(max(A))*ones(y-1,n); 1e5*ones(5,n)];

kin=ub./[n*ones(y-1,n);2e3*ones(5,n)]; 

[kout1,sspout,exitid,iter]=fmincon('model3fun',kin,[],[],[]
,[],lb,ub,'nonlcon1',options,x,T,A,n,I,id);

if id==4
k=I.*kout1(15:19,:)';
elseif id==2.2
k=I.*kout1(13:17,:)';
end

k1in=k(:,1)*ones(1,m1); k2in=k(:,2)*ones(1,m2);
k3in=k(:,3)*ones(1,m3);
k4in=k(:,4)*ones(1,m4); k5in=k(:,5)*ones(1,m5);

p1=[exp(-k1in.*t1m),exp(-k2in.*t2m),exp(-k3in.*t3m),exp(-
k4in.*t4m),exp(-k5in.*t5m)];

if id==4
B1=kout1(1:14,:);
elseif id==2.2
B1=kout1(1:12,:);
end

residual1=(A-B1*p1);

for ii=1:iternum-1

[kout2,sspout,exitid,iter]=fmincon('model3fun',kout1,[],[],[]
,[],lb,ub,'nonlcon1',options,x,T,A,n,I,id);
kout1=kout2;
end

if iternum<2
kout2=kout1; Bf=B1; pf=p1;
end

if id==4
kf=I.*kout2(15:19,:)';

```

```

elseif id==2.2
kf=I.*kout2(13:17,:)';
end

k1fin=kf(:,1)*ones(1,m1); k2fin=kf(:,2)*ones(1,m2);
k3fin=kf(:,3)*ones(1,m3);
k4fin=kf(:,4)*ones(1,m4); k5fin=kf(:,5)*ones(1,m5);
pf=[exp(-k1fin.*t1m),exp(-k2fin.*t2m),exp(-
k3fin.*t3m),exp(-k4fin.*t4m),exp(-k5fin.*t5m)] ;

if id==4
kkf=I.*kout2(15:19,:)';
elseif id==2.2
kkf=I.*kout2(13:17,:)';
end

if id==4
Bf=kout2(1:14,:);
elseif id==2.2
Bf=kout2(1:12,:);
end

residualf=(A-Bf*pf);

runtime=toc/60      %runtime in minutes

chi2=sum(sum(((Bf*pf-A).^2)./((0.04*ones(y-1,z-
1)+0.004*A).^2)));
rchi2=(chi2/((y-1)*(z-1)-(n*(y+4))-1))

Bff=[Bff,Bf];
rchi2ff=[rchi2ff;rchi2];
koutff=[koutff;kkf];
runt=[runt;runtime];
if id==4
save mod3res3 Bff rchi2ff koutff
else
save mod3del2 Bff rchi2ff koutff runt
end

figure(10)
eval(sprintf(' subplot(3,3,%d)',n));

```

```

plot(x,Bf); xlabel('wavelength
(nm)'); ylabel('absorbance');
axis([280 450 0 15]);

eval(sprintf('title('''%d components'''),n));
if n==1
title('1 component');
end

for j=1:n
eval(sprintf('text(410,Bf(y-1,%d),'''- %d'''),j,j));
end

mm=1:n;
figure(11)
plot(mm',rchi2ff,'o-')

end

```

```

function ssp=model3fun(kin,x,T,A,n,I,id)
% This m-file is the minimization routine for fmincon
% in mrunmodel3.m
if id==4 %'srfacut and srfa2
t1=T(1:21); t2=T(22:37); t3=T(38:54); t4=T(55:71);
t5=T(72:81);

elseif id==2.2 %'delaware10'
t1=T(1:20); t2=T(21:38); t3=T(39:54); t4=T(55:69);
t5=T(70:91);
end

[y,z]=size(A);
t1=ones(n,1)*t1; t2=ones(n,1)*t2; t3=ones(n,1)*t3;
t4=ones(n,1)*t4;
t5=ones(n,1)*t5;

m1=length(t1);
m2=length(t2);m3=length(t3);m4=length(t4);m5=length(t5);

if id==4
k=I.*kin(15:19,:)';
elseif id==2.2
k=I.*kin(13:17,:)';
end

k1in=k(:,1)*ones(1,m1); k2in=k(:,2)*ones(1,m2);
k3in=k(:,3)*ones(1,m3);
k4in=k(:,4)*ones(1,m4); k5in=k(:,5)*ones(1,m5);

p=[exp(-k1in.*t1),exp(-k2in.*t2),exp(-k3in.*t3),exp(-
k4in.*t4),exp(-k5in.*t5)];

if id==4
B=kin(1:14,:);
elseif id==2.2
B=kin(1:12,:);
end

ssp=sum(sum((A-B*p).^2));

```

```
function [c,ceq]=nonlcon1(kin,x,T,A,n,I,id);
% Nonlinear inequality and equality constraints on fmincon
% for model3.m

if id==4
c=[sum(kin(1:14,:),2)-37.5933*ones(14,1); -kin(15:19,1)];
elseif id==2.2
c=[sum(kin(1:12,:),2)-37.5933*ones(12,1); -kin(13:17,1)];
end

ceq=[ ];
```

```

% This mfile calculates the general ANOVA for increasing
% numbers of components. Requires Bff, koutff, data A, T,
% and m's.
% This file also calculates the broadband fits for SRFA.
% Thus it requires the data file bbsrfa.txt, which
% is in a form similar to the monochromatic bleaching data:
% 0 0 time
% 1 I Ab
% where 1 is the observation wavelengths, I is the
% irradiances, time is the time points of observations
% and Ab is the data

m=0;

for n=[1,2,4,7,11,16,22,29,37]

eval(sprintf('Bf%d=Bff(:,%d:%d+%d)',m+1,n,n,m));
eval(sprintf('kf%d=koutff(%d:%d+%d,:)',m+1,n,n,m));

m=m+1;
end

SSfm=[];SSrm=[];MSfm=[];MSrm=[];
Ftest=[]; Fitest=[];
SSf=[]; MSi=[];

for n=1:9

I = 1e-6*ones(n,1)*[27.2 66.0 25.7 72.5 36.8];
eval(sprintf('k=I.*kf%d;',n))

m1=length(t1);
m2=length(t2);m3=length(t3);m4=length(t4);m5=length(t5);
k1in=k(:,1)*ones(1,m1); k2in=k(:,2)*ones(1,m2);
k3in=k(:,3)*ones(1,m3);
k4in=k(:,4)*ones(1,m4); k5in=k(:,5)*ones(1,m5);
t1m=ones(n,1)*t1; t2m=ones(n,1)*t2; t3m=ones(n,1)*t3;
t4m=ones(n,1)*t4;
t5m=ones(n,1)*t5;

p=[exp(-k1in.*t1m),exp(-k2in.*t2m),exp(-k3in.*t3m),exp(
-k4in.*t4m),exp(-k5in.*t5m)];

eval(sprintf('fit=Bf%d*p;',n))
if n>1

```

```

SSf0=SSf1;
end
SSf1=sum(sum(((fit).^2)/1134));
%SSf1=sum(sum((fit)).^2)/1092;
SSr1=sum(sum((A-fit).^2))/1134;
%SSr1= sum(sum((A-fit).^2))/1092;

MSf1=SSf1/(19*n);
MSr1=SSr1/(1134-19*n-1);
F=MSf1/MSr1;

if n>1

SSi=SSf1-SSf0;
MSi=SSi/(19*n-19*(n-1));
Fi=MSi/MSr1;
Fitest=[Fitest,Fi];
end

Ftest=[Ftest,F];
SSfm=[SSfm,SSf1];
SSrm=[SSrm,SSr1];
MSfm=[MSfm,MSf1];
MSrm=[MSrm,MSr1];
end

figure(13)

n=1:9;
subplot(3,2,1)
plot(n,SSfm); title('SSf')
subplot(3,2,2)
plot(n,SSrm); title('SSr')
subplot(3,2,3)
plot(n,MSfm); title('MSf')
subplot(3,2,4)
plot(n,MSrm); title('MSr')
subplot(3,2,5)
plot(n,Ftest); title('Ftest')
subplot(3,2,6)
q=1:8;
plot(q,Fitest); title('Fitest')

figure(14)

```

```

for n=1:9
    eval(sprintf('subplot(3,3,%d)',n));
    eval(sprintf('plot(x,Bf%d);',n));
    xlabel('wavelength (nm)');ylabel('absorbance');
    axis([280 450 0 40]);

    eval(sprintf('title('''%d components'''),n));
    if n==1
        title('1 component');
    end

    for j=1:n
        eval(sprintf('text(410,Bf%d(y-1,%d), ''-
%d''',n,j,j));
    end
end

load bbsrfa.txt
dataab=bbsrfa;
[yb,zb]=size(dataab);
    xb=dataab(2:zb,1); %first column minus first
row
    Tb=dataab(1,3:zb); %first row minus first colum
    Ab=dataab(2:zb,3:zb); %normalized irradiation
values
    Ib=dataab(2:zb,2); %irradiation intensities

factor=[37.4772 32.7105 28.5143 24.8415 21.6676
18.8826 16.3506 14.0024 11.8627 10.0228 8.42413
7.03864 5.90144 4.98559]'; %converts from normalized data

Ab=factor*ones(1,zb-2).*Ab;

Ib=3*[6.39e-9 2.18e-7 2.87e-6 4.92e-6 6.73e-6]';
    % E m-2 s-1
    % factor of 3 is a correction
    % for the use of low irradiances
    % in the monochromatic fit
for n=1:9

    eval(sprintf('Abcalc=Bf%d*exp(-((kf%d*Ib)*Tb));',n,n));
    resid=((Ab-Abcalc)./Ab)*100;

figure(15)
eval(sprintf('subplot(3,3,%d)',n));

```

```
plot(Tb,Ab','o'); hold on; plot(Tb,Abcalc');hold off
eval(sprintf('title('''%d Component fit'''),n));
xlabel('time (hr)'); ylabel('Normalized absorbance')

figure(16)
eval(sprintf('subplot(3,3,%d)',n));
plot(Tb,resid')
eval(sprintf('title('''%d Component fit'''),n));
axis([0 100 -100 100])
xlabel('time (hr)'); ylabel('Percent Residual')

end
```

CHAPTER 5.

IRON EFFECTS ON THE PHOTOBLEACHING OF CDOM AND THE PHOTOPRODUCTION OF CO

Abstract

The photochemical transformations of terrestrially-derived chromophoric dissolved organic matter (CDOM) in coastal waters are as yet poorly understood. In particular, the effects of Fe on the photochemical transformations of CDOM are relatively unexplored. Strong spatial and temporal correlations have been observed between dissolved organic carbon (DOC) and Fe concentrations, and dissolved Fe in marine systems is dominated by organic complexes. Photochemical rates of Fe(III) reduction support the notion that Fe-related photochemistry may be important in CDOM photobleaching and photooxidation.

We conducted photobleaching experiments using a filtered xenon arc solar simulator on water samples collected from the Delaware Bay and on solutions of Suwannee River Fulvic Acid (SRFA). Fe was either added as FeCl_3 or rendered photochemically inactive by the addition of desferrioxamine B, a fungal siderophore. No differences in the photobleaching of either optical absorption or of CDOM fluorescence were observed.

We also examined the Fe dependence of the photochemical production of CO in the estuarine samples collected from the Delaware Bay. No systematic effect of Fe or DFOM addition on CO production from the estuarine samples was observed. This is in contrast to an optical buoy experiment conducted in the Sargasso Sea that indicated an ~20% reduction in the photoproduction of CO due to the addition of DFOM.

The results of these experiments suggest that neither indirect (OH^\bullet -mediated) nor direct photochemistry of Fe plays a significant role in photobleaching in estuaries, although OH^\bullet -mediated photobleaching may be of some importance during long-term photobleaching of some CDOM samples.

Introduction

The decomposition of nonliving organic matter, especially terrestrial plant matter, in part results in the formation of dissolved organic polymers that are somewhat resistant to further microbial breakdown and assimilation. A portion of this material is highly colored and is found in both freshwater and coastal marine aquatic systems (1,2). This chromophoric portion of dissolved organic matter (CDOM) plays many important roles in surface waters. CDOM is the dominant absorber of light in the near ultraviolet (UV) region, and often in the visible region as well. Thus, it protects the underwater ecosystem from the deleterious effects of UV (3-5) and contributes substantially to attenuation with depth of photosynthetically active radiation (PAR) (1,5-7), as well as influences the thermal structure of the water column (8). The photochemical decomposition of CDOM leads to the formation of a variety of organic products, including low molecular weight carbonyl compounds, dissolved inorganic carbon (DIC), and carbon monoxide (3,9-16). Photochemical alterations of CDOM also lead to increased microbial availability of what would otherwise be recalcitrant organic carbon, further contributing to the recycling of carbon to DIC as a crucial part of the carbon cycle (12,17-22).

CDOM absorption significantly complicates the application of remote sensing to the determination of chlorophyll in coastal waters (1,23), and renders remote sensing all but useless without extensive *in situ* validation in inland waters (24). Re-emission of absorbed light as fluorescence can also have an impact on remote sensing in coastal waters. CDOM fluorescence has a broad maximum in the 400-550 nm range, potentially impacting the detection of chlorophyll absorption (25,26). Substantial effort has been aimed at determining the contributions of CDOM to remote measurements of color (6,26-30). It has been argued that CDOM in coastal environments contributes far more color to remote observations than has been previously accounted for, thus biasing the interpretation of remote sensing data (6,26,28,31). Understanding the processes that control the absorption characteristics of coastal waters can help in the development of

more globally relevant algorithms for the deconvolution of the components of ocean color.

Photobleaching

Light absorption by CDOM is a necessary precursor to the photochemical reactions that significantly affect aquatic ecosystems. Photoreactions also ultimately lead to the destruction of the chromophores and hence to the loss of absorption and fluorescence ('bleaching' or 'fading'). These photobleaching reactions thus act as a sink for CDOM (28,32). Previous studies of CDOM photobleaching have demonstrated that this sink is significant compared to the mixing residence time of CDOM in both coastal and freshwaters. Absorption bleaching half-lives on the order of days have been found in bottle experiments in sunlight or simulated sunlight (12). Field studies of photobleaching have found that both minimum values of diffuse attenuation coefficients in lakes and significant decreases in CDOM absorption in stratified ocean waters relative to intermediate waters occur during the summer (28,33). Under certain conditions, the seasonal stratification of the water column in marine systems causes CDOM photobleaching to significantly increase the optical transparency of surface seawaters (28,33,34). These bleaching processes are thus important for understanding both the distributions of CDOM and the dynamics of CDOM influences on the aquatic environment.

Fluorescence has been observed to be directly correlated with absorption, and thus could potentially serve as a remote proxy for ocean color (27,29,35). Bleaching of fluorescence has also been observed to occur at significant rates in surface waters (28,36-38). This bleaching is most obvious in lower salinity 'lenses' of riverine or estuarine water in near coastal regions, where the mixing depth is constrained by the salinity gradient (39). Bleaching of absorption is also seen in these cases, and has been used to calculate the *in situ* photobleaching half-life of CDOM in coastal waters (28).

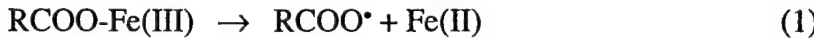
Role of Fe in CDOM photochemistry

A number of studies have indicated that Fe may play an important role in the photochemical reactions of CDOM (9,40-47). Previous investigators have found that Fe catalyzes the photochemical consumption of dissolved oxygen and the photomineralization of CDOM to DIC (9). A more recent study showed that the complexation of Fe by a non-photochemically active ligand reduced the photoproduction rates of DIC and CO from riverine CDOM by 55% and 27%, respectively (48).

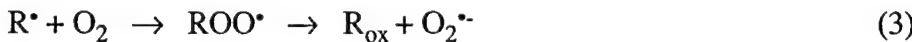
Photochemical reactions of CDOM-Fe complexes may take place either as homogeneous reactions (molecular association) or as heterogeneous reactions (on surfaces). Photochemical reactions occur at the surfaces of iron (hydr)oxide particles at appreciable rates (49). These photoreactions may include all the types of reactions seen in solution, such as the production of dissolved Fe(II) and H₂O₂, and the mineralization of DOM. Due to the formation of Fe and DOM colloids in estuaries, heterogeneous photoreactions may be very significant contributors to Fe photochemistry in these waters. If direct photochemical processes dominate, only the chromophoric portion of the DOM will be broken down, and the rates of photodecomposition and product formation will be proportional to the amount of light absorbed by the CDOM. If indirect photochemical processes are important, significant photodecomposition of non-chromophoric material is also possible. In this case, the rate of light absorption by CDOM will only control CDOM decomposition rates if CDOM photoreactions are the main source of the intermediates involved. There is no reason to assume that the same general mechanism is responsible for different processes of interest. For instance, photobleaching could proceed mostly via direct mechanisms while photomineralization and photoproduction of low molecular weight organic compounds could proceed mostly via indirect mechanisms.

Fe can play a role in both direct and indirect photochemical reactions. Fe-DOM interactions have been investigated, and the association between DOM in both freshwater and marine waters has been established (*vide infra*). Depending on the system, DOM may form surface coatings on iron-oxide surfaces and participate in surface reactions or molecular Fe-DOM complexes may form that react directly in a number of ways. These

reactions could include ligand to metal charge transfer (LMCT) reactions that would produce reduced Fe(II) and oxidized CDOM (Equation 1) and usually lead to photodecarboxylation (Equation 2):



Decarboxylation leads to the formation of a second radical (R^\bullet), most often a carbon-centered radical that then can react further with oxygen, leading to the formation of ROS such as superoxide (O_2^-) and organic peroxides:



The superoxide thus formed may redox cycle with Fe, Cu, or with CDOM itself, eventually forming hydrogen peroxide in an overall 2:1 stoichiometry (40,41,50-52).



In addition to stimulating the photoproduction of DIC, Fe may also play a role in the photoproduction of another form of inorganic carbon, carbon monoxide (CO). Zuo and Jones (1997) found a non-linear correlation between CO photoproduction rates and Fe concentrations in a variety of freshwaters, and were able to increase the photoproduction of CO by adding Fe to a sample from a humic lake (53). Gao and Zepp observed that addition of an iron ligand decreased the rate of CO photoproduction in Satilla River water by up to 27% (48). Pos *et al.* also suggested that transition metals in seawater might increase the photoproduction of radical intermediates that lead to acyl radicals and thence to CO (54).

The photoreduction of Fe(III) to Fe(II) must have an associated oxidation reaction, thus arguing that the rate of CDOM oxidation from Fe-associated mechanisms can be calculated from the rate of Fe(III) reduction. Photo-oxidation rates of CDOM in fulvic acid solutions due to several different mechanisms were calculated to be between $1.1 \times 10^{-10} \text{ Ms}^{-1}$ (dark reduction of Fe(III)) and $2.4 \times 10^{-10} \text{ Ms}^{-1}$ (LMCT surface reactions) for a system (pH 3-5) containing 40 μM crystalline iron oxide and 10 mg/L DOM (40). Previous work in seawater supports the inference that Fe could have a substantial effect on photo-oxidation in coastal waters. High concentrations of dissolved Fe(II) (~1-40 nM)

have been observed in sunlit waters (55-59), and typical H₂O₂ concentrations in these waters are also high (100 nM) (60). The higher Fe(II) steady-state measurements may be due to the measurement of *reducible* Fe, rather than reduced Fe. Regardless, at these concentrations, H₂O₂ is probably the dominant sink of Fe(II). As the rate constant of the reaction of H₂O₂ with Fe(II) is $5 \times 10^4 \text{ M}^{-1} \text{ s}^{-1}$ (61), in order to maintain a steady state concentration of 1 nM Fe(II) in sunlit seawaters (a concentration more commonly found using different types of Fe(II) measurement techniques), something (e.g. an organic ligand) must be oxidized by Fe(III) at a rate of at least $5 \times 10^{-12} \text{ M s}^{-1}$ ($0.018 \mu\text{M hr}^{-1}$) to balance the loss of the Fe(II). If LMCT reactions of organic matter are responsible for all of the reduction of Fe(III), then DOM is being photo-oxidized at this rate. In addition, the production of OH• by the reaction of Fe(II) with H₂O₂ may be as high as $5 \times 10^{-12} \text{ Ms}^{-1}$ based on the calculations above, and photobleaching of CDOM by OH• might be another important contributing mechanism of photooxidation. Rates of total DOC oxidation in seawater are on the order of 10^{-11} - 10^{-10} Ms^{-1} (0.036 - $0.36 \mu\text{M hr}^{-1}$), comparable in magnitude to these calculated oxidation rates (12,62). Additional DOC photo-oxidation reactions may take place on particle surfaces. These photoprocesses are not reflected in dissolved Fe(II) concentrations, as the Fe(II) produced during these photoreactions is most likely not released into solution (63). Photodecomposition may proceed both via direct photochemical reactions, following absorption of photons by CDOM, (60,64-66), or via indirect (sensitized) processes, involving DOM reactions with photochemically generated intermediates such as reactive oxygen species (ROS) (Chapter 3; (60)).

Estuarine processes

All previous studies of Fe effects on CDOM photochemistry have focussed on freshwater samples or extracts. Changes to both Fe and CDOM speciation occur as river water mixes with seawater in estuaries. The transport of terrestrial DOM from rivers through estuaries to the coastal ocean has been observed to be relatively conservative (67-69), although the loss of some fraction (an estimated 20%) has been observed by a number of investigators (70-73). Humic acids may compose the largest fraction of DOM removed by estuarine flocculation. Despite the attention paid to DOM transportation in

estuaries, very few studies have focussed on CDOM. A recent study has found 21% of the CDOM in the Tyne estuary to be removed by adsorption onto suspended sediments (74). On the other hand, CDOM may behave conservatively in some tropical riverine systems, although this conservative behavior appears to be seasonal in the Orinoco River system(30,75).

In contrast to the loss of CDOM observed in some estuarine systems, the production of fluorescent DOM (FDOM) has been observed in several estuaries (37,38,76). This contrasting behavior between the production of FDOM and loss of CDOM seen in a number of different estuaries is very interesting and apparently contradictory, as a linear relationship between DOM fluorescence and absorption has been observed a number of times (27-29).

The speciation and size distribution of Fe also appears to be substantially altered during estuarine mixing (71-73,77-80). In most estuaries studied, riverine Fe appears to coagulate to form colloids upon mixing of river water with seawater in the estuary. This may be due to aggregation of dissolved iron and small colloids to form larger colloids as a result of the reduction of electrostatic repulsion caused by the increased ionic strength of estuarine waters (79). These colloids are not necessarily removed from estuaries by settling, and total iron may for the most part be conserved within some estuaries (78). In particular, once initial coagulation occurs at low salinity, substantially less Fe may be removed during mixing to higher salinities. For example, in one study conducted during two different seasons, Fe losses ranged from only 15-30% of total dissolved Fe during mixing between estuarine waters (22 %) and offshore waters (30 %) of New Jersey (81). Concentrations of dissolved and colloidal Fe (<0.4 μ m filtered) measured in a number of different estuarine and near coastal waters ranged from 5 nM to 4.67 μ M, supporting the idea that Fe could be important to CDOM photochemistry in these systems (81-84). Most measured <0.2 μ m filtered Fe concentrations in the literature for salinities between 10-30 ‰ (estuaries and near coastal) fall between 15-100 nM (84-86). One exception is the New Jersey coastal region, which exhibited both high ‘inshore’ Fe concentrations (mean

($\pm 1\sigma$) 970 (± 140) nM, mean salinity 22‰) and high ‘offshore’ Fe concentrations (320 (± 20) nM, salinity 30 ‰) in 1986 and 1987 (81).

The size of Fe colloids and solubility of dissolved Fe in all marine waters appears to be controlled by organic matter (72,87-90). In estuarine and near coastal regions, this control may be exerted via co-coagulation of DOM with Fe and other metals. There appears to be a near linear relationship between measured DOM and Fe in several estuaries (91), supporting the idea that there is a physical association between Fe and DOM, or, more specifically, between Fe and humic acids (72,79), which compose the most highly colored portions of DOM.

The evidence for the role played by Fe in the photochemistry of CDOM in freshwaters led us to believe that Fe might play a role in the photobleaching of CDOM. To examine this hypothesis, we conducted photobleaching experiments on a set of estuarine samples and on an extracted freshwater fulvic acid sample to which we added Fe or a photochemically inert Fe ligand, desferrioxamine (DFOM). The concentration of Fe used (100 nM in most experiments) was chosen to fall at the high end of the measured range of filterable (< 0.2 µm) Fe concentrations (15-100 nM for salinities 10-30‰). We followed the photobleaching of both absorption and of fluorescence during irradiation with simulated sunlight (Xe arc). In addition, we examined the photoproduction of CO with and without photolabile Fe, and determined the apparent quantum yield of CO in these estuarine samples.

Methods

Samples

Seawater samples were collected during a transit of the Delaware Bay in April 1999 from the Teflon® surface water (~2 m) flow system of the R/V Henlopen. Samples were filtered online using sequential 0.45 µm and 0.2 µm cartridge filters (Gelman AquaPrep and MaxiCapsule) that had been acid-washed and extensively pre-rinsed. Samples were then stored in fluorinated HDPE carboys at 4° C in the dark until use, and refiltered before irradiation. Station S29 was located at the mouth of the Bay (salinity of

29‰), station S20 was located in the middle of the Bay (salinity of 20.1‰), and station S4 was located at the entrance to the Chesapeake Canal (salinity of 4‰).

Suwannee River fulvic acid reference material (SRFA) was obtained from the International Humic Substances Society. Solutions of 3 mg/L SRFA (1.5 mg C/l) were made up in unbuffered 18 MΩ deionized water (Millipore Co., Milli-Q).

Bog water was collected from Thoreau's Bog in Concord, MA by pressing an acid-washed Teflon bottle into the floating sphagnum moss bed. Samples were subsequently 0.2 µm filtered (Gelman MaxiCapsule).

Photobleaching

Photobleaching was performed using a 400 W ozone-free Xe arc in a Research Arc Housing (Oriel Corp.). The Xe-arc was run at 75% of maximum power (approximately 300 W). Airmass 0 and 1 (AM0 and AM1) filters were used to filter out wavelengths below 290nm and to simulate sunlight at a solar zenith angle of 0° at the earth's surface. The spectrum produced approximates solar irradiation at solar noon on the summer solstice at 43.4 N, 71.1 W as calculated for the same time using the program TUV, available from the National Center for Atmospheric Research (92) (**Figure 5.2**). An IR filter containing chilled Milli-Q water was used to minimize thermal effects. Solutions were contained in a specially-designed jacketed glass solar cell with a quartz window at the bottom. This design was chosen to minimize the surface-to-volume ratio of the irradiation vessel so as to minimize surface effects arising from interactions of the CDOM and Fe with the glass walls. A water jacket allowed the temperature to be maintained between 25 and 28 °C. Solutions were stirred from above using a Teflon paddle on a glass shaft (**Figure 5.1**). Sampling ports were sealed using Teflon stoppers. All glassware and Teflon was acid-washed using 5 M nitric acid and extensively rinsed with Milli-Q. Sample handling was performed in a positive-pressure clean room using acid-washed Teflon bottles. Irradiations were performed under optically thin conditions and samples were withdrawn periodically for analysis using pre-rinsed plastic pipettes. Care was taken to minimize changes in the optical pathlength of the samples to < 20%.

In order to examine the effects of Fe on photobleaching, Fe was either added to irradiation experiments or naturally present Fe was complexed by desferrioxamine B mesylate (DFOM, Sigma-Aldrich Chemicals), a fungal siderophore that produces photochemically inactive Fe complexes (see Results). Fe was added as Fe(III)Cl₃ from acidic stock solutions (pH < 2) and allowed to equilibrate for 30-60 minutes. DFOM (500 nM) was added at least 12 hours before irradiation experiments to allow any strongly chelated Fe to exchange. A recent study found that DFOM had a conditional stability constant in seawater (K_{Fe^3+L}) with respect to [Fe'] (all the inorganic dissolved Fe(III)) of 12.1, and a conditional stability constant with respect to free hydrated Fe³⁺ ($\log K_{Fe^{3+}L}$) of 22.1, versus a mean a conditional stability constant ($\log K_{Fe^3+L}$) of 20.3 for the strong unknown ligand in surface waters from the Northwestern Atlantic (89,93). MINEQL+ (94) calculations support the idea that all the dissolved Fe should be complexed by 500 nM DFOM. Marine ion concentrations and stability constants for DFOM were obtained from Morel and Hering (1993).

SRFA samples were treated similarly to seawater samples except that pH was controlled by the addition of small amounts of NaOH and continuous bubbling with a CO₂/air mixture. This bubbling allowed the adjustment of pH to pH 8 (near seawater) or to pH 6 ± 0.2. Unless noted, SRFA solutions were irradiated at pH 8.

Contrary to previous reports (48), the DFOM-Fe complex exhibits a photostable absorption band in the visible region, with an extinction coefficient (ϵ_{430}) of 2200 M⁻¹cm⁻¹. At the concentrations of iron complexed in this study (up to 100 nM), this absorption is negligible. At the higher concentrations of iron in other studies (up to 14 μM, giving an absorption value of 0.07 cm⁻¹ centered at 430nm) the DFOM-Fe complex might have contributed as much as 40% of the absorption value at 430nm, potentially biasing apparent quantum yield determinations above 400nm for both CO and DIC (48).

Gamma Radiolysis

Gamma radiolysis was performed as previously described (Chapter 3; (95)). Briefly, solutions to be exposed to gamma radiolysis were saturated with either N₂O or N₂O/O₂ (4:1 v/v) prior to radiolysis. Seawater samples were irradiated for 40 minutes,

producing 38 $\mu\text{M OH}^\bullet$, equivalent to ~20 days of surface sunlight, assuming 2 $\mu\text{M OH}^\bullet \text{ d}^{-1}$ (see Chapter 3). Bog water samples were irradiated for 70 minutes, producing 72 $\mu\text{M OH}^\bullet$. Samples were analyzed immediately for absorption and fluorescence.

Analyses

CDOM absorption was determined with an HP 8453 diode-array spectrophotometer using 10 cm cells. Milli-Q water served as the blank. The absorbance data was baseline corrected using the average absorbance from 700-725 nm. A peak at 735-740nm was identified as a thermal effect and seen in many spectra (96-98). Spectra were converted to spectral absorption coefficients, $a_{CM}(\lambda)$ using the relation

$$a_{CM}(\lambda) = 2.303 A(\lambda)/l \quad (5)$$

where $A(\lambda)$ is the optical density at wavelength λ and l is the cell pathlength (35). The spectral slopes (S) were obtained from plots of the natural log of the absorption coefficients versus wavelength by linear regression over the interval from 290 nm to 400 nm:

$$a(\lambda) = a(\lambda_o) e^{S(\lambda_o - \lambda)} \quad (6)$$

where λ_o is 400 nm. Bi-exponential fits of bleaching spectra were generated for normalized absorption plots using a non-linear fitting routine (SigmaPlot). The method of spectral decomposition developed in Chapter 4 was successfully applied to these broadband bleaching data. However, to be consistent with previous investigators, the data are presented here as bi-exponential fits.

CDOM fluorescence spectra were obtained on a Perkin-Elmer LS50 spectrofluorometer using 355 nm excitation, 4 nm slits, and 0.1 s integration and averaging 10 scans to reduce the signal to noise ratio. The fluorescence signal at the CDOM emission maximum (444-455 nm) was normalized to the water Raman signal at 394-405nm to produce the F/R ratio values, with relative units (29). The F/R values were transformed to $F_n(355)$ values by standardizing with a 10 $\mu\text{g l}^{-1}$ solution of quinine sulfate in 0.1 N sulfuric acid scanned in an identical way. The F/R value determined for quinine sulfate at this concentration is defined to be 10 $F_n(\lambda_{ex})$.

Excitation-emission spectra (EEMS) were obtained by scanning emission wavelengths from 250 to 650 nm in 0.5 nm increments and excitation wavelengths from 230 to 470 nm in 10 nm increments using 4 nm slits. Data analysis was performed using MATLAB. Spectra were normalized to a 4 nm wide band centered at the water Raman peak at $\lambda_{\text{ex}} = 330$ nm and $\lambda_{\text{em}} = 372$ nm. Fluorescence values at λ_{em} below $\lambda_{\text{ex}} + 6$ nm and above $2 \times \lambda_{\text{ex}} - 6$ nm were set to zero to avoid including the Raleigh scattering peaks.

Analyses of total iron were performed by spectrophotometric measurement of Fe(II) in 10cm quartz cells using 0.147 mM 4,4'-[3-(2-pyridinyl)-1,2,4-triazine-5,6-diyl]bis-benzenesulfonic acid (ferrozine) following acidic (HCl, pH 1) reduction of Fe_T to Fe(II) using hydroxylamine hydrochloride (6.00 mM). Although the recovery of Fe standards spiked into seawater and allowed to equilibrate was very good (*vide infra*), this method may not reduce all the Fe strongly bound to organic matter. The method of standard additions was used, in which known concentrations of Fe were added to samples containing an unknown concentration of Fe and a linear relationship was developed between the concentration of added Fe and measured Fe. All reagents were of the highest purity available and used as received from Sigma-Aldrich. The blank concentration of [Fe]_T was 8 ± 4 nM, most of which was derived from the reductant. Reported Fe concentrations are blank corrected. Recovery of Fe(III) spiked into seawater samples was $94 \pm 7\%$. This method has an inherent uncertainty of ± 4 nM derived from the photometric precision of the spectrophotometer (0.001 AU).

Carbon Monoxide Apparent Quantum Yields

The spectral dependence of carbon monoxide (CO) apparent quantum yields were determined using monochromatic irradiations of samples in long-path length cells (28 cm) from a Hg-Xe arc lamp and monochromator (Spectral Energy). This experimental setup is described in more detail in Xie *et al.* (in press). Samples to be irradiated were degassed with CO-free air ('zero-air') for 1-2 hours using acid-washed glass frits in methanol- and acid- rinsed Teflon bottles. Samples were then siphoned into cuvettes prior to irradiation to avoid contact with ambient air, which contained appreciable concentrations of CO (~2 ppmv). Glass rods encased in silicone rubber were used as

stoppers to minimize sample contact with organic materials. Samples were irradiated at different wavelengths corresponding to Hg emission lines (313 nm, 356 nm, and 405 nm) for different amounts of time, ranging from 10-100 minutes depending on the predicted CO production rates. Dark controls were maintained at room temperature during the course of all irradiations and analyzed after all prior CO analyses were performed on irradiated samples. Apparent quantum yields were calculated from initial absorption values:

$$\Phi = \frac{\text{moles CO produced min}^{-1}}{\text{moles of photons absorbed min}^{-1}} \quad (7)$$

The determinations of CO photoproduction are *apparent* quantum yields rather than true quantum yields, as the concentrations and molar absorption of the specific chromophores that produce CO are unknown. Thus, CO production rates were scaled to the total CDOM absorption. Irradiation intensities were determined by ferrioxalate actinometry. CO analyses were performed by gas chromatography with Hg detection after HgO oxidation of the reducing gas (CO) on a Trace Analytical Reduction Gas Analyzer (RGA-3) after 3 minutes of headspace equilibration of 35 ml aqueous samples in glass syringes with 5 ml CO-free air (99).

Carbon Monoxide Optical Buoy Incubations

Optical buoy experiments were conducted in the Sargasso Sea near the BATS station (32.03°N, 64.01°W) in March 2000 during Cruise EN335 of the R/V Endeavor. A brief description of the methods used is presented here. The use of optical buoys to determine CO production rates in surface waters is discussed more fully in (100)

Seawater for the optical buoy experiment was collected at local midnight from a depth of 20 m using a 30 L Go-Flo (General Oceanics) attached to a standard CTD rosette approximately 30 hours before optical buoy deployment. The water was pressure-filtered with clean N₂ using a prerinsed 0.2 µm membrane filter in a Teflon lined filter holder through Teflon tubing into acid rinsed 20L HDPE carboys. The sample in one 20L

carboy was allowed to equilibrate for 30 hours with 500 nM DFOM at room temperature in the dark. 50 nM Fe was added from acidic Fe(III)Cl₃ stock immediately prior to the beginning of the incubation. The water was then drained into 15 L acid-rinsed glass carboys and degassed through glass frits with CO-free air (medical grade) to reduce background CO prior to being sub-sampled into methanol- and acid-rinsed 500-mL quartz flasks. The optical buoy consisted of quartz flasks attached to stainless steel racks suspended at multiple depths beneath an open tripod of rods and floats. The quartz flasks were sealed with glass stoppers and attached to the cages upside down to minimize shadowing. The optical buoy was deployed near local dawn (0630) and retrieved near sunset (1830). Dark samples were maintained at room temperature (~20 C). CO was analyzed immediately after buoy retrieval using the headspace method as noted above, taking care to avoid any contact of the irradiated water with the atmosphere. Fe was analyzed in the initial sample using acidic reduction with hydroxylamine hydrochloride and ferrozine as noted above.

Results

Photobleaching of the CDOM in 0.2 μm filtered samples from three different stations in the Delaware Bay produced bleaching spectra that exhibit similar absorption bleaching curves (**Figure 5.3**). These curves are all best described by bi-exponential fits, with an initial fast loss of absorption followed by slower long-term bleaching (**Table 5.4**). The fast bleaching phase represented the majority (66±8%, range 59-85%) of the color bleached at 300nm in the initial 12 hours of each irradiation. This was followed by slow, nearly linear bleaching of a second portion. Both the initial spectra and the bleached spectra follow the characteristic pattern of featureless exponentially increasing absorption with decreasing wavelength (data not shown). However, SRFA absorption bleached more slowly than any of the seawater samples (**Figure 5.3**), despite containing approximately the same concentration of carbon (~1.5 mg C/l; 125 μM C). The fast-bleaching phase of SRFA was much smaller than the corresponding fast-bleaching phase of the seawater samples, and although the slower, long-term bleaching rates were similar, long-term bleaching rates for SRFA were also smaller (**Table 5.4**). The initial absorption

coefficients of the SRFA samples were comparable to that of the intermediate salinity samples (S20) and slightly less than that of the lowest salinity sample (S4). Bleaching of these samples caused the slope, S, of the optical spectra to increase in all cases (see **Table 5.3**). In agreement with previous studies, there is not a good correlation of S with salinity (30,75). The bleaching reaction of 70 μM $\text{OH}\cdot$ with 10 mg C l⁻¹ SRFA solutions did not change the spectral slopes significantly, but the reaction of S29 with half that amount of $\text{OH}\cdot$ measurably increased S.

Photobleaching of fluorescence

The bleaching of DOM fluorescence in the Delaware Bay samples was very similar to that of CDOM absorption. Comparable bi-exponential behavior was observed (**Figure 5.4; Table 5.5**). The initial rapid phase of photobleaching represented 87±7% (range 75-95%) of the total photobleaching of fluorescence in the first 12 hours of irradiation. This rapidly-bleaching portion made up more than 75% of the bleaching even after 30 hours of irradiation (equivalent to approximately 5 days of solar radiation, assuming 6 hours of insolation per day). The initial bleaching rates were significantly faster for fluorescence than absorption, while the slower, long-term rates were similar. This lead to greatly enhanced bleaching of fluorescence as compared to absorption for the same irradiation times. The more rapid fluorescence bleaching behavior was also observed in SRFA samples.

Effect of Fe on photobleaching

Neither the addition of 100 nM Fe nor the complexation of the Fe with DFOM to form a non-photoreactive Fe complex affected either the photobleaching of absorption or of fluorescence in any of the samples investigated (S4, S20, and SRFA solutions; **Figures 5.5-5.6**). The addition of larger concentrations of Fe, up to 2 μM , and a decrease of pH to 6, did not increase the photobleaching of SRFA (**Figure 5.6**).

Excitation-emission spectroscopy

Excitation-emission matrix spectroscopy (EEMS) is a fluorescence spectroscopy in which emission spectra are scanned at a number of different excitation wavelengths to

produce a matrix of fluorescence values. EEMS spectra of CDOM fluorescence for Delaware Bay seawater samples and for a solution of SRFA (**Figure 5.7**) exhibit the characteristic peaks identified as ‘humic-like’: one stimulated by UVC excitation (peak A), and one by UVA excitation (peak H, also known as peak C) (101). The peak positions for the lower salinity sample (S4) are A: $Ex_{max}/Em_{max} = 240/425$ nm, and H: $Ex_{max}/Em_{max} = 320/420$ nm. All sample peak positions are listed in **Table 5.6**. Peak H appears to be missing in the higher salinity sample (S29), and peak A is shifted toward lower excitation and emission wavelengths ($Ex_{max}/Em_{max} = 230/410$ nm) in accordance with the findings of Coble (1996). Both peak A and peak H were photobleached, despite the fact that the excitation wavelength of peak A is lower than the lowest wavelength of bleaching light (**Figure 5.8**). However, as might be expected, broadband light bleached peak H more than peak A, as can be seen by the increased values of the ratio of peak A to peak H after photobleaching (**Table 5.6**). Similarly to the emission spectra studied above, no alteration in the bleaching pattern of the EEMS upon addition of Fe or DFOM was observed.

EEMS spectra of seawater samples exposed to radiolytically-produced OH[•] indicate that both peak A and peak H are bleached by OH[•]. In the seawater samples, the A/H ratio increases as it does during photobleaching, although there A/H ratios in the difference spectra are less than in any of the photobleached spectra. This shift indicates that there is increased bleaching of peak A relative to peak H during bleaching with OH[•]. The A/H ratio is very close to 1 in the humic bog water difference spectrum, indicating almost equal bleaching in both peaks. This finding supports the possibility of OH[•] being partially responsible for the bleaching of a fluorophore that was not directly irradiated during the photobleaching experiments.

CO photoproduction

The spectral dependence of the apparent quantum yield (AQY) of CO in Delaware Bay seawater was also investigated (**Figures 5.10**). As has previously been described for both seawater and freshwater samples, the apparent quantum yield of CO photoproduction declined sharply from the UVB portion of the spectrum to the visible

(102). The values determined here (**Table 5.7**) are approximately one order of magnitude less than those previously determined for humic freshwaters, including the Suwannee River and the Satilla River (48,102), but extremely similar to CO AQY's determined in the Gulf of Maine and the Damariscotta River estuary (103). These values are only slightly larger than the AQY's determined for Sargasso Sea water (100). Interestingly, the AQY at 313 nm does not increase in a monotonic fashion with salinity (**Table 5.7**), but instead exhibits a lower value at S20 than at S4 or at S29. It is not clear what might produce this pattern specifically in the UVB region of the spectrum without affecting other portions of the spectrum. The CO production rate in S20 might have been decreased by the addition of Fe or DFOM, as was observed in the higher salinity sample, although the opposite result was obtained in the low salinity sample. As the CO production rate from an unmodified sample of S20 was not determined, this cannot be verified.

Fe effects on CO photoproduction

Fe did not appear to have a significant effect on CO photoproduction (**Figure 5.10**). Contrasting additions of Fe or DFOM to estuarine samples had similar, although inconsistent, results. In S4, both treatments increased the CO AQY slightly, while in S29 (and possibly S20) both decreased it slightly. The decreases in the CO AQY in S29 due to the addition of Fe or of DFOM might be a result of increased light scattering or absorption at 313 nm due to the formation of Fe colloids, or the tailing of the strong DFOM absorption band into the UVB region. The lack of replicate samples for S4 at 313nm does not allow a conclusion to be drawn as to the significance of the difference between the modified samples and the unamended sample. However, based on the errors in similar experiments, there is no significant difference between the sample treatments.

In contrast to the results in estuarine water, a ~20% decrease in CO photoproduction in marine surface waters after DFOM addition was observed during preliminary experiments performed in Sargasso Sea water during a cruise in March 2000 (**Figure 5.11** and (100)). The comparison between DFOM-incubated and 'unamended' Sargasso Sea water may not be completely valid due to a slight contamination of the Sargasso Sea water with Fe during sample manipulation. An Fe concentration of ~15 nM

was measured for the uncomplexed sample, far above Fe concentrations measured in the Sargasso Sea using clean sampling techniques (82). Additional preliminary experiments on the same cruise suggested that addition of Fe increased the photoproduction of CO slightly during deck incubations, although no increase was observed during the added-Fe optical buoy, and that DFOM reduced the photoproduction of CO by approximately 20 %, in accordance with the optical buoy work.

Discussion

Photobleaching of Absorption

The bi-exponential bleaching of CDOM absorption observed in this study was similar to that described by several previous investigators (12,28,39,104). The rapid initial bleaching may represent the preferential destruction of high-absorption chromophores, or the conversion of such chromophores into lower-absorbing, more bleaching-resistant chromophores which continue to be bleached at a much slower rate. This bi-exponential bleaching has been the observed pattern in previous studies of seawater samples (28,32). In several humic freshwater samples, investigators have instead observed mono-exponential (first order) decay of absorption (33,48). These same studies have found an increase in the slope S of logarithmic plot of absorption versus wavelength, in contrast to this study and to a number of other photobleaching studies (28,39,105). The difference between these observations may be due to a compositional difference between extremely humic riverine and lake water and the CDOM found in estuaries and coastal environments. However, in our bleaching of dilute SRFA solutions, we observed a very small rapid-bleaching component followed by slower, nearly linear bleaching. The extreme extraction processing that SRFA undergoes may cause compositional or structural changes that produce a small amount of rapidly bleaching material.

Our initial understanding suggested that indirect reactions of Fe, in particular the production of OH[•] via Fenton reactions, might be an important route to CDOM photooxidation. OH[•] reacts with CDOM with a bleaching efficiency of $3.0 (\pm 0.1) \times 10^4$ m⁻¹ per molar OH[•] for SRFA and $1.3 (\pm 0.2) \times 10^4$ m⁻¹ per molar OH[•] for S29 (Chapter 3;

(95)). The OH[•] production rate we expect in the low Fe systems (< 1 μM Fe) is a maximum of $1 \times 10^{-10} \text{ M s}^{-1}$ (0.36 μM hr⁻¹). The maximum bleaching rates we would expect from OH[•] are 0.01 m⁻¹ hr⁻¹ in the SRFA solutions and 0.005 m⁻¹ hr⁻¹ in the seawater samples. For the seawater samples, these rates are 0.3-1.3% of the initial rapid photobleaching rates observed, but 14-50% of the slower, long term photobleaching rates. For SRFA, the lower Fe samples would produce a OH[•]-supported bleaching rate that is 0.3-0.6% of the fast initial photobleaching, and 66-84% of the longer slow photobleaching (see **Table 5.4** for bleaching rates). Thus, OH[•]-supported bleaching may in fact be of some importance to long-term photobleaching rates. Because the SRFA bleaching experiments were performed in non-seawater matrices, it is possible that some component of seawater (such as Br⁻ or I⁻) reduces the bleaching efficiency of OH[•].

OH[•]-induced bleaching of CDOM does not exhibit multi-phased behavior. Instead, bleaching of CDOM is linear with increasing OH[•] dose (Chapter 3). The large percentage of the slow bleaching rate possibly attributable to OH[•] might help to explain both the linearity of these portions of the bleaching curves and the fact that these portions of the curves are almost parallel for different samples. However, the addition of Fe did not increase the bleaching rates in these samples (*vide infra*), suggesting either that indirect photoprocesses are not responsible for the bleaching behavior of CDOM, or that the addition of Fe did not stimulate the production of intermediates capable of indirectly bleaching CDOM.

Several factors may play a role in limiting the importance of OH[•] to CDOM bleaching. From previous work, we know that the reaction rate constants of OH[•] with DOM decrease with increasing dose (or in this case, photolysis time; Chapter 3, (95)). Other sinks of OH[•] will become increasingly important over time. Secondly, OH[•] photoproduction by CDOM will most likely decline during the course of a photolysis as chromophores are exhausted (106). The maximum OH[•] production rates used here are probably overestimates of the true OH[•] production rates. Thus, especially as regards to the long-term photobleaching rates, these estimates of the importance of OH[•]-mediated photobleaching may be large overestimates.

Photobleaching of Fluorescence

Similarly to absorption, the bi-exponential decay of fluorescence suggests either the presence of multiple fluorophores or the conversion of more rapidly bleached fluorophores to more slowly bleaching fluorophores. Similar bi-exponential fluorescence bleaching behavior has been previously observed, also in marine samples (36,107,108). The loss of the rapidly bleaching FDOM may be slowed in estuaries by vertical mixing of material, thus decreasing the residence time a particular parcel of FDOM-containing water spends undergoing photolysis, and allowing the material to be advected out of the estuary and into the coastal ocean. Alternatively, FDOM might be produced by biological activity, and this fresh material might be the source of the rapidly bleached fluorescence.

In the lower salinity samples studied here (SRFA, S4, and S20), fluorescence bleaching occurred more rapidly than absorption bleaching. The non-linear bleaching relationship between these two optical properties is illustrated in **Figure 5.12**. This is an interesting finding in light of field observations that fluorescence and absorption exhibit linear relationships in the Western North Atlantic (28,29). However, De Haan (1993) observed more rapid loss of fluorescence than absorption in a peaty freshwater lake (109). Interestingly, the highest salinity sample studied here (S29) actually exhibits a 1:1 relationship between absorption and fluorescence. These findings taken together suggest that during the course of FDOM residence time in this estuary, the extremely rapid photobleaching of a terrestrial DOM derived fluorescence leads to the loss of this material and the eventual establishment of a linear relationship, in which both CDOM and FDOM exhibit the same photobleaching rates. Alternatively, there could be significant non-photochemical alterations to the CDOM and the FDOM that reduce the bleaching differences between the two parameters such that FDOM becomes less bleachable.

Excitation-Emission Spectra

EEM spectra of low salinity samples from the Delaware Bay (S4, 4‰) exhibited characteristic ‘humic-like’ peaks A ($\text{Ex}_{\max}/\text{Em}_{\max} \sim 240/420 \text{ nm}$) and H ($\text{Ex}_{\max}/\text{Em}_{\max} \sim 320/420 \text{ nm}$). As has been previously observed in the Orinoco River/Gulf of Paria system

(75) and a number of other waters (101), the higher salinity sample (S29, 29‰) exhibited a much reduced peak H and a hypsochromic (blue) shift in both excitation and emission wavelengths of Peak A. This blue shift may be due to chemical changes to the fluorophores during CDOM transit through the estuary resulting in the shortening of conjugated systems, the elimination of substituents that contribute to hyperconjugation, and increases in the rigidity of the DOM molecules (75). Photobleaching of the higher salinity samples also leads to a slight hypsochromic shift in peak A, possibly due to the photooxidation of extended conjugated systems, such as highly absorbing aromatic systems.

Interestingly, peak A can be photobleached, although not as extensively as peak H. The ratio of peaks A/H increased in all samples and treatments during photobleaching (**Table 5.6**). Because peak A is excited by wavelengths of light below those used during irradiation ($\lambda_{\text{ex}} = 230\text{nm}$), this result suggests two different possibilities: (a) there is intramolecular transfer of energy during photobleaching that leads to the destruction of fluorophores absorbing below 290 nm, or (b) indirect photoproducts such as OH[•] are significant factors in these bleaching reactions.

Indirect photochemistry may play a significant role in certain systems, but the lack of any systematic significant effect of Fe or DFOM on the bleaching ratio of A/H suggests several possibilities. Assuming that Fe-driven photochemistry produces significant fluxes of indirect oxidants, either indirect photobleaching is a subtle effect in our systems or indirect photochemistry is not responsible for the bleaching of peak A. Alternatively, there may only be significant photo-Fenton production of OH[•] at low pH's and high Fe concentrations.

The role of one important indirect oxidant in bleaching processes was examined by examining the effect of radiolytically produced OH[•] (see also Chapter 3; (95)). During gamma radiolysis of two estuarine samples, the ratio of peaks A/H increased, in a fashion similar to the pattern observed during photolysis (**Table 5.6**). The fluorescence A/H ratio of the difference spectra (initial spectra – final spectra) produced from OH[•] bleaching was smaller than that produced during photobleaching. There is no reason to assume that

the quantum efficiency of fluorescence of the two fluorophores is similar. All that can be concluded is that OH• appears to bleach fluorophore A relative to fluorophore H more efficiently than photolysis does. This phenomena deserves further attention.

Similar results were obtained during the bleaching of humic bog samples, although the A/H ratio in the difference spectrum was very close to 1, indicating that this effect is not limited to seawater samples. However, as noted above, there is no systematic change in the A/H ratio of difference spectra upon addition of Fe, indicating that either OH• is not produced in significant enough concentrations to be an effective indirect photobleaching reagent or that indirect photobleaching processes are not completely responsible for the bleaching of fluorophores excited by shorter wavelengths than the lowest irradiation wavelengths.

Fe effects on photobleaching

We found no significant effect of Fe on the photobleaching rates of either estuarine samples or of low concentration solutions of SRFA. These findings are surprising in light of the extensive Fe photochemistry that has been described by a number of investigators (46-49). Most previous work on Fe photochemistry that has shown significant effects on DOM photoproduct formation rates has been performed in freshwater samples with very high Fe and DOM concentrations (9,43,45,48). Fe should have both direct and indirect effects on photoreactions. For Fe additions or photochemical inactivation via DFOM to fail to increase or decrease photobleaching rates indicates that *neither* mechanism of Fe photoreaction is significant in photobleaching reactions in estuarine waters or in dilute SRFA solutions.

One important issue that was not resolved in this study is the form taken by the Fe added to the samples. Much of this added Fe(III) most likely formed colloidal Fe(III) (hydr)oxides very rapidly. It is also likely that these Fe colloids incorporated some fraction of organic matter via coagulation with DOM or sorption of DOM to the freshly formed surfaces (79,110). In a number of different estuaries Fe has been found to occur largely in the colloidal phase (1kDa-0.2 µm) as has a significant fraction of the total organic matter (< 0.2 µm) (91,111-113). These natural colloids may form as riverborne

Fe comes into contact with seawater in estuaries. Thus, although the form and speciation of Fe in our experiments was not examined, it is reasonable to suggest that they are not completely dissimilar from the naturally occurring forms of Fe. The results of the DFOM addition experiments suggest that Fe already present in the samples, which presumably is more closely associated with the CDOM than the added Fe, also does not play a significant role in CDOM photobleaching.

Fe effects on CO photoproduction in estuarine waters

Fe does not appear to have a significant effect on CO photoproduction in estuarine waters. Contrasting additions of Fe or DFOM to estuarine samples either both increase the CO AQY slightly (S4), or both decrease it slightly (S29, possibly S20, *vide supra*). As mentioned above, these findings are surprising in light of the observations of Gao and Zepp (1998) that addition of DFOM decreased the rate of CO photoproduction in Satilla River water by 27%, and the preliminary experiments in the Sargasso Sea that indicated DFOM decreased CO photoproduction rates by ~20% in near-surface waters (48,100). The decreased photoproduction rates in the optical buoy experiments was observed only in the top 3 meters of the water column. It is possible that the CO photoproduction due to Fe is stimulated by short wavelength UV radiation that is rapidly attenuated by water. However, the optical conditions in the Sargasso Sea usually allow the penetration of most UV irradiation to depths greater than 3 m ($a_{300} = 0.2\text{-}0.4 \text{ m}^{-1}$; (34)). The contamination of the filtered samples with small amounts of Fe (15 nM) also confounds the issue of what effect Fe might have on *in-situ* CO photoproduction at natural Fe concentrations. The technical problems of maintaining both trace metal and organic clean conditions on a ship in rough weather may preclude the determination of these CO photoproduction values by the use of optical buoy techniques and instead require laboratory studies. In spite of the conflicting evidence from oceanic samples, the lack of an effect of Fe on CO photoproduction quantum yields in estuarine waters indicates that Fe does not have an effect on at least one important product of estuarine CDOM photooxidation. Oceanic CO photoproduction remains to be examined more closely.

Conclusions

Despite evidence for the involvement of Fe in the photooxidation of terrestrially-derived CDOM in fresh water, there appears to be no significant effect of Fe on the photobleaching or photoproduction of CO from estuarine samples. Furthermore, Fe does not increase the bleaching rates of an isolated terrestrial fulvic acid (SRFA). These findings lead to the conclusion that neither the direct nor the indirect OH[•]-mediated photochemistry of Fe plays a significant role in CDOM photooxidation processes in estuarine systems. CDOM photochemistry has been shown to have a significant effect on Fe speciation in marine systems, but a number of different processes, including the formation of Fe colloids, may have an inhibitory effect on the obverse processes of Fe-influenced CDOM photooxidation.

Photobleaching results obtained in this study support previous observations of spectral slope (S) increases and bi-exponential bleaching behavior observed in estuarine and coastal waters, and confirm differences between freshwater and estuary samples. More rapid fluorescence bleaching than absorption bleaching in low and intermediate salinity samples appears to preferentially remove a rapid-bleaching set of fluorophores, leading to a linear correlation between fluorescence and absorption in higher salinity samples, similar to that previously observed in the Mid-Atlantic Bight (28). Finally, the EEM spectral studies indicate the existence of so called 'off-axis' bleaching at wavelengths outside the irradiation wavelengths. This behavior is not completely explainable via OH[•]-induced bleaching, and suggests that the photochemical behavior of CDOM is more complicated than the simple superposition of multiple independent chromophores bleached by direct and indirect photoprocesses that had been the previous model.

Acknowledgements

I would like to thank O. Zafiriou, X. Hui, R. Najjar, J. Werner, L. Ziolkowski, C. Taylor, and J. Tolli for assistance with the CO optical buoy work. R. Kieber performed the Fe analysis of the CO buoy seawater sample. The captains and crews of the R/V

Endeavor cruise EN-335 and the R/V Cape Henlopen were essential for the CO optical buoy work and the collection of Delaware Bay seawater samples, respectively. This work was supported by NSF grants OCE9811208 and NSF OCE9819089.

References

1. Kirk, J. T. O. *Light and Photosynthesis in Aquatic Ecosystems*; 2 ed.; Cambridge University Press: Cambridge, 1994.
2. Aiken, G. R.; McKnight, D. M.; Wershaw, R. L.; MacCarthy, P. *Humic Substances in Soil, Sediment, and Water: Geochemistry, Isolation, and Characterization*; Aiken, G. R.; McKnight, D. M.; Wershaw, R. L.; MacCarthy, P., Ed.; Wiley-Interscience: New York, 1985, pp 691.
3. Zepp, R. G.; Callaghan, T. V.; Erickson, D. J. *J. Photochem. Photobiol. B: Biology* **1998**, *46*, 69-82.
4. Williamson, C. E. *Limnol. Oceanogr.* **1995**, *40*, 386-392.
5. Williamson, C. E.; Stemberger, R. S.; Morris, D. P.; Frost, T. M.; Paulsen, S. G. *Limnol. Oceanogr.* **1996**, *41*, 1024-1034.
6. DeGrandpre, M. D.; Vodacek, A.; Nelson, R. K.; Bruce, E. J.; Blough, N. V. *J. Geophys. Res.* **1996**, *101*, 22727-22736.
7. Schindler, D. W.; Curtis, P. J. *Biogeochem.* **1997**, *36*, 1-8.
8. Kirk, J. T. O. *J. Geophys. Res.* **1988**, *93*, 10897-10908.
9. Miles, C. J.; Brezonik, P. L. *Environ. Sci. Technol.* **1981**, *15*, 1089-1095.
10. Bertilsson, S.; Tranvik, L. *Limnol. Oceanogr.* **1998**, *43*, 885-895.
11. Granéli, W.; Lindell, M.; Tranvik, L. *Limnol. Oceanogr.* **1996**, *41*, 698-706.
12. Miller, W. L.; Zepp, R. G. *J. Geophys. Res.* **1995**, *22*, 417-420.
13. Zuo, Y.; Jones, R. D. *Naturwissenschaften* **1995**, *82*, 472-474.
14. Zhou, X.; Mopper, K. *Mar. Chem.* **1997**, *56*, 201-213.
15. Mopper, K.; Stahovec, W. L. *Mar. Chem.* **1986**, *19*, 305-321.
16. Kieber, R. J.; Zhou, X.; Mopper, K. *Limnol. Oceanogr.* **1990**, *35*, 1503-1515.
17. Amon, R. M.; Benner, R. *Geochim. Cosmochim. Acta* **1996**, *60*, 1783-1792.
18. Amon, R. M. W.; Benner, R. *Limnol. Oceanogr.* **1996**, *41*, 41-51.
19. Bertilsson, S.; Tranvik, L. *Limnol. Oceanogr.* **2000**, *45*, 753-762.
20. Bertilsson, S.; Allard, B. *Arch. Hydrobiol./Advanc. Limnol.* **1996**, *48*, 133-141.
21. Lindell, M. J.; Graneli, W.; Tranvik, L. J. *Limnol. Oceanogr.* **1995**, *40*, 195-199.
22. Tranvik, L. J.; Bertilsson, S. *Ecology Lett.* **2001**, *4*, 458-463.
23. Kirk, J. T. O. *Arch. Hydrobiol. Bieh. Ergeb. Limnol.* **1994**, *43*, 1-16.
24. Bukata, R. P.; Jerome, J. H.; Kondratyev, K. Y.; Pozdnyakov, D. V.; Kotykhov, A. A. *J. Great Lakes Res.* **1997**, *23*, 254-269.
25. Spitzer, D.; Dirks, R. W. *J. Appl. Opt.* **1985**, *24*, 444-445.
26. Vodacek, A.; Green, S.; Blough, N. V. *Limnol. Oceanogr.* **1994**, *39*, 1-11.
27. Vodacek, A.; Hoge, F. E.; Swift, R. N.; Yungel, J. K.; Peltzer, E. T.; Blough, N. V. *Limnol. Oceanogr.* **1995**, *40*, 411-415.
28. Vodacek, A.; Blough, N. V.; DeGrandpre, M. D.; Peltzer, E. T.; Nelson, R. K. *Limnol. Oceanogr.* **1997**, *42*, 674-686.
29. Hoge, F. E.; Vodacek, A.; Blough, N. V. *Limnol. Oceanogr.* **1993**, *38*, 1394-1402.
30. Blough, N. V.; Zafiriou, O. C.; Bonilla, J. J. *Geophys. Res.* **1993**, *98*, 2271-2278.

31. Muller-Karger, F. E.; McClain, C. R.; Fisher, T. R.; Esaias, W. E.; Varela, R. *Prog. Oceanogr.* **1989**, *23*, 23-64.
32. Kouassi, A. M.; Zika, R. G. *Toxicol. Env. Chem.* **1992**, *35*, 195-211.
33. Morris, D. P.; Hargreaves, B. R. *Limnol. Oceanogr.* **1997**, *42*, 239-249.
34. Nelson, N. B.; Siegel, D. A.; Michaels, A. F. *Deep-Sea Research Part I-Oceanographic Research Papers* **1998**, *45*, 931-957.
35. Green, S. A.; Blough, N. V. *Limnol. Oceanogr.* **1994**, *39*, 1903-1916.
36. Kouassi, A. M.; Zika, R. G.; Plane, J. M. C. *Netherl. J. Sea Res.* **1990**, *27*, 33-41.
37. Chen, R. F. *Organic Geochemistry* **1999**, *30*, 397-409.
38. Chen, R. F.; Bada, J. L. *Mar. Chem.* **1992**, *37*, 191-221.
39. Del Vecchio, R.; Blough, N. V. *Mar. Chem.* **submitted**.
40. Voelker, B. M.; Morel, F. M. M.; Sulzberger, B. *Environ. Sci. Technol.* **1997**, *31*, 1004-1011.
41. Voelker, B. M.; Sedlak, D. L. *Mar. Chem.* **1995**, *50*, 93-102.
42. Zuo, Y. G.; Hoigne, J. *Science* **1993**, *260*, 71-73.
43. Zepp, R. G.; Faust, B. C.; Hoigne, J. *Environ. Sci. Technol.* **1992**, *26*.
44. McKnight, D. M.; Kimball, B. A.; Bencala, K. E. *Science* **1988**, *240*, 637-640.
45. Faust, B. C.; Zepp, R. G. *Environmental Science & Technology* **1993**, *27*, 2517-2522.
46. Faust, B. C. *Aquatic and Surface Photochemistry*; Helz, G. R., Zepp, R. G. and Crosby, D. G., Ed.; Lewis Publishers: Boca Raton, FL, 1994, pp 3-38.
47. Waite, T. D.; Szymczak, R. *Aquatic and Surface Photochemistry*; Helz, G. R., Zepp, R. G. and Crosby, D. G., Ed.; Lewis Publishers: Boca Raton, FL, 1994, pp 39-52.
48. Gao, H. Z.; Zepp, R. G. *Environmental Science & Technology* **1998**, *32*, 2940-2946.
49. Sulzberger, B.; Laubscher, H.; Karametaxas, G. *Aquatic and Surface Photochemistry*; Helz, G. R., Zepp, R. G. and Crosby, D. G., Ed.; Lewis Publishers: Boca Raton, FL, 1994, pp 53-74.
50. Voelker, B. M.; Sedlak, D. L.; Zafiriou, O. C. *Environ. Sci. Technol.* **2000**, *34*, 1038-1042.
51. Zafiriou, O. C.; Voelker, B. M.; Sedlak, D. L. *J. Phys. Chem. A* **1998**, *102*, 5693-5700.
52. Goldstone, J. V.; Voelker, B. M. *Environ. Sci. Technol.* **2000**, *34*, 1043-1048.
53. Zuo, Y.; Jones, R. D. *Water. Res.* **1997**, *31*, 850-858.
54. Pos, W. H.; Riemer, D. D.; Zika, R. G. *Mar. Chem.* **1998**, *62*, 89-101.
55. Miller, W. L.; King, D. W.; Lin, J.; Kester, D. R. *Mar. Chem.* **1995**, *50*, 63-77.
56. O'Sullivan, D. W.; Hanson Jr., A. K.; Kester, D. R. *Mar. Chem.* **1995**, *49*, 65-77.
57. Johnson, K. S.; Coale, K. H.; A., E. V.; Tindale, N. W. *Mar. Chem.* **1994**, *46*, 319-334.
58. Kuma, K.; Nakabayashi, S.; Suzuki, Y.; Kudo, I.; Matsunaga, K. *Mar. Chem.* **1992**, *37*, 15-27.
59. Waite, T. D.; Szymczak, R.; Espey, Q. I.; Frunas, M. J. *Mar. Chem.* **1995**, *50*, 79-91.

60. Blough, N. V.; Zepp, R. G. *Active Oxygen in Chemistry*; Foote, C. S. and Valentine, J. S., Ed.; Chapman and Hall: New York, 1995, pp 280-333.
61. Moffett, J. W.; Zika, R. G. *Environ. Sci. Technol.* **1987**, *21*, 804-810.
62. Zafiriou, O. C.; Dister, B. J. *Geophys. Res.* **1991**, *69*, 99-4945.
63. Barbeau, K. *Influence of protozoan grazing on the marine geochemistry of particle reactive trace metals*; Barbeau, K., Ed.; Massachusetts Institute of Technology-Woods Hole Oceanographic Institute: Cambridge, MA, 1998.
64. Zafiriou, O. C. *Chemical Oceanography*; Academic Press: London, 1983; Vol. 8.
65. Zafiriou, O. C.; Joussot-Dubien, J.; Zepp, R. G.; Zika, R. *Environ. Sci. Technol.* **1984**, *18*, 358A-371A.
66. Cooper, W. J.; Zika, R. G.; Petasne, R. G.; Fischer, A. M. *Aquatic Humic Substances: Influence on Fate and Treatment of Pollutants*; Suffet, I. H. and MacCarthy, P., Ed.; American Chemical Society: Washington, DC, 1989; Vol. Advances in Chemistry Series No. 219.
67. Benner, R.; Opsahl, S. *Organic Geochemistry* **2001**, *32*, 597-611.
68. Mantoura, R. F. C.; Woodward, E. M. S. *Geochim. Cosmochim. Acta* **1983**, *47*, 1293-1309.
69. Miller, A. E. J. *Estuarine Coastal and Shelf Science* **1999**, *49*, 891-908.
70. Hedges, J. I.; Keil, R. G.; Benner, R. *Org. Geochem.* **1997**, *27*, 195-212.
71. Sholkovitz, E. R. *Geochim. Cosmochim. Acta* **1976**, *40*, 831-845.
72. Sholkovitz, E.; Boyle, E. A.; Price, N. B. *Earth Planet. Sci. Lett.* **1978**, *40*, 130-136.
73. Fox, L. E. *Geochim. Cosmochim. Acta* **1984**, *48*, 879-884.
74. Uher, G.; Hughes, C.; Henry, G.; Upstill-Goddard, R. C. *Geochem. Res. Lett.* **2001**, *28*, 3309-3312.
75. Del Castillo, C. E.; Gilbes, F.; Coble, P. G.; Muller-Karger, F. E. *Limnology and Oceanography* **2000**, *45*, 1425-1432.
76. Klinkhammer, G. P.; McManus, J.; Colbert, D.; Rudnick, M. D. *Geochim. Cosmochim. Acta* **2000**, *64*, 2765-2774.
77. Fox, L. E.; Wofsy, S. C. *Geochim. Cosmochim. Acta* **1983**, *47*, 211-216.
78. Mayer, L. M. *Geochim. Cosmochim. Acta* **1982**, *46*, 1003-1009.
79. Mayer, L. M. *Geochim. Cosmochim. Acta* **1982**, *46*, 2527-2535.
80. Hunter, K. A.; Leonard, M. W. *Geochim. Cosmochim. Acta* **1988**, *52*, 1123-1130.
81. Yan, L.; Stallard, R. F.; Key, R. M.; Crerar, D. A. *Geochim. Cosmochim. Acta* **1991**, *55*, 3647-3656.
82. Wu, J.; Luther III, G. W. *Geochim. Cosmochim. Acta* **1996**, *60*, 2729-2741.
83. Mackey, D. J.; O'Sullivan, J. E.; Watson, R. J.; Dal Pont, G. *Mar. Chem.* **1997**, *59*, 113-126.
84. Kuma, K.; Katsumoto, A.; Nishioka, J.; Matsunaga, K. *Estuarine, Coastal, and Shelf Sci.* **1998**, *47*, 275-283.
85. El-Nady, F. E.; Dowidar, N. M. *Estuar. Coast. Shelf Sci.* **1997**, *45*, 345-355.
86. Shiller, A. M.; Boyle, E. A. *Geochim. Cosmochim. Acta* **1991**, *55*, 3241-3251.
87. Wu, J.; Luther III, G. W. *Mar. Chem.* **1995**, *50*, 159-177.
88. van den Berg, C. M. G. *Mar. Chem.* **1995**, *50*, 139-157.

89. Rue, E. L.; Bruland, K. W. *Mar. Chem.* **1995**, *50*, 117-138.
90. Kawaguchi, T.; Wahl, M. H.; Aelion, C. M.; McKellar, H. N. *Journal of Environmental Science and Health Part a- Environmental Science and Engineering & Toxic and Hazardous Substance Control* **1994**, *29*, 1761-1776.
91. Powell, R. T.; Landing, W. M.; Bauer, J. E. *Mar. Chem.* **1996**, *55*, 165-176.
92. Madronich, S.; Flocke, S. *Handbook of Environmental Chemistry*; Boule, P., Ed.; Springer-Verlag: Heidelberg, 1998, pp 1-26.
93. Witter, A. E.; Hutchins, D. A.; Butler, A.; Luther III, G. W. *Mar. Chem.* **2000**, *69*, 1-17.
94. Environmental Research Software *MINEQL+*; 3.0 ed.; Environmental Research Software, Ed.; Procter and Gamble Company: Hallowell, ME, 1994.
95. Goldstone, J. V.; Pullin, M. J.; Bertilsson, S.; Voelker, B. M. *Environ. Sci. Technol.* **in press**.
96. Stedmon, C. A.; Markager, S.; Kaas, H. *Estuarine Coastal and Shelf Science* **2000**, *51*, 267-278.
97. Trabjerg, I.; Hojerslev, N. K. *Appl. Optics* **1996**, *35*, 2635-2658.
98. Pegau, W. S.; Zaneveld, J. R. *Limnol. Oceanogr.* **1993**, *38*, 188-192.
99. Xie, H.; Andrews, S. S.; Martin, W. R.; Miller, J.; Ziolkowski, L.; Taylor, C. D.; Zafiriou, O. C. *Mar. Chem.* **in press**.
100. Xie, H.; Goldstone, J. V.; Taylor, C. D.; Wang, W.; Zafiriou, O. C. **manuscript in preparation**.
101. Coble, P. G. *Mar. Chem.* **1996**, *51*, 325-346.
102. Valentine, R. L.; Zepp, R. G. *Environ. Sci. Technol.* **1993**, *27*, 409-414.
103. Ziolkowski, L. A. *Marine photochemical production of carbon monoxide*; Ziolkowski, L. A., Ed.; Dalhousie University: Halifax, N.S., Canada, 2000, pp 121.
104. Andrews, S. S.; Caron, S.; Zafiriou, O. C. *Limnol. Oceanogr.* **2000**, *45*, 267-277.
105. Grzybowski, W. *Chemosphere* **2000**, *40*, 1313-1318.
106. Vaughn, P. P.; Blough, N. V. *Environ. Sci. Technol.* **1998**, *32*, 2947-2953.
107. Hayasi, K.; Tsubota, H.; Sunada, I.; Goda, S.; Yamazaki, H. *Mar. Chem.* **1988**, *25*, 373-381.
108. Kramer, C. J. M. *Netherlands J. Sea Res.* **1979**, *13*, 325-329.
109. De Hann, H. *Limnol. Oceanogr.* **1993**, *38*, 1072-1076.
110. Santschi, P. H.; Lenhart, J. J.; Honeyman, B. D. *Mar. Chem.* **1997**, *58*, 99-125.
111. Wells, M. L.; Smith, G. J.; Bruland, K. W. *Marine Chemistry* **2000**, *71*, 143-163.
112. Wen, L.-S.; Santschi, P. H.; Tang, D. *Geochim. Cosmochim. Acta* **1997**, *61*, 2867-2878.
113. Wen, L.-S.; Santschi, P. H.; Gill, G.; Paternostro, C. *Mar. Chem.* **1999**, *63*, 185-212.

Table 5. 1

Characteristics of water samples used in photobleaching experiments.

Sample	Salinity (%)	Initial $a_{CM}(300)$ (m^{-1})	Initial F/R (FLU)
S4	4	9.39	2.2
S20	20	5.80	0.8
S29	29	3.62	0.2
SRFA	n.a.	6.82	1.0

Table 5. 2

Measured Fe concentrations in irradiation samples. $[Fe(II)]$ was measured spectrophotometrically using ferrozine after acid reduction of $[Fe]_T$ (see Methods). The errors are 1σ for the averages of two or three replicate determinations.

Sample	Measured $[Fe]_T$ (nM)
SRFA	7 ± 1.5
SRFA +Fe	27 ± 3
S4 Initial	20 ± 5
S4 Fe	54 ± 5
S20 Initial	13 ± 4
S20 Fe	143 ± 4
S29 Initial	33^a

^a This sample may have been inadvertently contaminated with Fe

Table 5. 3

Spectral slopes (S) of absorption curves determined from least-squares regression of log-linearized absorption values ($a(\lambda)$, m^{-1}) from 250 nm to 450 nm. All fits have $r^2 > 0.98$. In all cases, S increases or does not change significantly (SRFA) as a result of bleaching. The effect of OH[•] bleaching on the spectral slope of two samples is also shown. The SRFA solution was 10 mg C l-1 and was exposed to 70 μM OH[•], while the S29 sample was exposed to 35 μM OH[•].

Sample	Initial $a_{\text{CM}}(300)$ (m^{-1})	Slope at t_0	Slope at $t \sim 78\text{hr} (\pm 2 \text{ hr})$
S4	9.39	0.0156	0.0170
S4 + Fe	9.36	0.0157	0.0174
S4 +DFOM	9.36	0.0157	0.0173
S20 ^a		0.0176	0.0190 ^b
S20 +Fe	5.99	0.0159	0.0167
S20 +DFOM	5.79	0.0163	0.0170
S29	3.62	0.0115	0.0185
SRFA	6.82	0.0158	0.0169
SRFA +Fe	6.92	0.0160	0.0162
SRFA +DFOM	6.81	0.0160	0.0164
SRFA + OH [•]	29.3	0.0180	0.0181 ^c
S29 + OH [•]	2.95	0.0171	0.0183 ^d

^a This sample was 0.02 μm filtered prior to irradiation. ^b Irradiation time is 48 hours (final timepoint). ^c Exposed to 70 mM OH[•]. ^d Exposed to 35 mM OH[•].

Table 5.4

Fitting constants for bi-exponential fits of absorption photobleaching. Normalized absorption values at 300nm were fit to the equation $A = a_1 \exp(-k_1 t) + a_2 \exp(-k_2 t)$, with t in hours, using a non-linear fitting routine. These values must thus be multiplied by the initial absorptions in **Table 5.1** to obtain the rates in $\text{m}^{-1} \text{ hr}^{-1}$. Note that there are extremely small differences between sample treatments, although there are different rate constants for different samples. Note also that SRFA seems to have a much smaller rapidly bleaching component, as can be seen in **Figure 5.3**.

Sample	a₁	k₁ (hr⁻¹)	a₂	k₂ (hr⁻¹)
S4	0.079	0.168	0.915	3.23e-3
S4 + Fe	0.065	0.182	0.934	3.69e-3
S4 +DFOM	0.109	0.108	0.885	3.11e-3
S20 +Fe B	0.0670	0.103	0.928	2.88e-3
S20 +DFOM	0.0564	0.239	0.943	2.99e-3
S29	0.233	0.108	0.787	2.79e-3
SRFA	0.0376	0.462	0.962	2.19e-3
SRFA +Fe	0.0348	0.225	0.965	1.99e-3
SRFA +DFOM	0.0400	0.310	0.959	1.75e-3

Table 5. 5

Fitting constants for bi-exponential fits of photobleaching of fluorescence. Normalize fluorescence/Raman values were fit to the equation $Fl = f_1 \exp(-k_1 t) + f_2 \exp(-k_2 t)$, with t in hours, using a non-linear fitting routine. These values must thus be multiplied by the initial fluorescence values in **Table 5.1** to obtain the rates in FLU hr^{-1} . Note that there are extremely small differences between sample treatments, although there are different rate constants for different samples.

Sample	f₁	k₁ (hr⁻¹)	f₂	k₂ (hr⁻¹)
S4	0.355	0.166	0.626	7.17e-3
S4 + Fe	0.284	0.448	0.711	1.06e-2
S4 +DFOM	0.394	0.134	0.582	6.63e-3
S20 +Fe B	0.449	0.124	0.576	3.43e-3
S20 +DFOM	0.349	0.119	0.644	4.57e-3
S29	0.434	0.028	0.613	5.53e-4
SRFA	0.489	0.177	0.493	6.50e-3
SRFA +Fe	0.245	0.248	0.753	8.88e-3
SRFA +DFOM	0.475	0.291	0.513	9.90e-3

Table 5. 6

Excitation and emission peak wavelengths (in nm) determined from EEMS. Peaks A and H are the so-called ‘humic-like’ fluorescence peaks. The ratio of peak A to peak H in the initial material, the final spectrum, and in the difference spectrum (‘Bleached’: the fluorescence lost during photobleaching) are shown in the final columns.

The samples bleached with OH[•] were exposed to ~40 μM OH[•], corresponding to approximately 20 days of solar bleaching, assuming an OH[•] production rate of 2 μM d⁻¹.

Sample	Hours irrad.	Peak A (Ex _{max} /Em _{max})	Peak H (Ex _{max} /Em _{max})	Initial	Final	Ratio A/H Bleached
S4	110.3	240/425	320/420	1.95	2.04	1.81
S4 Fe	78.5	240/425	320/420	1.96	2.15	1.89
S4 DFOM	104.9	240/425 (0)	320/420 (5)	1.95	2.04	1.89
S20 Fe	106.3	240/415	320/420	2.15	2.18	2.12
S20 DFOM	123.2	240/420	320/420	2.17	2.61	1.80
S29	97.8	230/410	none ^a	(2.57) ^b	(2.77) ^b	(2.07) ^b
SRFA	123.8	230/430	320/440	2.29	3.42	1.87
SRFA Fe	95.7	230/430	330/435	2.49	3.53	1.61
SRFA DFOM	120.8	230/430	320/440	2.33	2.95	2.01
S4 bleached with OH [•]		240/425	320/420	1.97	2.19	1.56
S29 bleached with OH [•]		230/410	none ^a	(2.12) ^b	(2.91) ^b	(1.83) ^b
Bog bleached with OH [•]		250/445	340/450	0.78	0.71	0.94

^a Peak was not present. ^b The value at 320/420 was used to calculate A/H.

Table 5. 7

Apparent quantum yields of CO from seawater samples in mole per photon absorbed at 3 different wavelengths. The values in parentheses are standard deviations from duplicate determinations.

Sample	Apparent Quantum Yield x 10 ⁵		
	313nm	365nm	405nm
S4	5.67	1.44	0.758
S4 Fe	7.17	1.78	0.497
S4 DFOM	7.31	1.36	0.267
S20 Fe	2.71 (0.11)	0.826	0.397
S20 DFOM	2.65 (0.22)	0.819	1.00 ^a
S29	5.18 (0.07)	0.742 (0.06)	0.260
S29 Fe	3.26 (0.7)	0.757 (0.02)	0.347
S29 DFOM	3.23 (0.06)	0.653 (0.3)	0.254
S29 Cu	8.36 (0.39)	1.09 (0.03)	0.959

^a This value was biased by an anomalous absorption value for this sample at 405nm. The CO production rates (nM/hr) were the same for both S20 Fe and S20 DFOM at 405 nm.

Figure 5.1

Schematic diagram of photobleaching apparatus. A: Research lamp housing 400 W Xe arc. B: IR filter containing chilled Milli-Q water. C: Dichroic mirror. D: Custom solar cell with sampling ports, quartz bottom, outside waterjacket for cooling, and mechanical stirring rod.

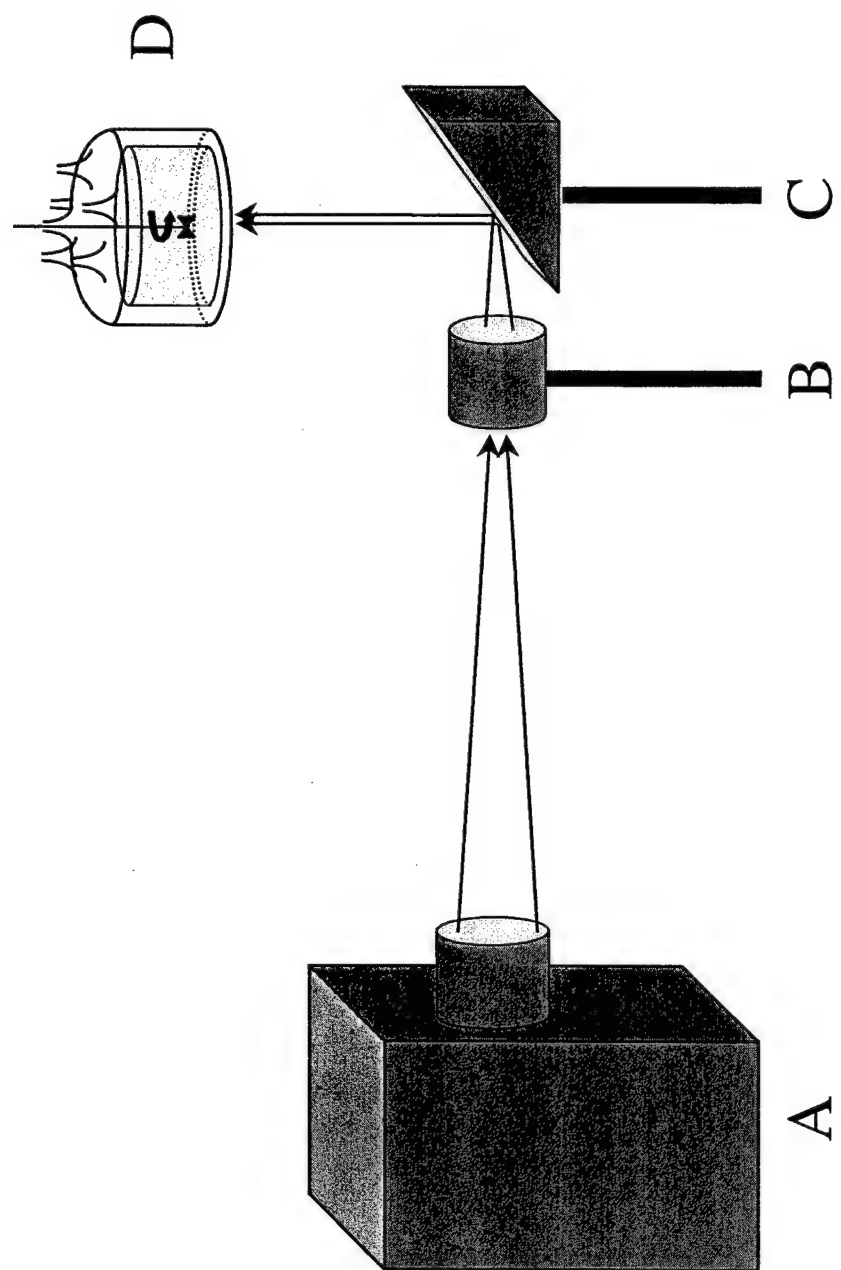


Figure 5. 2

Irradiance spectrum of solar simulator and a solar spectrum at 43.4 N, 71.1 W at solar noon calculated using TUV.

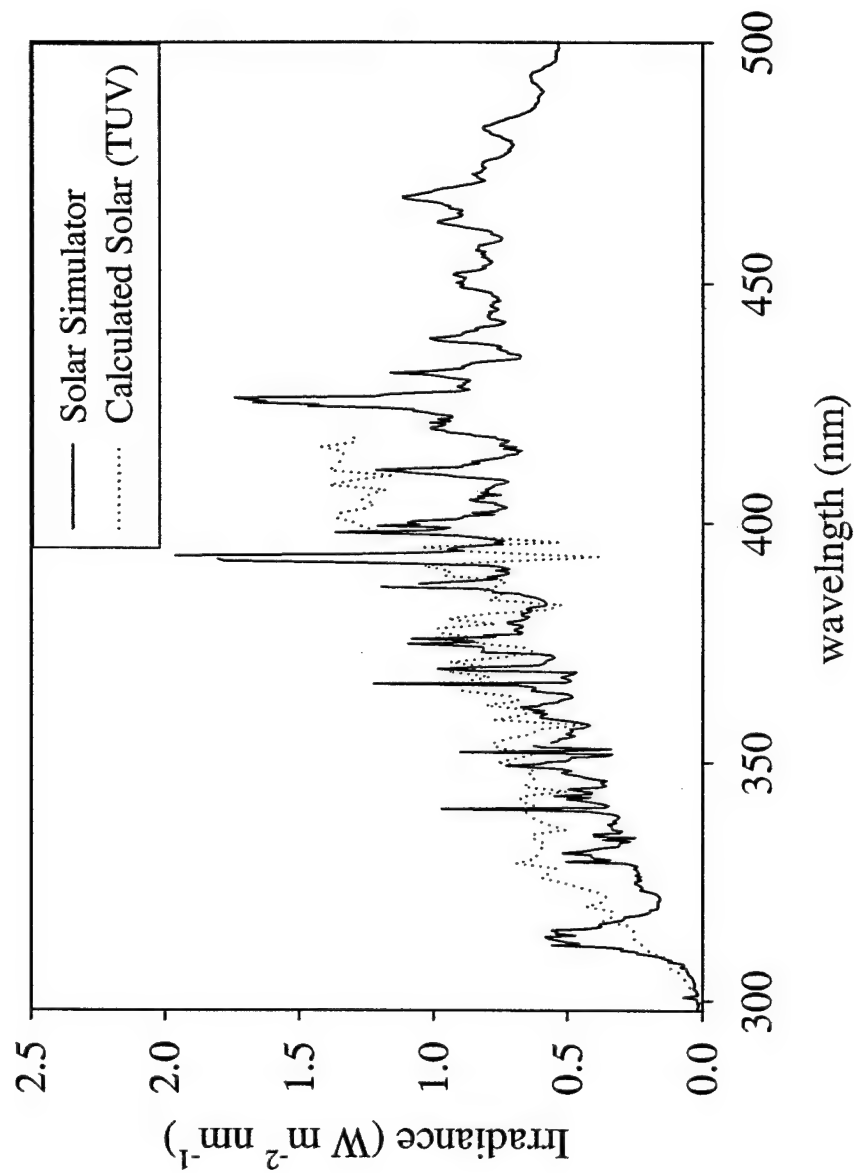


Figure 5. 3

Normalized photobleaching curves of CDOM absorption at 300nm in three unaltered seawater samples from the Delaware Bay (S4, 4%, ∇ ; S20Fe, 20%, \blacksquare ; and S29, 29%, \diamond) and one fulvic extract (SRFA, 2.5 mg C/l in Milli-Q water, \bullet). The lines are bi-exponential fits to the data.

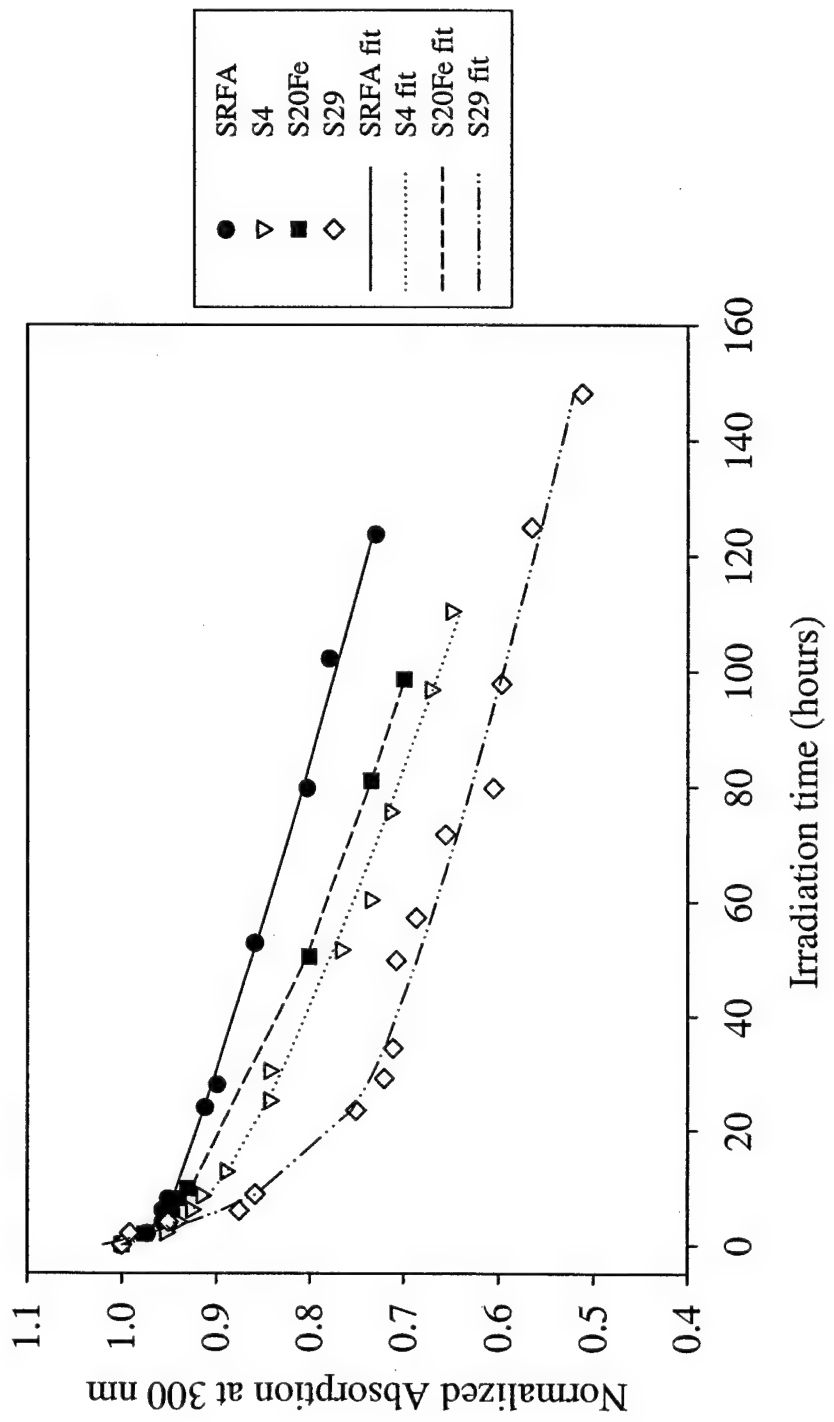


Figure 5. 4

Normalized photobleaching curves of CDOM fluorescence F/R values (see Methods) for three unaltered seawater samples from the Delaware Bay (S4, ∇ ; S20Fe, \blacksquare ; and S29, \diamond) and one fulvic extract (SRFA, \bullet). The lines are bi-exponential fits to the data. Note that the bleaching of the CDOM fluorescence is significantly faster than the bleaching of the CDOM absorption.

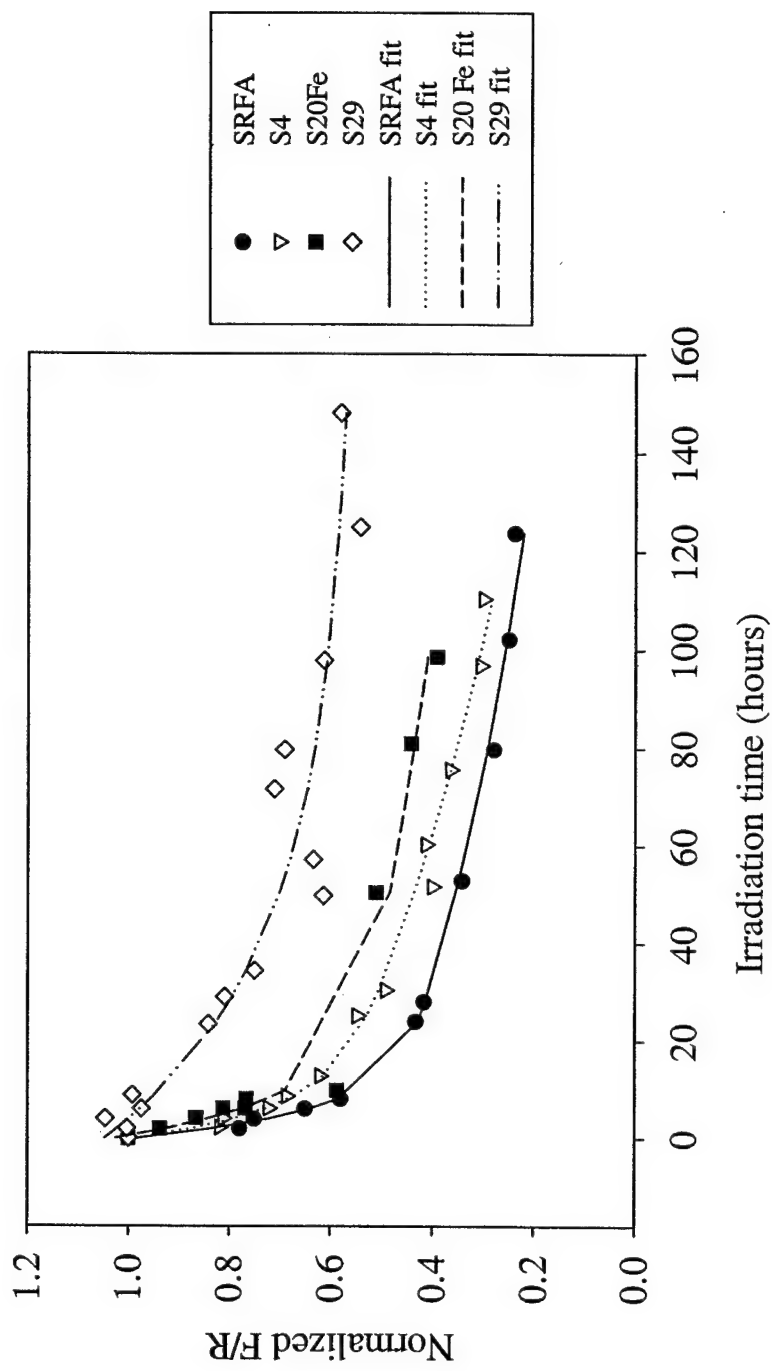


Figure 5. 5

Normalized bleaching curves of CDOM absorption and fluorescence F/R values for three treatments of two different seawater samples: Fe (100 nM Fe(III) added, ● and ○), DFOM (500 nM DFOM incubated, ▼ and ▽), and unamended (nothing added, ■ and □). A: S4, B: S20. There is no significant difference in the bleaching rates of either the absorption or of the fluorescence.

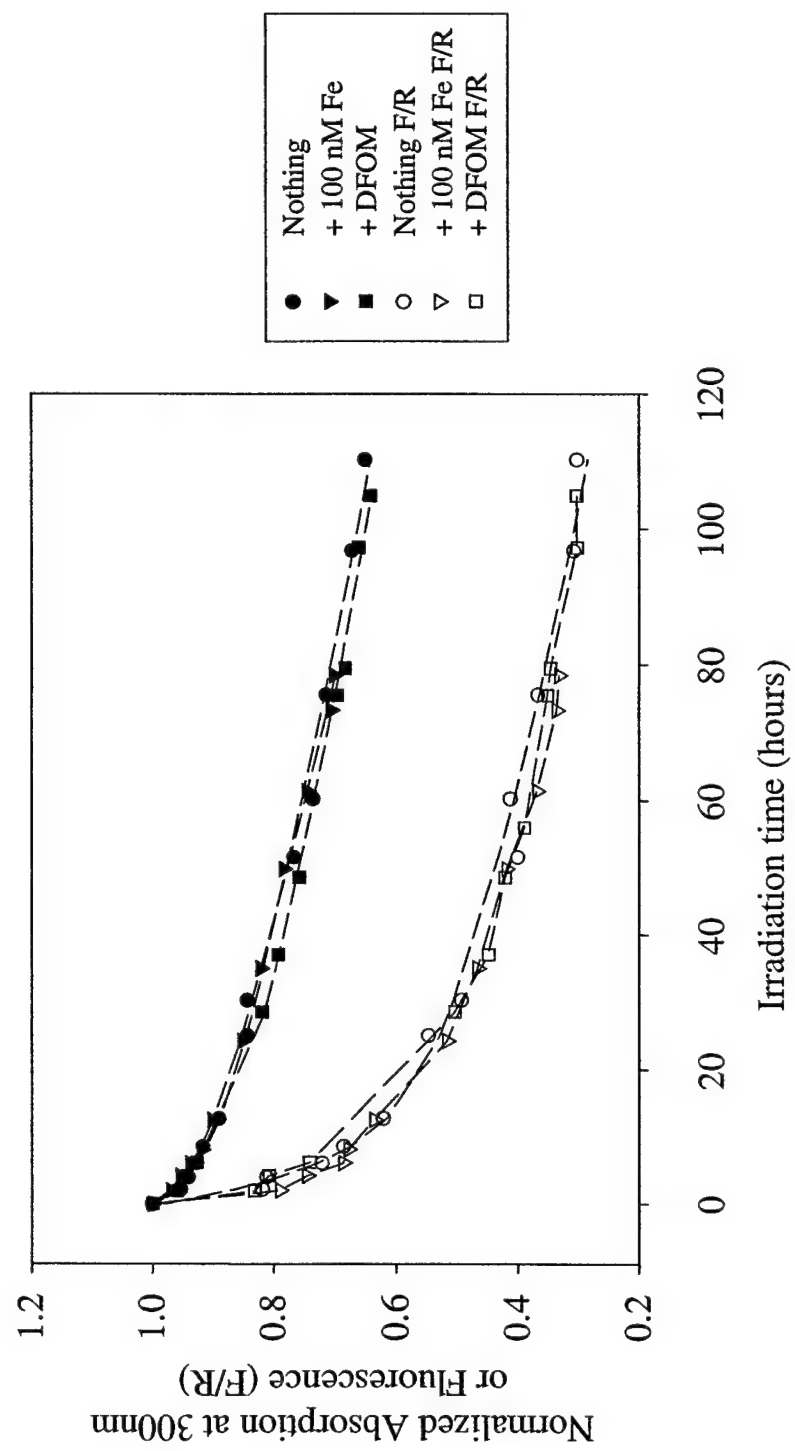


Figure 5.6

Normalized bleaching curves of CDOM absorption and fluorescence F/R values for additions of Fe to 2.5 mg C/l SRFA solutions: unamended (nothing added, ●), 500nM DFOM (▽), 100 nM Fe pH 8 (■), 100 nM Fe, pH 6 (◇), 2 μM Fe, pH 6 (▲). The lines are bi-exponential fits.

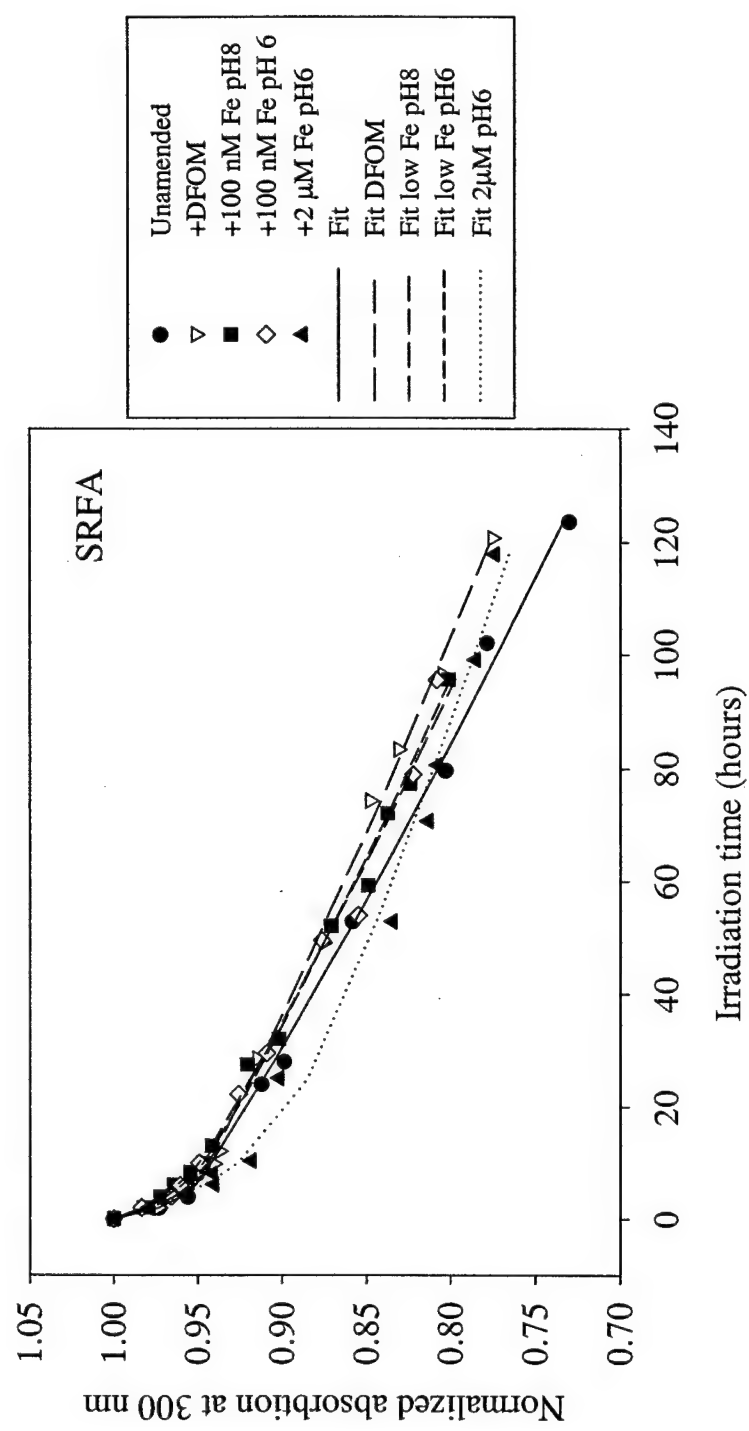


Figure 5. 7

Excitation-emission matrix spectra (EEMs) for 4 different water samples: S4, S20Fe, S29, and SRFA.

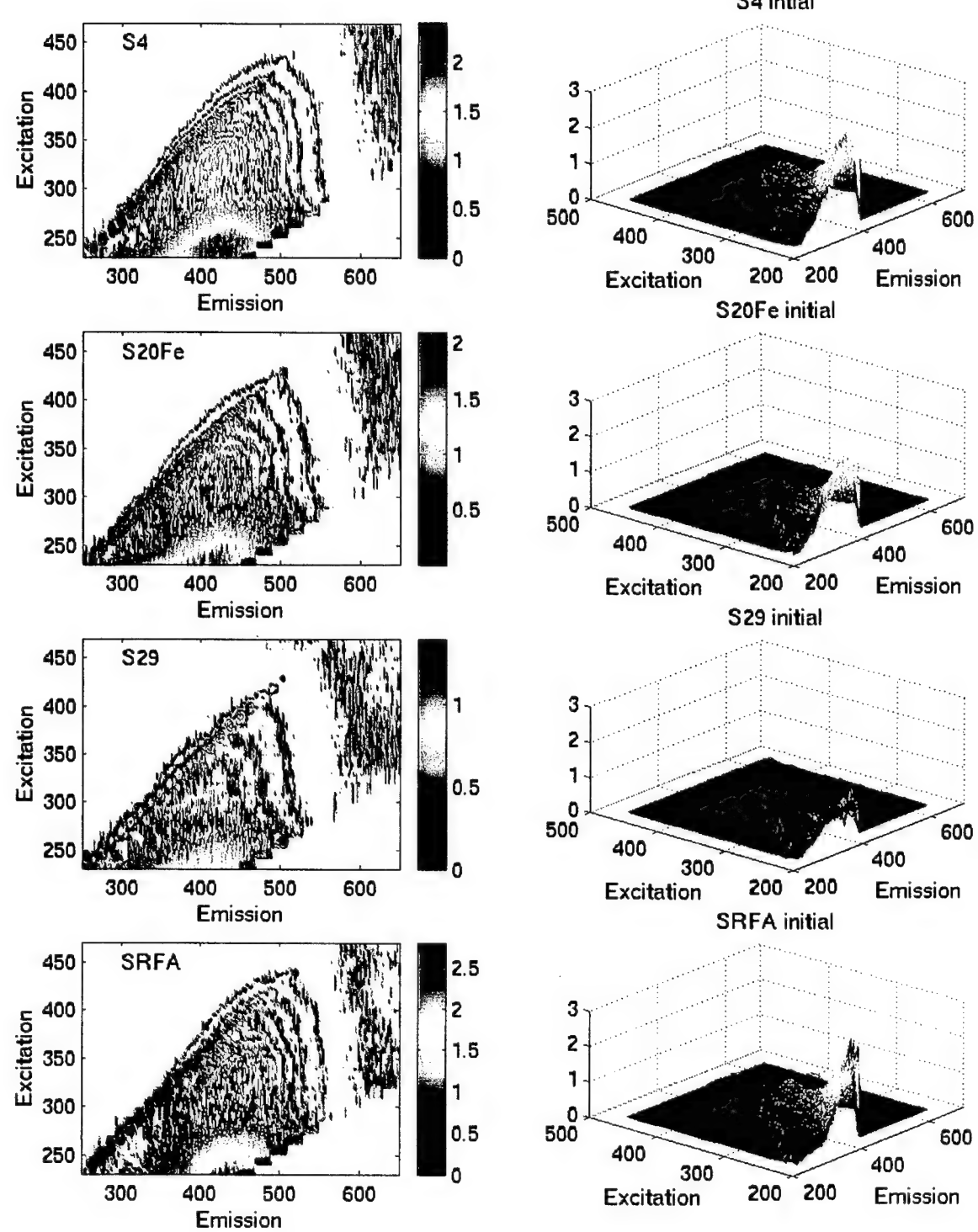


Figure 5.8

EEMs difference spectra showing the bleaching of the two fluorescence peaks (A and H).
From top to bottom: S4, S20Fe, S29, and SRFA.

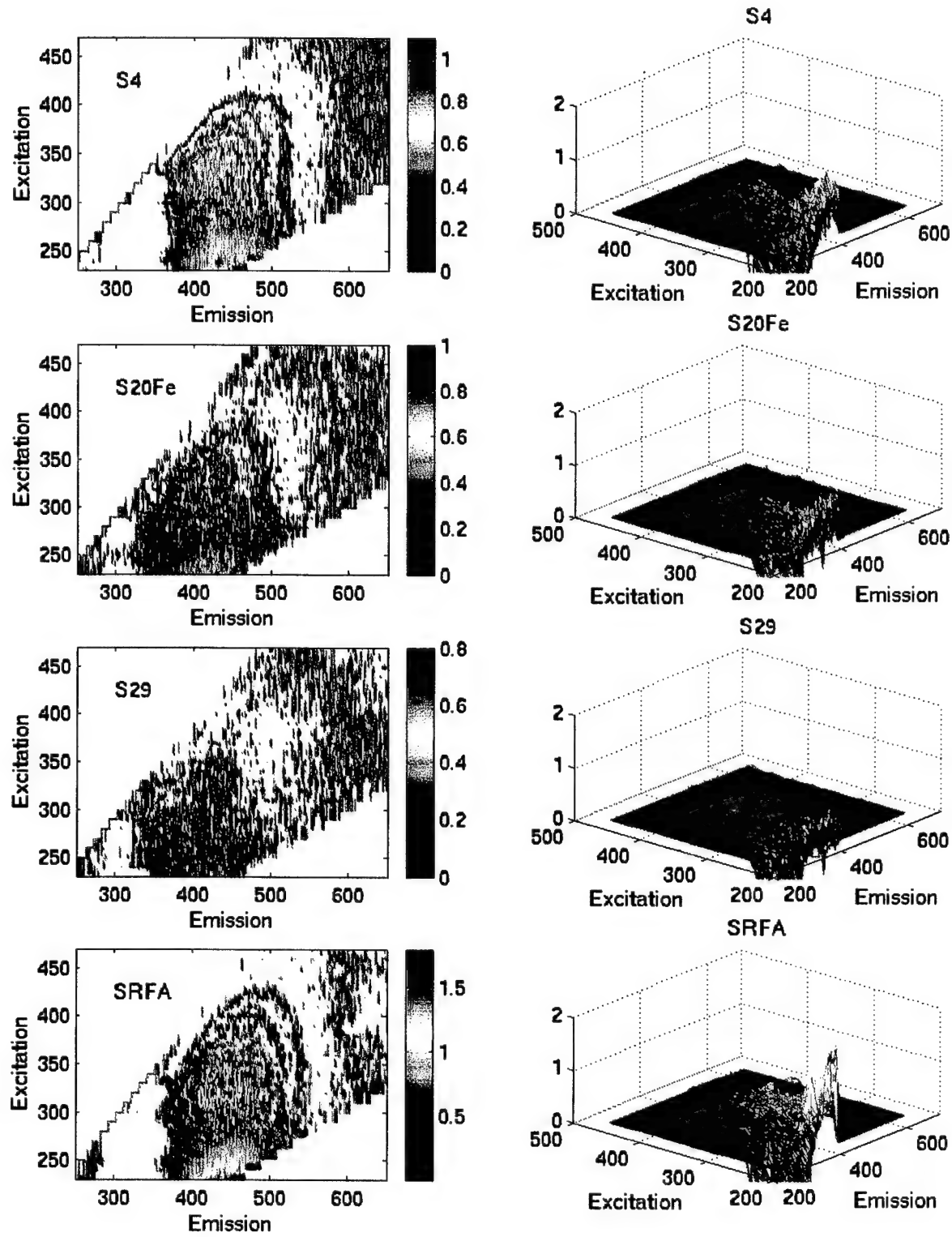


Figure 5.9

EEMS difference spectra showing the bleaching of fluorescence by radiolytically-produced OH[•]. From top to bottom: S4, S29, humic bog water.

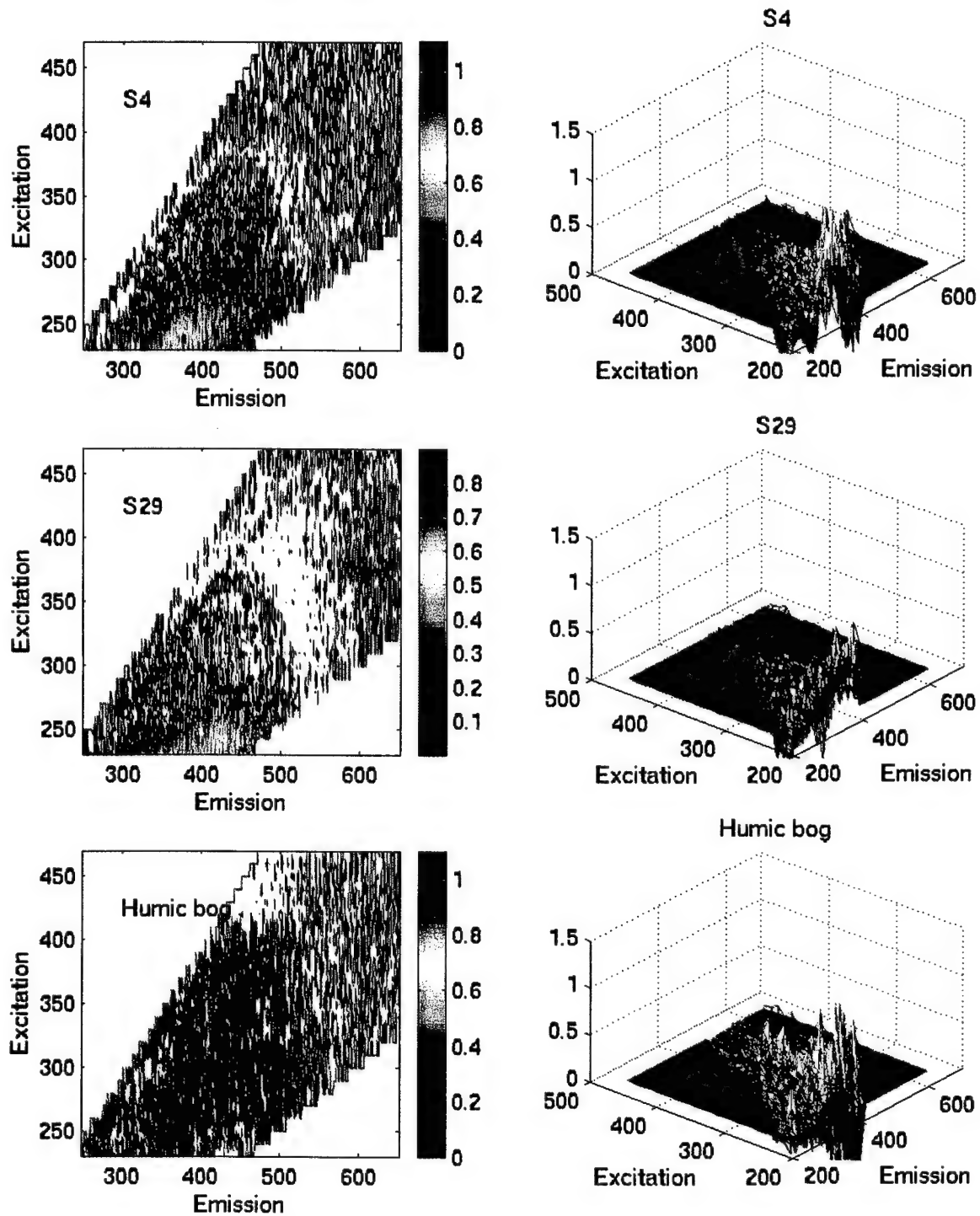


Figure 5.10

Apparent quantum yields (AQY) of CO photoproduction from estuarine seawater for different treatments: unaltered (■), 100 nM Fe(III) (●), 500 nM DFOM (∇), or 50nM Cu(II) (\diamond). These values are calculated from short term (< 90 min) irradiations at the given wavelengths. Where error bars are present, they are the standard deviation of duplicate determinations. A: S4, B: S20, C: S29.

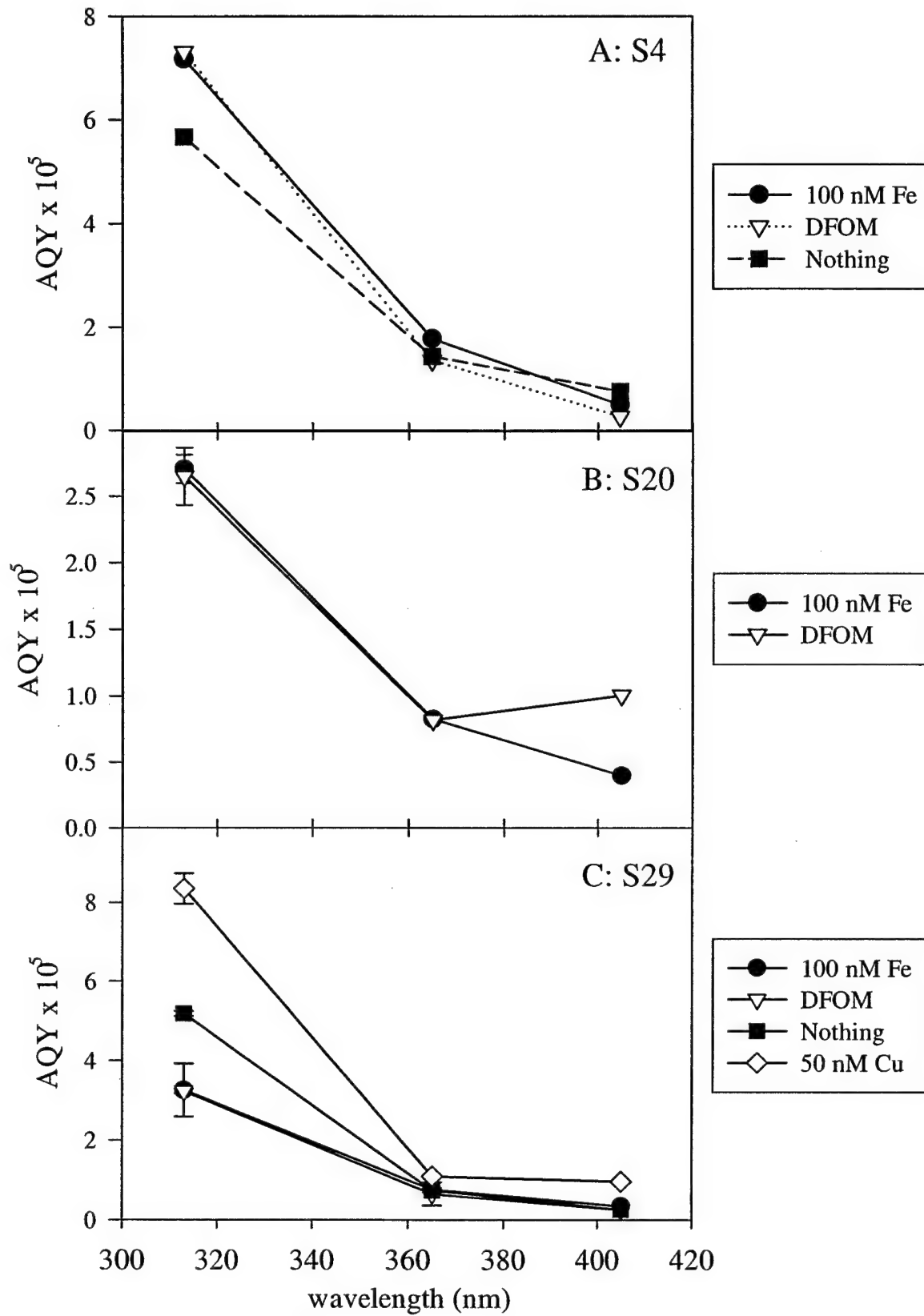


Figure 5.11

CO photoproduction from Sargasso Sea water during one daylight period as determined using an optical buoy (see Methods). Quartz flasks were suspended from an open frame at predetermined depths from dawn to dusk. 500 nM DFOM (V) was added to one set of flasks, and duplicate determinations were made for each flask. Samples were 0.2 μ m filtered sterilized. Left: effects of added DFOM (500 nM). Right: effects of added Fe (50 nM).

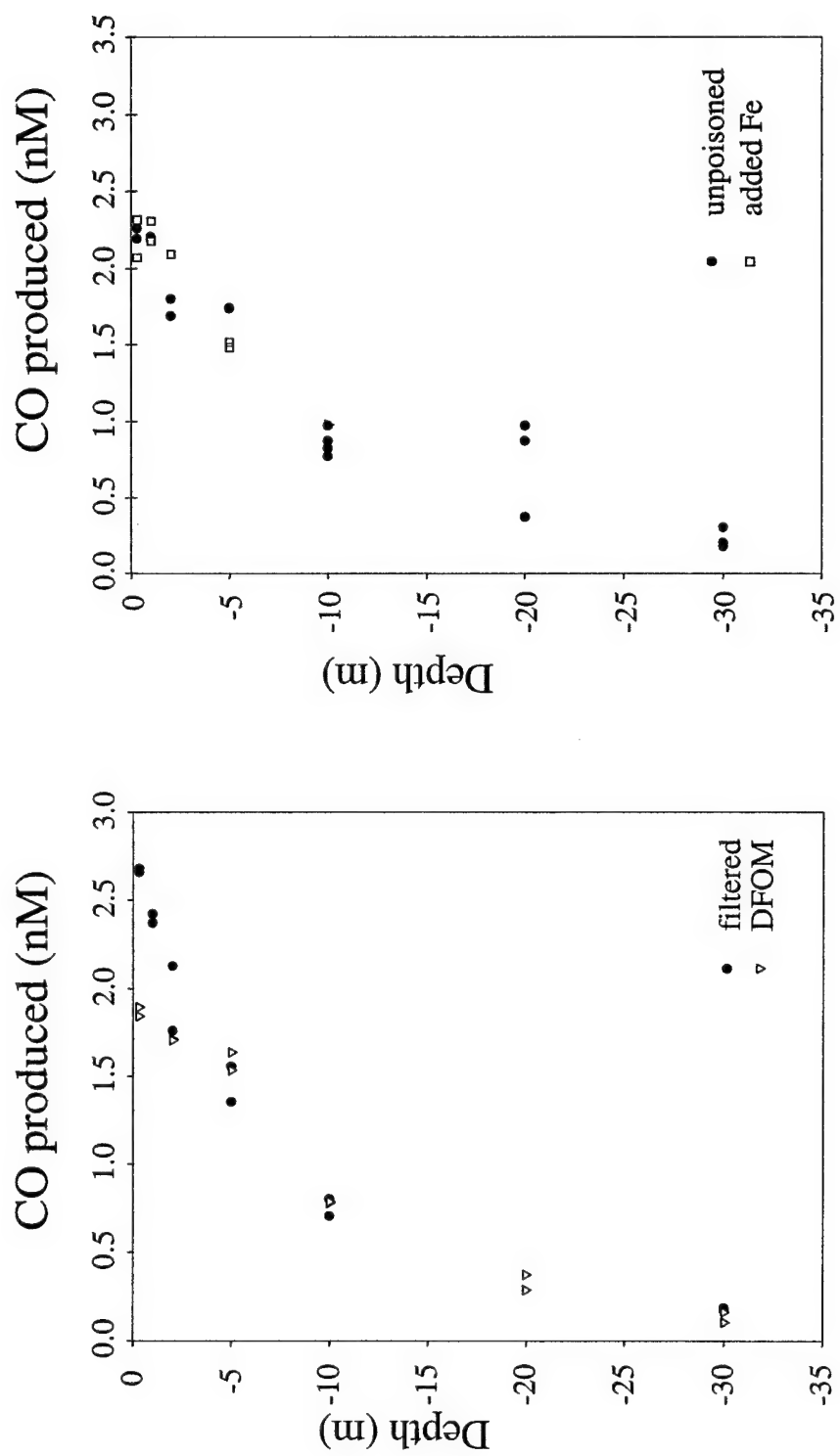
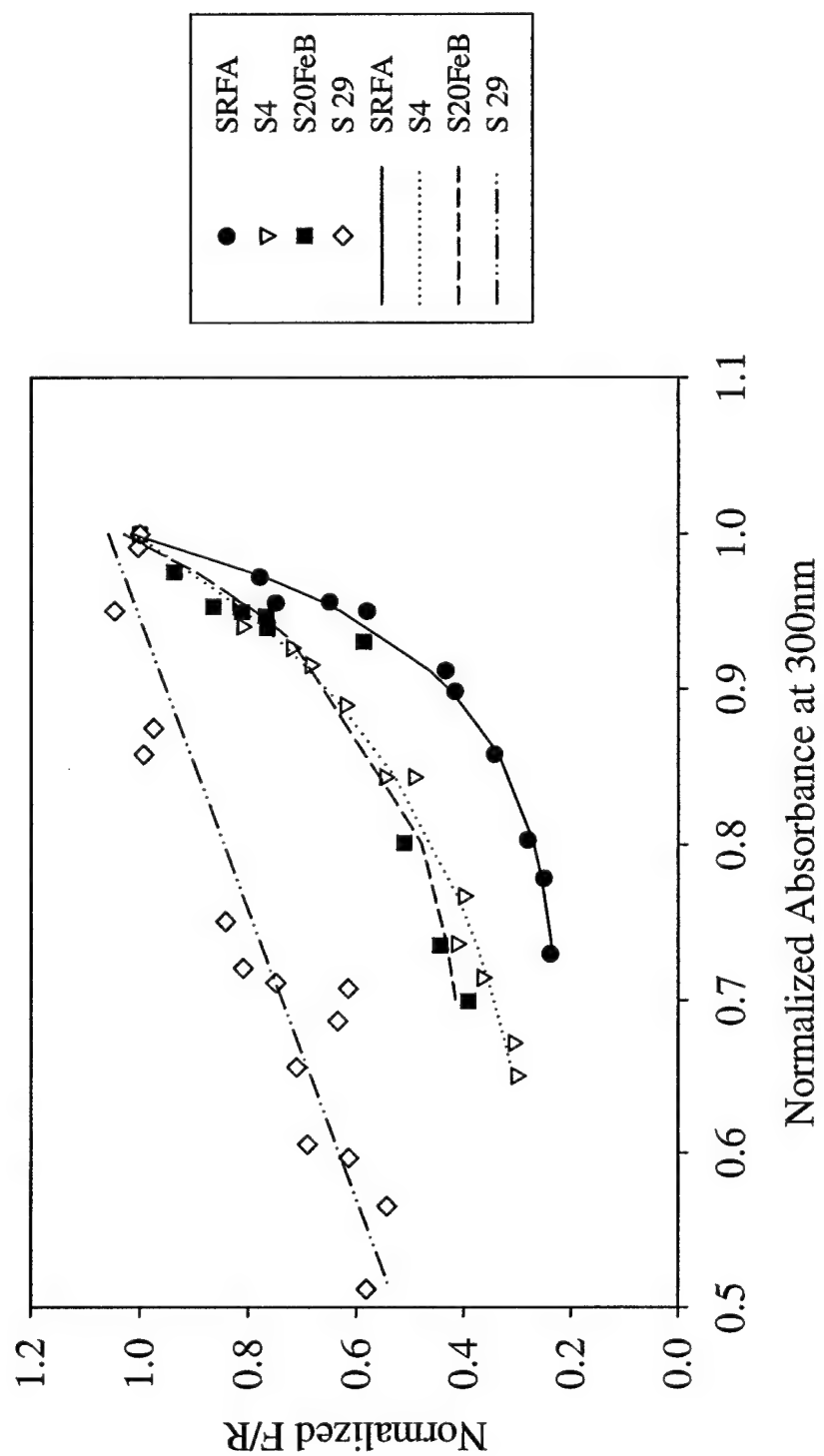


Figure 5.12

Bleaching of fluorescence versus bleaching of absorption for 4 different samples: SRFA (●), S4 (▽), S20FeB (■), and S29 (◇). The lines are single exponential fits, except for S29, which has a linear fit. Note that as the sample becomes progressively less ‘terrestrial’ in nature, the slope of the relationship flattens out.



CHAPTER 6.
THESIS DISTILLATION AND FUTURE WORK

Geochemical Significance

Significant transformations of terrestrial dissolved organic matter take place in estuarine and coastal waters. These transformations are in part effected by photochemical processes. In particular, there is a significant loss of chromophoric dissolved organic matter (CDOM). Photobleaching of the chromophores responsible for light absorption leads both to the greater penetration of light into the ocean and to a reduction in the production rates of photolysis products, including reactive oxygen species (ROS), carbon monoxide, and possibly reduced metals such as Fe(II). The photochemical decomposition of CDOM leads to the formation of a variety of biologically available products, including carbon monoxide and low molecular weight carboxylic acids and carbonyl compounds, that could represent an important source of carbon substrates to microorganisms.

Photomineralization of CDOM to dissolved inorganic carbon (DIC) may also constitute a significant flux in the global carbon cycle. CDOM photochemistry may also have an effect on the cycling of iron, a biogeochemically important element in marine systems. In order to further the study of these processes, this thesis has focused on several main issues: the photobleaching of CDOM, the roles of reactive oxygen species in the photochemistry of CDOM, and the roles that iron may play in CDOM photochemistry.

Photodecomposition may proceed both via direct photochemical reactions, following absorption of photons by CDOM, or via indirect processes, involving DOM reactions with photochemically generated intermediates such as reactive oxygen species (ROS). Prior work on CDOM photobleaching has not attempted to investigate the relative importance of these two mechanisms. If the mechanisms of photobleaching can be understood, then it may be possible to make predictions of CDOM photobleaching rates, given a few measurements of important parameters and knowledge of solar irradiance values. These predictions would be useful in modeling light penetration in marine systems, a crucial factor in many models of oceanographic surface processes.

The ROS that appear to play important roles in DOM chemistry are superoxide (O_2^-) and hydroxyl radical ($OH\cdot$). Of these, $OH\cdot$ is the likeliest candidate for having significant effects on DOM decomposition. $OH\cdot$ is a powerful oxidant known to react

with many organic compounds at nearly diffusion-limited rates. In this thesis I have determined the OH[•]-mediated bleaching rates of CDOM. In most natural systems, the production rates of OH[•] are too low to allow indirect bleaching reactions of OH[•] to play a significant role in CDOM photobleaching. However, there are indications that OH[•] contributes to long-term photobleaching rates, especially in freshwater systems, and to the bleaching of CDOM fluorescence. In particular, OH[•] may be responsible for bleaching fluorophores that absorb light at wavelengths below 290 nm, the lowest wavelength in the solar spectrum at the earth's surface.

Fe has been established to be of some importance in the photochemistry of CDOM in freshwaters (1-3). In this thesis I established that Fe does *not* play a significant role in the photobleaching and photooxidation of CDOM in coastal and estuarine waters. These results indicate that Fe does not have to be taken into account when examining the photobleaching of CDOM in coastal systems. In addition, Fe does not play a significant role in CO photoproduction, at least in coastal waters. These findings stand in contrast to the fact that Fe can affect photochemical processes in atmospheric and fresh waters.

It is clear that in both marine and freshwater systems, CDOM photochemistry plays a role in Fe speciation (4-11). One mechanism by which this occurs is through the redox reactions of O₂[−] with Fe. Prior investigations suggested that dissolved Fe might control O₂[−] steady-state concentrations. We found that CDOM appears to act as an organic redox catalyst in the decomposition of O₂[−] to O₂ and HOOH. In combination with the catalytic activity of various organic and inorganic copper complexes, this activity severely limits the steady-state concentration of O₂[−] in seawater. Instead of controlling O₂[−] steady-state concentrations, dissolved Fe speciation may be significantly affected by O₂[−] steady-state levels (12). The effect of O₂[−] on CDOM is less clear, but as CDOM appears to catalytically cycle with O₂[−], the net effect may be null.

This thesis adds to the few measurements of CO photochemical quantum yields in coastal waters. Photoproduction of carbon monoxide (CO) is potentially an important part of CDOM mineralization. Furthermore, CO is nearly always supersaturated in the surface ocean relative to the atmosphere, and in the atmosphere CO is a scavenger of gas phase

$\text{OH}\cdot$. As $\text{OH}\cdot$ is an important atmospheric oxidant, especially of organic pollutants, understanding the photoproduction of CO in the surface ocean is also important for our understanding of atmospheric chemistry. The quantum yields determined for the Delaware Bay seawater are extremely similar to the pooled quantum yields determined for three stations in the Gulf of Maine (13). The extension of these numbers to global photoproduction rates of CO produce an estimated annual CO photoproduction of 250-415 Tg CO yr⁻¹, a much smaller range than the previous estimates (150-1400 Tg CO yr⁻¹; (13-15)). Note that these are estimates of total production and not of fluxes, as they do not take into account the sinks of CO. These photoproduction rates are smaller than the estimated anthropogenic contribution of 1560 Tg CO yr⁻¹ (16).

A model of CDOM photobleaching that can successfully reproduce CDOM photobleaching under simulated solar irradiation was developed. This model incorporates time- and bleaching-wavelength-dependent behavior that represents an improvement over current models photobleaching. Although the mechanistic investigations of CDOM photobleaching chemistry in this thesis may not yield results of immediate use in predicting CDOM photobleaching, this model provides an empirical method of predicting CDOM bleaching, and thus may be of general utility in the modeling of geochemical phenomena affected by light penetration into marine surface waters.

Future Work

Each part of this thesis leads to a myriad of different investigative paths. I will highlight a few of the more interesting directions for future inquiry. I am indebted to my advisor and thesis committee members for the fruitful interactions which have stimulated these ideas.

A broader examination of O_2^- photoproduction rates would enable investigators to better assess the roles of this important photointermediate. Measurements of O_2^- photoproduction rates have so far been limited to the western North Atlantic and the Caribbean due to the extreme difficulty of these analyses (17,18). All estimates of the O_2^- steady-state concentration, and thus the results of redox modeling of trace metals in seawater, are based on these values.

The indirect photoredox cycling of humic substances by O_2^- in aquatic environments warrants further study. Reduced humic materials produced by chemical reactions with a bulk reductant such as sulfide have also been shown to reduce aquatic pollutants such as nitroaromatic compounds (19). Superoxide creates reduced humic materials during catalytic dismutation, and therefore electron transfer to other substances such as iron oxides or aquatic pollutants might occur at significant rates if the steady-state concentration of reduced humic materials is high enough.

Hydroxyl radicals may play a role in the photolytic decomposition of certain types of biomolecules that are otherwise recalcitrant to decomposition. In this thesis, bacterial growth potential as an indirect measure of the impact of hydroxyl radical on DOM substrate quality and bioavailability was assessed for very limited types of DOM (Suwannee River fulvic and humic acids) that are not good representatives of most aquatic DOM. A valuable addition would be an examination of the role of OH^\bullet in altering the bioavailability of the DOM in both marine and non-marine whole water samples, especially in conjunction with an equivalent assessment of the similar role of photochemical processes on the same material.

The role that OH^\bullet plays in the long-term photoreactions of CDOM in seawater is another avenue of inquiry. Some component of seawater may interfere with the reactivity of OH^\bullet with CDOM, for example by acting as a sink for both OH^\bullet and any reactive radical species produced from the reactions of Br^- and OH^\bullet . In addition, due to analytical constraints, I was unable to examine the possible role of OH^\bullet on DIC photoproduction in seawater. This line of investigation may also lead to a greater understanding of the mechanisms of photolytic mineralization.

Finally, the development of an accurate predictive model of CDOM photobleaching that could be applied to depth-dependent irradiance models would greatly aid not only photochemists but also the remote sensing community. The multicomponent model presented here is a step in the direction of providing such a model, but more work remains to be done to assess the validity of this approach.

References

1. Gao, H. Z.; Zepp, R. G. *Environmental Science & Technology* **1998**, *32*, 2940-2946.
2. Zuo, Y.; Jones, R. D. *Water. Res.* **1997**, *31*, 850-858.
3. Miles, C. J.; Brezonik, P. L. *Environ. Sci. Technol.* **1981**, *15*, 1089-1095.
4. Voelker, B. M.; Sedlak, D. L. *Mar. Chem.* **1995**, *50*, 93-102.
5. Voelker, B. M.; Morel, F. M. M.; Sulzberger, B. *Environ. Sci. Technol.* **1997**, *31*, 1004-1011.
6. Waite, T. D.; Szymczak, R.; Espey, Q. I.; Frunas, M. J. *Mar. Chem.* **1995**, *50*, 79-91.
7. Miller, W. L.; King, D. W.; Lin, J.; Kester, D. R. *Mar. Chem.* **1995**, *50*, 63-77.
8. Emmenegger, L.; Schonenberger, R.; Sigg, L.; Sulzberger, B. *Limnol. Oceanogr.* **2001**, *46*, 49-61.
9. Fukushima, M.; Tatsumi, K. *Colloids and Surfaces a-Physicochemical and Engineering Aspects* **1999**, *155*, 249-258.
10. Faust, B. C. *Aquatic and Surface Photochemistry*; Helz, G. R., Zepp, R. G. and Crosby, D. G., Ed.; Lewis Publishers: Boca Raton, FL, 1994, pp 3-38.
11. Sulzberger, B.; Laubscher, H.; Karametaxas, G. *Aquatic and Surface Photochemistry*; Helz, G. R., Zepp, R. G. and Crosby, D. G., Ed.; Lewis Publishers: Boca Raton, FL, 1994, pp 53-74.
12. Rose, A. L.; Waite, T. D. *Env. Sci. Technol.* **2002**, *in press*.
13. Ziolkowski, L. A. *Marine photochemical production of carbon monoxide*; Ziolkowski, L. A., Ed.; Dalhousie University: Halifax, N.S., Canada, 2000, pp 121.
14. Valentine, R. L.; Zepp, R. G. *Environ. Sci. Technol.* **1993**, *27*, 409-414.
15. Zuo, Y.; Jones, R. D. *Naturwissenschaften* **1995**, *82*, 472-474.
16. Khalil, M. A. K.; Rasumssen, R. A. *Chemosphere* **1990**, *20*, 227-242.
17. Zafiriou, O. C.; Dister, B. *J. Geophys. Res.* **1991**, *69*, 99-4945.
18. Micinski, E.; Ball, L. A.; Zafiriou, O. C. *J. Geophys. Res.* **1993**, *98*, 2299-2306.
19. Dunnivant, F. M.; Schwarzenbach, R. P.; Macalady, D. L. *Environ. Sci. Technol.* **1992**, *26*, 2133-2141.

AUTHOR'S BIOGRAPHY

I, Jared Verrill Goldstone, was born in Washington, D.C. on December 8, 1971 to Martha Welsh Goldstone, originally of Cambridge, MA, and Dr. Donald Edward Goldstone, originally of Baltimore, MD. I have two younger brothers, Tobias Evan (2.3 years younger) and Benjamin Tibbets (6.5 years younger). With the exception of summers, I grew up in Washington, DC. Summers we spent in Boothbay, Maine, where my mother's parents had retired to a former dairy farm. I attended Lafayette Elementary until 6th grade, followed by Maret School until graduation in 1989.

I attended Yale University from the fall of 1989 until graduation in the spring of 1993, where I was a member of Branford College, the Yale Banner, the Yale Precision Marching Band, as well as sundry other organizations, and majored in Chemistry. My undergraduate thesis advisor was Robert Crabtree, and my thesis research involved the synthesis of novel ligands for rhodium-mediated C-H bond activation. During the fall of 1991 I spent three months at McMurdo Station, Antarctica assisting in the assessment of UV effects on indigenous phytoplankton assemblages as part of a Research Experience for Undergraduates (REU) program. My advisors during this project were Michael Lesser and Patrick Neale.

After graduation from Yale, I enrolled in the doctoral program of Department of Chemistry at the Massachusetts Institute of Technology. In the spring of 1996, after working for Professor Alan Davison on rhenium oxygen atom transfer catalysis and technetium radiopharmaceutical characterization, I received a Master's Degree (S.M.). Three months later I enrolled in the MIT-WHOI Joint Program in Oceanography and began to work for Tina Voelker in the Department of Civil and Environmental Engineering at MIT. During subsequent summers I worked for Ollie Zafiriou at WHOI on carbon monoxide photoproduction in marine systems. I have participated in several research cruises, including two to the BATS station near Bermuda, and one in the Chesapeake Bay, and presented a number of papers at several different conferences.

My post-graduate work will begin with Neil Blough at the University of Maryland in College Park.

Document Library

Distribution List for Technical Report Exchange—November 1999

University of California, San Diego
SIO Library 0175C
9500 Gilman Drive
La Jolla, CA 92093-0175

Working Collection
Texas A&M University
Dept. of Oceanography
College Station, TX 77843

Hancock Library of Biology & Oceanography
Alan Hancock Laboratory
University of Southern California
University Park
Los Angeles, CA 90089-0371

Fisheries-Oceanography Library
151 Oceanography Teaching Bldg.
University of Washington
Seattle, WA 98195

Gifts & Exchanges
Library
Bedford Institute of Oceanography
P.O. Box 1006
Dartmouth, NS B2Y 4 A2
CANADA

Library
R.S.M.A.S.
University of Miami
4600 Rickenbacker Causeway
Miami, FL 33149

NOAA/EDIS Miami Library Center
4301 Rickenbacker Causeway
Miami, FL 33149

Maury Oceanographic Library
Naval Oceanographic Office
Building 1003 South
1002 Balch Blvd.
Stennis Space Center, MS 39522-5001

Research Library
U.S. Army Corps of Engineers
Waterways Experiment Station
3909 Halls Ferry Road
Vicksburg, MS 39180-6199

Library
Institute of Ocean Sciences
P.O. Box 6000
Sidney, B.C. V8L 4B2
CANADA

Institute of Geophysics
University of Hawaii
Library Room 252
2525 Correa Road
Honolulu, HI 96822

National Oceanographic Library
Southampton Oceanography Centre
European Way
Southampton SO14 3ZH
UK

Marine Resources Information Center
Building E38-320
MIT
Cambridge, MA 02139

The Librarian
CSIRO Marine Laboratories
G.P.O. Box 1538
Hobart, Tasmania
AUSTRALIA 7001

Library
Lamont-Doherty Geological Observatory
Columbia University
Palisades, NY 10964

Library
Proudman Oceanographic Laboratory
Bidston Observatory
Birkenhead
Merseyside L43 7 RA
UK

Library
Serials Department
Oregon State University
Corvallis, OR 97331

IFREMER
Centre de Brest
Service Documentation-Publications
BP 70 29280 PLOUZANE
FRANCE

Pell Marine Science Library
University of Rhode Island
Narragansett Bay Campus
Narragansett, RI 02882

REPORT DOCUMENTATION PAGE	1. REPORT NO. MIT/WHOI 2002-05	2.	3. Recipient's Accession No.
4. Title and Subtitle Direct and Indirect Photoreactions of Chromophoric Dissolved Organic Matter: Roles of Reactive Oxygen Species and Iron		5. Report Date February 2002	
		6.	
7. Author(s) Jared Verrill Goldstone		8. Performing Organization Rept. No.	
9. Performing Organization Name and Address MIT/WHOI Joint Program in Oceanography/Applied Ocean Science & Engineering		10. Project/Task/Work Unit No. MIT/WHOI 2002-05	
		11. Contract(C) or Grant(G) No. (C) OCE-9811208; OCE-9529448; (G) OCE-9819089; OCE-9521628	
12. Sponsoring Organization Name and Address National Science Foundation		13. Type of Report & Period Covered Ph.D. Thesis	
		14.	
15. Supplementary Notes This thesis should be cited as: Jared Verrill Goldstone, 2002. Direct and Indirect Photoreactions of Chromophoric Dissolved Organic Matter: Roles of Reactive Oxygen Species and Iron. Ph.D. Thesis. MIT/WHOI, 2002-05.			
16. Abstract (Limit: 200 words) Photochemical transformations of chromophoric dissolved organic matter (CDOM) are one of the principal processes controlling its fate in coastal waters. Photoreactions ultimately lead to the destruction of the chromophores and hence to the loss of absorption and fluorescence (bleaching), thus acting as a sink for CDOM and photodecomposition may proceed both via direct photochemical reactions or via indirect processes, involving photochemically generated intermediates such as reactive oxygen species (ROS). Superoxide (O_2^-) reactions with CDOM did not appear to degrade the CDOM. Instead, CDOM catalysed the dismutation of O_2^- to O_2 and HOOH. This reactivity has the effect of limiting the steady-state concentration of O_2^- in most coastal waters. Reactions of CDOM with radiolytically produced hydroxyl radical (OH^\bullet) formed CO_2 and several low molecular weight carboxylic acids, as well as bleached both the absorption and fluorescence at slow rates. These reactions did not increase the bioavailability of this material to a microbial consortium. Addition of iron to several coastal seawater samples and to solutions of Suwannee River Fulvic Acid neither increased the rate of photobleaching nor the apparent quantum yield (AQY) of CO. Similarly, the addition of the siderophore desferrioxamine B did not change the photobleaching rates or the CO AQYs. In combination with prior results, these findings suggest that indirect photoreactions do not increase the photobleaching rates of CDOM in coastal systems. A model of CDOM photobleaching based on the assumption of negligible indirect photobleaching processes and multiple non-interacting chromophores was created utilizing photobleaching data produced with monochromatic light to calculate the spectra and exponential decay rates of independent components. These components were then used to calculate bleaching spectra for broadband light and compared with actual bleaching spectra.			
17. Document Analysis a. Descriptors photochemistry CDOM hydroxyl radical			
b. Identifiers/Open-Ended Terms			
c. COSATI Field/Group			
18. Availability Statement Approved for publication; distribution unlimited.		19. Security Class (This Report) UNCLASSIFIED	21. No. of Pages 255
		20. Security Class (This Page)	22. Price